

Universidade Estadual Paulista "Júlio de Mesquita Filho"
Instituto de Biociências
Campus Botucatu

**Avaliação funcional das proteínas desacopladoras mitocondriais
em *Arabidopsis thaliana* utilizando mutantes de inserção**

Rômulo Pedro Macêdo Lima

Botucatu – SP

Março 2022

Universidade Estadual Paulista “Júlio de Mesquita Filho”
Instituto de Biociências
Campus Botucatu

**Avaliação funcional das proteínas desacopladoras mitocondriais
em *Arabidopsis thaliana* utilizando mutantes de inserção**

Rômulo Pedro Macêdo Lima

Orientador/Supervisor: Dr. Ivan de Godoy Maia

Tese apresentada ao Programa de Pós-graduação em Ciências Biológicas (Genética) do Instituto de Biociências de Botucatu, Universidade Estadual “Júlio de Mesquita Filho”, para obtenção do título de Doutor em Genética.

Botucatu – SP

Março 2022

FICHA CATALOGRÁFICA ELABORADA PELA SEÇÃO TÉC. AQUIS. TRATAMENTO DA INFORM.
DIVISÃO TÉCNICA DE BIBLIOTECA E DOCUMENTAÇÃO - CÂMPUS DE BOTUCATU - UNESP

BIBLIOTECÁRIA RESPONSÁVEL: ROSANGELA APARECIDA LOBO-CRB 8/7500

Lima, Rômulo Pedro Macêdo.

Avaliação funcional das proteínas desacopladoras
mitocondriais em *Arabidopsis thaliana* utilizando mutantes de
inserção / Rômulo Pedro Macêdo Lima. - Botucatu, 2022

Tese (doutorado) - Universidade Estadual Paulista "Júlio
de Mesquita Filho", Instituto de Biociências de Botucatu
Orientador: Ivan de Godoy Maia
Capes: 20203004

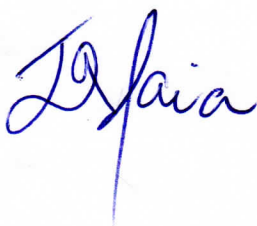
1. Mutagênese insercional. 2. Expressão gênica.
3. Metaboloma. 4. Mitocôndrias. 5. Proteínas de
desacoplamento mitocondrial.

Palavras-chave: Duplo-mutante; Expressão gênica;
Metaboloma; Mitocôndria; Proteína desacopladora.

ATA DA DEFESA PÚBLICA DA TESE DE DOUTORADO DE RÔMULO PEDRO MACÊDO LIMA, DISCENTE DO PROGRAMA DE PÓS-GRADUAÇÃO EM CIÊNCIAS BIOLÓGICAS (GENÉTICA), DO INSTITUTO DE BIOCIÊNCIAS - CÂMPUS DE BOTUCATU.

Aos 08 dias do mês de abril do ano de 2022, às 09:00 horas, por meio de Videoconferência, realizou-se a defesa de TESE DE DOUTORADO de RÔMULO PEDRO MACÊDO LIMA, intitulada **Avaliação funcional das proteínas desacopladoras mitocondriais em Arabidopsis thaliana utilizando mutantes de inserção**. A Comissão Examinadora foi constituída pelos seguintes membros: Prof. Dr. IVAN DE GODOY MAIA (Orientador(a) - Participação Virtual) do(a) Departamento de Ciências Químicas e Biológicas / Instituto de Biociências de Botucatu - UNESP, Prof. Dr. DOUGLAS SILVA DOMINGUES (Participação Virtual) do(a) Departamento de Biodiversidade / Instituto de Biociências de Rio Claro - UNESP, Prof. Dr. EDVALDO APARECIDO AMARAL DA SILVA (Participação Virtual) do(a) Departamento de Produção Vegetal / Faculdade de Ciências Agrômicas de Botucatu - UNESP, Prof. Dr. JORGE MAURICIO COSTA MONDEGO (Participação Virtual) do(a) Instituto Agrônomo de Campinas, Prof. Dr. CELSO LUIS MARINO (Participação Virtual) do(a) Departamento de Ciências Químicas e Biológicas / Instituto de Biociências de Botucatu - UNESP. Após a exposição pelo doutorando e arguição pelos membros da Comissão Examinadora que participaram do ato, de forma presencial e/ou virtual, o discente recebeu o conceito final: APROVADO. Nada mais havendo, foi lavrada a presente ata, que após lida e aprovada, foi assinada pelo(a) Presidente(a) da Comissão Examinadora.

Prof. Dr. IVAN DE GODOY MAIA



Agradecimentos

À Deus, por minha vida, a de meus familiares e amigos.

Ao meu orientador, Dr. Ivan de Godoy Maia, pela orientação, confiança, ensinamentos passados e imensurável contribuição neste trabalho.

Aos colegas doutores Luís Fernando Rolim, Pedro Barreto e Douglas Domingues, pelas enormes contribuições e sugestões transmitidas no exame geral de qualificação.

Aos amigos e colegas do Departamento de Ciências Químicas e Biológicas (Setor Genética), do Laboratório de Biotecnologia e Genética Molecular (BIOGEM), do Programa de Pós-Graduação em Ciências Biológicas (Genética) e do Centro de Convivência Infantil (CCI) “Pertinho da Mamãe”, por todas as pessoas que passaram por mim e deixaram uma marca de aprendizado, incentivo e carinho aqui na cidade de Botucatu, em especial à Camila Baldin, Priscila Medeiros, Tháris Gabryel, Amanda Tanamachi, Erasmo Oliveira, Alessandra Nunes-Laitz, Cristiane Rosa, Ricardo Manoel, Maiara Cornacini, Marcelo Alcântara, Darlin Zaruma, Valdeir Carvalho, Rafael Mendonça, Carlos Barreira, dona Malvina, Zé, Simone Campos, Talita Aleixo, Rafael Nakajima, Bruna Jerônimo, Prof. Robson Carvalho, Jeferson Souza, Paula Freire, Sarah Cury, Silvana Melo e Vanessa Rafaela.

Aos ex-colegas amigos e professores do Centro de Citricultura (CCSM) pelos anos de aprendizado e convivência, em especial ao Nicholas Vinícius, por todo conhecimento transmitido na parte de RNA-Seq e ciências “ômicas” da vida.

A toda “galera da Bio”, amigos e professores da época de graduação na UESB, em especial ao professor Dr. Antonio Carlos de Oliveira, pelos encontros online durante esta pandemia e também nas idas para a Bahia, com conversas de motivação e descontração, obrigado mesmo por tudo, se hoje estou aqui vocês têm contribuído imensamente para esta formação.

A todos os meus amigos da minha cidade natal (Poções-Bahia) e meus familiares da “Macedônia” e “Rocha Lima”, em especial a Wallas Meira e Lêda Cristina, conterrâneos e amigos queridos que carrego comigo aonde quer que eu vá.

Aos amigos de Vitória da Conquista-Bahia, principalmente os familiares da minha esposa, em especial a minha sogra Eliane e meu sogro Gildásio, minhas cunhadas Elaine e Tamiris, minha sobrinha de coração Maria Fernanda, pelas palavras de incentivo, conforto e confiança, e a Aline (“Né”), por ter vindo com a gente para Botucatu e ter nos ajudado com os cuidados da minha filha Maria Liz logo no início do doutorado.

A minha avó, Lacimi Caires, por todo amor e dedicação comigo, a minha mãe, Vanuza Macêdo, por todo suporte, paciência e amor incondicional transmitidos, e a meu pai (in memoriam), por sempre ter me dado forças e coragem para percorrer os obstáculos da vida.

A minha família incrível que construí desde a Bahia com esta admirável e forte mulher, Jakeline Oliveira, que a cada devaneio e desânimo me fortaleceu com suas palavras de ajuda e força, pelas conversas sobre o meio acadêmico e também sobre genética. Você vai longe!!! A minha filhota linda e que sou completamente apaixonado, Maria Liz, muito obrigado pela ternura, amor e pelo conforto nos momentos mais difíceis. E

a Kiara, nossa filhota felina que me acompanha desde o Mestrado, obrigado pelos inúmeros afagos e conforto durante esta caminhada. Amo vocês!!!

Ao apoio financeiro essencial para a realização desta pesquisa, pela concessão das bolsas de estudo da Coordenação de Aperfeiçoamento de Pessoal de Nível Superior (CAPES) – Código de financiamento 001, e da Fundação de Amparo à Pesquisa do Estado de São Paulo (FAPESP), Processo nº 2018/19021-1. Obrigado!!!

A todos que contribuíram de alguma forma para a realização deste trabalho.

Epígrafe

“Mas tu não deves esquecer. Tu te tornas eternamente responsável por aquilo que cativas.”

Antonie de Saint-Exupéry

Resumo

As proteínas desacopladoras mitocondriais (UCPs) são proteínas especializadas no transporte mitocondrial capazes de dissipar o gradiente eletroquímico de prótons gerados na respiração independente da síntese de ATP. Essas proteínas fazem parte da família de carreadores aniônicos mitocondriais e desempenham um papel fundamental na manutenção da função mitocondrial. Em plantas, a importância das UCPs como componentes da tolerância celular ao estresse oxidativo já foi demonstrada em estudos prévios. Três genes codificando UCP já foram descritos em *Arabidopsis thaliana* (nomeados *AtUCP1-3*), sendo boa parte dos dados funcionais obtidos para a isoforma *AtUCP1*. Portanto, o papel desempenhado pelas demais isoformas é ainda pouco estudado. Diante disso, mutantes de inserção de *Arabidopsis* foram empregados para investigar a existência de redundância funcional entre essas isoformas. Para tal, numa primeira abordagem, duplo-mutantes de inserção para diferentes combinações gênicas (*atucp1/atucp2*, *atucp1/atucp3* e *atucp2/atucp3*) foram obtidos e analisados funcionalmente durante o desenvolvimento vegetativo e reprodutivo. Em uma segunda etapa foram empreendidas análises de metabólitos durante a fase vegetativa destes duplo-mutantes. Em paralelo, baseado em dados prévios da primeira abordagem que indicaram fenótipos mais evidentes na fase vegetativa do duplo-mutante *atucp1/atucp3* em relação ao controle selvagem, o perfil global de expressão gênica deste duplo-mutante na fase vegetativa foi determinado usando RNA-Seq. Análises subsequentes de bioinformática com datasets encontrados na literatura foram empreendidas. Os dados obtidos na primeira etapa indicam que as três isoformas parecem atuar de forma complementar em diferentes processos associados ao crescimento e desenvolvimento de *A. thaliana*. As isoformas *AtUCP1* e *AtUCP2* atuam de forma conjunta na manutenção da homeostase e função mitocondrial durante a fase reprodutiva. Por outro lado, as isoformas *AtUCP2* e *AtUCP3* teriam maior relevância funcional na atividade fotossintética, enquanto que a *AtUCP1* atuaria na manutenção do aparato fotossintético. Além disso, as isoformas *AtUCP2* e *AtUCP3* atuam em conjunto na manutenção do equilíbrio redox. Os dados indicam ainda que todas as três isoformas atuam em conjunto para a redução das espécies reativas de oxigênio (ERO) na mitocôndria. Cabe ressaltar que o duplo *knockdown* dos genes *AtUCP1* e *AtUCP3* foi o que promoveu as maiores alterações fenotípicas e de função mitocondrial na fase vegetativa. Curiosamente, uma maior atividade respiratória foi registrada no duplo-mutante *atucp2/atucp3*, o que pode ser justificado pela forte expressão compensatória do gene *AtUCP1* sob condições normais. De maneira similar, uma forte expressão compensatória da isoforma não inativada foi detectada em todas as três combinações de duplo-mutantes crescidos em condições normais ou em presença de estresse (salino e osmótico), o sugerindo uma redundância parcial entre elas. As análises de metabólitos revelaram profundas alterações no teor de alguns metabólitos primários (açúcares, aminoácidos, ácidos orgânicos e componentes de ácidos nucleicos) e secundários nos três duplo-mutantes. Em consonância, diversos genes diferencialmente expressos associados ao cloroplasto, mitocôndria e à resposta aos estresses abióticos foram detectados no duplo-mutante *atucp1/atucp3*. As análises comparativas de RNA-Seq para validação com o dataset selecionado de *A. thaliana* tipo selvagem reforçam os impactos causados por toda a célula. Em conjunto, os resultados obtidos evidenciaram uma intensa reprogramação transcricional e metabólica em decorrência do duplo *Knockdown* de genes *AtUCP1* and *AtUCP3*. As análises apontaram ainda para a existência de uma redundância funcional parcial entre as três isoformas, que atuam

ora de forma isolada, ora de maneira conjunta na manutenção da homeostase e função mitocondrial durante o crescimento e desenvolvimento de *A. thaliana*. Essas descobertas fornecem novos subsídios para fundamentar o papel desempenhado pelas diferentes isoformas e fornecem *insights* sobre a atuação *in planta* da isoforma AtUCP3 em associação com a AtUCP1.

Palavras-chave: Proteína desacopladora, mitocôndria, duplo-mutante, expressão gênica e metaboloma.

Abstract

Mitochondrial uncoupling proteins (UCP) are specialized proteins involved in mitochondrial transport, which are able to dissipate the proton electrochemical gradient generated by respiration independent of ATP synthesis. These proteins belong to the mitochondrial anionic carrier family and play a key role in the maintenance of the mitochondrial function. In plants, their relevance as components of cell tolerance to oxidative stress has already been shown in previous studies. Three genes encoding UCP have been described in *Arabidopsis thaliana* (named *AtUCP1-3*), with most functional data being obtained for the *AtUCP1* isoform. Therefore, the role played by the other isoforms is still poorly understood. In view of this, we decided to investigate the occurrence of functional redundancy between these isoforms using *Arabidopsis* insertion mutants. For this, in a first approach, double-insertion mutants for different gene combinations (*atucp1/atucp2*, *atucp1/atucp3* and *atucp2/atucp3*) were obtained and functionally analyzed during vegetative and reproductive development. In a second step, metabolome analysis was carried out during the vegetative phase of these double mutants. In parallel, based on previous data from the first approach indicating more evident phenotypes in the vegetative phase of the *atucp1/atucp3* mutant compared with the wild-type (WT) control, the global gene expression profile of this double mutant in the vegetative phase was determined using RNA-Seq. Subsequent bioinformatics analyzes with datasets found in the literature were carried out. The data obtained in the first approach indicate that the three isoforms act in a complementary way in different processes associated with *A. thaliana* growth and development. The concerted action of the *AtUCP1* and *AtUCP2* isoforms seems to be required for maintaining homeostasis and mitochondrial function during the reproductive phase. On the other hand, our data suggest that the *AtUCP2* and *AtUCP3* isoforms have higher functional relevance in the photosynthetic activity, while *AtUCP1* would act in favor of photosynthetic apparatus maintenance. In addition, a concerted action of the *AtUCP2* and *AtUCP3* isoforms seems to be required for maintaining the redox balance. All three isoforms are necessary to reduce reactive oxygen species (ROS) in mitochondria. Of note, the double knockdown of the *AtUCP1* and *AtUCP3* promoted the highest phenotypical changes and alterations in mitochondrial function in the vegetative phase. Interestingly, the *atucp2/atucp3* mutant showed a higher respiratory activity, which can be explained by the strong compensatory expression of *AtUCP1* under normal conditions. Similarly, a strong compensatory expression of the non-inactivated isoform was detected in all three double mutants grown under normal and stressed conditions (saline and osmotic), thus suggesting a partial redundancy between the isoforms. Additionally, the metabolome analysis revealed profound changes in the content of some primary (sugars, amino acids, organic acids and nucleic acid components) and secondary metabolites in all three double mutants. Accordingly, several differentially expressed genes associated with chloroplast, mitochondria and response to abiotic stresses were detected in *atucp1/atucp3* double mutant plants. Comparative analysis of RNA-Seq for validation with the selected dataset of wild-type *A. thaliana* reinforce the impacts caused throughout the cell. Overall, these results indicate that an intense transcriptional and metabolic reprogramming occurs as a consequence of the double knockdown of *AtUCP1* and *AtUCP3* genes. Our data revealed the existence of a partial functional redundancy between the three isoforms, which would act either alone or in a concerted way for the maintenance of homeostasis and mitochondrial function during *A. thaliana* growth and development. These findings provide clues for the functionality of different *AtUCP*

isoforms and give insights for the role played by the AtUCP3 isoform in association with AtUCP1 in the entire plant level.

Keywords: Uncoupling protein, mitochondria, double mutant, gene expression and metabolome.

Avaliação funcional das proteínas desacopladoras mitocondriais em
Arabidopsis thaliana utilizando mutantes de inserção

Rômulo Pedro Macêdo Lima

Orientador: Dr. Ivan de Godoy Maia

Sumário

Introdução geral e justificativa	11
Objetivos	19
Referências bibliográficas	20
Capítulo I: The Double Knockdown of the Mitochondrial Uncoupling Protein Isoforms Reveals Partial Redundant Roles During <i>Arabidopsis thaliana</i> Vegetative and Reproductive Development.....	23
Capítulo II: Effects of Mitochondrial Disturbances on Transcriptional and Metabolite Profiles of <i>Arabidopsis ucp</i> double mutant plants	60
Considerações Finais.....	171

Introdução geral e justificativa

Devido à imobilidade, as plantas passam por constantes adaptações às adversidades do ambiente. Neste contexto, as mitocôndrias vegetais também tiveram que se adaptar adquirindo atributos metabólicos únicos em comparação aos animais, como por exemplo, a biossíntese do ácido ascórbico, do folato e a aquisição de uma via respiratória alternativa (Millar et al., 2011). Por participarem de uma série de processos celulares importantes, as mitocôndrias atuam ativamente nos diversos mecanismos de resposta aos diferentes tipos de estresses ambientais, o que as tornam sítios de detecção de desequilíbrios funcionais e alterações energéticas (Jacoby et al., 2012).

Apesar de ser uma área que necessita de maior investigação, principalmente em plantas, a relação entre sinalização retrógrada mitocondrial e a resposta aos estresses permite refutar a ideia de que as mitocôndrias são organelas independentes, necessárias apenas para o metabolismo energético. A resposta coordenada entre a mitocôndria e o núcleo, especialmente em presença de algum fator estressante, envolve adaptações metabólicas e bioquímicas de curto e longo prazo que conferem à célula uma maior resistência. Essa resposta mediada por alguma disfunção mitocondrial recebe a denominação de *mitohormesis* (Figura 1), que atualmente está sendo estudada em vários organismos-modelo. Em plantas, a *mitohormesis* é bastante associada aos mecanismos moleculares que levam à alteração na expressão de genes nucleares envolvidos no processo de biogênese mitocondrial e na resposta a algum tipo de estresse (Welchen et al., 2014; Yun & Finkel, 2014).

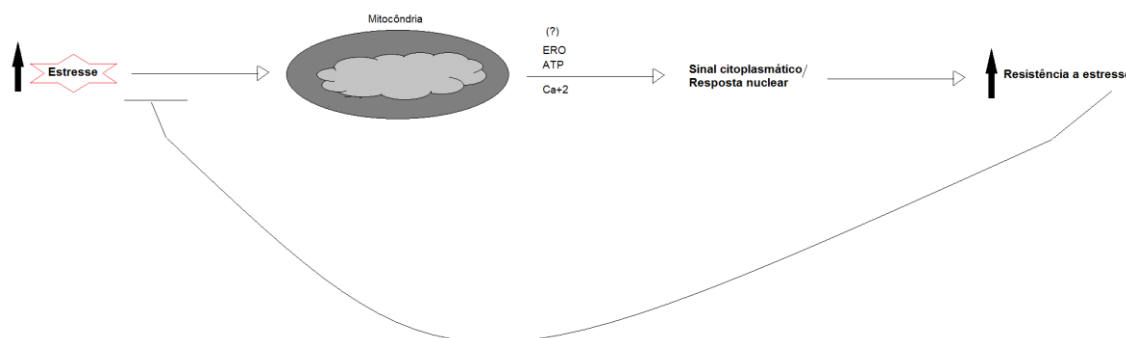


Figura 1. Mitohormesis. Com uma perturbação da função mitocondrial por algum tipo de estresse (seja interno ou externo), ocorre um intenso processo de sinalização dessa perturbação ao citosol por meio de diferentes mecanismos, como a geração de ERO, ATP e íons Ca^{+2} , que geram um sinal citoplasmático e uma subsequente resposta nuclear (representada pela alteração transcricional de genes) indutores de uma proteção celular (resistência) a curto e longo prazo. (Adaptado de Yun & Finkel, 2014)

Sabe-se que vários estresses ambientais podem induzir alterações significativas na expressão de diferentes genes pela sinalização ao núcleo do acúmulo mitocondrial de espécies reativas de oxigênio (ERO) (Hartl & Finkemeier, 2012). O aumento rápido e excessivo de ERO ocorre de maneira contínua na cadeia transportadora de elétrons da mitocôndria em dois principais complexos (I e III). Duas enzimas respiratórias alternativas, a oxidase alternativa (AOX) e a NADH desidrogenase, fazem parte dessa cadeia em plantas e não estão presentes em mamíferos. Em condições de estresse, a AOX, que está envolvida na sinalização mitocôndria-núcleo e funciona como um marcador de disfunção mitocondrial bem como de estresse oxidativo, é frequentemente induzida (Almeida et al., 1999; Moller, 2001; Vanlerberghe, 2013). Por outro lado, estudos prévios detectaram a presença de outro grupo de proteínas dissipadoras de energia nas mitocôndrias de plantas que atuam como reguladoras do acúmulo de ERO mitocondrial e na proteção contra o estresse oxidativo, as chamadas proteínas desacopladoras mitocondriais (uncoupling mitochondrial protein; UCPs) (Vercesi et al., 1995; Maxwell et al., 1999).

De forma geral, o processo de respiração celular para produção de energia ocorre em três estágios: produção de acetilcoenzima A (acetil-CoA); oxidação do acetil-CoA; além da transferência de elétrons e fosforilação oxidativa. A primeira etapa ocorre no citosol e se inicia pela oxidação de substratos como glicose (via glicólise) ou ácidos graxos (via beta-oxidação), o que gera moléculas menores (piruvato e depois acetil-CoA), além de energia na forma de elétrons conservada nos compostos intermediários NADH (Nicotinamida-Adenina-Dinucleotídeo) e FADH₂ (Flavina-Adenina-Dinucleotídeo). Os intermediários NADH e FADH₂ produzidos no citoplasma são posteriormente transportados para a mitocôndria, em que alimentarão o ciclo de Krebs e a cadeia respiratória. O acetil-CoA, resultante da metabolização do piruvato, entra no ciclo de Krebs e participa de uma série de reações de oxirredução que irá culminar na liberação de gás carbônico (CO₂), sendo que parte da energia livre gerada é retida na forma das coenzimas reduzidas NADH e FADH₂ na matriz mitocondrial (Krauss et al., 2005). Por fim, as coenzimas reduzidas NADH e FADH₂ geradas são transportadas para a cadeia respiratória ou cadeia transportadora de elétrons (complexo de proteínas da membrana interna mitocondrial), o que acarreta na doação e transferência de seus elétrons por todo o complexo, resultando no consumo de oxigênio molecular (O₂) e formação de água (H₂O). Esse processo de transporte de

elétrons ao longo da cadeia respiratória ocasiona liberação de energia, que por sua vez, pode ser dissipada na forma de calor ou utilizada para a manutenção do gradiente eletroquímico de prótons (H^+) da matriz mitocondrial (local de menor concentração) para o espaço intermembranar (local de maior concentração) (Barreto, 2014).

Na fosforilação oxidativa, o fluxo de prótons estabelecido pela oxidação de NADH e $FADH_2$ é usado para sintetizar ATP a partir de ADP e fosfato inorgânico (P_i) por um complexo proteico da membrana mitocondrial interna chamado ATP sintase (processo denominado de fosforilação oxidativa). Assim, na respiração acoplada, o complexo ATP sintase permite a reentrada de prótons para a matriz mitocondrial gerando energia contida nas moléculas de ATP. Entretanto, a cadeia transportadora de elétrons pode não estar totalmente acoplada à fosforilação oxidativa já que os íons H^+ podem retornar para a matriz mitocondrial pela ação de outras proteínas presentes na membrana interna. Dentre essas proteínas, encontram-se as chamadas proteínas desacopladoras mitocondriais (UCPs; *uncoupling protein mitochondrial*), que facilitam a reentrada de prótons para a matriz mitocondrial, tudo isso sem que esteja ocorrendo a produção de energia na forma de ATP. Como consequência, o potencial de membrana é ligeiramente reduzido e a energia derivada da oxidação dos substratos é perdida de forma independente à síntese de ATP. Tal atividade desacopladora é dependente de ácidos graxos e sensível aos nucleotídeos purínicos. Por fim, o carreador ADP/ATP exporta o ATP recém-sintetizado para o citosol em forma de ADP (Figura 2) (Nicholls, 2001; Ledesma et al., 2002; Vercesi et al., 2006; Nunes, 2010; Laitz, 2014).

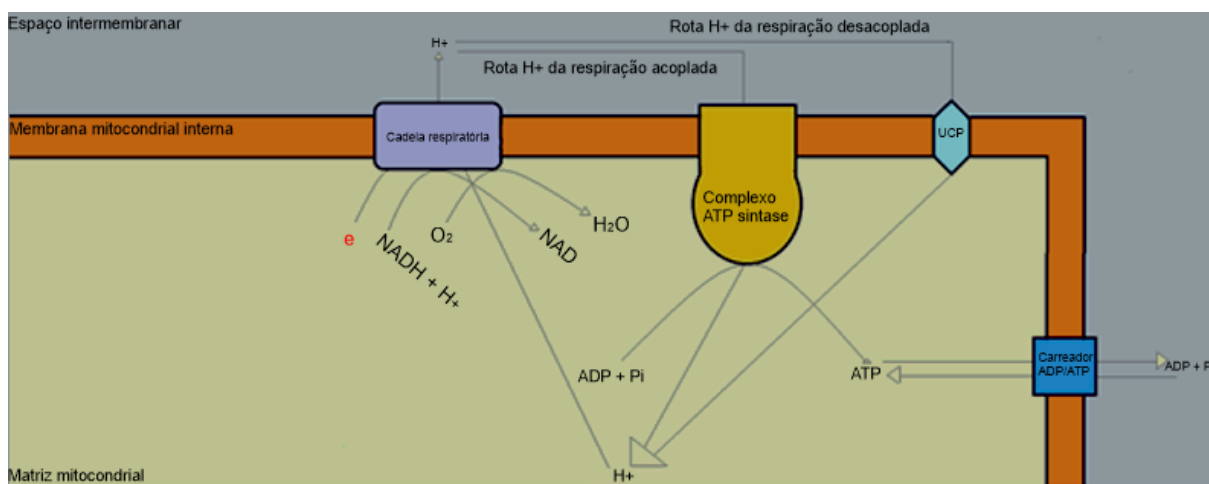


Figura 2. As UCPs provocam o desacoplamento entre o transporte de elétrons e a fosforilação oxidativa (oxidação de NADH e síntese de ATP a partir de ADP), o que permite a dissipação de energia. Durante a respiração, elétrons (e^-) são transportados e perpassam o complexo de proteínas da membrana mitocondrial interna (cadeia respiratória), enquanto prótons H^+ são bombeados para o espaço intermembranar gerando um gradiente eletroquímico que é usado pelo complexo ATP sintase

para a produção de ATP. As UCPs propiciam uma reentrada de prótons H^+ para a matriz mitocondrial, dissipando assim o gradiente eletroquímico gerado. Por fim, o ATP sintetizado é exportado para o espaço intermembranar e logo em seguida para o citosol pelo Carreador ADP/ATP em troca de ADP. (Adaptado de Ledesma et al., 2002)

As UCPs, presentes na membrana interna da mitocôndria, foram descritas inicialmente em mitocôndrias de tecido adiposo marrom de camundongos e relacionadas ao processo de termogênese (produção de calor) (Vercesi et al., 2006). Foram evidenciadas pela primeira vez em plantas por Vercesi et al. (1995), que demonstraram em mitocôndrias isoladas de batata a presença de proteínas com potencial atividade desacopladora, estado alcançado apenas na ausência de nucleotídeos purínicos e na presença de ácidos graxos. Como em mamíferos, as UCPs de plantas são codificadas por pequenas famílias multigênicas (Borecký et al., 2006; Nogueira et al., 2011). A análise detalhada do genoma de *Arabidopsis thaliana*, por exemplo, permitiu a identificação de uma família gênica composta por seis genes, denominados inicialmente *AtPUMP1-6*, e posteriormente renomeados *AtUCP1-6* (Borecký et al., 2006). Em estudos posteriores, entretanto, os produtos de três destes genes (*AtUCP4-6*) foram funcionalmente associados a transportadores de dicarboxilatos (Palmieri et al., 2008), o que restringiu esta família a apenas três membros (*AtUCP1-3*). Apesar da conhecida existência destas três isoformas em *A. thaliana*, até o presente momento, grande parte dos dados funcionais relevantes foram obtidos empregando o gene *AtUCP1* como modelo.

Desde que foi identificada a primeira UCP (UCP1) com atividade desacopladora em *arabidopsis*, poucos estudos têm sido feitos para tentar compreender o papel e a relevância fisiológica das outras duas isoformas presentes nesta planta modelo (*AtUCP2* e *AtUCP3*). Neste sentido, Monné et al. (2018) demonstraram que as isoformas *AtUCP1* e *AtUCP2* compartilham 72% de identidade de aminoácidos em suas sequências proteicas e apresentam várias propriedades de transporte semelhantes, enquanto a *AtUCP3* compartilha apenas 35% e 37% com *AtUCP1* e *AtUCP2*, respectivamente. Com isso, as proteínas *AtUCP1* e *AtUCP2* são mais próximas e relacionadas entre si, enquanto a *AtUCP3* é uma proteína mais distante. Já estudos de expressão gênica (Borecký et al., 2006; Nogueira et al., 2011) indicaram que os genes *AtUCP1-3* apresentam expressão ubíqua, mas com níveis distintos de expressão ao longo do desenvolvimento, *i.e.*, o gene *AtUCP1* apresenta expressão mais alta (de 3 a 9 vezes em relação aos demais) e variável nos diferentes órgãos/tecidos da planta, enquanto os genes *AtUCP2* e *AtUCP3* possuem uma

expressão mais baixa e constitutiva. O pico de expressão do gene *AtUCP1* ocorre durante o processo de germinação das sementes (1 a 6 dias) enquanto que o gene *AtUCP2* é mais expresso durante a fase reprodutiva (Nogueira et al., 2011). A expressão do gene *AtUCP3*, por outro lado, é praticamente invariável ao longo do desenvolvimento (Nogueira et al., 2011). No trabalho de Borecký et al. (2006) ficou constatado também que os genes *AtUCP1-3* têm a expressão modulada por diferentes estresses abióticos de acordo o tempo de exposição. Sendo assim, os padrões diferenciais de expressão gênica observados sugerem que essas três isoformas podem não atuar de forma redundante.

Resultados experimentais gerados por diferentes estudos sugerem que as UCPs de plantas desempenham um papel fundamental na defesa celular contra o estresse oxidativo mitocondrial (Kowaltowski et al., 1998; Houton-Cabassa et al., 2002; Brandalise et al., 2003; Smith et al., 2004; Pastore et al., 2007). Considera-se que o desacoplamento entre a respiração e a fosforilação oxidativa mediado por essas proteínas é capaz de aumentar a velocidade respiratória, levando a uma significativa redução na geração mitocondrial de ERO. Essas observações iniciais sugeriram que o principal papel dessas proteínas seria, portanto, o de moderar a produção desses radicais durante a ocorrência de estresses (Vercesi et al., 2006).

Com base nessa premissa, estudos empregando plantas transgênicas demonstraram que a superexpressão do gene *AtUCP1* em tabaco conduz a uma maior tolerância aos estresses oxidativo, salino e osmótico, além de promover a biogênese mitocondrial e induzir a expressão de diversos genes de defesa por meio de comunicação retrógrada (Brandalise et al., 2003; Begcy et al., 2011; Barreto et al., 2014). Adicionalmente, Barreto et al. (2015) revelaram que a superexpressão do gene *AtUCP1* promove uma resposta intrínseca de hipóxia que possibilita melhor desempenho sob condição de estresse. Recentemente, Barreto et al. (2022) reforçaram essa ideia e reportaram a existência de um novo mecanismo envolvendo a sinalização retrógrada mitocondrial mediada pela *AtUCP1* que influencia a via de detecção do oxigênio. Neste cenário, as proteínas desacopladoras funcionariam como um gatilho de ativação da resposta à hipóxia, porém esta funcionalidade permanece restrita à *AtUCP1*. Em contrapartida, Sweetlove et al. (2006) demonstraram que o mutante de inserção de T-DNA *atucp1* apresenta reduzida taxa de assimilação fotossintética de carbono bem como um estresse oxidativo localizado. Esse fato,

entretanto, não afeta a capacidade do mutante em suplantar determinados tipos de estresses abióticos, tais como baixa temperatura, exposição a metal pesado e tratamento com herbicida. Neste trabalho, entretanto, a possível contribuição dos genes *AtUCP2* e *AtUCP3* no fenótipo observado não foi considerada, e nenhuma investigação sobre uma possível complementação e redundância funcional entre as diferentes isoformas foi empreendida.

O papel desempenhado pelas UCPs no equilíbrio redox foi evidenciado em outras espécies vegetais, corroborando assim os estudos prévios empregando *arabidopsis*. Em tomate, por exemplo, a superexpressão do gene *LeUCP* provocou um aumento na eficiência quântica do fotossistema II, do coeficiente de extinção fotoquímico e da taxa de transferência de elétrons, além de reduzir o acúmulo de ERO (Chen et al., 2013). As plantas com superexpressão foram mais tolerantes ao estresse térmico e à infecção pelo fungo *Botrytis cinerea*, sugerindo um papel importante das UCPs na resposta do tomateiro aos estresses abióticos e bióticos (Chen et al., 2013). Baseados em experimentos de silenciamento gênico, estes autores propuseram que o gene *LeUCP* é essencial para manter o equilíbrio redox e a atividade de enzimas antioxidantes em resposta ao estresse oxidativo, reduzindo assim a superprodução de ERO (Chen et al., 2014).

Recentemente, Monné et al. (2018) propuseram novas funções para as UCPs em plantas. Esses autores mostraram, por intermédio de sistemas de reconstituição, que as proteínas *AtUCP1* e *AtUCP2* atuam como transportadores de aminoácidos, como glutamato e aspartato, além de dicarboxilatos, como o malato, entre outros metabólitos. Adicionalmente, investigando mudanças nos perfis metabólicos dos mutantes simples de inserção de T-DNA *atucp1* e *atucp2*, os mesmos autores evidenciaram alterações importantes nos teores de alguns ácidos orgânicos, como o malato e o fumarato, tanto em condições normais de crescimento quanto sob imposição de estresse salino. Os dados obtidos apontam que essas duas isoformas representam os primeiros transportadores mitocondriais em *arabidopsis* capazes de transportar aspartato e glutamato, contribuindo possivelmente para o transporte de equivalentes redutores via troca aspartato/glutamato na fotorrespiração (Monné et al., 2018).

Por estarem envolvidas na regulação do estado redox e na tolerância ao estresse oxidativo como descrito anteriormente, as UCPs representam um ótimo

modelo para entender o papel desempenhado pelo desacoplamento mitocondrial na resposta aos estresses em plantas, bem como para demonstrar a efetiva participação destas proteínas em possíveis mecanismos de comunicação mitocôndria-núcleo. Como uma prova de conceito, nosso grupo demonstrou recentemente que a superexpressão do gene *AtUCP1* em tabaco promove importante reprogramação transcricional com alterações significativas na expressão de genes relacionados com o metabolismo energético, a fotossíntese, a fotorrespiração e a homeostase redox (Laitz et al., 2015). Da mesma maneira, Barreto et al. (2014) observaram incremento na expressão de genes de resposta a estresses, incluindo aqueles associados com o sistema antioxidante, nas referidas plantas com superexpressão do gene *AtUCP1*.

Como destacado anteriormente, grande parte dos dados funcionais obtidos até o momento utilizou a *AtUCP1* como modelo, sendo que o papel desempenhado pelas duas outras isoformas presentes em *Arabidopsis* (*AtUCP2* e *AtUCP3*) ainda é pouco estudado. Neste contexto, resultados recentes obtidos pelo nosso grupo de pesquisa utilizando os mutantes simples de inserção *atucp1* e *atucp2* revelaram que o mutante *atucp2* apresenta alterações fenotípicas significativas, como redução no número de folhas, atraso no florescimento e aumento no número de siliques estéreis, em comparação ao genótipo selvagem (Arcuri et al., 2021). Tais fenótipos, possivelmente resultantes de alterações na homeostase e função mitocondrial, carecem de maior investigação. O fato do mutante de inserção *atucp1* também apresentar alterações similares no número de siliques estéreis, além de redução significativa no comprimento das siliques, reforça ainda mais a hipótese de que as UCPs desempenham papel importante durante a fase reprodutiva, fornecendo indícios de distúrbios na fertilidade. Neste contexto, dados adicionais indicam que perturbações na função mitocondrial, e por consequência na atividade respiratória, podem conduzir à infertilidade (Busi et al., 2011). O fato de plantas jovens destes mutantes, em especial do *atucp2*, apresentarem alterações significativas na razão ATP/ADP, consumo de oxigênio e eficiência fotossintética também sugerem um importante papel destes genes durante o desenvolvimento vegetativo (Arcuri et al., 2021).

Partindo-se desta premissa e visando exacerbar os fenótipos descritos e observados empregando os mutantes simples, o presente estudo propôs a obtenção e caracterização de duplo-mutantes de inserção para os referidos genes (*atucp1 atucp2*, *atucp1 atucp3* e *atucp2 atucp3*). Em posse de tais duplo-mutantes, ensaios

visando investigar a relevância destas isoformas e a redundância funcional entre elas foram empreendidos. Neste contexto, diferentes abordagens com o objetivo de detectar possíveis alterações genéticas, fisiológicas, metabólicas e de estado redox, dentre outras, decorrentes da expressão alterada dos genes *AtUCPs* foram empregadas para melhor compreender as respectivas funções in *planta* das referidas proteínas. Pretendeu-se, desta maneira, contribuir para melhor compreensão do papel desempenhado pelos genes *UCPs* nas fases vegetativa e reprodutiva.

Objetivos

Objetivo geral

O presente estudo teve por principal objetivo empreender a caracterização funcional de duplo-mutantes de inserção em diferentes combinações gênicas visando um melhor entendimento do papel funcional das isoformas AtUCP1-3 em arabidopsis.

Objetivos específicos

Na tentativa de elucidar o papel das UCPs no desenvolvimento vegetativo e reprodutivo, os seguintes objetivos específicos foram propostos:

1. Empreender a obtenção dos duplo-mutantes *atucp1 atucp2*; *atucp1 atucp3* e *atucp2 atucp3* e avaliar o fenótipo dos mesmos em condições normais e sob estresse;
2. Avaliar as alterações fisiológicas, de estado redox e metabólicas dos referidos duplo-mutantes de inserção;
3. Avaliar o grau de redundância funcional nos duplo-mutantes a partir de alterações no nível de expressão dos genes *AtUCP1-3* em condições normais e sob estresse;
4. Avaliar as alterações transcricionais em duplo-mutantes, selecionados com base nas análises fenotípicas a partir de estágios específicos do desenvolvimento vegetativo em *A. thaliana*, usando a técnica de RNA-Seq e análises de bioinformática;
5. Avaliar o perfil de metabólitos dos duplo-mutantes durante a fase vegetativa.

Referências bibliográficas

- ALMEIDA, A.M.; JARMUSZKIEWICZ, W.; KHOMSI, H.; ARRUDA, P.; VERCESI, A.E.; SLUSE, F.E. **Cyanide-resistant, ATP-synthesis-sustained, and uncoupling-protein-sustained respiration during postharvest ripening of tomato fruit.** *Plant Physiol.*, v.119, p.1323-1329, 1999.
- ARCURI, M.L.C.; NUNES-LAITZ, A.V.; LIMA, R.P.M.; BARRETO, P.; MARINHO, A.N.; ARRUDA, P.; MAIA, I.G. The Knockdown of Mitochondrial Uncoupling Proteins 1 and 2 (AtUCP1 and 2) in *Arabidopsis thaliana* Impacts Vegetative Development and Fertility. *Plant Cell and Physiol.*, v.00, p.1-15, 2021.
- BARRETO, P.; DAMBIRE, C.; SHARMA, G.; VICENTE, J.; OSBORNE, R.; YASSITEPE, J.; GIBBS, D.J.; MAIA, I.G.; HOLDSWORTH, M.J.; ARRUDA, P. Mitochondrial retrograde signaling through UCP1-mediated inhibition of the plant oxygen-sensing pathway. *Curr. Biol.*, v.32, p.1-9, 2022.
- BARRETO, P.; OKURA, V.; PENA, I.A.; MAIA, R.; MAIA, I.G.; ARRUDA, P. **Overexpression of mitochondrial uncoupling protein 1 (UCP1) induces a hypoxic response in *Nicotiana tabacum* leaves.** *J. Exp. Bot.*, v.67, p.301-313, 2015.
- BARRETO, P.; OKURA, V.K.; NESHICH, L.A.; MAIA, I.G.; ARRUDA, P. **Overexpression of UCP1 in tobacco induces mitochondrial biogenesis and amplifies a broad stress response.** *BMC Plant Biol.*, v.14, p.144-159, 2014.
- BEGCY, K.; MARIANO, E.D.; MATTIELLO, L.; NUNES, A.V.; MAZZAFERA, P.; MAIA, I.G.; MENOSSI M. **An *Arabidopsis* mitochondrial uncoupling protein confers tolerance to drought and salt stress in transgenic tobacco plants.** *PLOS ONE*, v.6, p.1-10, 2011.
- BORECKÝ, J.; NOGUEIRA, F.T.S.; DE OLIVEIRA, K.A.P.; MAIA, I.G.; VERCESI, A.E.; ARRUDA, P. **The plant energy-dissipating mitochondrial systems: depicting the genomic structure and expression profiles of the gene families of uncoupling protein and alternative oxidase in monocots and dicots.** *J. Exp. Bot.*, v.57, p.849-864, 2006.
- BRANDALISE, M.; MAIA, I.G.; BORECKY, J.; VERCESI, A.E.; ARRUDA, P. **Overexpression of plant uncoupling mitochondrial protein in transgenic tobacco increases tolerance to oxidative stress.** *J. Bioenerg. Biomembr.*, v.35, p.203-209, 2003.
- BUSI, M.V.; GOMEZ-LOBATO, M.E.; RIUS, S.P.; TUROWSKI, V.R.; CASATI, P.; ZABALETA, E.J.; GOMEZ-CASATI, D.F.; ARAYA, A. **Effect of mitochondrial dysfunction on carbon metabolism and gene expression in flower tissues of *Arabidopsis thaliana*.** *Mol. Plant.*, v.4, p.127-43, 2011.
- CHEN, S.; LIU, A.; JI, D.; LIN, X.; LIU, Z.; XIA, X.; LIU, D.; AHAMMED, G.J. **Silencing of tomato mitochondrial uncoupling protein disrupts redox poise and antioxidant enzymes activities balance under oxidative stress.** *J. Plant Biol.*, v.57, p.9-19, 2014.

CHEN, S.; LIU, A.; ZHANG, S.; LI, C.; CHANG, R.; LIU, D.; AHAMMED, G.J.; LIN, X. **Overexpression of mitochondrial uncoupling protein conferred resistance to heat stress and *Botrytis cinerea* infection in tomato.** *Plant Physiol. Biochem.*, v.73, p.245-253, 2013.

HARTL, M.; FINKEMEIER, I. **Plant mitochondrial retrograde signaling: posttranslational modifications enter the stage.** *Front. Plant Sci.*, v.3, p.253, 2012.

HOUTON-CABASSA, C.; MESNEAU, A.; MIROUX, B.; ROUSSAUX, J.; RICQUIER, D.; ZACHOWSKI, A.; MOREAU, F. **Alteration of plant mitochondrial proton conductance by free fatty acids. Uncoupling protein involvement.** *J. Biol. Chem.*, v.277, p.41533-41538, 2002.

JACOBY, R.P.; LI, L.; HUANG, S.; PONG LEE, C.; MILLAR, A.H.; TAYLOR, N.L. **Mitochondrial composition, function and stress response in plants.** *J. Integr. Plant Biol.*, v.54, p.887-906, 2012.

KOWALTOWSKI, A.J.; COSTA, A.D.; VERCESI, A.E. **Activation of the potato plant uncoupling mitochondrial protein inhibits reactive oxygen species generation by the respiratory chain.** *FEBS Letters*, v.425, p.213-216, 1998.

LAITZ, A.V.N.; ACENCIO, M.L.; LEMKE, N.; RIBOLLA, P.E.M.; MAIA, I.G. **Transcriptome response signatures associated with the overexpression of a mitochondrial uncoupling protein (AtUCP1) in tobacco.** *PLOS ONE*, v.10, p.1-13, 2015.

MAXWELL, D.P.; WANG, Y.; MCINTOSH, L. **The alternative oxidase lowers mitochondrial reactive oxygen species production in plant cells.** *Proc. Natl. Acad. Sci. USA*, v.96, p.8271-8276, 1999.

MILLAR, A.H.; WHELAN, J.; SOOLE, K.L.; DAY, D.A. **Organization and regulation of mitochondrial respiration in plants.** *Ann. Rev. Plant Biol.*, v.62, p.79-104, 2011.

MOLLER, I.M. **Plant mitochondria and oxidative stress: Electron transport, NADPH Turnover, and metabolism of reactive oxygen species.** *Ann. Rev. Plant Physiol.*, v.52, p.561-91, 2001.

MONNÉ, M.; DADDABBO, L.; GAGNEUL, D.; OBATA, T.; HIELSCHER, B.; PALMIERI, L.; MINIERO, D.V.; FERNIE, A.R.; WEBER, A.P.M.; PALMIERI, F. **Uncoupling proteins 1 and 2 (UCP1 and UCP2) from *Arabidopsis thaliana* are mitochondrial transporters of aspartate, glutamate, and dicarboxylates.** *J. Biol. Chem.*, v.293, n.11, p.4213-4227, 2018.

NICHOLLS, D.G. **A history of UCP1.** *Biochem. Soc. Trans.*, v.29, p.751-755, 2001.

NOGUEIRA F.T.; SASSAKI F.T.; MAIA I.G. ***Arabidopsis thaliana* Uncoupling Proteins (AtUCPs): insights into gene expression during development and stress response and epigenetic regulation.** *J. Bioenerg. Biomembr.*, v.43, p.71-79, 2011.

PALMIERI, L.; PICAULT, N.; ARRIGONI, R.; BESIN, E.; PALMIERI, F.; HODGES, M. **Molecular identification of three *Arabidopsis thaliana* mitochondrial**

dicarboxylate carrier isoforms: organ distribution, bacterial expression, reconstitution into liposomes and functional characterization. *Biochem. J.*, v.410, p. 621-629, 2008.

PASTORE, D.; TRONO, D.; LAUS, M.N.; DI FONZO, N.; FLAGELLA, Z. **Possible plant mitochondria involvement in cell adaptation to drought stress. A case study: durum wheat mitochondria.** *J. Exp. Botany*, v.58, p.195-210, 2007.

SMITH, A.M.; RATCLIFFE, R.G.; SWEETLOVE, L.J. **Activation and function of mitochondrial uncoupling protein in plants.** *J. Biol. Chem.*, v.279, p.51944-51952, 2004.

SWEETLOVE, L.J.; LYTOVCHENKO, A.; MORGAN, M.; NUNES-NESE, A.; TAYLOR, N.L.; BAXTER, C.J.; EICKMEIER, I.; FERNIE, A.R. **Mitochondrial uncoupling protein is required for efficient photosynthesis.** *Proc. Natl. Acad. Sci. USA*, v.103, p.19587-19592, 2006.

VANLERBERGHE, G.C. **Alternative Oxidase: A Mitochondrial Respiratory Pathway to Maintain Metabolic and Signaling Homeostasis during Abiotic and Biotic Stress in Plants.** *Int. J. Mol. Sci.*, v.14, p.6805-6847, 2013.

VERCESI, A.E.; BORECKÝ, J.; MAIA, I.G.; ARRUDA, P.; CUCCOVIA, I.M.; CHAIMOVICH, H. **Plant uncoupling mitochondrial proteins.** *Ann. Rev. Plant Biol.*, v.57, p.383-404, 2006.

VERCESI, A.E.; MARTINS, I.S.; SILVA, M.P.A.; LEITE, H.M.F.; CUCCOVIA, I.M.; CHAIMOVICH, H. **PUMPing plants.** *Nature*, v.375, p.24-25, 1995.

WELCHEN, E.; GARCIA, L.; MANSILLA, N.; GONZALEZ, D. H. **Coordination of plant mitochondrial biogenesis: keeping pace with cellular requirements.** *Frontiers in Plant Science*, v.4, n.551, p.1-12, 2014.

YUN, J.; FINKEL, T. **Mitohormesis.** *Cell metabolism*, v.19, n.6, p.757-766, 2014.

Capítulo I

O capítulo I corresponde ao manuscrito intitulado “**The Double Knockdown of the Mitochondrial Uncoupling Protein Isoforms Reveals Partial Redundant Roles During *Arabidopsis thaliana* Vegetative and Reproductive Development**” que foi submetido ao periódico *Plant Science*. Este estudo descreve a caracterização molecular e as análises funcionais dos duplo-mutantes de inserção *atucp1 atucp2*, *atucp1 atucp3* e *atucp2 atucp3*. Análises fenotípicas, bioquímicas, fisiológicas e metabólicas foram realizadas com o intuito de melhor compreender o papel das três isoformas *in planta*.

The Double Knockdown of the Mitochondrial Uncoupling Protein Isoforms Reveals Partial Redundant Roles During *Arabidopsis thaliana* Vegetative and Reproductive Development

Rômulo Pedro Macêdo Lima¹, Alessandra Vasconcellos Nunes-Laitz², Mariana de Lara Campos Arcuri¹, Felipe Girotto Campos³, Thaís Arruda Costa Joca³, Gean Charles Monteiro¹, Hélio Kushima⁴, Giuseppina Pace Pereira Lima¹, Luiz Fernando Rolim de Almeida³, Pedro Barreto¹, Ivan de Godoy Maia^{1,*}

¹Departamento de Ciências Químicas e Biológicas, Instituto de Biociências, UNESP, 18618-689, Botucatu, SP, Brasil

²Instituto Federal de Educação, Ciência e Tecnologia de Rondônia, IFRO, 76821-001, Colorado do Oeste, RO, Brasil

³Departamento de Bioestatística, Biologia Vegetal, Parasitologia e Zoologia, Instituto de Biociências, UNESP, 18618-689, Botucatu, SP, Brasil

⁴Departamento de Biofísica e Farmacologia, Instituto de Biociências, UNESP, 18618-689, Botucatu, SP, Brasil

Running title: Functional evaluation of *UCPs* using double mutants

*Author for correspondence. E-mail: ivan.maia@unesp.br

ABSTRACT

Mitochondrial uncoupling proteins (UCPs) are specialized proteins capable of dissipating the proton electrochemical gradient generated in respiration independent of ATP synthesis. Three *UCP* coding genes with distinct expression patterns have been identified in *Arabidopsis thaliana* (namely *UCP1*, *UCP2* and *UCP3*). Here, we generated T-DNA double-insertion mutants (*ucp1 ucp2*, *ucp1 ucp3* and *ucp2 ucp3*) to investigate the functionality of the *Arabidopsis UCP* isoforms. A strong compensatory effect of the wild-type *UCP* gene was found in the double knockdown lines. Higher levels of reactive oxygen species (ROS) were observed in vegetative and reproductive organs of double mutant plants. This exacerbated oxidative stress in plants also increased lipid peroxidation but was not compensated by the activation of the antioxidant system. Alterations in O₂ consumption and ADP/ATP ratio were also

observed, suggesting a change in mitochondrial energy-generating processes. Deficiencies in double mutants were not limited to mitochondria and also changed photosynthetic efficiency and redox state. Our results indicate that *UCP2* and *UCP3* have complementary function with *UCP1* in plant reproductive and vegetative organ/tissues, as well as in stress adaptation. The partial redundancy between the *UCP* isoforms suggests that they could act separately or jointly on mitochondrial homeostasis during *A. thaliana* development.

KEYWORDS: uncoupling protein, mitochondria, double mutant, *Arabidopsis thaliana*

Introduction

By participating in a number of cellular processes related to energy metabolism in plants, such as respiration and photorespiration, mitochondria and their structural components act actively in response to different types of internal and external stress elicitors [1]. The inner membrane of plant mitochondria contains an internal group of energy-dissipating proteins, the so-called mitochondrial uncoupling proteins (UCPs), which have been reported to play a protective role against oxidative stress [2-4]. Classically, UCPs catalyze the uncoupling between mitochondrial oxidative phosphorylation and ATP synthesis. In other words, they facilitate the reentry of protons from the inner membrane space back to the mitochondrial matrix without the simultaneous production of ATP by the ATP synthase complex. Consequently, the membrane potential is slightly reduced, and the energy derived from the oxidation of substrates is lost independently of ATP synthesis. Such uncoupling activity is dependent on fatty acids and sensitive to purine nucleotides [5,6].

New functions have been recently attributed to plant UCPs. Through reconstitution assays, UCPs have been shown to transport glutamate and aspartate possibly as part of the mitochondrial malate-aspartate shuttle [7]. In this regard, due to their ability to exchange amino acids for several dicarboxylates [7], a role for plant UCPs in nitrogen metabolism has been postulated [8,9]. Although it remains unclear whether plant UCPs act predominantly as an uncoupler or as a solute transporter, these proteins have well-established roles in the maintenance of mitochondrial homeostasis [10] and in cellular defense against reactive oxygen species (ROS) generation [11-15].

The role played by plant UCPs is not exclusively restricted to ROS alleviation inside the mitochondria, since their action on redox metabolism has been also evidenced in the cytoplasm and chloroplast [8,16-18]. In tomatoes, for example, overexpression of *LeUCP*, apart reducing ROS accumulation, also triggered an increase in the quantum yield of photosystem II (PSII), in the photochemical dissipation and in the electron transport rate [19]. In another study based on gene silencing assays, it has been proposed that *LeUCP* is essential to maintain photosynthetic capacity, redox balance and activity of antioxidant enzymes in response to oxidative stress, consequently reducing ROS overproduction [20].

Among the *UCP* genes present in *Arabidopsis thaliana*, namely *UCP1*, *UCP2* and *UCP3*, the founder member of the family (*UCP1*) has been the most extensively studied. At first, the main interests were on *UCP1* biochemical activity and physiological roles, particularly during plant exposure to stresses [6]. In this context, some conflicting results have been reported. Brandalise et al. [13], for example, showed that *UCP1* overexpression in tobacco decreased ROS generation in leaf tissues subjected to hydrogen peroxide (H₂O₂)-induced oxidative stress. Similar results have been obtained thereafter using the same overexpression lines, indicating improved tolerance to ROS-generating stresses [17,21]. In contrast, *UCP1* knockdown in *A. thaliana* resulted in localized oxidative stress without rendering the plant more susceptible to different types of abiotic stresses [16]. In this study, however, the possible contribution of the *UCP2* and *UCP3* genes in the observed phenotype was not addressed, and no investigation on possible complementation and functional redundancy between the different isoforms was undertaken.

Until now, the exact role and physiological relevance of the *UCP2* and *UCP3* isoforms are far from understood. Worth noting is that *UCP1* and *UCP2* are closely related (72% amino acid identity) and share a number of similar transport properties [7], whereas *UCP3* is a more distantly related protein. In relation to their subcellular location, the mitochondrial localization of both *UCP1* and *UCP2* has been experimentally demonstrated [7]. Interestingly, previous gene expression studies have indicated that *UCP2* and *UCP3* display distinctive expression patterns compared to *UCP1*, which is expressed in all organs/tissues but in variable levels depending on the developmental stage [22,23]. In contrast, although being also ubiquitous, *UCP2* and *UCP3* show a lower and constitutive expression [22,23]. Moreover, all *Arabidopsis*

UCP coding genes are differentially modulated by abiotic stresses depending on the time-length of exposure. Taken together, these evidences suggest that these isoforms, as observed in mammals, may potentially play distinct non-redundant roles.

The use of T-DNA insertion mutants represents a good strategy to infer possible *in vivo* functions of gene family members and to investigate the existence (or not) of functional redundancy between them. In this context, higher order mutants can be obtained from combinations between single mutants, giving rise to double mutants, which may show more exacerbated phenotypes than their parental single mutants [24,25]. Here, to obtain novel insights into the physiological relevance of the *UCP* family members in *A. thaliana* and further extend the observations obtained previously using *ucp1* and *ucp2* single-insertion mutants [26], we generated double mutants for different gene sets (*ucp1 ucp2*, *ucp1 ucp3* and *ucp2 ucp3*). The double mutant lines were phenotypically and physiologically evaluated during vegetative and reproductive development. Clear alterations in energy metabolism, photosynthetic performance and redox homeostasis were observed. Overall, the data present herewith gives a better insight of the roles played by *UCP* genes at the entire plant level.

Material and Methods

Plant material, molecular characterization and relative expression using RT-qPCR

All mutants used in this study are in the *A. thaliana* Columbia ecotype background (Col-0). The *UCP1* (At3g54110) and *UCP2* (At5g58970) T-DNA insertion lines (SAIL_536_G01; ABRC stock #CS874648 and SALK_037074, respectively) have been functionally characterized previously [16,26]. The mutant line (SALK_123501C) containing a T-DNA insertion in the promoter region (position 182) of *UCP3* (At1g14140) was obtained from the Arabidopsis Biological Resource. Wild-type (WT) Col-0 was used as control in all the assays. Seeds were kept at 4°C for at least 72 h in darkness for dormancy breaking and then germinated in plastic pots containing Carolina Soil® substrate or in Petri plates containing one-half-strength Murashige and Skoog medium (½ MS) [27]. Plants were maintained in a growth chamber (Fitotron, Conviron® Model CPM6050) with 16 h day/8 h night photoperiod cycle, photosynthetic

photon flux density (PPFD) of 150 $\mu\text{mol photons m}^{-2} \text{s}^{-1}$, temperature of 19°C and relative humidity around 65%, receiving daily irrigations.

Double mutants were obtained by crossing the homozygous *ucp1*, *ucp2* and *ucp3* single-insertion mutants [26] in different combinations (*ucp1 ucp2*, *ucp1 ucp3* and *ucp2 ucp3*). To identify homozygous double mutant lines, genomic DNA was extracted from leaf tissues using the CTAB (Cetyl Trimethyl Ammonium Bromide) method as described by Doyle et al. [28]. Homozygosity was confirmed by PCR amplification using GoTaq Master Mix (Promega), 100 ng/ μL of genomic DNA and 0.1 μL of gene-specific (*UCP1* to *UCP3*) primers (at 10 μM) together with the primers of the inserted T-DNA (Supplemental Table S1A). PCR reaction consisted of an initial denaturation cycle at 95°C for 5 min, followed by 35 amplification cycles of 94°C for 30 s, 51°C for 1 min and 72°C for 1 min and a final extension step at 72°C for 7 min. Genomic DNA extracted from WT and the *ucp1* to *ucp3* single mutants were used as control. Amplification products were sequenced for verification. At least three homozygous lines for each double mutant were obtained.

The relative expression of *UCP1*, *UCP2*, *UCP3* and *AOX1a* in 21-day-old plants ($n=3$ per genotype) grown in $\frac{1}{2}$ MS medium was determined by quantitative reverse transcription PCR (RT-qPCR) using SYBR Green master mix (Applied Biosystems) as described [18]. The glyceraldehyde-3-phosphate dehydrogenase (*GAPDH*; At1G13440) gene was used as endogenous controls [29]. Reactions were performed in triplicates and a pool of WT plants was used as calibrator for relative quantification using the $2^{-\Delta\Delta\text{CT}}$ method [30]. Treatments for determining the expression of the three *UCP* genes under stress were performed essentially as described [31]. For that, double mutant plants (21-day-old) were incubated in $\frac{1}{2}$ MS liquid medium and kept under constant agitation (67 rpm) with continuous light for 7 days. Subsequently, the medium was replaced by new $\frac{1}{2}$ MS liquid medium supplemented with 125 mM NaCl or 250 mM mannitol. The treated plants were sampled at different time points (6, 12, 24 and 48 h) for subsequent RNA extraction and RT-qPCR analysis. As control, untreated plants grown in $\frac{1}{2}$ MS liquid medium and sampled at the same time points were used. Two biological replicates per time point were employed. The primers used in expression analysis are described in Supplemental Table S1B.

Plant phenotyping and water content

The following growth and development parameters were evaluated: germination rate (G_R), primary root length (PRL), rosette area and leaf number on the rosette. Germination rate (G_R) and PRL were evaluated under control and stressed conditions (salt and osmotic stresses). For this purpose, seeds and 7-day-old seedlings of the different genotypes were placed in Petri plates containing $\frac{1}{2}$ MS medium supplemented with 125 mM NaCl or 250 mM mannitol, respectively. These concentrations were defined in preliminary assays and are considered moderate [21,26]. G_R analyzes were performed as described by Begcy et al. [21]. The number of germinated seeds, defined by hypocotyl emergence, was counted daily after dormancy breaking, and expressed in percentage of total number of plated seeds. For each treatment, three Petri plates containing 30 seeds of each genotype were used. Means and standard error were obtained, with average values being added one day after the other. For PRL analyzes, 7-day-old seedlings ($n=5$ per genotype) were grown vertically on Petri plates (3 per treatment) for 10 days. Then, the root system was digitized and the PRL parameter was measured using RootNav v1.8.1 software (<<http://sourceforge.net/projects/rootnav/files/>>).

To evaluate the parameters of leaf development in adult plants, the rosette area of 30-day-old plants was measured ($n=10$ per genotype) by scanning the images captured using ImageJ software. Concomitantly, the leaf number on rosettes was scored. To evaluate fresh weight (FW), dry weight (DW) and relative water content (RWC), 28-day-old plants ($n=10$ per genotype) were separated into roots and aerial part. FW was estimated by weighing on a precision balance. Then, the material was placed in paper bags and dried in air circulating oven at 70°C for 72 h. Elapsed this time, the material was reweighed to estimate the DW. RWC values were estimated by the relationship: $RWC (\%) = \{[(FW-DW)/FW] \times 100\}$.

To assess parameters related to flowering time, floral transition (days) and first flower opening (days) were evaluated. For that, substrate-grown plants ($n=10$ per genotype) were monitored daily in the growth chamber until 55 days after sowing (DAS). Subsequently, when the plants reached 60 DAS, siliques were collected (10 per plant; total of 100 siliques per genotype) and their length (cm) measured. Seed weight was scored after silique maturation (around 80 DAS) on a precision balance using seed pools ($n=10$ per genotype).

ROS detection and quantification

Superoxide (O_2^-) accumulation in mitochondria was estimated using MitoSOX Red probe according to manufacturer's protocol (Invitrogen). For this purpose, young leaves collected from 21-day-old plants grown in $\frac{1}{2}$ MS medium under normal conditions were used ($n=3$ per genotype). The collected leaves were immersed in $\frac{1}{2}$ MS liquid medium supplemented or not with 125 mM NaCl or 10 mM H_2O_2 (salt and oxidative stresses, respectively), and incubated under constant light and agitation on a shaker table for 20 h. After this time, the leaves were incubated at room temperature for 25 min in the dark in a solution containing 5 μ M MitoSOX Red diluted in water and then washed with $\frac{1}{2}$ MS liquid medium for at least three times. Light intensity and fluorescence emission were detected at 488/585-615 nm (Em/Ex) using a Leica TCS SP5 laser scanning confocal microscope with a 10x objective.

The presence of H_2O_2 in leaves and open flowers at stage 12 [32] was evaluated using 3,3-diaminobenzidine (DAB) staining according to Daudi and O'Brien [33]. For that, leaves and open flowers were collected from $\frac{1}{2}$ MS-grown plants (21-day-old) and substrate-grown plants (45-day-old), respectively ($n=3$ plants per genotype). The collected samples were subjected to infiltration by Speed-vac in a 1 mg/mL DAB solution (pH 3.0) in 10 mM sodium phosphate dibasic (Na_2HPO_4) buffer for 7 min. As a staining control, 10 mM Na_2HPO_4 buffer was used. After being infiltrated, the samples were placed on a shaker table at 100 rpm and incubated for 4 h in the dark at room temperature. Then, the DAB solution was replaced by the bleaching solution (ethanol: acetic acid: glycerol = 3:1:1), and the samples were immediately incubated in a water bath at 90°C for 15 min. Finally, the bleaching solution was removed, and the samples were kept in stand by for 30 min in new bleaching solution until the images were captured. The images were viewed using an Olympus SZX16 stereo microscope with a numerical aperture (NA) of 1.6.

Quantification of H_2O_2 content was performed according to Alexieva et al. [34] using 21-day-old plants and open flowers as described in the DAB assays. Pools of plants and floral tissues ($n=3$ pools per genotype; each pool containing three plants and 20 open flowers) were macerated in liquid nitrogen, and 30 mg of the fine powder was homogenized with gently agitation in 0.1% trichloroacetic acid (TCA) solution. The homogenized samples were centrifuged at 10000 rpm for 15 min at 4°C, with 500 μ L of the supernatant being transferred to test tubes. The tubes with extracts received 2.5

mL of a cocktail containing 0.5 mL of 0.1 M phosphate-buffered saline (PBS) buffer (pH 7.0) and 2 mL of 1 M potassium iodide (KI). The reactions were incubated in the dark at room temperature for 1 h, and thereafter, the absorbance at 390 nm was determined using a spectrophotometer. The samples were read in duplicate, and a calibration curve was obtained from H₂O₂ standard solutions prepared with 0.1% TCA.

Determination of lipid peroxidation and activity of antioxidant enzymes

Lipoperoxide content was quantified as described by Heath and Packer [35] and adapted by Rama Devi and Prasad [36]. Approximately 30 mg of plant material from 21-day-old plants (n=3 per genotype) grown in ½ MS medium was macerated in liquid nitrogen. The fine powder was homogenized with gently agitation in 5 mL of a solution containing 0.25% thiobarbituric acid (TBA) and 10% TCA and incubated in a water bath at 90°C for 1 h. After that, the homogenates were centrifuged at 10000 rpm for 15 min at 4°C, and the supernatants collected. Absorbance readings were taken at 560 nm and 600 nm using a spectrophotometer. A malondialdehyde (MDA) compound extinction coefficient equal to 155 mM cm⁻¹ was adopted and the difference between the two absorbencies was estimated.

To evaluate the activity of superoxide dismutase (SOD) and catalase (CAT), protein extracts (n=3 extracts per genotype) were obtained from 21-day-old plants (30 mg) grown in ½ MS medium. The plants were macerated in liquid nitrogen, and 0.5 mL of extractor buffer containing 100 mM potassium phosphate buffer (pH 7.5), 1.27 mM Ethylenediaminetetraacetic acid (EDTA), 3 mM DL-Dithiothreitol (DTT) and 2.7 mM Polyvinylpolypyrrolidone (PVPP) was added to the fine powder for protein extraction. The extracts were centrifuged at 10000 rpm for 15 min at 4°C, and the supernatant was used to determine specific enzymatic activities. The determination of total SOD (EC 1.15.1.1) activity was based on the inhibition of photoreduction of nitro blue tetrazolium (NBT) as described by Sun et al. [37]. One unit of SOD activity (UA) was considered as the amount of enzyme needed to inhibit 50% in photoreduction of NBT compared with the blank reaction (without the protein extract), being its specific activity expressed as UA min⁻¹ gFW⁻¹ µgPTN⁻¹. The total CAT (EC 1.11.1.6) activity was determined by the decrease in consumption of H₂O₂ according to Kar and Mishra [38]. The CAT specific activity was calculated by the ratio between its total activity (expressed in nmol H₂O₂ min⁻¹ gFW⁻¹) and the amount of total soluble protein

(expressed in gPROT gFW⁻¹), being expressed as nmol H₂O₂ min⁻¹ gFW⁻¹ gPTN⁻¹. The concentration of total soluble proteins was estimated following the Bradford's method [39].

ADP/ATP ratio and respiratory rate

The levels of ADP and ATP were determined using ATP Assay kit (Invitrogen) following the manufacturer's recommendations. For that, 21-day-old plants (n=3 per genotype) grown in ½ MS medium were used. Plants were collected at the end of the night period and macerated in liquid nitrogen. Thirty mg of fine powder was homogenized in 1 mL of methanol/chloroform/water (4:2:1) and maintained on ice for 30 min with gentle agitation. Then, 1 mL of water was added, and the samples were centrifuged at 10000 rpm for 5 min for phase separation. The supernatant was dried in a Speed-vac for 2 h, and the resulting pellet was resuspended in 10 mM PBS buffer (pH 7.4). ADP (later converted to ATP) and ATP contents were measured according to Napolitano and Shain [40] using a BioTek Synergy™ HTX Multi-Mode Microplate Reader, with the reactions being performed in triplicates. Standard curves were generated using a purified ATP solution to enable the conversion of luminescence signals into ATP concentrations. After quantification of the ADP and ATP levels, the ADP/ATP ratio was determined.

Oxygen (O₂) consumption was measured using an Oxygraph-2k (Oroboros, Innsbruck, Austria). For that, leaves at the same position in the rosette were harvested from 21-day-old plants (n=3 per genotype) maintained in the dark for at least 1 h at room temperature. Approximately 10 mg of the fresh detached leaves were sectioned, and the longitudinal and transverse sections were transferred to 2.1 ml of air saturated MS medium. The O₂ consumption per mass was monitored in the dark at 25°C with continuous stirring (80 rpm). Data were sampled in consecutive 120 stable points (1/second) despising the first two minutes.

Quantification of mitochondrial DNA (mtDNA)

Mitochondrial DNA (mtDNA) was quantified by qPCR using SYBR Green master mix (Applied Biosystems) essentially as described by Barreto et al. [17]. For that, genomic DNA from 21-day-old plants (n=3 per genotype) grown in ½ MS medium was

$\text{m}^2 \text{s}^{-1}$], intercellular CO_2 concentration (C_i) [ppm] and leaf transpiration rate (E) [$\text{mmol H}_2\text{O m}^{-2} \text{s}^{-1}$], adopting a maximum PPFD of $1000 \mu\text{mol photons m}^{-2} \text{s}^{-1}$ in the equipment (light saturation condition). The instantaneous water-use efficiency was determined by A_{net}/E ratio [$(\mu\text{molCO}_2 \text{m}^{-2} \text{s}^{-1}) (\text{mmolH}_2\text{O m}^{-2} \text{s}^{-1})^{-1}$] as described by Berry and Downton [45]. Already the instantaneous carboxylation efficiency, given by A_{net}/C_i ratio [$(\mu\text{mol CO}_2 \text{m}^{-2} \text{s}^{-1}) (\text{ppm})^{-1}$], was determined as described by Von Caemmerer and Farquhar [46].

Fluorescence measurements under light conditions and derived ratios and extinction coefficients were estimated and analyzed according to Baker [47]. For this, the chamber with the IRGA fluorometer was adjusted to have an actinic light pulse of $4500 \mu\text{mol photons m}^{-2} \text{s}^{-1}$. Once stabilized, the first measurement of chlorophyll fluorescence was captured, corresponding to the steady-state fluorescence (F') [mV]. Then, the saturated pulse was applied to obtain maximum fluorescence (F_m') [mV]. With the shutdown of the light, the basal or minimum fluorescence (F_o') [mV] was scored. The derived photochemical parameters from the three fluorescence measurements were calculated: Electron Transport Rate (ETR), given by the formula: $ETR = \{[(F_m' - F') / F_m'] \times \text{PPFD} \times 0.5 \times 0.85\}$, which represents the photon flow directed to PSII [47,48]; photochemical dissipation coefficient or quenching photochemical (qP), given by the formula: $qP = [(F_m' - F') / (F_m' - F_o')]$, indicating the opening degree of the reaction centers of PSII and representing the simultaneous occurrence of photosynthesis and photorespiration processes [47,48]; and quantum yield of PSII (Φ_{PSII}), given by the formula: $\Phi_{\text{PSII}} = [(F_m' - F') / F_m']$, which indicates the fraction of photons absorbed and used in the photochemical pathway [47,48].

Statistical analyzes

Unless otherwise stated, the statistical analyzes were performed using PRISM 5.0 (GraphPad Software Inc., US) by obtaining the average values and standard error, and significance was assessed by comparing the means of each double mutant and WT Col-0 by paired t-test. For statistical analyzes of relative expression and mtDNA quantification, $2^{-\Delta\Delta\text{CT}}$ data were \log_2 -transformed. For gene expression analysis under stressed conditions, paired t-test was performed using the means of each treated double mutant relative to untreated it at a corresponding time point. For FW, DW and RWC, the data obtained were submitted to ANOVA followed, when significant by the

F-test, by a Scott-Knott test at 5% probability for comparison of the means. Percentage data of RWC value were transformed in arc sen ($\sqrt{x/100}$) before being subjected to F-test.

Results

Molecular characterization of the double mutant lines

As depicted by PCR genotyping, homozygous double mutant lines were obtained for three different *UCP* gene combinations (*ucp1 ucp2*, *ucp1 ucp3* and *ucp2 ucp3*) (Supplemental Fig. 1). The corresponding single mutant lines harbored T-DNA insertions in the 5'-UTR region of *UCP1* [16], in the first intron of *UCP2* [26] and in the promoter region of *UCP3* (Fig. 1A). As expected, transcript accumulation of the targeted *UCP* genes in the corresponding double mutant lines was clearly reduced (below 0.38-fold) compared with WT (Fig. 1B). To reveal possible compensatory expression, the transcript accumulation of the wild-type *UCP* genes in each double mutant was evaluated. We found significant increases in the relative expression of WT *UCP3* (4.27-fold), *UCP2* (3.58-fold) and *UCP1* (7.27-fold) in the *ucp1 ucp2*, *ucp1 ucp3* and *ucp2 ucp3* double mutants, respectively, grown under normal conditions (Fig. 1B). Interestingly, the strongest compensatory effect was found for *UCP1* in *ucp2 ucp3*. When subjected to salt and osmotic stresses, a compensatory increase in the expression of the respective WT *UCP* genes was also detected in the double mutant lines (Fig. 1C, 1D and 1E). In the case of the *ucp2 ucp3* mutant, the transcript abundance of *UCP1* was significantly increased in the early stages (6 and 12 h) of salt or osmotic stress imposition and clearly reduced at the end of the assay (Fig. 1C). In contrast, the transcript levels of *UCP2* were increased in the *ucp1 ucp3* mutant throughout the assay (Fig. 1D), suggesting a more prominent role under stress. In addition, when the *ucp1 ucp2* mutant was subjected to the mentioned stresses, a significant increase in *UCP3* transcript accumulation was observed at 24 h followed by a decrease at 48 h (Fig. 1E). Overall, these results indicate that the double *UCP* knockdown is buffered by the transcriptional upregulation of the WT copy under control conditions and in a time-dependent manner under stress.

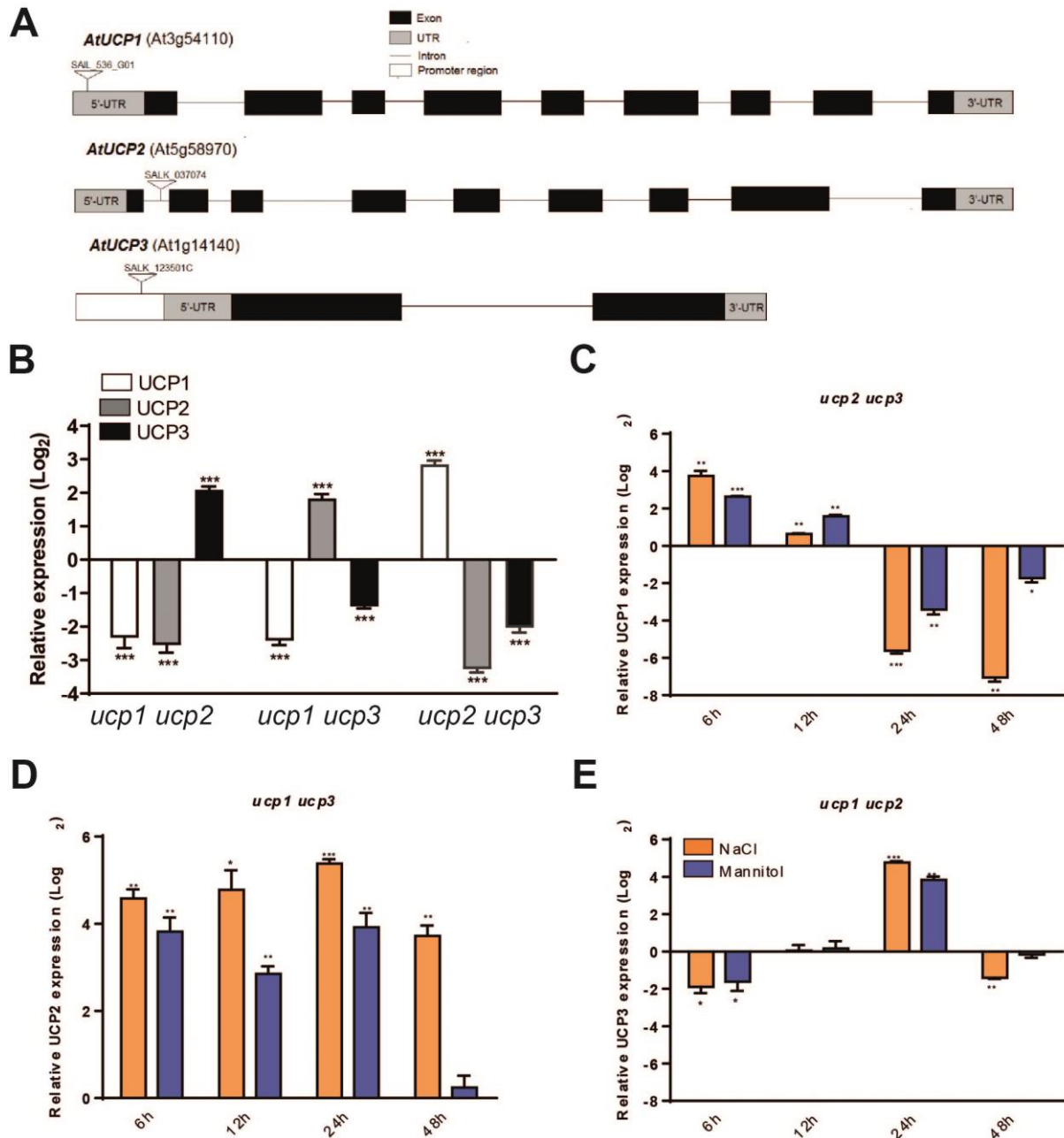


Fig. 1. Molecular characterization of the *ucp* double mutants. (A) Schematic representation of the *UCP1*, *UCP2* and *UCP3* gene structure showing the sites of T-DNA insertions. Exons and introns are depicted by boxes and lines, respectively. (B) Relative expression (Log₂) of *UCP1*, *UCP2* and *UCP3* in each double mutant. The expression of the target genes in wild-type (WT) Col-0 plants was used as calibrator (expression arbitrarily set to zero). Expression of (C) *UCP1*, (D) *UCP2*, and (E) *UCP3* in *ucp2 ucp3*, *ucp1 ucp3* and *ucp1 ucp2* plants (21-day-old), respectively, submitted to salt (NaCl) and osmotic (Mannitol) stresses. The plants were sampled at different time points (6, 12, 24 e 48 h) after stress imposition. Untreated double mutant plants were used as control (expression arbitrarily set to zero). *GAPDH* was used as endogenous control in all reactions. The bars represent the means with their respective standard errors (\pm SE) from three biological replicates per genotype. Asterisks denote significant differences when compared with WT (*p < 0.05, **p < 0.005 and ***p < 0.0005).

Phenotypic evaluation of the double mutants

The three double mutant lines performed similarly to the WT plants during seed germination under normal conditions (Fig. 2A). At five DAS, the G_R of WT and double mutant seeds reached 100% and approximately 97%, respectively, with no further differences observed thereafter. In contrast, the double mutant lines showed delayed G_R when seeds were germinated in media supplemented with salt and mannitol (Fig. 2A). The *ucp2 ucp3* seeds were the most affected reaching a final G_R of 64% under salt stress when compared with the WT, a performance that reflects a lower tolerance when compared to osmotic stress (final G_R of 82%). Under these stresses, the maximum G_R for WT seeds was reached at six DAS, while at the same time point, only 48% (salt) and 59% (osmotic) of the *ucp2 ucp3* seeds germinated. In contrast, no differences in G_R were found between *ucp1 ucp2* or *ucp1 ucp3* and the WT during germination under stress.

Primary root length (PRL) was also evaluated under normal ($\frac{1}{2}$ MS medium) or stressed conditions (salt and osmotic). A significant reduction in PRL was observed in *ucp1 ucp2* and *ucp1 ucp3* mutants under normal conditions when compared with WT (Fig. 2B). Under stress, all genotypes showed shorter PRL when compared with WT, but the observed differences were only statistically significant for *ucp1 ucp2* and *ucp1 ucp3* (Fig. 2B). In contrast, no differences in lateral root formation were observed among mutants. Overall, these results suggest that *UCP1*, among the other isoforms, is important for maintaining root growth under normal and adverse conditions.

Growth parameters during vegetative phase were also quantitatively evaluated. Despite showing a similar rosette area relative to the WT (Fig. 2C and 2D), all double mutants had a significant reduction in leaf number (Fig. 2E). Complementary assays to evaluate FW, DW and RWC of the aerial parts and root system revealed a pronounced decrease in root (68% and 44% for FW and DW, respectively) and shoot (50% and 48% for FW and DW, respectively) biomasses of the *ucp1 ucp3* double mutant as compared with the WT (Table 1). This was reflected by the major differences found in the RWC of roots and aerial parts of *ucp1 ucp3* compared with the other evaluated genotypes. The RWC of *ucp1 ucp2* roots was also affected and differed significantly from WT and *ucp2 ucp3*. This agrees with the results obtained for PRL (Fig. 2B). On the other hand, all genotypes, except *ucp1 ucp3*, showed no differences in FW, DW and RWC of the aerial parts.

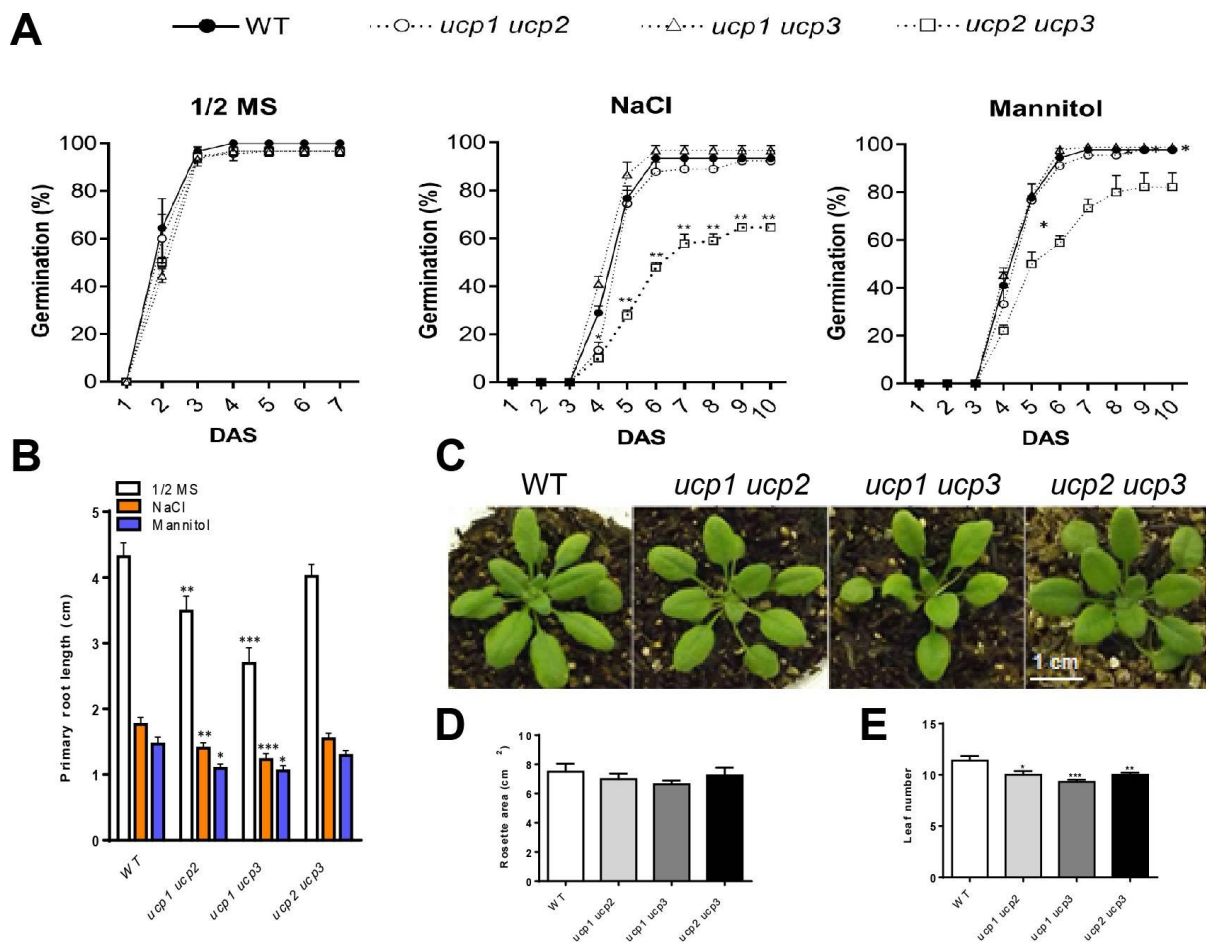


Fig. 2. Effects of the double knockdown of *UCP* genes in germination rate (G_R), primary root length (PRL) and vegetative development. (A) G_R of wild-type (WT) Col-0 and *ucp* double mutant seeds sown on $\frac{1}{2}$ MS medium supplemented or not (control) with NaCl (125 mM) and Mannitol (250 mM). Time points are a mean of three biological replicates (each replicate is the average of 30 seeds per genotype). (B) PRL of WT and *ucp* double mutant seedlings grown vertically for 10 days on $\frac{1}{2}$ MS medium supplemented or not (control) with NaCl (125 mM) and Mannitol (250 mM). The bars represent the means with their respective standard errors (\pm SE) from 15 biological replicates per genotype. (C) Representative images of WT and *ucp* double mutant plants (30-day-old), and corresponding rosette area (D) and leaf number (E). The bars represent the means with their respective standard errors (\pm SE) from 10 biological replicates per genotype. Asterisks denote significant differences when compared with WT (* p <0.05, ** p <0.005 and *** p <0.0005).

Table 1. Fresh weight (FW), dry weight (DW) and relative water content (RWC) of wild-type (WT) Col-0 and double mutants (*ucp1 ucp2*, *ucp1 ucp3* and *ucp2 ucp3*) plants (28-day-old) grown under normal conditions.

Treatments	Root FW ¹ (g)	DW ¹ (g)	RWC ^{1,2}	Aerial part FW ¹ (g)	DW ¹ (g)	RWC ^{1,2}
WT	0.022 \pm 0.002a	0.0039 \pm 0.0003a	1.13 \pm 0.01a	0.18 \pm 0.02a	0.021 \pm 0.002a	1.22 \pm 0.01a
<i>ucp1 ucp2</i>	0.018 \pm 0.003a	0.0042 \pm 0.0006a	1.04 \pm 0.03b	0.16 \pm 0.01a	0.017 \pm 0.001a	1.23 \pm 0.01a
<i>ucp1 ucp3</i>	0.007 \pm 0.001b	0.0022 \pm 0.0003b	0.95 \pm 0.04c	0.08 \pm 0.003b	0.011 \pm 0.001b	1.19 \pm 0.01b
<i>ucp2 ucp3</i>	0.023 \pm 0.003a	0.0033 \pm 0.0004a	1.17 \pm 0.01a	0.17 \pm 0.02a	0.021 \pm 0.001a	1.21 \pm 0.01a
CV (%)	29.53	29.66	7.79	24.09	25.48	1.72

¹Means \pm SE followed by same letter are not significantly different (p <0.05) by Scott-Knott test. Ten biological replicates were used in each treatment.

²Data transformed in arc sen ($\sqrt{x/100}$).

The double knockdown of *UCP* genes alters mitochondrial metabolism associated with energy and ROS production during the vegetative phase

In order to correlate the growth differences observed between WT and double mutants with UCP function, we decided to evaluate parameters related to mitochondrial metabolism. At first, as UCPs are classically linked with the detoxification of ROS [11,13], we investigated mitochondrial O_2^- accumulation in WT and double mutant lines using MitoSOX Red staining. As a result, a visual increase in superoxide labeling (red staining) under control and stressed conditions could be observed in double mutant leaves compared with WT (Supplemental Fig. 2). Subsequently, the presence of H_2O_2 in WT and double mutant leaves was detected using DAB and then quantified in entire plants. As shown in Fig. 3A, DAB staining was more intense in double mutant leaves than in WT leaves, a feature that was positively correlated with an increase in H_2O_2 levels in double mutant plants (Fig. 3B). Overall, these results point to the occurrence of an exacerbated oxidative stress in mutants. In fact, oxidative damage assessed through lipid peroxidation measurements increased significantly in double mutant lines when compared with the WT (Fig. 3C).

We further looked to the antioxidant defense system in mutants by measuring the enzymatic activities of SOD and CAT. SOD activity was significantly reduced in *ucp1 ucp2* (34%) and *ucp2 ucp3* (26%) double mutant plants when compared with WT (Fig. 3D). On the other hand, no significant changes in CAT activity were detected between the investigated genotypes (Fig. 3E). These results suggest that the investigated double mutants are less effective in signaling and counteracting ROS-induced damage.

Next, to assess the effect of the investigated double knockdowns in mitochondrial energy metabolism, we measured ATP and ADP levels and O_2 consumption in mutant and WT plants. Significant decreases in ADP levels have been observed in *ucp1 ucp3* and *ucp2 ucp3* double mutant plants (Supplemental Fig. 3A), while the ATP levels were significantly increased in the *ucp1 ucp2* and *ucp1 ucp3* mutants compared with the WT (Supplemental Fig. 3B). In this regard, an imbalanced ADP/ATP ratio was observed in the three double mutants, reaching a reduction of at least 79% relative to the WT (Fig. 3F). On the other hand, although no significant effect in O_2 consumption was detected in *ucp1 ucp2* when compared with the WT, a significant reduction was registered for *ucp1 ucp3*, whereas an increase was observed

in *ucp2 ucp3* (Fig. 3G). To further substantiate the impact of the double knockdown on mitochondrial metabolism, we determined the relative expression of a marker nuclear gene associated with mitochondrial function, namely *AOX1a*. Previous observations have shown that alterations in *UCP1* expression affect nuclear gene expression, in particular of genes implicated in alternative respiratory pathways [17,18]. In fact, *AOX1a* expression was differently affected according to the double mutant analyzed (Supplemental Fig. 3C), being down-regulated in *ucp1 ucp2* and *ucp1 ucp3* and upregulated in *ucp2 ucp3*. Collectively, these data support the idea that the double knockdown of *UCP* genes is reflected by perturbations in mitochondrial metabolism. In addition, we assessed mitochondrial biogenesis through the relative quantification of mtDNA content (Fig. 3I). In this context, a decrease in the relative amount of mtDNA was observed in *ucp1 ucp2* (0.85-fold) and *ucp2 ucp3* (0.76-fold), but this reduction was significant only for *ucp2 ucp3*. Interestingly, *ucp1 ucp3* had an increase (1.32-fold) in amount of mtDNA when compared with WT.

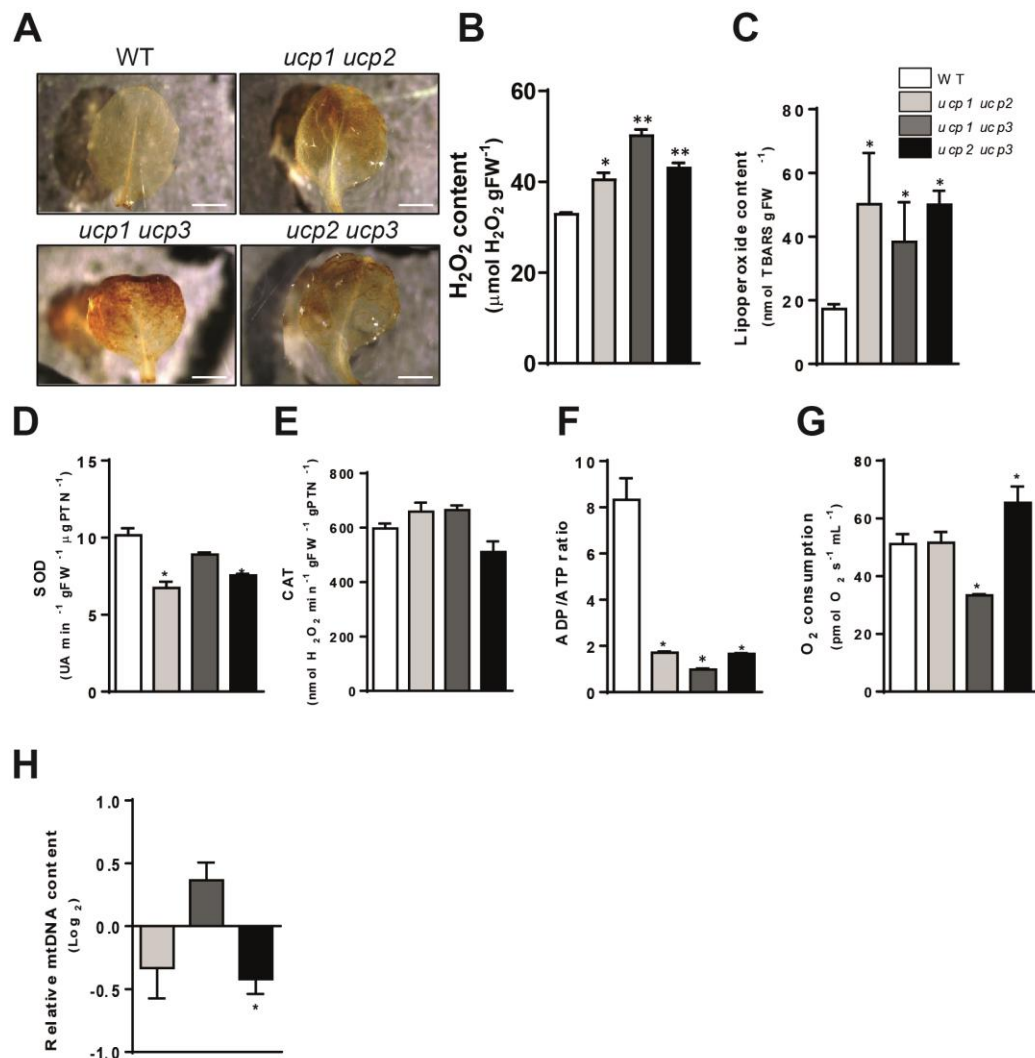


Fig. 3. Effects of the double knockdown of *UCP* genes on ROS homeostasis and mitochondrial metabolism. (A) *In situ* detection of H_2O_2 in leaves from wild-type (WT) Col-0 and *ucp* double mutant plants (21-day-old) using DAB. Representative images were taken using an Olympus SZX16 stereo microscope (scale bar = 1000 μ m). (B) H_2O_2 and (C) lipoperoxide contents in WT and *ucp* double mutant plants (21-day-old). (D) Superoxide dismutase (SOD) and (E) catalase (CAT) activities in 21-day-old plants. (F) ADP/ATP ratio of plants (21-day-old) collected in the dark. (G) O_2 consumption rate in detached leaves from WT and *ucp* double mutant plants (21-day-old). The mean of the negative slopes from three most homogeneous biological replicates per genotype was taken into account. (H) Relative mitochondrial DNA (mtDNA) content (\log_2). Quantification in WT plants was used as control (expression arbitrarily set to zero). The bars represent the means with their respective standard errors (\pm SE) from three biological replicates per genotype. Asterisks denote significant differences when compared with WT (* $p < 0.05$, ** $p < 0.005$ and *** $p < 0.0005$).

Cellular redox balance and photosynthesis are remotely affected by the knockdown of *UCP* genes during vegetative phase

Previous characterization of the *ucp1* single mutant revealed altered redox state in the cytosol [8]. This feature is in line with the newly hypothesized function of UCP as part of the malate-aspartate shuttle implicated in the regulation of redox balance between the mitochondria and the cytosol [7,10]. To check whether the cellular redox balance could be impacted by the double knockdown of the *UCP* genes, the dinucleotide pools (Supplemental Fig. 3) and associated NADH/NAD⁺ and NADPH/NADP⁺ ratios were determined (Fig. 4A and 4B). No significant changes in NADH levels were found between the three double mutants and WT (Supplemental Fig. 3D). In contrast, NAD⁺ levels were significantly higher in the *ucp1 ucp2* and *ucp2 ucp3* mutants compared with the WT (Supplemental Fig. 3E). Moreover, *ucp1 ucp2* and *ucp1 ucp3* mutants showed increased levels of NADPH (Supplemental Fig. 3F), while all double mutants exhibited increased levels of NADP⁺ (Supplemental Fig. 3G). These alterations in the dinucleotide pools led to a significant reduction in the cellular NADH/NAD⁺ ratio was observed in *ucp1 ucp2* (16.5%) and *ucp2 ucp3* (33%) when compared with WT (Fig. 4A). Likewise, the NADPH/NADP⁺ ratio decreased significantly in both *ucp1 ucp3* (30%) and *ucp2 ucp3* (24%) compared with WT (Fig. 4B). Overall, these results indicate that the cellular redox homeostasis is disturbed in the mentioned double mutants.

Given that plant UCP activity has important impacts not only in the mitochondria, but also in other cell compartments, especially in the chloroplast [8,16], the photosynthetic performance of the double mutants and other possible associated physiological effects were investigated by performing whole-plant gas exchange

measurements (Fig. 4). The three double mutants showed lower A_{net} values when compared with WT. However, this reduction was significant only for *ucp1 ucp3* (36%) and *ucp2 ucp3* (66%) (Fig. 4C). Moreover, g_s and C_i values were significantly decreased in *ucp1 ucp2* (36% and 18%, respectively) and *ucp2 ucp3* (55% and 14%, respectively) (Fig. 4D and 4E). The *ucp2 ucp3* double mutant was the only one with significant decreases in g_s , A_{net} , C_i and E (49%; Fig. 4F). When compared with WT, the *ucp1 ucp3* and *ucp2 ucp3* double mutants displayed significant reductions in A_{net}/C_i (32% and 60%, respectively) but no alterations in A_{net}/E ratio (Fig. 4G and 4H). Therefore, we can infer that the lower photosynthetic efficiency of these double mutants could be a result of reduced carboxylation efficiency of Rubisco (A_{net}/C_i ratio). In addition to gas exchange parameters, fluorescence measurements of chlorophyll α in the presence of light were determined. In this case, both *ucp1 ucp2* and *ucp1 ucp3* mutants showed lower F_m' (Fig. 4I), F_o' (Fig. 4J) and F' (Fig. 4K) values when compared with WT. However, even though the detected decreases, the derived ratios (ETR , qP and Φ_{PSII}) remained unchanged compared with WT (Fig. 4L, 4M and 4N).

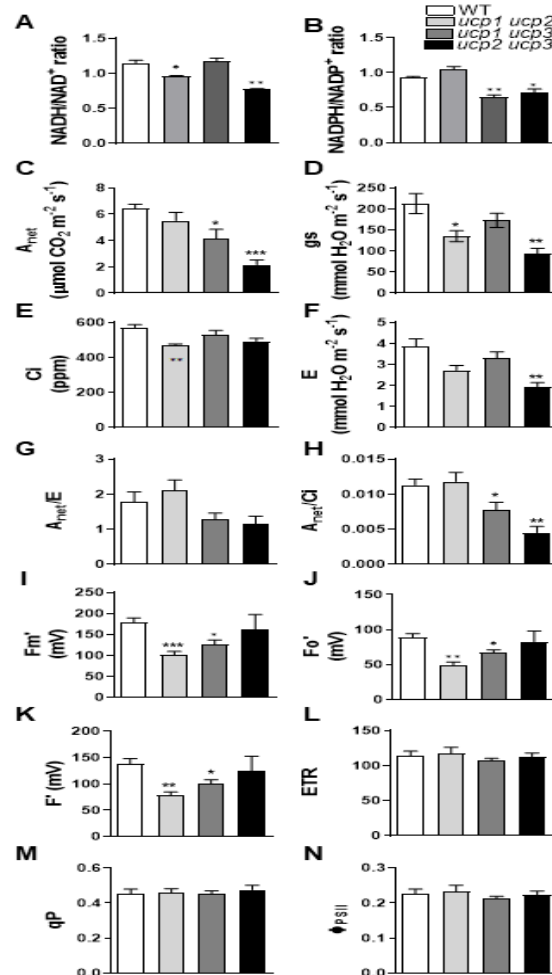


Fig. 4. Impacts of the double knockdown of *UCP* genes in cellular redox state, gas exchange and chlorophyll α fluorescence parameters. (A) NADH/NAD⁺ and (B) NADPH/NADP⁺ ratios of wild-type (WT) Col-0 and *ucp* double mutant plants (21-day-old). The bars represent the means with their respective standard errors (\pm SE) from three biological replicates per genotype. (C) Net photosynthetic rate (A_{net}), (D) stomatal conductance (g_s), (E) intercellular CO₂ concentration (C_i), (F) leaf transpiration rate (E), (G) instantaneous water-use efficiency (A_{net}/E) and (H) instantaneous carboxylation efficiency (A_{net}/C_i) of WT and *ucp* double mutant plants (21-day-old). (I) Maximum fluorescence (F_m'), (J) basal fluorescence (F_o'), (K) steady-state fluorescence (F'), (L) electron transport rate (ETR), (M) photochemical dissipation (qP) and (N) quantum yield of PSII (Φ_{PSII}) of WT and *ucp* double mutant plants (21-day-old). The bars represent the means with their respective standard errors (\pm SE) from five biological replicates per genotype. Asterisks denote significant differences when compared with WT (* p <0.05, ** p <0.005 and *** p <0.0005).

The double knockdown of *UCP* genes impacts plant reproduction

The success of plant reproduction relies on the source tissues to provide energy to the flowers [49]. This is highly dependent on chloroplastic metabolism in leaves [49], as well as mitochondrial energy generation in flowers [50]. It has been previously reported that an increased *UCP1* content influences the balance between source and sink tissues thus contributing to increase seed production in tobacco plants subjected to drought stress [51]. Due to their higher mitochondrial content, flower tissues are much more prone to oxidative stress than leaf tissues [52].

To test whether the double knockdown could exacerbate oxidative stress during the reproductive phase, we addressed accumulation of H₂O₂ in open flowers. Indeed, a clear increase in endogenous accumulation of H₂O₂ (brown precipitate) in open flowers from the three double mutants was evidenced by DAB staining (Fig. 5A), a feature that was further confirmed by H₂O₂ quantification (Fig. 5B). These results are indicative of an increased oxidative stress in the reproductive organs of mutant plants and are in line with the high levels of ROS accumulation observed in flowers of the *ucp1* and *ucp2* single mutants [26].

To find out whether such an enhanced ROS accumulation in the double mutant flowers would lead to phenotypic changes during the reproductive phase, parameters related to flowering time, floral transition and opening were examined. A delay in the flowering time of *ucp1 ucp2* and *ucp2 ucp3* double mutants when compared with WT was observed (Fig. 5C and 5D). In both double mutants, the numbers of days for floral transition and for first flower opening were significantly increased. Moreover, the siliques and seeds of all double mutants were reduced in size when compared with WT (Fig. 5E). Concerning silique length, the strongest reduction was observed in *ucp1*

ucp2 (26%; Fig. 5F). Likewise, although showing a normal phenotype with a similar brown color coating, mutant seeds were visually smaller than WT seeds (Fig. 5E). Hence, a decrease of approximately 65% in seed fresh weight was observed in *ucp1 ucp2* and *ucp2 ucp3* double mutants (Fig. 5G).

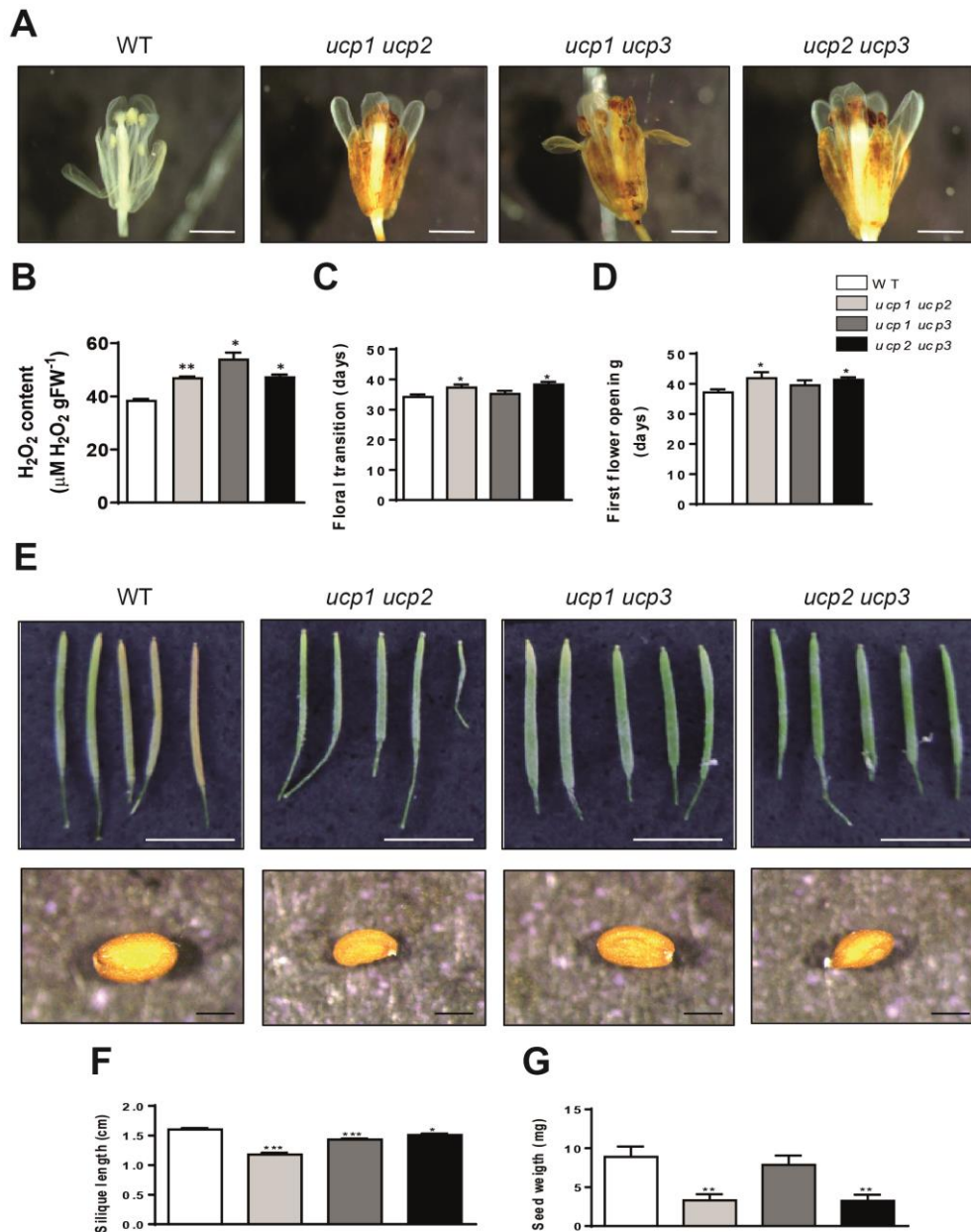


Fig. 5. Effects of the double knockdown of *UCP* genes on the reproductive phase. (A) *In situ* detection of H_2O_2 in open flowers from wild-type (WT) Col-0 and *ucp* double mutant plants (45-day-old) using DAB. Representative images were taken using an Olympus SZX16 stereo microscope (scale bar = 1000 μm). (B) H_2O_2 content in open flowers from WT and *ucp* double mutant plants (45-day-old). The bars represent the means with their respective standard errors ($\pm SE$) from three biological replicates per genotype. (C) Floral transition (days) and (D) First flower opening (days). The bars represent the means with their respective standard errors ($\pm SE$) from 10 biological replicates per genotype. (E) Representative image of siliques (scale bar = 1 cm) and seeds (scale bar = 200 μm) from WT and *ucp* double mutant plants. (F) Silique length.

The bars represent the means with their respective standard errors (\pm SE) from 100 biological replicates per genotype. (G) Seed weight. Seeds were harvested from 10 siliques randomly collected from 10 distinct plants. The bars represent the means with their respective standard errors (\pm SE) from 10 biological replicates per genotype. Asterisks denote significant differences when compared with WT (* p <0.05, ** p <0.005 and *** p <0.0005).

Discussion

Although *UCP1* from *A. thaliana* was discovered almost 20 years ago, the biological role and molecular function of the other isoforms present in this species still a matter of debate [10]. Here, to gain further insights into the physiological relevance of the different UCP isoforms, double knockdown mutants for different gene combinations were generated. These double mutants were viable and reproduced some of the phenotypes previously observed in the *ucp1* and *ucp2* single mutants [26]. Intriguingly, a strong compensatory expression of the WT *UCP* genes in double mutants under normal or stressed (salt and osmotic) conditions was detected, suggesting the existence of partial redundancy between them. This is in agreement with the compensatory expression also registered for the *ucp1* and *ucp2* single mutants [26] and corroborated by *in silico* analyzes indicating that these genes, although showing distinct spatio-temporal expression patterns, are ubiquitously expressed [23].

A classical phenotype reported for *UCP1* overexpression is enhanced tolerance to abiotic and biotic stresses [13,19,21]. Tobacco lines overexpressing the *A. thaliana* *UCP1*, for example, showed a better performance and higher tolerance to salt and osmotic stresses during seed germination [21]. Here we observed that the simultaneous double knockdown of *UCP2* and *UCP3* resulted in a relevant negative effect in seed germination under stress. Intriguingly, seeds from the *ucp1* single mutant were previously shown to be more sensitive to salt and osmotic stresses than *ucp2* seeds [26]. It seems therefore that a concerted action of *UCP2* and *UCP3* is required to cope with stress during seed germination. On the other hand, a prominent role for *UCP1* during primary root growth could be envisaged based on the root growth phenotypes of both *ucp1 ucp2* and *ucp1 ucp3* mutants. It is noteworthy that *UCP1* is the most highly expressed isoform during early plant development [23] and that a reduced primary root growth phenotype under control and stressed conditions is reminiscent of the *ucp1* single mutant [26]. In this context, the compensatory expression of *UCP1* observed in the *ucp2 ucp3* double mutant may underline the

absence of a significant root growth phenotype in this line. When looking to the vegetative phase, the *ucp1 ucp3* mutant was the only one showing reduced leaf number and negative effects in FW, DW and RWC of rosettes and roots. Likewise, a significant reduction in the DW of the aerial part when compared with the WT was observed in the *ucp1* single mutant [16].

Several reports attributed the stress tolerance found in *UCP1* overexpressing lines to an increase in mitochondrial uncoupling that would reduce ROS production inside mitochondria [13,14,17,19,21]. In line with these observations, our results revealed that both accumulation of H₂O₂ and lipid peroxidation increased in all double mutants. It is relevant to note that *UCP1* is activated by products of lipid peroxidation such 4-hydroxy-2-nonenal as part of a mechanism to reduce ROS production [14], which could also be the case for *UCP2* and *UCP3*. It seems, therefore, that physiological levels of all isoforms are required to maintain mitochondrial function and ROS homeostasis under normal conditions. Intriguingly, the resulting oxidative stress in double mutants was not compensated by an increase in the activity of the antioxidant enzymes SOD and CAT, a peculiarity that was also observed in tomato plants with a silenced UCP gene (*LeUCP*) [20]. This could be linked to the postulated role played by UCPs in retrograde redox signaling [10,17,55]. In animals, it has been proposed that a concerted action of UCPs and the antioxidant system is required to keep mitochondrial ROS at low levels [53].

The exacerbation of ROS generation in double mutant leaves is suggestive of disturbances in mitochondrial homeostasis. This was in part confirmed by the decreased ADP/ATP ratio found in double mutants, which suggests a functional relevance of the *UCP* isoforms in acting as mitochondrial uncouplers. In accordance, significant alterations in the ATP/ADP ratio were previously observed in the *ucp1* and *ucp2* single mutants [26]. Also compatible with our results, a decrease in ATP content associated with an increase in mitochondrial respiration in tobacco plants overexpressing *UCP1* has been previously reported [17]. Another interesting feature associated with enhanced UCP activity is the increase of oxygen consumption [6]. Here, although an expected significant decrease in O₂ consumption was detected in *ucp1 ucp3* leaves, the contrary was exclusively noticed in *ucp2 ucp3* leaves, a feature that might be linked to the detected increase in *AOX1a* expression in this double mutant. This suggests that the alternative respiratory pathway is activated when both

UCP2 and *UCP3* are knocked down, resulting in an increased mitochondrial respiration in the *ucp2 ucp3* mutant. This assumption is strengthened by previous results showing an increase in *AOX1a* expression in the *ucp1* and *ucp2* single mutants [26]. By contrast, we also found a correlation between the knockdown of *UCP1* in any gene combination and the downregulation of *AOX1a* expression. This is consistent with a previous finding showing that the *ucp1* single mutant accumulates low levels of total AOX protein [17]. It is worth mentioning that stimulation of alternative respiratory pathways is a hallmark of mitochondrial respiration deficiencies and it is generally associated with the over reduction of the electron transport chain and intracellular ROS accumulation [54]. In this respect, it seems that the compensatory expression of *UCP1* and the concomitant upregulation of *AOX1a* in the *ucp2 ucp3* mutant might be sufficient to trigger an increase in respiratory activity. In line with this observation, the *ucp2 ucp3* mutant also showed a significant decrease in mtDNA content, thus reinforcing its negative impact on mitochondrial homeostasis.

In addition to their function in controlling ROS homeostasis, plant UCP activity has been reported to promote alterations in nuclear gene expression [17,18], cellular redox status [7,8] and photosynthetic efficiency [16,26,55]. Here we show that the redox balance is also affected by the double knockdown of the *UCP* genes. Generally used as a cofactor for energy transfer in all living cells, the intermediate compounds NAD and NADP act in electron transport from redox reactions as well as in cell signaling [56]. Changes in NADH/NAD⁺ and NADPH/NADP⁺ ratios are generally associated with alterations in carbon and nitrogen metabolism within living cells [57]. Earlier results have suggested that regulated UCP1-mediated proton gradient dissipation grants NADH oxidation in the mitochondrial matrix to sustain continued photorespiration [16]. According to our findings, the double knockdown of *UCP2* and *UCP3* was the only combination that determined simultaneous reductions in NADH/NAD⁺ and NADPH/NADP⁺ ratios. These two isoforms could, therefore, play a more relevant role in adjusting cellular redox balance.

Photosynthetic metabolism was also affected by the knockdown of the *UCP* genes as noticed by decreases in A_{net} in *ucp1 ucp3* and *ucp2 ucp3*. Consistent with our data, the *ucp1* single mutant also exhibited reduced A_{net} due to a deficiency in photorespiration [16]. In this regard, the UCP-mediated uncoupling of mitochondrial respiration has been postulated to support NAD⁺ regeneration, especially when the

malate-oxalacetate shuttle is unable to consume all of the NADH produced during photorespiration. This activity allows appropriate redox balance to be maintained [10,16], which in turn ensures continued photorespiration during daytime. Interestingly, photosynthesis was also negatively affected by a single *UCP2* knockdown [26]. According to our results, however, the major changes in gas exchange parameters resulted from the knockdown of *UCP3* in any combination, indicating that this isoform also contributes to sustain the photosynthetic metabolism. Noteworthy, mutant plants carrying a knockdown in *UCP3* displayed decreased NADPH levels and, consequently, increased NADP⁺ accumulation, a condition that limits ribulose-1,5-bisphosphate (RuBP) regeneration and therefore lower net carbon assimilation. Additional data also revealed significant reductions in fluorescence values in *ucp1 ucp2* and *ucp1 ucp3* double mutants, which reinforces the importance of *UCP1* not only in the maintenance of photosynthetic efficiency as already reported [16], but also to reduce damage to the photosynthetic apparatus in *A. thaliana*. In accordance with our results, an increase in chlorophyll fluorescence triggered by overexpression of *LeUCP* was observed in tomato plants under cold stress [19].

It has been suggested by previous studies that mitochondrial dysfunctions, especially those leading to energy deficiency and oxidative stress as observed in double mutants, has a negative impact on plant fertility [54,58,59]. Here we found that the disruption of the *UCP* genes in all tested double mutants resulted in increased H₂O₂ content in reproductive tissues. This is consistent with previous results showing increased oxidative stress in the reproductive organs of the *ucp1* and *ucp2* single mutants [26]. Interestingly, all mutants also exhibited a significant inhibition of silique growth, a phenotype that was also documented in the *ucp1* and *ucp2* single mutants and attributed to defects in male and female fertility [26]. It should be highlighted that silique elongation depends on adequate fertilization and successful seed development [60,61]. In this regard, the significant reduction in seed size and in seed production observed in *ucp1 ucp2* and *ucp2 ucp3* double mutants highlight the importance of *UCP2* in the maintenance of plant fertility. Nonetheless, the implication of *UCP1* in this process should not be precluded since the knockdown of *UCP1* in combination with *UCP2* negatively affected several reproductive parameters. Further highlighting the importance of UCP in plant fertility, an increase in the weight of seeds per silique was evidenced in tobacco plants overexpressing *UCP1* [51]. Overall, these evidences

suggest that *UCP1* and *UCP2* may contribute in a partially redundant way to fertility maintenance in *A. thaliana*, collaborating for metabolic adjustments and concomitant reduction of ROS accumulation in mitochondria. In this context, the possible addictive role played by *UCP3* needs to be further addressed.

In conclusion, our systematic analysis revealed important disturbances in the entire plant due to the double knockdown of *UCP* genes in *A. thaliana*, which promotes alterations in mitochondrial homeostasis and function. Our data provided good evidence of isolated and concerted functionality of these three *UCP* isoforms at entire plant level, pointing out the existence of a partial redundancy between them.

Funding

This work was supported by Fundação de Amparo à Pesquisa do Estado de São Paulo [Processes 17/25139-2 and 18/19021-1 to R.P.M.L.]; Coordenação de Aperfeiçoamento de Pessoal do Ensino Superior (Financing code 001 to R.P.M.L. and CAPES/PRINT to P.B.) and Conselho Nacional de Desenvolvimento Científico e Tecnológico [Process 301043/2018-1 to I.G.M.].

Author Contributions

R.P.M.L. and I.G.M. conceived and designed the experiments; A.V.N.L., M.L.C.A., F.G.C., T.A.C.J., G.C.M., H.K. and R.P.M.L. performed the experiments; I.G.M., G.P.P.L., L.F.R.A. and R.P.M.L. interpreted the data; R.P.M.L., P.B. and I.G.M. wrote and edited the manuscript.

Acknowledgements

We thank Dra. Alicia J. Kowaltowski (Instituto de Química – USP/São Paulo) who provided the equipment for analysis of O₂ consumption, and Dr. André S. Pupo (Departamento de Farmacologia e Biofísica – UNESP/Botucatu) who provided the equipment for analysis of ADP/ATP ratio.

The authors have no conflicts of interest to declare.

References

- [1] R.P. Jacoby, L. Li, S. Huang, C. Pong Lee, A.H. Millar, N.L. Taylor, Mitochondrial composition, function and stress response in plants, *J. Integr. Plant Biol.* 54 (2012) 887-906.
- [2] A.E. Vercesi, I.S. Martins, M.P.A. Silva, H.M.F. Leite, I.M. Cuccovia, H. Chaimovich, PUMPing plants, *Nature* 375 (1995) 24-25.
- [3] M. Laloi, M. Klein, J.W. Reismeier, B. Muller-Rober, C. Fleury, F. Bouillaud, D. Ricquier, A plant cold-induced uncoupling protein, *Nature* 389 (1997) 135-136.
- [4] I.G. Maia, C.E. Benedetti, A. Leite, S.R. Turcinelli, A.E. Vercesi, P. Arruda, AtPUMP: an *Arabidopsis* gene encoding a plant uncoupling mitochondrial protein, *FEBS Letter* 429 (1998) 403-406.
- [5] D.G. Nicholls, A history of UCP1, *Biochem. Soc. Trans.* 29 (2001) 751-755.
- [6] A.E. Vercesi, J. Borecký, I.G. Maia, P. Arruda, I.M. Cuccovia, H. Chaimovich, Plant uncoupling mitochondrial proteins, *Annu. Rev. Plant Biol.* 57 (2006) 383-404.
- [7] M. Monné, L. Daddabbo, D. Gagneul, T. Obata, B. Hielscher, L. Palmieri, D.V. Miniero, A.R. Fernie, A.P.M. Weber, F. Palmieri, Uncoupling proteins 1 and 2 (UCP1 and UCP2) from *Arabidopsis thaliana* are mitochondrial transporters of aspartate, glutamate, and dicarboxylates, *J. Biol. Chem.* 293 (2018) 4213-4227.
- [8] A. Gandin, M. Denysyuk, A.B. Cousins, Disruption of the mitochondrial alternative oxidase (AOX) and uncoupling protein (UCP) alters rates of foliar nitrate and carbon assimilation in *Arabidopsis thaliana*, *J. Exp. Bot.* 65 (2014) 3133-3142.
- [9] M. Monné, A. Voza, F.M. Lasorsa, V. Porcelli, F. Palmieri, Mitochondrial carriers for aspartate, glutamate and other amino acids: a review, *Int. J. Mol. Sci.* 20 (2019) 4456.
- [10] P. Barreto, R.M. Couñago, P. Arruda, Mitochondrial uncoupling protein-dependent signaling in plant bioenergetics and stress response, *Mitochondrion* 53 (2020) 109-120.
- [11] A.J. Kowaltowski, A.D. Costa, A.E. Vercesi, Activation of the potato plant uncoupling mitochondrial protein inhibits reactive oxygen species generation by the respiratory chain, *FEBS Letter* 425 (1998) 213-216.
- [12] C. Houton-Cabassa, A. Mesneau, B. Miroux, J. Roussaux, D. Ricquier, A. Zachowski, F. Moreau, Alteration of plant mitochondrial proton conductance by free fatty acids. Uncoupling protein involvement, *J. Biol. Chem* 277 (2002) 41533-41538.

- [13] M. Brandalise, I.G. Maia, J. Borecký, A.E. Vercesi, P. Arruda, Overexpression of plant uncoupling mitochondrial protein in transgenic tobacco increases tolerance to oxidative stress, *J. Bioenerg. Biomembr.* 35 (2003) 203-209.
- [14] A.M. Smith, R.G. Ratcliffe, L.J. Sweetlove, Activation and function of mitochondrial uncoupling protein in plants, *J. Biol. Chem.* 279 (2004) 51944-51952.
- [15] D. Pastore, D. Trono, M.N. Laus, N. Di Fonzo, Z. Flagella, Possible plant mitochondria involvement in cell adaptation to drought stress. A case study: durum wheat mitochondria, *J. Exp. Bot.* 58 (2007) 195-210.
- [16] L.J. Sweetlove, A. Lytovchenko, M. Morgan, A. Nunes-Nesi, N.L. Taylor, C.J. Baxter, I. Eickmeier, A.R. Fernie, Mitochondrial uncoupling protein is required for efficient photosynthesis, *PNAS* 103 (2006) 19587-19592.
- [17] P. Barreto, V.K. Okura, L.A. Neshich, I.G. Maia, P. Arruda, Overexpression of UCP1 in tobacco induces mitochondrial biogenesis and amplifies a broad stress response, *BMC Plant Biol.* 14 (2014) 144-159.
- [18] A.V.N. Laitz, M.L. Acencio, N. Lemke, P.E.M. Ribolla, I.G. Maia, Transcriptome response signatures associated with the overexpression of a mitochondrial uncoupling protein (AtUCP1) in tobacco, *PLOS ONE* 10 (2015) 1-13.
- [19] S. Chen, A. Liu, S. Zhang, C. Li, R. Chang, D. Liu, G.J. Ahammed, X. Lin, Overexpression of mitochondrial uncoupling protein conferred resistance to heat stress and *Botrytis cinerea* infection in tomato, *Plant Physiol. Biochem.* 73 (2013) 245-253.
- [20] S. Chen, A. Liu, D. Ji, X. Lin, Z. Liu, X. Xia, D. Liu, G.J. Ahammed, Silencing of tomato mitochondrial uncoupling protein disrupts redox poise and antioxidant enzymes activities balance under oxidative stress. *J. Plant Biol.* 57 (2014) 9-19.
- [21] K. Begcy, E.D. Mariano, L. Mattiello, A.V. Nunes, P. Mazzafera, I.G. Maia, M. Menossi, An *Arabidopsis* mitochondrial uncoupling protein confers tolerance to drought and salt stress in transgenic tobacco plants, *PLOS ONE* 6 (2011) 1-10.
- [22] J. Borecký, F.T.S. Nogueira, K.A.P. De Oliveira, I.G. Maia, A.E. Vercesi, P. Arruda, The plant energy-dissipating mitochondrial systems: depicting the genomic structure and expression profiles of the gene families of uncoupling protein and alternative oxidase in monocots and dicots, *J. Exp. Bot.* 57 (2006) 849-864.
- [23] F.T. Nogueira, F.T. Sasaki, I.G. Maia, *Arabidopsis thaliana* Uncoupling Proteins (AtUCPs): insights into gene expression during development and stress response and epigenetic regulation, *J. Bioenerg. Biomemb.* 43 (2011) 71-79.

- [24] F.E. Tax, D.M. Vernon, T-DNA-associated duplication/translocations in *Arabidopsis*. Implications for mutant analysis and functional genomics, *Plant Physiol.* 126 (2001) 1527-1538.
- [25] G.C. Briggs, K.S. Osmont, C. Shindo, R. Sibout, C.S. Hardtke, Unequal genetic redundancies in *Arabidopsis* – a neglected phenomenon?, *Trends Plant Sci.* 11 (2006) 492-498.
- [26] M.L.C. Arcuri, A.V. Nunes-Laitz, R.P.M Lima, P. Barreto, A.N. Marinho, P. Arruda, I.G. Maia, The Knockdown of Mitochondrial Uncoupling Proteins 1 and 2 (AtUCP1 and 2) in *Arabidopsis thaliana* Impacts Vegetative Development and Fertility, *Plant Cell Physiol.* 00 (2021) 1-15.
- [27] T. Murashige, F. Skoog, A revised medium for rapid growth and bioassays with tobacco tissues cultures, *Physiol. Plant.* 15 (1962) 473-497.
- [28] J.J. Doyle, J.L. Doyle, L.H.B. Hortorium, Isolation of plant DNA from fresh tissue, *Focus* 12 (1987) 13-15.
- [29] T. Czechowski, M. Stitt, T. Altmann, M.K. Udvardi, W. Scheible, Genome-wide identification and testing of superior reference-genes for transcript normalization in *Arabidopsis*, *Plant Physiol.* 139 (2005) 5-17.
- [30] K.J. Livak, T.D. Schmittgen, Analysis of relative gene expression data using real-time quantitative PCR and the 2- $\Delta\Delta$ Ct method, *Methods* 25 (2001) 402-408.
- [31] C.C. Matioli, J.P. Tomaz, G.T. Duarte, F.M. Prado, L.E.V. Del Bem, A.B. Silveira, L. Gauer, L.G.G. Corrêa, R.D. Drumond, A.J.C. Viana, P. Di Mascio, C. Meyer, M. Vincentz, The *Arabidopsis* bZIP gene AtbZIP63 is a sensitive integrator of transient abscisic acid and glucose signals, *Plant Physiol.* 1570 (2011) 692-705.
- [32] D.R. Smyth, J.L. Bowman, E.M. Meyerowitz. Early flower development in *Arabidopsis*, *Plant Cell* 2 (1990) 755-767.
- [33] A. Daudi, J.A. O'Brien, Detection of hydrogen peroxide by DAB staining in *Arabidopsis* leaves, *Bio-Protocol* 2 (2012) 1-4.
- [34] V. Alexieva, I. Sergiev, S. Mapelli, E. Karanov, The effect of drought and ultraviolet radiation on growth and stress markers in pea and wheat, *Plant Cell Environ.* 24 (2001) 1337-1344.
- [35] R.L. Heath, L. Packer, Photoperoxidation in isolated chloroplasts I. Kinetic and stoichiometry of fatty acid peroxidation, *Arch. Biochem. Biophys.* 125 (1968) 189-198.

- [36] S. Rama Devi, M.N.V. Prasad, Copper toxicity in *Ceratophyllum demersum* L. (Coontail), a free floating macrophyte: response of antioxidant enzymes and antioxidants, *Plant Sci.* 138 (1998) 157-165.
- [37] Y.I. Sun, L.W. Oberley, Y. Li, A simple method for clinical assay of superoxide dismutase, *Clin. Chem.* 34 (1988) 497-500.
- [38] M. Kar, D. Mishra, Catalase, peroxidase, and polyphenol oxidase activities during rice leaf senescence, *Plant Physiol.* 57 (1976) 315-319.
- [39] M.M. Bradford, A rapid and sensitive method for the quantitation of microgram quantities of protein utilizing the principle of protein-dye binding, *Anal. Biochem.* 72 (1976) 248-254.
- [40] M.J. Napolitano, D.H. Shain, Quantitating adenylate nucleotides in diverse organisms, *J. Biochem. Biophys. Methods* 63 (2005) 69-77.
- [41] D.Y. Wang, Q. Zhang, Y. Liu, Z.F. Lin, S.X. Zhang, M.X. Sun, Sodmergen. The levels of male gametic mitochondrial DNA are highly regulated in angiosperms with regard to mitochondrial inheritance, *Plant Cell* 22 (2010) 2402-2416.
- [42] M.H. Hameed, Hypoxia up-regulates mitochondrial genome-encoded transcripts in *Arabidopsis* roots, *Genes Genet. Syst.* 90 (2015) 325-334.
- [43] S. Shevtsov, K. Nevo-Dinur, L. Faigon, L.D. Sultan, M. Zmudjak, M. Markovits, O. Ostersetzer-Biran, Control of organelle gene expression by the mitochondrial transcription termination factor mTERF22 in *Arabidopsis thaliana* plants, *PLOS ONE* 13 (2018) 1-31.
- [44] Y. Gibon, F. Larher, Cycling assay for nicotinamide adenine dinucleotides: NaCl precipitation and ethanol solubilization of the reduced tetrazolium, *Anal. Biochem.* 251 (1997) 153-157.
- [45] J.A. Berry, W.J.S. Downton, Environmental regulation of photosynthesis, in: Govindjee (Ed.), *Photosynthesis*, Academic Press, London, 1982, pp. 263-343.
- [46] S. Von Caemmerer, G.D. Farquhar, Some relationships between the biochemistry of photosynthesis and the gas exchange of leaves, *Planta* 153 (1981) 376-387.
- [47] N. R. Baker, Chlorophyll fluorescence: a probe of photosynthesis in vivo, *Annu. Rev. Plant Biol.* 59 (2008) 89-113.
- [48] E.F. Belshe, M.J. Durako, J.E. Blum, Photosynthetic rapid light curves (RLC) of *Thalassia testudinum* exhibit diurnal variation. *J. Exp. Marine Biol. Ecol.* 342 (2007) 253-265.

- [49] R. Lemoine, S.L. Camera, R. Atanassova, F. Dédaldéchamp, T. Allario, N. Pourtau, J.L. Bonnemain, M. Laloi, P. Coutos-Thévenot, L. Maurousset, M. Faucher, C. Girousse, P. Lemonnier, J. Parrilla, M. Durand, Source-to-sink transport of sugar and regulation by environmental factors, *Front. Plant Sci.* 4 (2013) 1-21.
- [50] L. Chen, Y.G. Liu, Male sterility and fertility restoration in crops, *Annu. Rev. Plant Biol.* 65 (2014) 579-606.
- [51] P. Barreto, J.E.C.T. Yassitepe, Z.A. Wilson, P. Arruda, Mitochondrial uncoupling protein 1 overexpression increase yield in *Nicotiana tabacum* under drought stress by improving source and sink metabolism, *Front. Plant Sci.* 8 (2017) 1836.
- [52] F. Müller, I. Rieu, Acclimation to high temperature during pollen development, *Plant Reprod.* 29 (2016) 107-118.
- [53] Y.C. Tseng, R.D. Chen, M. Lucassen, M.M. Schmidt, R. Dringen, D. Abele, P.P. Hwang, Exploring uncoupling proteins and antioxidant mechanisms under acute cold exposure in brains of fish, *PLOS ONE* 6 (2011) 1-15.
- [54] J. Dahan, G. Tcherkez, D. Macherel, A. Benamar, K. Belcram, M. Quadrado, N. Arnal, H. Mireau, Disruption of the CYTOCHROME C OXIDASE DEFICIENT 1 gene leads to cytochrome c oxidase depletion and reorchestrated respiratory metabolism in *Arabidopsis thaliana*, *Plant Physiol.* 166 (2014) 1788-1802.
- [55] P. Barreto, V. Okura, I.A. Pena, R. Maia, I.G. Maia, P. Arruda, Overexpression of mitochondrial uncoupling protein 1 (UCP1) induces a hypoxic response in *Nicotiana tabacum* leaves, *J. Exp. Bot.* 67 (2016) 301-313.
- [56] W. Shen, Y. Wei, M. Dauk, Y. Tan, D.C. Taylor, G. Selvaraj, J. Zou, Involvement of a glycerol-3-phosphate dehydrogenase in modulating the NADH/NAD⁺ ratio provides evidence of a mitochondrial glycerol-3-phosphate shuttle in *Arabidopsis*, *Plant Cell* 18 (2006) 422-441.
- [57] H. Takahashi, K. Takahara, S. Hashida, T. Hirabayashi, T. Fujimori, M. Kawai-Yamada, T. Yamaya, S. Yanagisawa, H. Uchimiya, Pleiotropic modulation of carbon and nitrogen metabolism in *Arabidopsis* plants overexpressing the NAD kinase2 gene, *Plant Physiol.* 151 (2009) 100-113.
- [58] M.V. Busi, M.E. Gomez-Lobato, S.P. Rius, V.R. Turowski, P. Casati, E.J. Zabaleta, D.F. Gomes-Casati, A. Araya, Effect of mitochondrial dysfunction on carbon metabolism and gene expression in flower tissues of *Arabidopsis thaliana*, *Mol. Plant* 4 (2011) 127-143.

- [59] D.A. Geisler, C. Pöpke, T. Obata, A. Nunes-Nesi, A. Matthes, K. Schneitz, E. Maximova, W.J. Araújo, A.R. Fernie, S. Persson, Downregulation of δ -subunit reduces mitochondrial ATP synthase levels, alters respiration, and restricts growth and gametophyte development in *Arabidopsis*, *Plant Cell* 24 (2012) 2792-2811.
- [60] J. Keskitalo, G. Bergquist, P. Gardeström, S. Jansson, A cellular timetable of autumn senescence, *Plant Physiol.* 139 (2005) 1635-1648.
- [61] C. Wagstaff, T.J.W. Yang, A.D. Stead, V. Buchanan-Wollaston, J.A. Roberts, A molecular and structural characterization of senescing *Arabidopsis* siliques and comparison of transcriptional profiles with senescing petals and leaves, *Plant J.* 57 (2009) 690-705.
- [62] L. Palmieri, N. Picault, R. Arrigoni, E. Besin, F. Palmieri, M. Hodges, Molecular identification of three *Arabidopsis thaliana* mitochondrial dicarboxylate carrier isoforms: organ distribution, bacterial expression, reconstitution into liposomes and functional characterization, *Biochem. J.* 410 (2008) 621-629.

SUPPLEMENTARY DATA

Table S1A. List of primers used in this study. Primers designed for genotyping the double-mutants (*ucp1 ucp2*, *ucp1 ucp3* and *ucp2 ucp3*).

Gene	Forward primer (5'→3')	Reverse primer (5'→3')	T-DNA primer (5'→3')	References
<i>UCP1</i>	GACGAAGATGTGAAGTAG ACC	CAAAGAGAAGATACATGT TG	SAILLb3 TAGCATCTGAATTTTCATAACCAATCTCG ATACA	Palmieri et al., 2008; Sweetlove et al., 2006
<i>UCP2</i>	AAGAGGGTCTATCTAATG ACG	GCCACAAACCAATAAATA GAA	SALK ATTTTGCCGATTTCGGAA	Palmieri et al., 2008
<i>UCP3</i>	ACTCTTTCTGATTGTAGGA	GACTTTAAAGCCCAATAT TAT		Palmieri et al., 2008

Table S1B. List of primers used in this study. Primers designed for relative quantification of *UCP1* to *UCP3* and *AOX1a* expression by RT-qPCR.

Gene	Description	Forward primer (5'→3')	Reverse primer (5'→3')	References
<i>UCP1</i>	Mitochondrial Uncoupling Protein 1	GATGGTGCGGCTGGTA	CGCCGACGCAAGCAG	Palmieri et al., 2008
<i>UCP2</i>	Mitochondrial Uncoupling Protein 2	CATAACAATGGCGGATTTCAAA	CGCTGCAAATGAAGGTTTCA	
<i>UCP3</i>	Mitochondrial Uncoupling Protein 3	GGAGCCGAGTGACCAGAGAA	CGCAGAGAGTGAAGCAAGCA	
<i>AOX1a</i>	Alternative Oxidase 1a	CCGACGATTGGAGGTATG	CGGTGGATTCTGTTCTCTG	Barreto et al., 2014
Endogenous control				
<i>GAPDH</i>	Glyceraldehyde-3-phosphate Dehydrogenase	GCCAAGGCTGGGATTGC	GTCGTACCATGACACCAACTTCA	Czechowski et al., 2005

Table S1C. List of primers used in this study. Primers designed for relative quantification of mitochondrial DNA (mtDNA) quantification by qPCR.

Gene	Description	Forward primer (5'→3')	Reverse primer (5'→3')	References
<i>MatR</i>	Maturase R	GCCGACGACTTACTACTGG	GCCTACCCAAAGGTTTCAGG	Wang et al., 2010
<i>CoxI</i>	Cytochrome c Oxidase I	GTCTTCGGGTATCTAGGCATG	GGTATCTACGTCTAAGCCCACAG	
Endogenous control				
<i>RPOTmt</i>	Mitochondrial Phage-type RNA Polymerase	CTGTCTCTCCCTCTCCTTGAT C	GTCCACGATTCTGCTTACTG	Shevtsov et al., 2018

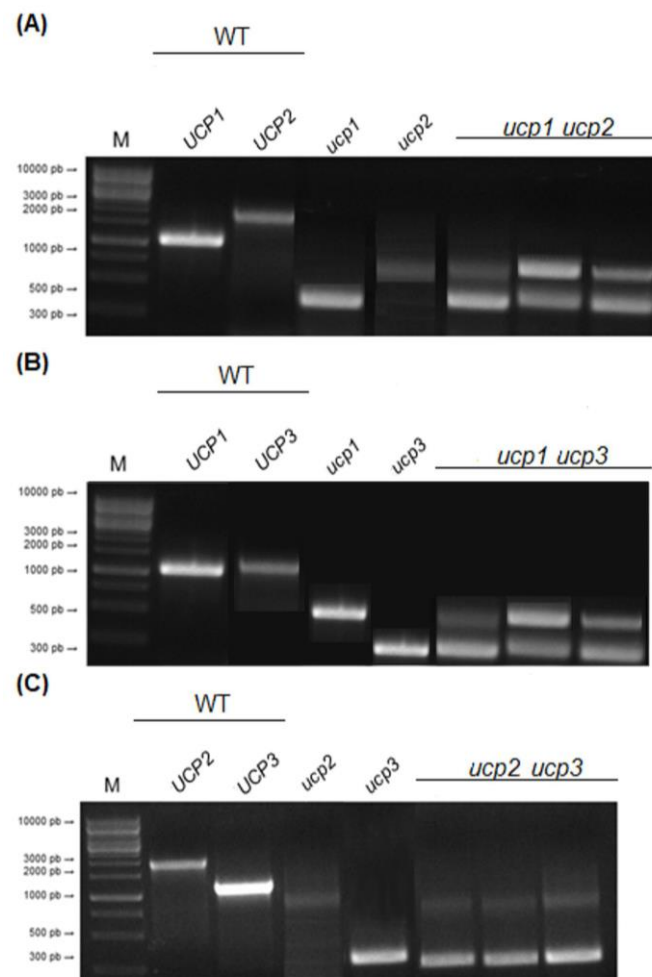


Fig. S1. Identification of homozygous double mutant lines by genomic PCR amplification. Amplification products generated using gene-specific and T-DNA left border (LB) primers are shown for (A) *ucp1 ucp2*, (B) *ucp1 ucp3* and (C) *ucp2 ucp3* lines. Amplification products in the wild-type (WT) Col-0 and *ucp* single mutant backgrounds are also shown as control. Agarose gel (1%) stained with ethidium bromide. M = 1 Kb Marker.

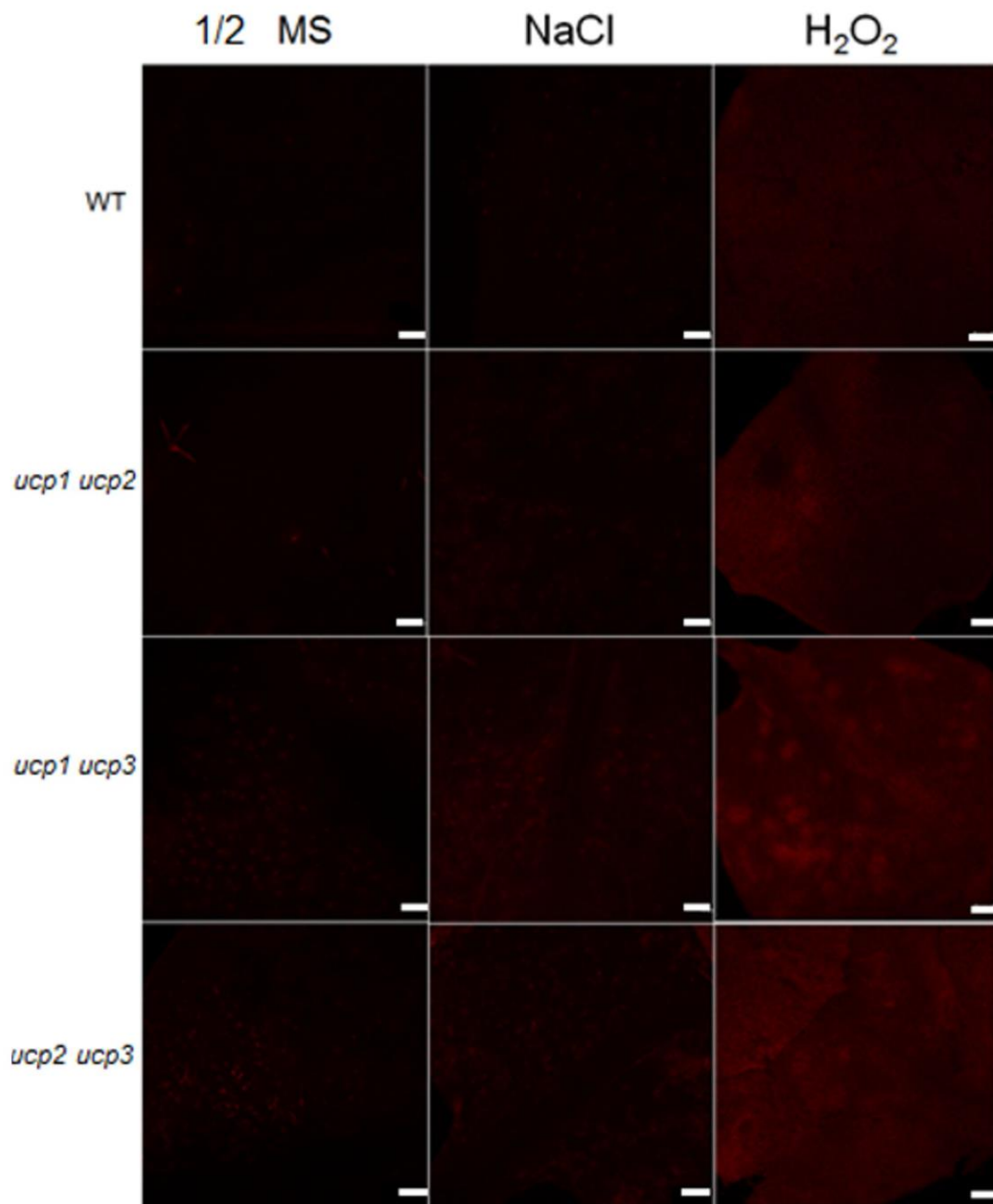


Fig. S2. Mitochondrial superoxide (O_2^-) accumulation in leaves of wild-type (WT) Col-0 and *ucp* double mutant plants (21-day-old). The leaves were incubated in $\frac{1}{2}$ MS liquid medium without supplementation (first column) or supplemented with 125 mM NaCl (middle column) and 10 mM hydrogen peroxide (last column) for 20 h. The tissues were stained with MitoSOX Red and visualized in a Leica TCS SP5 laser scanning confocal microscope. Representative confocal images from three independent assays are shown. Scale bar = 100 μ m.

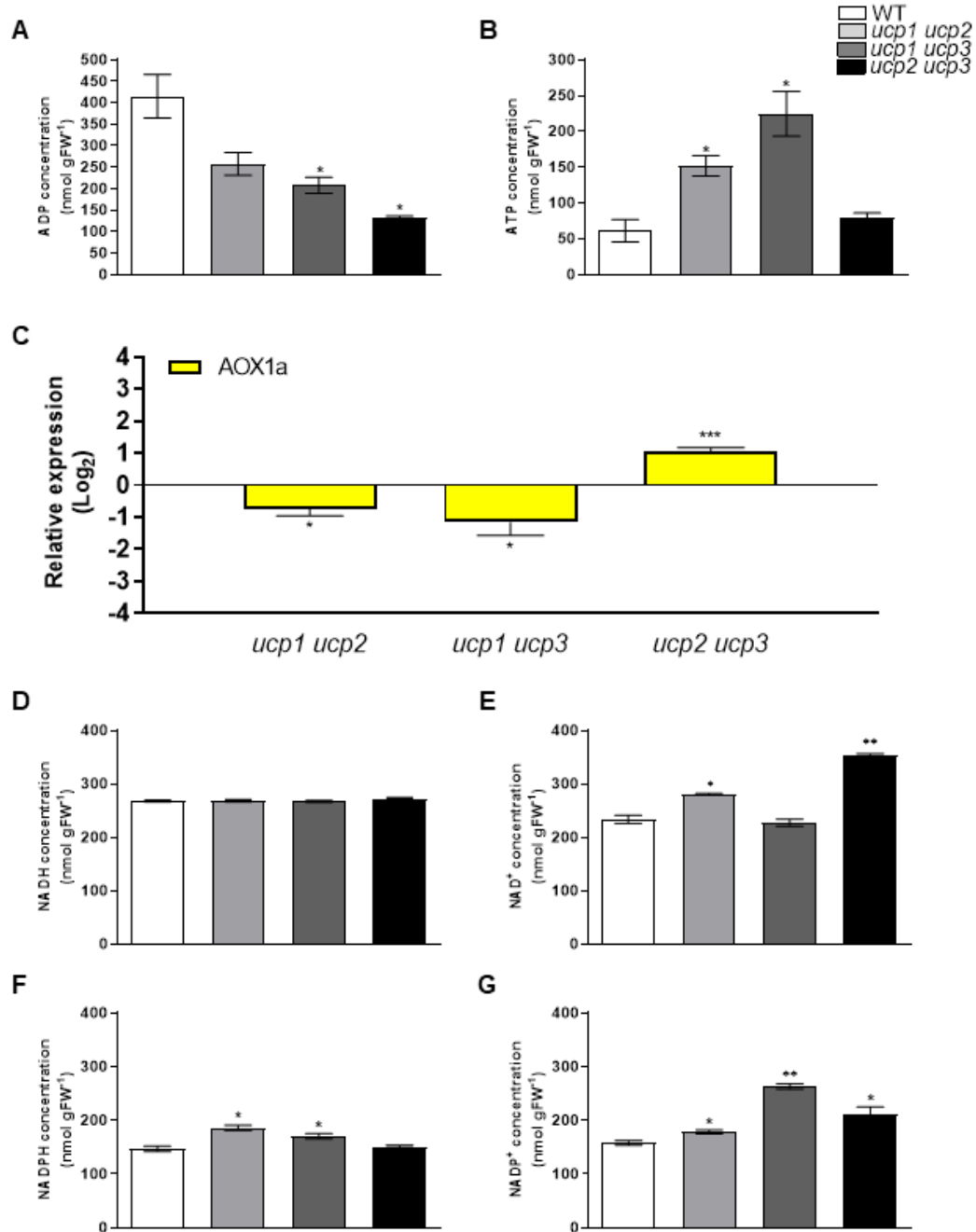


Fig. S3. Levels of ADP, ATP, NADH, NAD⁺, NADPH, NADP⁺ and relative expression of *AOX1a* gene in the *ucp* double mutants. (A) ADP and (B) ATP levels in wild-type (WT) Col-0 and *ucp* double mutant plants (21-day-old). (C) Relative expression (log₂) of *AOX1a* in each double mutant. *GAPDH* was used as endogenous control and the expression of the target genes in WT plants was employed as calibrator (expression arbitrarily set to zero). (D) NADH, (E) NAD⁺, (F) NADPH and (G) NADP⁺ levels in WT and *ucp* double mutant plants (21-day-old). The bars represent the means with their respective standard errors (\pm SE) from three biological replicates per genotype. Asterisks denote significant differences when compared with WT (* p <0.05, ** p <0.005 and *** p <0.0005).

Capítulo II

O capítulo II corresponde ao manuscrito intitulado “**Effects of Mitochondrial Disturbances on Transcriptional and Metabolite Profiles of *Arabidopsis ucp* double mutant plants**” que será submetido ao periódico *International Journal of Molecular Science*. O manuscrito disponibiliza os dados de RNA-Seq de plantas do duplo-mutante *atucp1/atucp3*, o qual foi escolhido com base nos dados de fenotipagem descritos no Capítulo I. Adicionalmente, foram empreendidas análises comparativas de predição em *datasets* de transcriptoma de plantas do tipo selvagem Col-0. Paralelamente, os resultados relativos às análises de metabólitos em plantas inteiras dos três duplo-mutantes em comparação com o selvagem são relatados.

Effects of Mitochondrial Disturbances on Transcriptional and Metabolite Profiles of *Arabidopsis ucp* double mutant plants

Rômulo P. M. Lima^{1*}, Jakeline Santos Oliveira², Leandro Costa do Nascimento³, Mônica Teresa Veneziano Labate⁴, Carlos Alberto Labate⁴, Pedro Barreto¹, Ivan de Godoy Maia^{1*}

¹Departamento de Ciências Químicas e Biológicas (Setor Genética), Instituto de Biociências, UNESP, CEP 18618-689, Botucatu, SP, Brasil

²Departamento de Biologia Estrutural e Funcional (Setor Fisiologia) Instituto de Biociências, UNESP, CEP 18618-689, Botucatu, SP, Brasil

³Laboratório de Genômica e Expressão, Instituto de Biologia, UNICAMP, CEP 13083-970, Campinas, SP, Brasil

⁴Departamento de Genética, Escola Superior de Agricultura “Luiz de Queiroz”, USP, CEP 13418-260, Piracicaba, SP, Brasil

*Correspondence: romulo.lima@unesp.br (Brazil); ivan.maia@unesp.br (Brazil); Tel.: +55-14-99121-6611; +55-14-3880-0363

Abstract

Three genes encoding mitochondrial uncoupling proteins (UCPs) have been described in *Arabidopsis thaliana* (*UCP1* to *UCP3*). In plants, they are characterized as regulators of oxidative stress, and, for instance, much of the biological data were obtained for the *UCP1* and *UCP2* isoforms compared with *UCP3*. To gain further insights, we investigated the transcriptome profiles of *ucp1 ucp3* double mutant plants and evaluated the metabolome of all three types of *ucp* double mutants (*ucp1 ucp2*, *ucp1 ucp3* and *ucp2 ucp3*) during vegetative phase. We found that the double knockdown of *UCP1* and *UCP3* promotes important transcriptional reprogramming with clear alterations in the expression of genes related to mitochondrial and chloroplast function as well as those responsive to abiotic stress, suggesting that profound disturbances occur throughout the cell. The comparison of our transcriptome data with the selected dataset of wild-type *A. thaliana* in the same growth conditions reinforces the impacts caused throughout the cell, respectively. The observed changes in the transcriptome were well correlated with the metabolomic data, which detected alterations in various

metabolites related to primary and secondary metabolisms in the *ucp* double mutants. These findings support a better elucidation for effects of *UCP* genes and provide insights into the role of UCP3 isoform together with UCP1 in the entire plant.

Keywords: uncoupling protein, double mutant, mitochondria, chloroplast, abiotic stress, transcriptome comparison, metabolomics, functional role

INTRODUCTION

The mitochondrial uncoupling process that facilitates the reentry of protons into the mitochondrial matrix independent of ATP synthesis is mediated by a class of proteins present in the mitochondrial inner membrane called mitochondrial uncoupling proteins (UCPs) (Maxwell et al., 1999; Nicholls, 2001; Vercesi et al., 2006). Currently, phylogenetic, functional and genome sequencing analysis revealed the presence a small multigene family (*UCP1*, *UCP2* e *UCP3*) in the model plant *Arabidopsis thaliana* (Borecký et al., 2006; Palmieri et al., 2008). Just like other energy-dissipating proteins present in the plant mitochondria, such as the Alternative oxidase (AOX) and NADH dehydrogenase (NADH-D), UCP-mediated mild uncoupling have been implicated in the control of reactive oxygen species (ROS) production and protection against oxidative stress (Maxwell et al., 1999; Brandalise et al., 2003; Smith et al., 2004).

Due to their action on ROS homeostasis, plant UCPs are able to promote tolerance to different abiotic and biotic stresses, such as salt, drought, heat, hypoxia, turnip crinkle virus and *Botrytis cinerea* infections (Begcy et al., 2011; Figueira & Arruda, 2011; Chen et al., 2013; Barreto et al., 2015; Pu et al., 2016). Additionally, UCP has previously been shown to play a role in the maintenance of cellular redox balance (Chen et al., 2014; Lima et al., submitted), in sustaining photosynthesis and photorespiration through a crosstalk with the chloroplast (Chen et al., 2013; Chen et al., 2014; Lima et al., submitted), in retrograde communication (Brandalise et al., 2003; Begcy et al., 2011; Barreto et al., 2014) and in the transport of metabolites across the inner mitochondrial membrane (Monné et al., 2018).

Despite the known existence of three *UCP* genes in *A. thaliana*, to date, much of the relevant functional data was obtained using the *UCP1* gene as a model, with few studies demonstrating the role and physiological relevance of the other two isoforms. Arcuri et al. (2021) characterized and investigated the phenotypes of single-insertion

mutants for two of these isoforms (UCP1 and UCP2). Among the results obtained, the data support a role of these genes in vegetative development and overall plant fertility, with the *ucp2* single mutant showing clear changes in energy metabolism and very contrasting phenotypes, such as reduction in the number of leaves, delay in flowering and increased number of sterile siliques. An additional study using double-insertion mutants (*ucp1 ucp2*, *ucp1 ucp3* and *ucp2 ucp3*) revealed that UCP2 and UCP3 act in concert with UCP1 during vegetative and reproductive development, thus suggesting a partial redundancy between these isoforms (Lima et al., submitted). Interestingly, the double knockdown of *UCP1* and *UCP3* (Lima et al. submitted) produced the most evident phenotypes in plants at 21-day-old, with clear reductions in the number of leaves and water content, as well as significant changes in photosynthetic efficiency and energy metabolism.

Data from previous studies that sought to investigate alterations in the transcriptome of transgenic tobacco plants overexpressing *UCP1* revealed significant changes in the expression of genes related to energy metabolism, photosynthesis, photorespiration and redox homeostasis (Laitz et al., 2015) as well as a broad induction of genes associated with abiotic and biotic stress responses, in special those implicated in response to hypoxia (low oxygen) (Barreto et al., 2014; Barreto et al., 2015). In line, the metabolic profiling of these UCP1-overexpressing plants revealed a strong accumulation of metabolites related to hypoxia adaptation (e.g., alanine, TCA intermediates) similarly to that found in wild-type plants under hypoxic conditions (Barreto et al., 2015). In fact, an UCP1-mediated retrograde signaling that influences nuclear response to hypoxia through the inhibition of the oxygen sensing pathway has been recently described (Barreto et al., 2022).

Considering the lack of information of the potential role of UCP3 *in planta*, we employed an *A. thaliana ucp1 ucp3* double insertion mutant, which showed a clear phenotype during the vegetative growth (Lima et al. submitted), to assess the transcriptomic alterations associated with this combined genetic defect. In addition, a metabolite profile was carried out using all three types of *ucp* double mutants (*ucp1 ucp2*, *ucp1 ucp3* and *ucp2 ucp3*) generated by Lima et al. (submitted). Clear alterations were observed in genes related to chloroplast, mitochondria and response to abiotic stresses, while there were several changes in the accumulation of metabolites related to primary (amino acids, organic acids, sugars and nucleic acid compounds) and

secondary metabolisms. Our results highlight that the double knockdown of *UCP* genes promotes important disturbances throughout the cell and extends knowledge of underlying roles played by the *UCP3* gene at the entire plant.

RESULTS

Illumina RNA-Seq and functional annotation of differentially expressed genes (DEGs) by the double knockdown of *UCP1* and *UCP3* genes in plants

RNA-Seq experiment was performed to evaluate the global transcriptional changes associated with the double knockdown of *UCP1* and *UCP3* compared with WT control plants. Overall, the normalized count data from samples were used to verify the biological variability between them by Principal Component Analysis (PCA). As shown in Figure 1A, according to PCA, control (pink circles) and mutant (blue circles) sample groups showed distinctive global expression profiles. The first component (PC1) accounted for 63% of the variance and visibly separated the samples by treatment (control x mutant). Except for one out of three control samples, all samples from the same group clustered together. Volcano plot from the RNA-Seq analysis demonstrated a wide deregulation in the two directions (up- and downregulation) in plants of the *ucp1 ucp3* double mutant (Figure 1B). In fact, 668 differentially expressed genes (DEGs) were detected using DESeq2 package and defined by $P_{adj} < 0.1$. Among them, 356 DEGs were upregulated (Table S2A), while 312 downregulated (Table S2B) (Figure 1C).

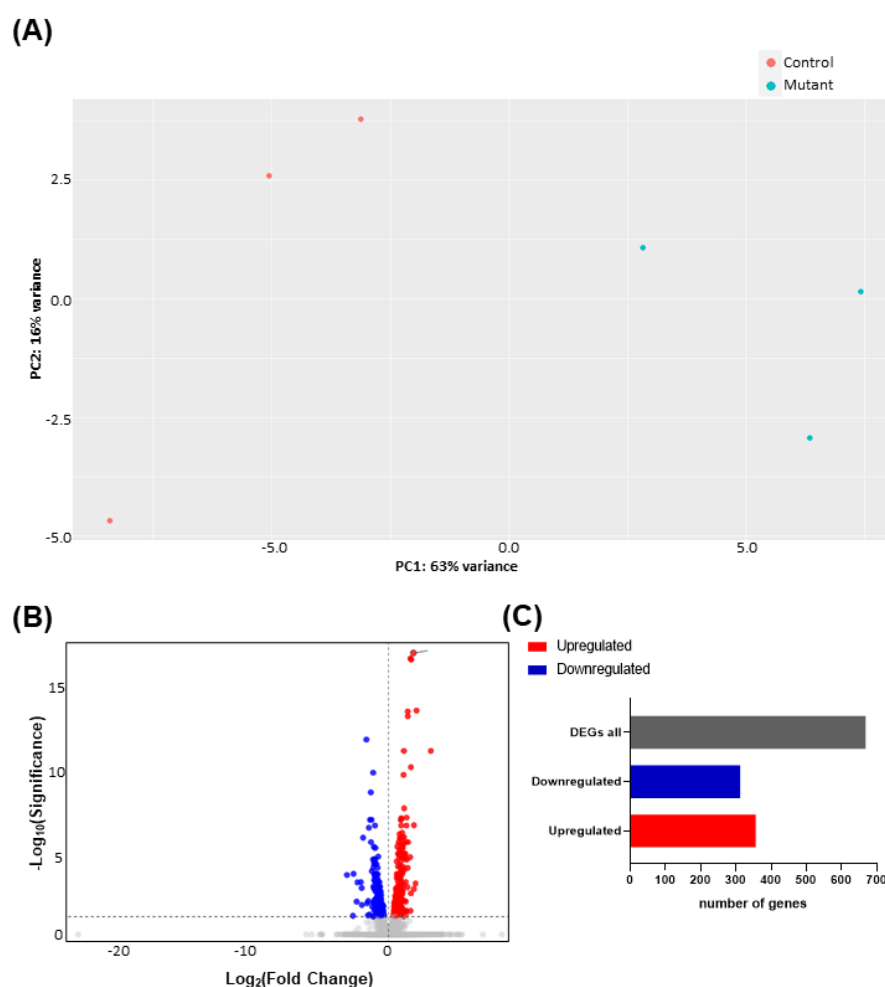


Figure 1. Overview of the *Arabidopsis thaliana ucp1 ucp3* double mutant transcriptome. (A) PCA of normalized count data from control (WT) and mutant (*ucp1 ucp3*) samples. (B) Volcano plot of negative log-transformed Padj ($-\log_{10}\text{Padj}$) and $\log_2(\text{Fold Change})$ for each gene in *ucp1 ucp3* plants compared with WT control. (C) Number of DEGs all, up- and downregulated DEGs in *ucp1 ucp3* plants (21-day-old) compared with WT control. DEGs were identified using DESeq2 package and defined by $\text{Padj} < 0.1$. Up- and downregulated DEGs are shown in red and blue, respectively. WT: wild-type; PCA: Principal Component Analysis; Padj: adjusted p-value; DEG: differentially expressed gene.

To elucidate potential gene functions, a functional annotation of the DEGs was carried out against the GO and KEGG databases using DAVID. According to the GO analysis (corrected p-value ≤ 0.05), the upregulated mutant-related DEGs were assigned to 24 GO biological process (BP) terms (Figure S1A), seven GO molecular function (MF) terms (Figure S1B) and 23 GO cellular component (CC) terms (Figure S1C). In contrast, a total of eight GO BP terms (Figure S2A), four GO MF terms (Figure S2B) and 24 GO CC terms (Figure S2C) were significantly observed for the downregulated mutant-related DEGs. The BP and CC categories had the highest number of terms for both directions, with emphasis on CC that had representative

number of DEGs associated with terms in both up- and downregulated directions. In the CC category, the ontologies 'chloroplast', 'plasma membrane', 'plasmodesma' and 'chloroplast envelope' were assigned for both up- and downregulated DEGs, with no other GO category having common terms for both directions. The most highly represented ontologies among the upregulated DEGs were 'response to abscisic acid', 'protein binding' and 'chloroplast', respectively, while 'response to cadmium ion', 'ATP binding' and 'chloroplast', respectively, figured among the downregulated DEGs.

Overall, the generated data indicate that the observed DEGs are mainly involved in abiotic stress responses and they drastically impact important molecular processes (e.g., transcription, translation, splicing), as well as the chloroplastic metabolism and cell energy production. The great number of DEGs associated with the CC term 'chloroplast' (first place both up and down) and the concomitant enrichment of GO terms related to the chloroplast clearly illustrate that the double knockdown of *UCP1* and *UCP3* during the vegetative phase remotely and markedly affected the chloroplast organelle.

KEGG analysis (corrected p-value ≤ 0.05) demonstrated that the up- and downregulated DEGs enriched in *ucp1 ucp3* plants were assigned to three and two KEGG pathways, respectively (Figures S1D and S2D). 'Photosynthesis – antenna proteins' (13 DEGs), 'photosynthesis' (night DEGs) and 'alpha-Linolenic acid metabolism' (six DEGs) were the pathways associated with the upregulated genes, while 'protein processing in endoplasmic reticulum' (14 DEGs) and 'ribosome biogenesis in eukaryotes' (10 DEGs) were those associated with the downregulated. Thus, the most representative pathways associated with the upregulated DEGs are related to the photosynthetic process and to the chloroplast, which is consistent with the GO analysis. In contrast, the over-represented pathways for the downregulated DEGs were related to the endoplasmic reticulum and its quality control in protein processing within cells. These data reinforce that the double knockdown of *UCP1* and *UCP3* during vegetative phase engages a cross-talk between the mitochondria and other cellular compartments, such as the chloroplast and the endoplasmic reticulum, and it produces effects throughout the cell.

The top 30 functions associated with the identified DEGs are shown in Figure 2A. Among them, 17 were associated to GO CC, ten to GO BP, two to GO MF and one to KEGG pathway. Overall, an overrepresentation of terms associated with the

chloroplast and DNA metabolism, plant response to abiotic stress and other cellular components, such as vacuole, cell wall, nucleolus and ribosome was observed. The DEGs assigned to all GO categories or related to the KEGG pathway 'photosynthesis – antenna proteins' in the upregulated direction demonstrate a coordinated plastid-related expression, which highlights the importance of the UCP activity in the cross-talk between mitochondria and chloroplast. In contrast, in the downregulated direction the most prominent terms were associated with the nucleolus and related to basic processes such as ribosome and protein folding and DNA metabolism. Interestingly, the CC GO analysis revealed that most of the upregulated DEGs encode membrane proteins, such as those located in the chloroplast thylakoid, while the downregulated DEGs encode inner space proteins, such as those located in cytosol and the chloroplast stroma.

Consistent with the enrichment analysis shown in Figure 2A, the upregulated DEGs enriched in at least two terms and pathways (13 in total) were associated with the pathway 'photosynthesis – antenna proteins' (Figure 2B). All of them are members of the light-harvesting complexes (LHCs), a modular antenna system which constitute the photosynthetic apparatus in plants. The LHC protein superfamily contributes to the photosynthetic antenna complexes of Photosystems I (LHCIs) and II (LHCIIIs) (Leister & Schneider, 2003). Likewise, CAB proteins are components of LHCIIIs and play a role in maintaining the structure of the thylakoid membrane, as well as in transmission and distribution of the energy to PSI and PSII reaction centers (Liu et al., 2008; Wei et al., 2016). Among the most enriched downregulated DEGs (3 in total), two of them (*BIP2* and *mtHsc70-1*), which are members of the of the 70-kD heat shock proteins (HSP70s) multigene family, are associated with the pathway 'protein processing in endoplasmic reticulum'. HSP70s are induced by plants in response to heat stress and play in the chaperone network a key role that controls cellular protein processes, such as protein translocation, folding and refolding (Kampinga & Craig, 2010). Protein-Protein Interaction (PPI) networks of these key components were built via STRING analysis to clarify the interconnections among them. The results showed that the 13 antenna proteins were highly clustered, with evidences of non-centrality by the predicted functional relationship between them. On the other hand, the three heat shock proteins formed another clustered interaction network having *BIP2*, which is the only one that interacts with the other two proteins, as central protein (Figure 2C). *BIP2* plays an

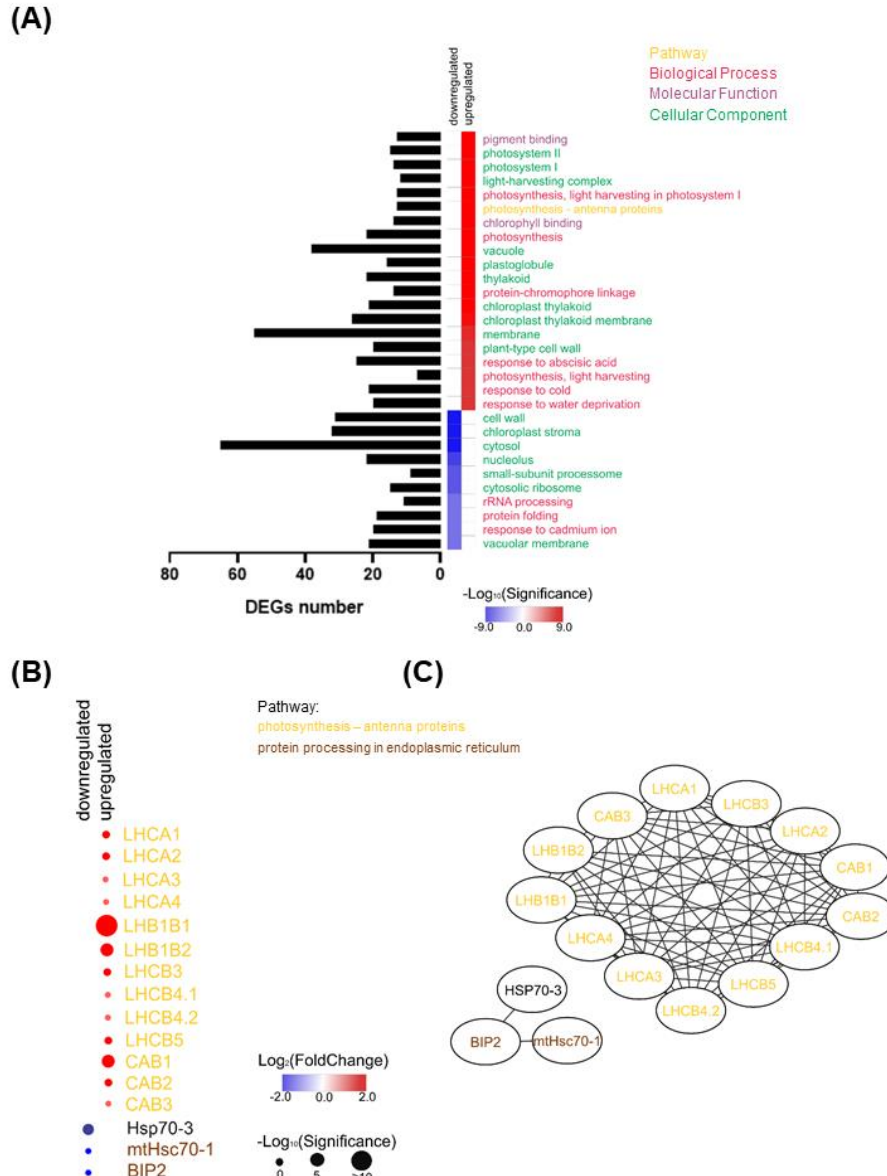


Figure 2. Functions and components of the *ucp1 ucp3* double mutant transcriptome. (A) The top 30 functions from up- (right column in red) and downregulated (left column in blue) DEGs significantly enriched in the *ucp1 ucp3* plants (21-day-old) compared with WT. Names to the right of the heatmap are colored according to the DAVID bioinformatics resources 6.8: Kyoto Encyclopedia of Genes and Genomes (KEGG), GO Biological Process, GO Molecular Function and GO Cellular Component. The intensity of the color in the heatmap indicates the enrichment significance (corrected p-value) by the Benjamini-Hochberg test correction, in which the most significant GO terms or KEGG pathways from each directional regulation are shown by the $-\text{Log}_{10}p \geq 4$ filter and excluding common ones. Horizontal bars plot to the left of the heatmap depicts the DEGs number (black bars) for each GO term or KEGG pathway. (B) A heat-scatter plot showing $\text{Log}_2(\text{Fold Change})$ values and corresponding negative log-transformed Padj ($-\text{Log}_{10}\text{Padj}$) for the 16 DEGs most enriched in the *ucp1 ucp3* plants compared with WT. Up- and downregulated DEGs are shown in red and

blue, respectively. The color and size of the circles correspond to the $\text{Log}_2(\text{Fold Change})$ and $-\text{Log}_{10}\text{Padj}$ values, respectively, from the RNA-Seq data. The DEG names are colored according to the KEGG pathway. **(C)** PPI networks retrieved from STRING database of the up- and downregulated DEGs most enriched in the *ucp1 ucp3* plants compared with WT. Network-predicted interactions are adjusted by the Cytoscape software v. 3.8.2 and filtered with high confidence (0.700) from STRING. WT: wild-type; DEG: differentially expressed gene; p: corrected p-value; Padj: adjusted p-value; PPI: protein-protein interactions; STRING: search tool for recurring instances of neighboring genes.

Major metabolic pathways associated with the DEGs between *ucp1 ucp3* plants and WT

The resulting 668 DEGs were then mapped against the *A. thaliana* major metabolic pathways (Figure 3). The DEGs mapped into carbon fixation process related to photosynthesis light reactions were mostly upregulated in mutant plants (Figure 3). This is in line with our previous enrichment analysis shown in Figure 2 that revealed an intense upregulation of the pathway ‘photosynthesis – antenna proteins’. Furthermore, the pathways related to lipid, carbon (starch and sucrose synthesis) and cell wall metabolisms were predominantly associated with upregulated DEGs. On the other hand, there were some metabolic pathways, such as amino acid (AA), energy [oxidative pentose phosphate (OPP) and tricarboxylic acid cycle (TCA)] and secondary metabolisms, with up- and downregulated DEGs in the same proportion, showing transcriptional response for both directions (Figure 3). In order to visualize the impacts in the mitochondrial metabolism, a MapMan overview of the transcriptome related to mitochondrial electron transport chain and metabolite transporters was also performed (Figure S3). We found a total of seven DEGs mapped into this pathway being most of them downregulated. Among them, we observed *AOX1a*, which is involved in alternative respiratory pathway, genes encoding solute and dicarboxylate transporters (*AT3G51870* and *DiT1*), and members of the *UCP* family (*UCP1* and *UCP3*). In contrast, only two genes, *UCP2* and another metabolite transporter (*AT3G62650*), were upregulated.

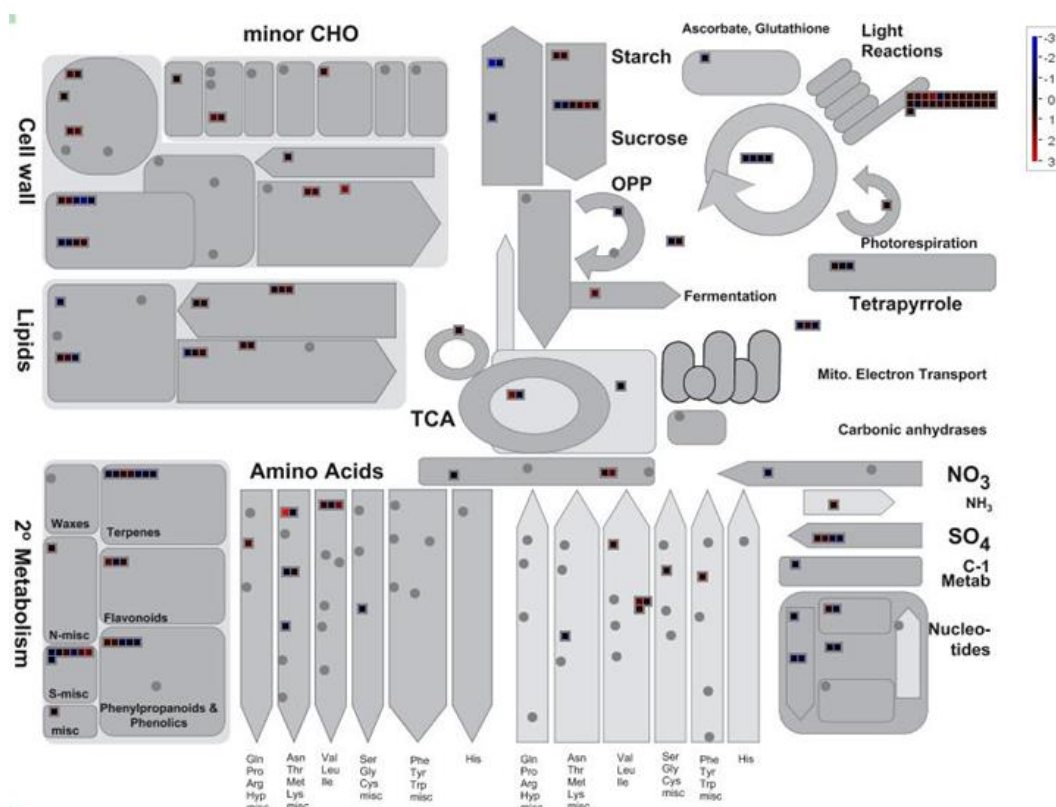


Figure 3. Metabolic overview of the *ucp1 ucp3* double mutant transcriptome. The 668 DEGs ($P_{adj} < 0.1$) were used against the *Arabidopsis thaliana* major metabolic pathways. The $\text{Log}_2(\text{Fold Change})$ values for each up- and downregulated DEG detected by MapMan analysis were plotted onto boxes. Red and blue boxes indicate up- and downregulated DEGs, respectively. DEG: differentially expressed gene; P_{adj} : adjusted p-value.

The double knockdown of *UCP1* and *UCP3* genes alters a coordinated gene network related to chloroplast and mitochondria organelles during vegetative phase

Interestingly, the GO and KEGG enrichment analysis showed several up- and downregulated DEGs functionally associated to chloroplastic metabolism in the *ucp1 ucp3* plants (Figures S1 and S2). To get further insights, we analyzed the functional annotation (according to metabolic type and process) as well as the expression of the DEGs exclusively associated with the GO term chloroplast (GO:0009507). When the 93 upregulated DEGs were functionally analyzed (Table S3), two major groups were detected: one assembling of genes related to photosynthetic process (28%) and a second grouping of genes associated with carbon and AA metabolism (27%). The other representative categories of metabolic type and process were transport activity (13%), DNA metabolism (11%) and plant growth, development and response to stress (11%), while three minor groups each corresponded to less than 10% of the total

(Figure 4A). In the other direction, among the 123 downregulated DEGs analyzed (Table S3), a major group assembling of genes involved in DNA metabolism (50%) was observed. The other representative categories were carbon and AA metabolism (16%), transport activity (7%), unknown function (7%), secondary metabolism (6%) and signaling pathway (5%), while three minor groups each corresponded to less than 5% of the total (Figure 4A). Overall, these results are consistent with the enrichment analysis shown in Figure 2A, especially in relation to the major groups of each direction.

Motivated by the large number of deregulated DEGs in both directions associated with the CC chloroplast that appeared in our RNA-Seq data, we performed further functional analysis using the top ten up- and downregulated chloroplast-related DEGs for each metabolic type and process, excluding ‘Photosynthesis’, ‘Plant growth, development and response to stress’ and ‘Unknown’. This revealed that the majority of the highly upregulated chloroplast-related transcripts was involved in three major groups related to carbon and AA metabolism, transport activity and DNA metabolism, respectively (Figure 4B). Regarding their function, the majority of the top ten genes related to carbon and AA metabolism is associated with the BP ‘tryptophan and carbohydrate metabolic process’ (*BGLU18*, *TGG2*, *TSA1*, *TGG1* and *CYP79B3*). With respect to transport activity and DNA metabolism, we observed transcripts associated with the BP functions water transport (*DELTA-TIP*, *PIP1C*, *TIP2;2*, *TIP2* and *PIP1B*) and purine metabolism (*APS3* and *APS4*), respectively. The minor groups corresponded to genes that participate in lipid metabolism and signaling pathway, fatty acid biosynthetic process (*FATB* and *FAD3*) and proteolysis (*IAR3* and *RD21A*), respectively. Some of the upregulated chloroplast-related transcripts were also associated with the MF terms structural constituent of ribosome (*AT5G24490*), glutamyl-tRNA reductase activity (*HEMA1*) and ATP binding (*ERD1* and *CAC3*). Interestingly, the most highly expressed genes of each major group were *BGLU18* and *TGG2* (Figure 4B), which encode “atypical” and classical thioglucosidases, respectively (Nakano et al., 2017; Meier et al., 2019). Subsequently, we found genes encoding plant aquaporins with high interaction *DELTA-TIP* and *PIP1C* (Chaumont et al., 2000; Gawwad et al., 2013), as well as *AT2G29670* and *AT5G24490*, which are involved in two closely related transcriptional processes. The induced expression of the mentioned genes is indicative of imbalances on primary metabolism, water

transport system and transcription process promoted by the double knockdown of *UCP1* and *UCP3*.

On the other hand, most of the significantly downregulated chloroplast-related DEGs were equally associated with the three major groups observed for the upregulated genes (Figure 4B). The other representative categories of metabolic type and process were transcripts involved to signaling pathway (six genes) and secondary metabolism (seven genes). Many of the downregulated transcripts associated with carbon and AA metabolism were related to the BP 'cysteine metabolic process' (*APR2*, *APR3* and *MS2*) and the pathway 'protein processing in endoplasmic reticulum' (*PDIL2-2* and *PDIL1-2*). With respect to DNA metabolism, four genes (*Hsp70-3*, *AT2G37690*, *AT1G56050* and *Cpn60beta2*) were associated with the MF 'ATP binding' and three (*AT4G30825*, *AT5G02830* and *cpHsc70-2*) with 'protein processing in endoplasmic reticulum'. The other major group of transport activity encompassed genes with a diversity of functions, including two transmembrane transport genes (*EAAC* and *AT5G43745*) and one (*UCP1*) related to mitochondrial transport. In parallel, many of the genes related to signaling pathway were associated with the BPs 'proteolysis' (*SPPA*, *T12E18_90* and *EMB3144*) and 'signal transduction' (*GUN1* and *ROC3*), while those related to secondary metabolism with the pathway 'terpenoid biosynthesis' (*HPT1*, *ABC4* and *GGPS1*). The top-ranking downregulated chloroplast-related DEGs of each major group were *APR2*, which encodes a protein involved with cysteine synthesis for cell sulfur homeostasis (Birke et al., 2015), *Hsp70-3*, encoding a heat shock protein (Kampinga & Craig, 2010), *AAC2*, encoding an isoform of the mitochondrial adenylate carrier involved in redox energy balance, photosynthesis and photorespiration (Palmieri et al., 2011), *SPPA*, encoding a component of the chloroplast proteolytic machinery from *A. thaliana* (Lensch et al., 2001), and *CYP706A6*, a member of the plant *CYP* family associated with the flavonoid biosynthetic pathways (Yonekura-Sakakibara et al., 2019) (Figure 4B). Overall, these results revealed a wide range of impaired processes on primary (e.g., sulfur and energy balance, chloroplastic protein degradation, crosstalk between mitochondria and chloroplast) and secondary (e.g., terpenoid and flavonoid biosynthesis) metabolisms.

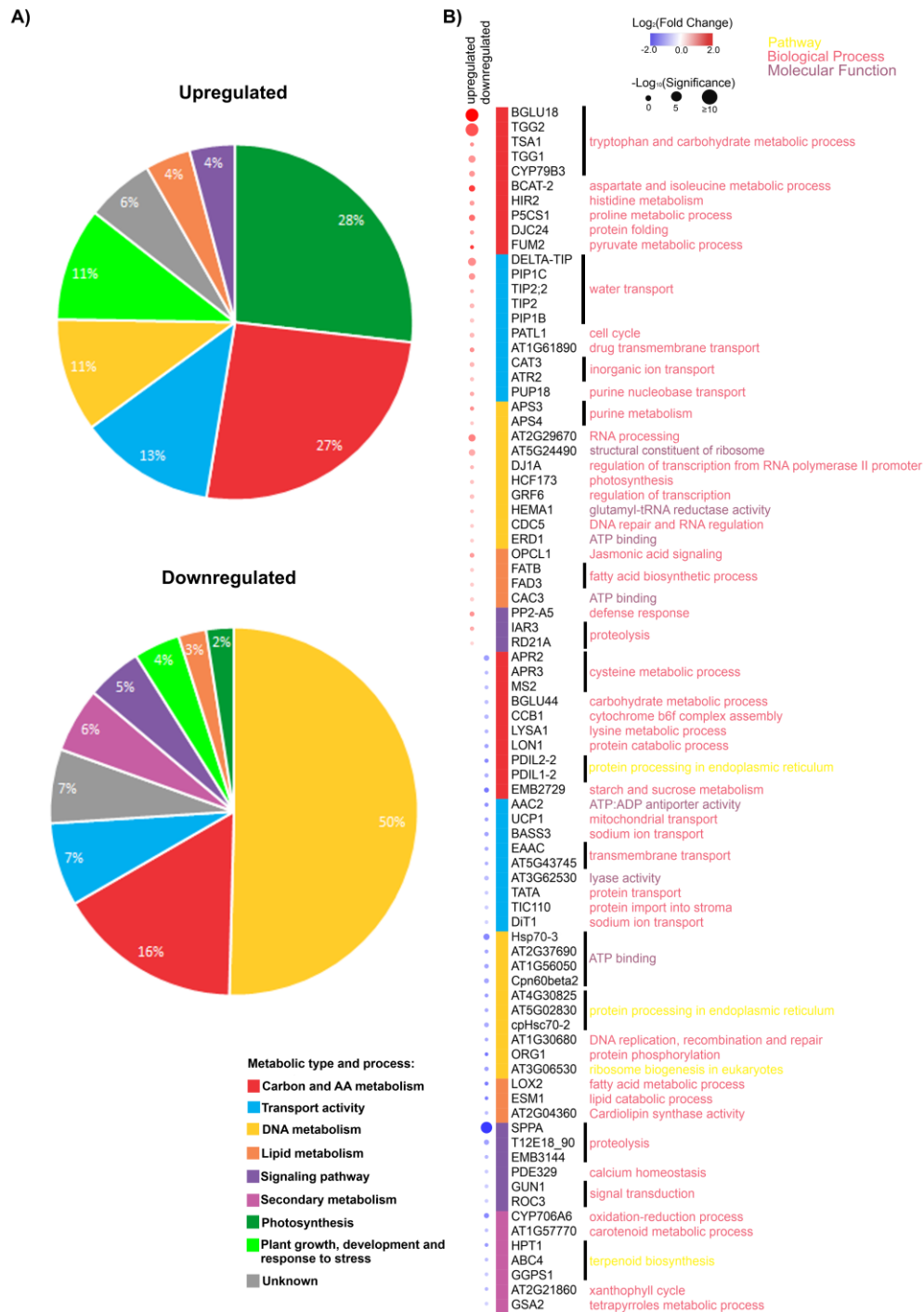


Figure 4. Impacts of the *UCP1* and *UCP3* double knockdown on the chloroplast. **(A)** Pie charts demonstrating the distribution of the metabolic type and process from a total of 216 up- and downregulated chloroplast-related DEGs. These DEGs were identified from GO enrichment analysis of the cellular component (CC) term 'chloroplast' (GO:0009507) using a corrected $p(\text{Benjamini-Hochberg}) \leq 0.05$. **(B)** A heat-scatter plot showing the top ten up- or downregulated chloroplast-related DEGs for each metabolic type and process, excluding 'Photosynthesis', 'Plant growth, development and response to stress' and 'Unknown'. The color and size of the circles correspond to the $\text{Log}_2(\text{Fold Change})$ and $-\text{Log}_{10}(\text{Padj})$ values, respectively, from the RNA-Seq data. The colored column to the left of the DEGs follows the same legend for each metabolic type and process in pie charts. Names to the right of the DEGs are colored according to the enrichment analysis for each one performed using DAVID:

Kyoto Encyclopedia of Genes and Genomes (KEGG), GO Biological Process and GO Molecular Function. Similar DEG functions are indicated with a black line. DEG: differentially expressed gene; Padj: adjusted p-value.

The aforementioned analysis was subsequently performed to investigate the possible impacts of the double knockdown on mitochondria. For that, the DEGs associated with the GO term mitochondria (GO: 0005739) were employed. The results revealed that only one direction was strongly affected, with 55 mitochondrial-related genes being downregulated (Table S4). One major group assembling genes related to DNA metabolism (51%) was detected. The other representative groups were carbon and AA metabolism (16%), transport activity (13%), signaling pathway (7%) and plant growth, development and response to stress (5%), while three minor groups each corresponded to less than 5% of the total (Figure 5A). Overall, these results are consistent with the enrichment analysis for the downregulated chloroplast-related DEGs shown in Figure 2A and Figure 4A. Additional functional analysis using the top ten downregulated mitochondrial-related DEGs for each metabolic type and process, excluding 'Plant growth, development and response to stress' and 'Unknown', revealed that the majority was associated with carbon and AA metabolism, transport activity and DNA metabolism (Figure 5B). The other categories of metabolic type and process encompassed transcripts associated to signaling pathways (four genes), cellular respiration (two genes) and secondary metabolism (one gene). Regarding their function, many of the downregulated transcripts associated with DNA metabolism were related to the pathway 'protein processing in endoplasmic reticulum' (*AT4G30825*, *AT5G02830* and *CNX1*) and the MF 'ATP binding' (*AT2G37690*, *Cpn60beta2* and *SYCO ARATH*). The other major group carbon and AA metabolism encompassed genes with a variety of functions, including two genes for the BP 'carbohydrate and malate metabolic process' (*MDH* and *mMDH1*). With respect to transport activity, two expected genes (*UCP1* and *UCP3*) were involved to BP 'mitochondrial transport' and two (*EAAC* and *K15C23.2*) with the BP 'transmembrane transport'. Gene functions related to MF 'mitochondrial ribosome binding' and BPs 'proteolysis', 'protein phosphorylation' and 'calcium homeostasis' were markedly affected highlighting the role of mitochondria as a signaling organelle. Alterations in secondary metabolism associated with 'carotenoid metabolic process' were also observed. In addition, the expression of two genes (*AOX1A* and *AT4G21105*) encoding proteins involved in

cellular respiration was clearly altered in *ucp1 ucp3* plants compared with WT (Figure 5B).

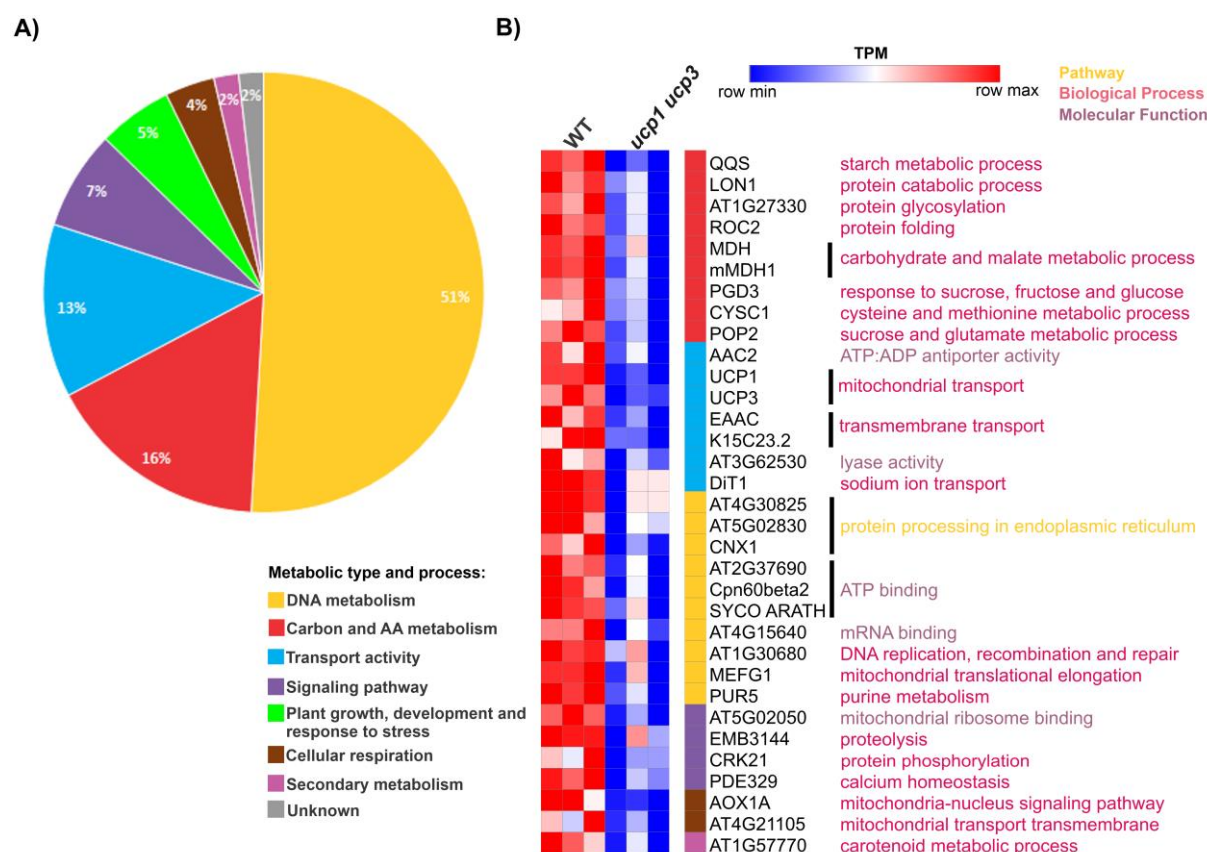


Figure 5. Impacts of the *UCP1* and *UCP3* double knockdown on the mitochondria. (A) A pie chart demonstrating the distribution of the metabolic type and process from a total of 55 downregulated mitochondrial-related DEGs. These DEGs were identified from GO enrichment analysis of cellular component (CC), term 'mitochondria' (GO: 0005739) using a corrected p (Benjamini-Hochberg) ≤ 0.05 . (B) A heatmap showing the top ten downregulated mitochondrial-related DEGs for each metabolic type and process, excluding 'Plant growth, development and response to stress' and 'Unknown'. The expression scale according to TPM data of the three biological replicates per genotype varies from dark blue (downregulation) to dark red (upregulation). The colored column to the left of the DEGs follows the same legend for each metabolic type and process in pie chart. Names to the right of the DEGs are colored according to enrichment analysis for each one performed using DAVID: Kyoto Encyclopedia of Genes and Genomes (KEGG), GO Biological Process and GO Molecular Function. Similar DEG functions are indicated with a black line. DEG: differentially expressed gene; TPM: Transcripts Per Kilobase Million.

Transcriptomic responses to abiotic stress are markedly impacted by the double knockdown of *UCP1* and *UCP3* genes during vegetative phase

Previous studies have demonstrated that the overexpression of *UCP1* in tobacco markedly affected the expression of genes responsive to several abiotic stresses, such as heat, cold, osmotic, water deprivation, hypoxia, salt, oxidative and

cadmium stresses (Barreto et al., 2014; Barreto et al., 2015). Therefore, we decided to investigate whether the double knockdown of *UCP1* and *UCP3* in plants would affect abiotic stress-responsive transcripts as suggested by our GO analysis (Figures S1 and S2). For that, the DEGs of GO terms in the BP category associated with responses to abiotic stress were further investigated. When the 78 upregulated abiotic stress-responsive DEGs were functionally analyzed (Table S5), five major groups encompassing genes responsive to light (37%), water deprivation (28%), cold (28%), salt stress (24%) and oxidative stress (18%) were detected (Figure 6A). Four minor groups were also observed i.e., osmotic stress (8%), all (4%), which corresponds to genes associated with several types of abiotic stress, hypoxia (3%) and heat (1%). On the other hand, we observed three groups encompassing the 24 downregulated abiotic stress-responsive DEGs (Table S5) i.e., heat (17%), cadmium ion (33%) and a major group of both stresses (50%) (Figure 6A). Thus, these results demonstrate different abiotic stress profiles for each expression direction, which is consistent with Figure 2.

Further functional analysis using the top six upregulated and the top ten downregulated abiotic stress-responsive DEGs was performed. Six major groups (light, water deprivation, cold, salt, oxidative and osmotic stress) encompassed each of the top six upregulated abiotic stress-responsive DEGs. The other groups showed transcripts associated to all (four genes), hypoxia (two genes) and heat (one gene) stresses (Figure 6B). Surprisingly, among the 42 upregulated abiotic stress-responsive DEGs shown in the heat-scatter plot, 25 (60%) were associated with abscisic acid (ABA) responsiveness, which is in line with Figure 2. Among the top six upregulated DEGs related with light, we identified three transcripts (*LHB1B1*, *LHB1B2* and *FRO6*) associated with light stimulus, while the other three were involved with light absence (*ASN1*, *ACBP3* and *BCB*) (Figure 6B). The top-ranking upregulated abiotic stress-responsive DEGs of each major group were *LHB1B1*, *LHB1B2* and *ASN1*, the first two belonging to the photosynthetic LHCII and the last one involved in plant nitrogen assimilation, being highly expressed in the absence of light (Lam et al., 2003; Leister & Schneider, 2003). The other genes observed in sequence were: *BGLU18* gene, encoding an endoplasmic reticulum β -glucosidase critical for water deprivation and salt stress (Han et al., 2020), *COR413IM1*, encoding a protein involved in water deprivation and in response to cold stress present in chloroplast inner membrane (Woldesemayat & Ntwasa, 2018), *FUM2*, which encodes a cytosolic fumarase associated with TCA

cycle and responsive to salt treatment (Eprintsev et al., 2021), *SEN1* and the transcription factor *MYC2*, two genes involved in JA signaling and in response to oxidative stress (Schenk et al., 2005; Yoon et al., 2020), and *COR6.6*, a ABA-responsive gene associated with osmotic, cold and salt stresses (Kreps et al., 2002) (Figure 6B). In sum, the RNA-Seq data revealed a wide upregulation of abiotic stress-responsive genes in the *ucp1 ucp3* plants, especially those related with light, water deprivation, cold, salt, oxidative and osmotic stresses.

On the other hand, the RNA-Seq data also revealed a critical downregulation of DEGs involved with cadmium ion and heat stress as also demonstrated in Figure 6B. Of the 22 downregulated abiotic stress-responsive DEGs shown in the heat-scatter plot, ten are exclusively associated with cadmium ion, four with heat and eight with both stresses. Intriguingly, seven of these DEGs are implicated in biotic stress responses, including the transcription factor *WRKY33*, which belongs to the *WRKY* family that modulates numerous host defense responses (Pandey & Somssich, 2009), while ten encode heat shock proteins localized in various compartments (e.g., cytosol, endoplasmic reticulum, mitochondria, chloroplast) and belonging to different families, such as *HSP60* and *HSP70/HSP80* (Al-Whaibi, 2010). In comparison with the upregulation direction, few transcripts encoding abiotic stress-responsive proteins were repressed in *ucp1 ucp3* plants (Figure 6B). Of these, the most significant and lowest expressions of each group detected were *NRT1.8*, a member of nitrate transporter (*NRT1*) family that mediates cadmium tolerance (Li et al., 2010), as well as *Hsp70-2*, *Hsp70-3* and *HSP81-3*, three *HSP* genes which participate in heat stress defense and perform chaperoning functions (e.g., folding and refolding of target proteins) (Swindell et al., 2007). Overall, these results indicate disturbances in heat and cadmium tolerances by the double knockdown of *UCP1* and *UCP3*.

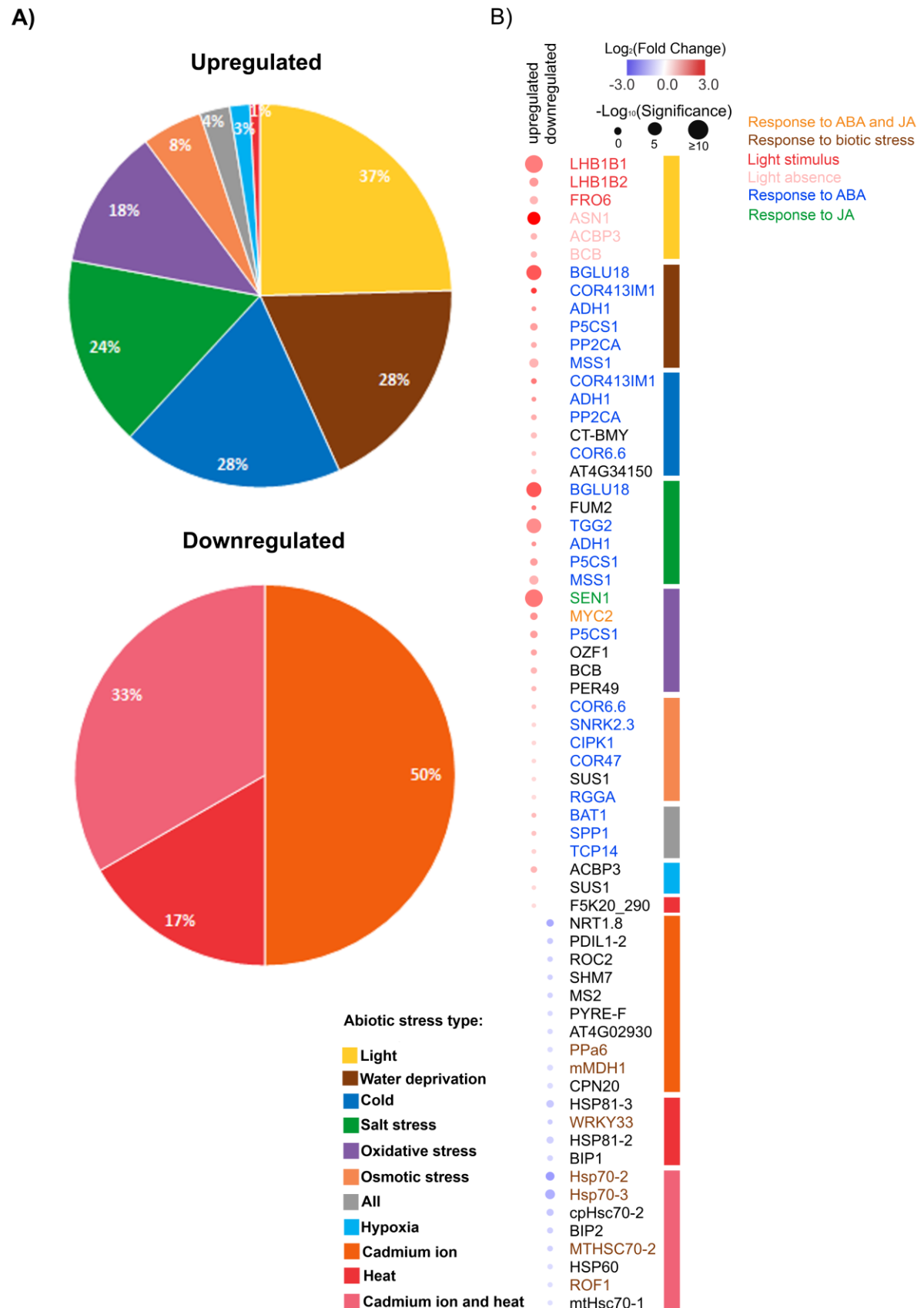


Figure 6. Impacts of the *UCP1* and *UCP3* double knockdown on the expression of abiotic stress-responsive DEGs. (A) Pie charts demonstrating distribution of the metabolic type and process from a total of 102 up- and downregulated abiotic stress-

responsive DEGs. These DEGs were identified using a corrected p (Benjamini-Hochberg) ≤ 0.05 in the DAVID bioinformatics resources 6.8 from GO enrichment analysis of biological process (BP), all terms related to 'abiotic stress'. **(B)** A heat-scatter plot showing at most the top six upregulated and top ten downregulated abiotic stress-responsive DEGs for each type of abiotic stress. The color and size of the circles correspond to the $\text{Log}_2(\text{Fold Change})$ and $-\text{Log}_{10}\text{P}_{\text{adj}}$ values, respectively, from the RNA-Seq data. The colored column to the right of the DEGs follows the same legend for each type of abiotic stress in pie charts. Names of the DEGs are colored according to hormonal signaling or light response type for upregulated DEGs, or type of biotic stress for downregulated DEGs, while DEGs non-classified in this approach are depicted in black. DEG: differentially expressed gene; P_{adj} : adjusted p -value.

TF families impacted by the double mutation of *UCP1* and *UCP3*

Thirty-three TFs representing different families were identified as differentially expressed between mutant and WT (Table S6). Several of them, such as bHLH, bZIP, TCP, AP2-ERF, NAC and WRKY, are known to play regulatory roles in stress response. The over-represented TF families for the upregulated DEGs were bHLH (three members), bZIP (three members), C3H (two members) and TCP (two members), while for the downregulated DEGs were WRKY (five members), NAC (three members), AP2-ERF (two members) and bHLH (two members). The top ten TFs for each direction according to average $\text{Log}_2(\text{Fold Change})$ values are shown in Figure 7A. The top-ranking up- and downregulated DEG TFs were, respectively, WRI4, which belongs to AP2-SHEN family, and NAC047, one of the three repressed members of the NAC family. As shown in Figure 7B, the categorized perturbations (circles) that impacted the expression of these TFs (rectangles) in the same direction as RNA-Seq data was determined using Genevestigator. This allowed the identification of 25 interactions between some of the top ten TFs and different stress conditions. Eleven interactions were detected for five upregulated TFs and six perturbations, three of them related to osmotic stress. In contrast, 14 interactions between seven downregulated TFs and five stress conditions were observed. Among them, five were associated with oxidative and three with salt stress. Interestingly, seven differentially expressed TFs were modulated by cold stress i.e., three upregulated (*ERF2*, *OZF1* and *GRF3*) and four downregulated (*FBH4*, *NAC3*, *HRA1* and *LBD41*). *BZIP9* was the upregulated TF that had the most interactions being induced by heat, hypoxia, light stimulus and biotic stress. In the opposite direction, *NAC3* was downregulated by cold, oxidative, salt and biotic stress (Figure 7B).

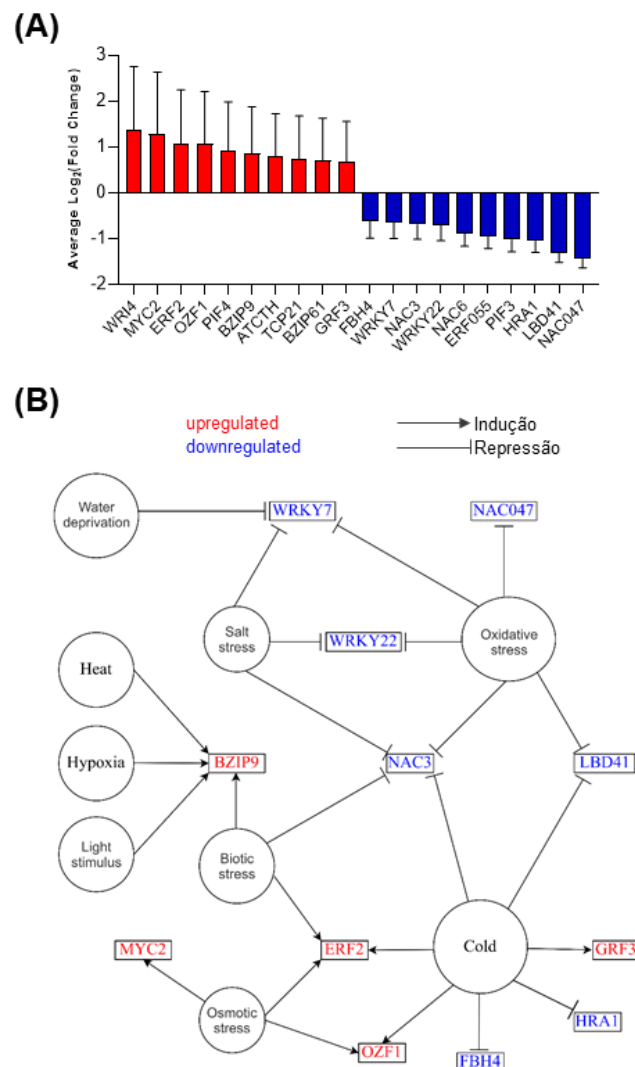


Figure 7. Functional characterization of the transcription factors (TFs) differentially expressed between *ucp1 ucp3* double mutant and WT. (A) Bar plot showing the top ten up- (red bars) or downregulated (blue bars) differentially expressed TFs. The bars represent the means with their respective standard errors (\pm SE) from TPM data in three biological replicates per genotype. (B) Representative diagram demonstrating the categorized perturbations (circles) that impacted the expression of TFs (rectangles) in the same direction. The most up- or downregulated TFs were selected and evaluated using the treatments (perturbations related to light intensity, biotic and abiotic stresses) obtained through Genevestigator. The perturbations that significantly affected each TF expression by more than 1-Log₂(Fold Change) (p-value < 0.01) were selected and ranked to determine the expression average for each stress condition, setting at expression average \geq 1-Log₂(Fold Change). Names of the categorized TFs are colored according to their expression direction in RNA-Seq data, being red for upregulated and blue for downregulated TFs, respectively. TPM: Transcripts Per Kilobase Million.

Transcriptome comparison with datasets of WT *A. thaliana* in the same growth conditions

In order to give further confidence to the transcriptome results generated for *ucp1 ucp3* plants, two datasets (SRR1_WT and SRR2_WT) from WT *A. thaliana* Col-0 available in online repositories were obtained. The normalized count data from samples were used to verify the biological variability between the data generated in house for WT and *ucp1 ucp3* mutant and the SRR1_WT and SRR2_WT datasets by Principal Component Analysis (PCA). According to PCA, the SRR2_WT (green circles) was the closest to both in house WT (purple circles) and mutant (blue circles) in comparison to SRR1_WT (pink circles) (Figure S4A). Therefore, SRR2_WT was chosen to proceed with the analysis. The first component (PC1) accounted for 88% of the variance and visibly separated the SRR1_WT group from all the other three groups. Except for one out of three mutant samples, all samples from the same group grouped assembled together. Volcano plot from RNA-Seq analysis demonstrated a new transcriptional profile for the *ucp1 ucp3* double mutants relative to *A. thaliana* WT_SRR2 Col-0, with a strong deregulation in the two directions (up- and downregulation) (Figure S4B). In fact, 7904 DEGs were detected using DESeq2 package and defined by $P_{adj} < 0.1$. Among them, 4445 DEGs were upregulated, while 3459 downregulated (Figure S4C).

A comparison of the two RNA-Seq data from deregulated DEGs showed common and specific changes between our in-house transcriptome analysis and *ucp1 ucp3*/SRR2_WT RNA-Seq (Figure 8A). A number of 484 overlapping DEGs were found with the majority (316; 65%) presenting the same directional expression. On the other hand, the others 168 (35%) were non-directional. Among the DEGs that have the same direction in both RNA-Seq data, 182 are up-directional and 134 down-directional (Figure 8A). Among the ten clusters formed, five were composed of the up-directional DEGs and five also of the down-directional (Figure S5).

A number of 30 directional DEGs from GO terms associated with chloroplast, mitochondria and abiotic stress were then thoroughly reviewed to confirm their expression profiles (Figure 8B). Of the ten chloroplast-related DEGs, seven (*BCAT3*, *BGLU44*, *CIA2*, *cpHsc70-2*, *GSA2*, *LOX2* and *OSB3*) were downregulated in *ucp1 ucp3* plants compared with the two WT groups, while three (*GRF6*, *PP2-A5* and *SEN1*) were upregulated. The downregulated *cpHsc70-2* gene, which encodes a 70-kD heat shock protein (HSP70) essential for chloroplast development and involved in protein folding and transport across membranes (Latijnhouwers et al., 2010), was the only one

largely induced at three samples of each WT group, while all the three upregulated chloroplast-related genes were induced in the *ucp1 ucp3* group (Figure 8B). Among the ten mitochondrial-related DEGs, seven (*AOX1a*, *AT3G51870*, *AT5G02050*, *DiT1*, *mtHsc70-1*, *UCP1* and *UCP3*) were downregulated and three (*AT3G62650*, *FUM2* and *UCP2*) upregulated. In this regard, the downregulated genes *AOX1a*, an isoform of AOX family involved in alternative respiratory pathway, as well as the two isoforms *UCP1* and *UCP3*, which were knockdown in the mutant plants, had their expressions widely repressed in all samples of the *ucp1 ucp3* group. The upregulated genes *UCP2* and *FUM2*, which encodes a cytosolic fumarase, were the only ones that had their expressions strongly repressed in all samples of both WT groups (Figure 8B). Concerning the ten abiotic stress-responsive DEGs, seven (*ASN1*, *COR27*, *COR47*, *GDH1*, *GLY3*, *GRF3* and *OZF1*) were upregulated and three (*Hsp70-2*, *HSP81-2* and *HSP81-3*) downregulated. Among the upregulated genes, those with strongly induction in all *ucp1 ucp3* samples were *COR27* and *GLY3*, which are highly expressed in response to cold and salt stress, respectively. In the other direction, all the three downregulated abiotic stress-responsive genes, which encode heat shock proteins, were repressed in all samples of the mutant group (Figure 8B).

Another heatmap (Figure 8C) was constructed to show the relationships among these 30 directional DEGs employing a similarity matrix with the Pearson correlation distance as a metric (difference degree in a range of -1 to 1). By the comparison of the congruence pattern of the expression profiles, the more yellow the color, more intense is the interaction between two DEGs, demonstrating a higher congruence and smaller distance between their expressions. In this regard, smaller distance was observed between the abiotic stress-responsive DEGs among themselves and with the mitochondrial- and chloroplast-related DEGs. Except *OZF1*, the other nine directional genes related to abiotic stress had a strong interaction between their expressions. In addition, these transcripts strongly interacted with six mitochondrial (*AOX1a*, *AT3G51870*, *AT5G02050*, *UCP1*, *UCP2* and *UCP3*) and four chloroplastic (*BGLU44*, *GRF6*, *PP2-A5* and *SEN1*) DEGs (Figure 8C). The three *UCP* genes also showed high interaction between them and with *AOX1A*, which is consistent with their roles of mitochondrial energy dissipation systems (Pu et al., 2015).

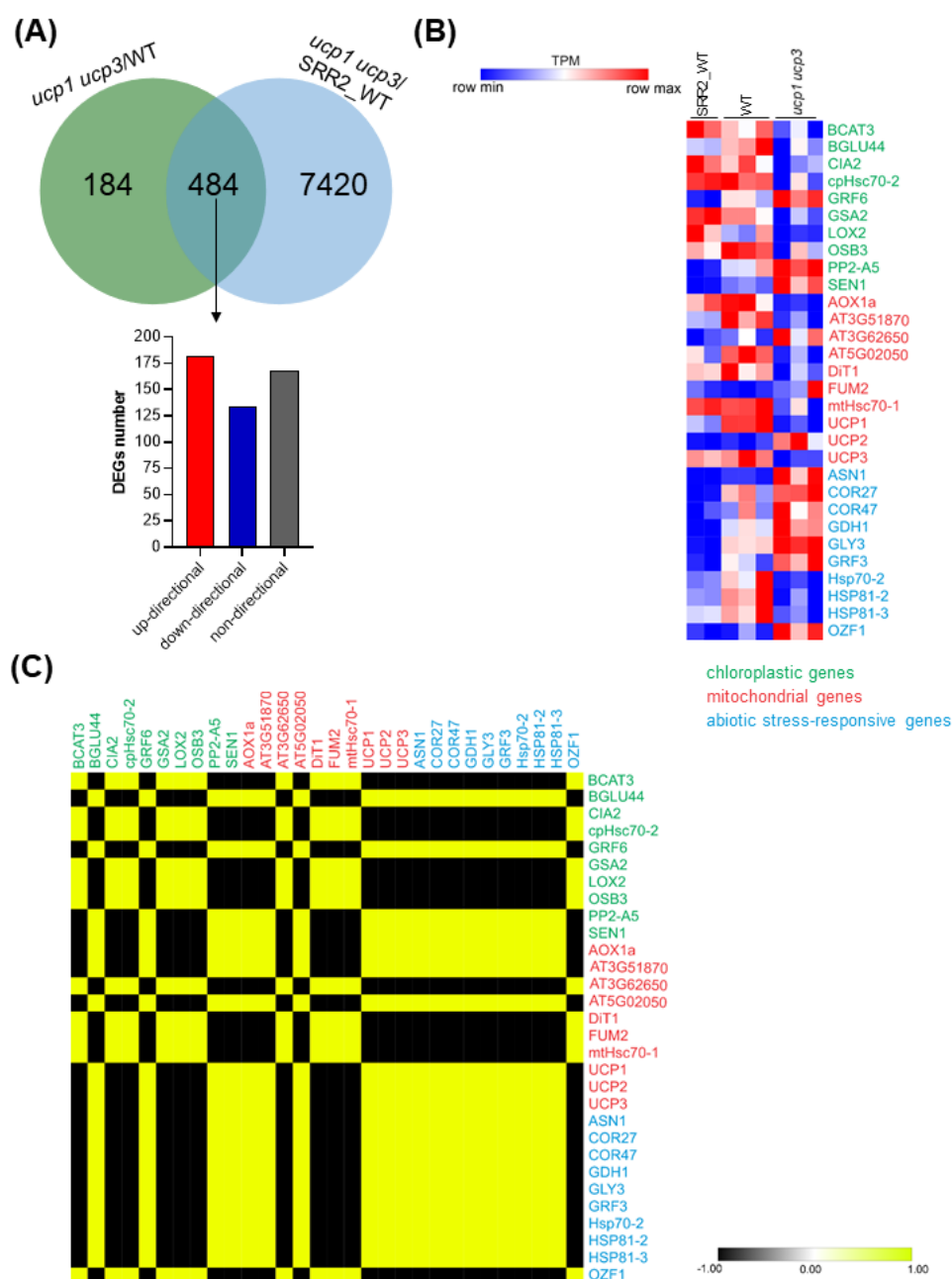


Figure 8. Bioinformatics analysis validation of the *ucp1 ucp3* double mutant transcriptome. **(A)** Schematic representation showing the amount and direction of the overlapping DEGs between *ucp1 ucp3* plants and two WT treatments in each RNA-Seq counterpart. A Venn diagram was constructed indicating the amount of the overlapping DEGs. The bar plot indicates the direction of the overlapping DEGs number. **(B)** A heatmap showing the expression profiles of thirty selected directional DEGs related to chloroplast, mitochondria and abiotic stress (ten of each) relative to WT and mutant groups of the transcriptome together with SRR2_WT selected dataset. The expression scale according to TPM data of the three biological replicates per genotype varies from dark blue (downregulation) to dark red (upregulation). **(C)** A heatmap representing the similarity matrix of the selected directional DEGs from the paired comparison between *ucp1 ucp3* mutant group with the two WT treatments in each RNA-Seq counterpart. Log₂(Fold Change) values from each RNA-Seq and Pearson correlation were used as metric. The Color scale represents the degree of

similarity: black indicates low correlation, yellow high correlation. DEG: differentially expressed gene; WT: wild-type; TPM: Transcripts Per Kilobase Million.

Metabolite profiles of *ucp* double mutant plants under normal growth conditions

The metabolic disturbances associated with the double knockdown of *UCP* genes during vegetative phase under normal growth conditions were investigated using GC-MS. As a result, a total of 105 metabolites was identified in the entire experiment after screening (Table S7). To determine the metabolite profiles, the relative abundance compared to the WT control was performed. A total of 71 metabolites, including amino acids, nitrogenous bases, organic acids, sugars and others (e.g., secondary metabolites, inorganic acids), was detected in the double mutants relative to WT (Figure 9).

The annotation analysis classified these metabolites into five groups being sugars, sugars alcohols and sugars intermediates the major one (30%), followed by organic acids and organic acids intermediates (27%), amino acids and amino acids intermediates (22%), others (17%) and nitrogenous bases (4%) (Figure 9A). It should be noted that the Log₂Fold Change values of few metabolites into all groups were significantly different in the three double mutants compared with WT, revealing that most metabolite levels were concentrated in the range of -5 to 5, and that the average values of Log₂Fold Change in each group were relatively close to 1 or -1 (Figures 9B, 9C and 9D). Conversely, the group composed by nitrogenous bases showed higher decreases for the three double mutants, what can be justified by the significant decreases in guanine observed in all of them (10B, 10C, 10D and 10E).

Of the alterations observed for *ucp1 ucp2* plant under normal growth conditions, there were mostly decreases in metabolite levels for all groups, except for the amino acid class, which had a higher amount of metabolite accumulation compared with the other groups (Figure 9B). These double mutant plants showed only significant decreases for the alanine and glycine amino acids, as well as for the gluconic and glyceric organic acids, while a single accumulation was recorded significantly for the glutamate amino acid (Figure 9E). In relation to *ucp2 ucp3* plants, they had higher decreases for the group of others, while higher metabolite accumulations into amino acid and sugar groups (Figure 9C). There were significant decreases in 2-methylalanine, an intermediate precursor of the alanine amino acid, and glycine, following five organic acids and their intermediates (3-deoxytetronic acid, glyceric acid, monopalmitin, palmitic acid and stearic acid) (Figure 9E). On the other hand, significant

accumulations also were evident in these double mutants, with higher levels relative to WT plants of aspartate, glutamate and tyrosine amino acids, as well as ribose-5-phosphate, a sugar intermediate which is essential precursor in nucleotide synthesis, and urea, which is associated with root uptake and nitrogen homeostasis in plants (Figure 9E).

Among the three double mutants, the *ucp1 ucp3* plants were the ones that presented the higher number of metabolic changes. They presented higher accumulations in relation to WT plants of several metabolites, mainly belonging to organic acids and others groups (Figure 9D). Although no significant change in amino acids was detected, other metabolic alterations were observed for these double mutants, including significant decreases only in two sugars (galactose and psicofuranose) and several significant accumulations in three groups corresponding to organic acids and their intermediates (4-hydroxybutyric acid, dimethoxymandelic acid, fumaric acid, lactic acid, monopalmitin, sitosterol and threonic acid), sugars, sugars alcohols and their intermediates (arabinose, glycerol monostearate and myo-inositol [phosphate]) and others (dioctyl isophthalate, erythrono-1,4-lactone, phenylpropanolamine and sinapinic acid) (Figure 9E). The cluster analysis showed that the *ucp1 ucp3* double mutant presented a more distinct metabolite profile than the other two in comparison with WT plants. Overall, these results indicate that the three events from double knockdown of *UCP* genes alters drastically the plant metabolism with different metabolic changes and it reinforces that there is a partial redundancy between the three isoforms (Lima et al., submitted).

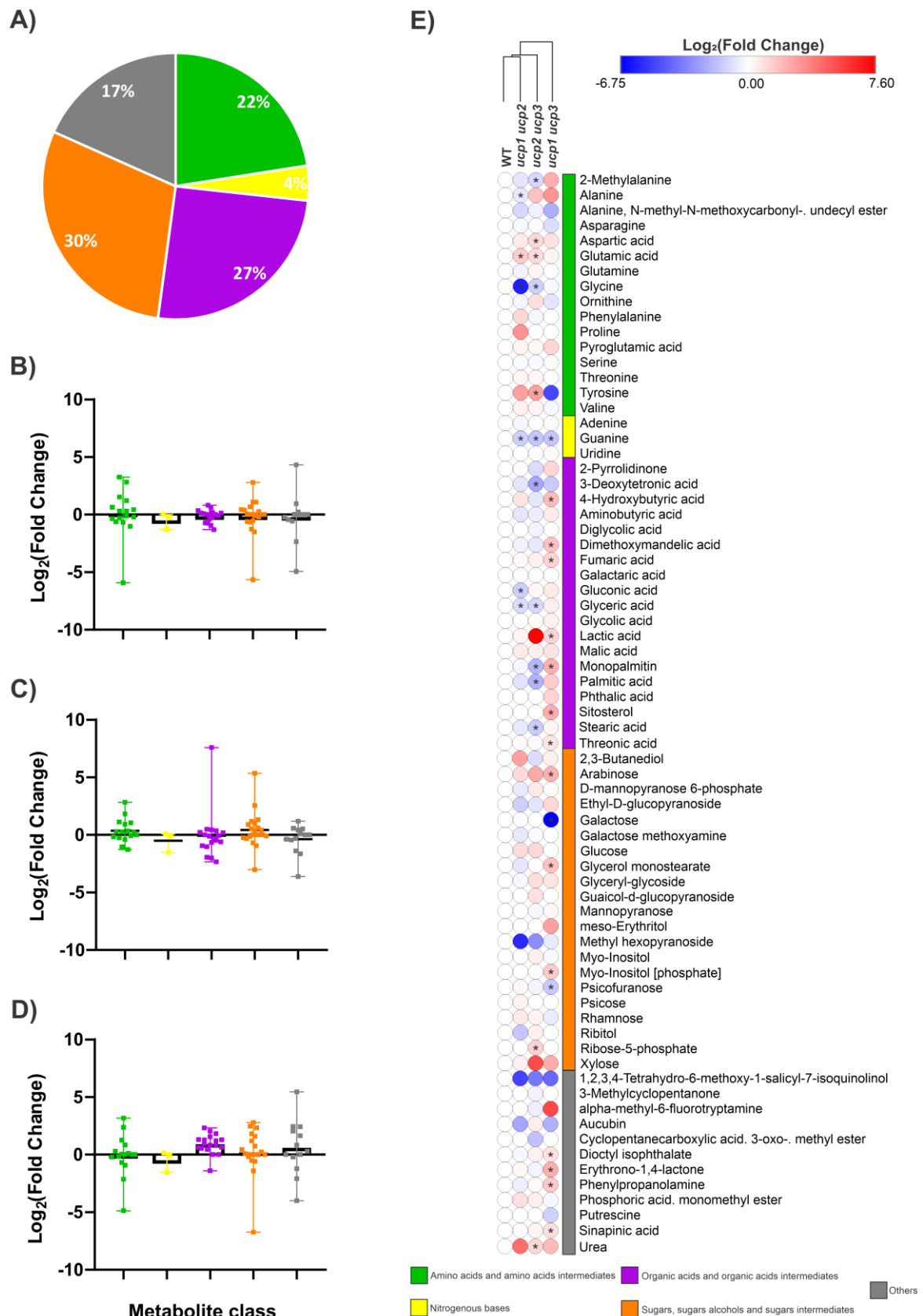


Figure 9. Changes in relative abundance of metabolites in *ucp* double mutant plants grown under normal conditions. (A) A pie chart demonstrating distribution of detected metabolites as measured by GC-MS in *A. thaliana ucp1 ucp2*, *ucp1 ucp3*, *ucp2 ucp3* and WT plants (21-day-old). Scatter plots showing the relative abundance

of metabolite levels per class using means with range from relative $\text{Log}_2(\text{Fold Change})$ values for **(B)** *ucp1 ucp2*, **(C)** *ucp2 ucp3* and **(D)** *ucp1 ucp3* double mutant plants (21-day-old). **(E)** A heatmap representing the alterations in the relative abundance of the metabolites detected in the *ucp* double mutants in comparison to WT control. Relative $\text{Log}_2(\text{Fold Change})$ values of metabolite levels were normalized in relation to mean calculated for the WT (arbitrarily set to zero). Asterisks denote significant differences compared with WT (*p-value ≤ 0.05) according to Student's *t* test. Values are means from five biological replicate samplings. WT: wild-type.

DISCUSSION

All living organism needs a supply of energy to develop the vital processes (e.g., growth, development, reproduction) that enables their survival. In plants, all development phases demand the correct functioning of energy metabolism and, consequently, of mitochondria (McBride et al., 2006). As the 'energy powerhouse of the cell', mitochondria has different functional marker genes that are involved in retrograde communication with the nucleus, which in turn can impact several cellular processes (Rhoads et al., 2005; Sweetlove et al., 2006; Rhoads & Subbaiah, 2007; Barreto et al., 2014; Gandin et al., 2014; Monné et al., 2018). Among these genes, *UCP1* has been recently shown to be implicated in retrograde signaling by inhibiting oxygen-sensing (Barreto et al 2022). Interestingly, the single knockdown of *UCP* genes has clear impacts not only on the mitochondrial metabolism associated with energy and ROS production, but also produces effects throughout the cell (Arcuri et al. 2021). In this regard, previous results showed interesting phenotypic changes during the reproductive phase of such mutants as well as physiological alterations particularly associated to low photosynthetic efficiency and reduced respiratory rate. Intriguingly, *ucp1 ucp3* double mutant plants displayed interesting disturbances during the vegetative phase (Lima et al., submitted) that merits further investigation. Here, we sought to investigate the impact of the double knockdown of *UCP1* and *UCP3* at the transcriptome level using RNA-Seq. In addition, metabolic profiles of different *ucp* double mutants were determined.

The transcriptome analysis of *ucp1 ucp3* plants revealed that among 668 DEGs, 53% were upregulated, whereas the other 47% were downregulated. GO and KEGG enrichment analyses revealed a wide gene expression adjustment in the double mutant that broadly affected extensive biological processes, molecular functions, cellular components and pathways mainly outside the mitochondria. Comparable findings were also observed when the *AOX1a* gene was knocked down in *A. thaliana* (Giraud et al., 2008). These results agree with other transcriptome studies

demonstrating that UCP1 activity, in addition to being critical for energy metabolism, is also involved in a spectrum of cellular events and metabolic processes, including the transcriptional regulation of nuclear genes encoding proteins associated with the metabolism of DNA, carbon and AA, response to abiotic stress, transport activity and signaling pathway (Barreto et al., 2014; Barreto et al., 2015; Laitz et al., 2015).

Previous studies have demonstrated that the plant photosynthetic capacity is remotely affected by UCP activity (Sweetlove et al., 2006; Chen et al., 2013; Gandin et al., 2014; Arcuri et al., 2021), a feature that is consistent with the low photosynthetic efficiency of *ucp1 ucp3* double mutant plants (Lima et al., submitted). In fact, a detailed analysis of the mutant transcriptome revealed an important transcriptional reprogramming with strong induction of chloroplastic components associated with photosynthesis and the antenna complex, a feature that reinforces the proposed cross-talk between the mitochondria with other cellular components. In an opposite direction, a broad repression of several genes involved with the photosynthetic apparatus was observed in tobacco plants overexpressing *AtUCP1* (Barreto et al. 2015). In view of these results, we hypothesized that the knockdown of *UCP1* and *UCP3* causes the two photosystems (PSI and PSII) to absorb more energy than can be handled, leading to an upregulation of genes encoding antenna proteins and to energy overload. This energy imbalance may be in part responsible for the low photosynthetic efficiency seen in the *ucp1 ucp3* double mutants. Alternatively, this energy overload may be a result of the strong compensatory expression of *UCP2* observed in double mutant plants (Lima et al., submitted), which may represent an alternative route for the respiratory process.

Intriguingly, the verified upregulation of many plastid-related genes contrasts with the downregulation of several mitochondrial-related genes, including those encoding electron transport chain components and a set of metabolite transporters. These results agree with previous transcriptome data of *AtUCP1* overexpressing tobacco plants showing that several GO terms associated with chloroplastic and mitochondrial metabolisms were significantly enriched among the up- and downregulated transcripts, respectively (Barreto et al., 2015). It seems therefore that an opposite metabolic reconfiguration of chloroplast and mitochondria occurs in response to decreased uncoupling activity. It should be noted that, in mutant plants, several genes encoding membrane and cell wall proteins showed higher transcript

levels compared to those encoding inner space proteins. In this regard, Busi et al. (2011) investigated the transcriptional responses associated with a mitochondrial dysfunction promoted by the expression of two unedited forms of the *u-ATP9* (ATP synthase subunit 9) gene in flowers tissues of *A. thaliana* and found, among the significant categories with ascribed function, a high number of transcripts encoding membrane proteins

When looking to the downregulated DEGs, the vast majority displayed functions associated with DNA metabolism. It has been postulated that the involvement of mitochondria in retrograde signaling provides a powerful communication network through dual-targeting of proteins (e.g., heat shock proteins and chaperones) to mitochondria and other cellular components, such as chloroplast, cytosol, endoplasmic reticulum and peroxisomes (Silva-Filho, 2003; Millar et al., 2008). Our results reflect, for example, a possible disrupted crosstalk between the mitochondria and the endoplasmic reticulum by the downregulation of genes encoding heat shock proteins involved with the pathway ‘protein processing in endoplasmic reticulum’, as well as of genes associated with molecular processes such as rRNA processing and protein folding. This is supported by a recent study indicating a role for UCP1 and AOX1a in the protection of the endoplasmic reticulum against reductive stress (Fuchs et al., 2022).

Given the multiple biological roles attribute to the plant UCP isoforms (Barreto et al., 2020), it is reasonable to expect that the double knockdown of *UCP1* and *UCP3* during the vegetative phase could affect several metabolic processes within the primary metabolism. Indeed, mutant plants had upregulated several genes connected to DNA, carbon, lipid, AA and energy metabolisms as well as those encoding components of different signaling pathways, transport activity and cellular respiration. On the other hand, some pathways associated with secondary metabolism (e.g., flavonoid and carotenoid metabolic processes) were negatively affected in the double mutant. Another interesting transcriptomic outcome of the double knockdown of *UCP1* and *UCP3* was the upregulation of genes encoding proteins with potential metabolic functions in cell homeostasis, such as thioglucosidases, aquaporins and some involved with transcriptional processes. These proteins are implicated in the functional coordination of plant development particularly associated with sulfur and nitrogen assimilation, water transport across cell membranes and molecular processes

associated with plastid gene expression machinery (Chaumont et al., 2000; Gawwad et al., 2013; Jarvis & López-Juez, 2013; Nakano et al., 2017; Meier et al., 2019). In the opposite direction, a large set of genes with decreased expression encode heat shock proteins, proteins associated with sulfur homeostasis, mitochondrial and other membrane transporters involved with energy metabolism, chloroplast proteolytic machinery, as well as those connected to protein and ion signaling within the cell, ATP binding, protein processing in endoplasmic reticulum and several proteins linked to carbon and AA metabolism. These observations suggest a disrupted gene network affecting both chloroplasts and mitochondria communication that in turn impacts several biological processes.

Our transcriptome analysis also revealed that *ucp1 ucp3* mutant plants had upregulated the expression of several genes involved in stress responses, particularly those associated with light, water deprivation, cold, salt, oxidative, osmotic and hypoxia stresses. This is in line with previous data showing that *ucp* single and double mutants (e.g., *ucp1 ucp3*) grown under normal conditions accumulate high levels of superoxide (O_2^-) and hydrogen peroxide (H_2O_2) in young leaves and plants, thus indicating the occurrence of strong oxidative stress in these mutants (Arcuri et al., 2021; Lima et al., submitted). Therefore, the observed upregulation of stress-responsive genes could be in part attributed to a more stressed state of the double mutant plants compared with the WT. Another compatible finding was the detected upregulation of genes associated with the response to ABA, a phytohormone known to mediate some physiological responses to different environmental constraints (Wani et al., 2016; Vishwakarma et al., 2017). In this regard, a crosstalk between ABA and ROS has been reported (Jiang & Zhang, 2001; Zhang et al., 2001; Wang & Song, 2008). On the other hand, genes involved in heat and cadmium ion stresses, including those encoding heat shock proteins, were found downregulated in mutant plants. Among them, the *NRT1.8* gene plays a central role in cadmium ion tolerance (Li et al., 2010). Overall, these results can be attributed to a disrupted retrograde signaling function of both isoforms during stress.

In line with the detected induction of a spectrum of stress-responsive genes, we found that many important stress-associated transcription factors belonging to different families, such as bHLH, bZIP, TCP, AP2-ERF, NAC, C3H and WRKY (Welchen et al., 2014; Wang et al., 2016), were deregulated in mutant plants. Our results demonstrated

that among the top ten differentially expressed TFs of each direction, six were upregulated and belonging to three large families (bHLH, bZIP and C3H) related to various abiotic stresses, while seven were downregulated and also distributed in three wide families (bHLH, NAC and WRKY) associated with environmental perturbations. The altered expression of these transcriptional regulators probably reflects a compensatory response or a negative disruption for the reduced expression of *UCP1* and *UCP3*, which in turn promotes important changes in the transcriptional network of the mutant plants. Interestingly, the activation of many stress-responsive pathways was also detected in mutant plants using Genevestigator. In this regard, a set of 12 TFs showing multiple interactions with various perturbations, including cold, oxidative, salt, osmotic and biotic stress, was put in evidence. Overall, these results provide evidences of an intense transcriptional reconfiguration in *ucp1 ucp3* plants that takes place via several predicted interactions between transcriptional regulators and different stress-responsive genes.

Overall, the comparison of the *ucp1 ucp3* transcriptome with datasets of WT *A. thaliana* (WT x SRR2_WT x *ucp1 ucp3*) revealed both similarities and differences between them. This fact can be attributed to an existing variability within the WT group or differences in RNA-Seq techniques and steps. Despite that, both transcriptome analyzes demonstrate an intense transcriptional reprogramming of these overlapping DEGs found with same directional expression throughout the course of the double knockdown of *UCP1* and *UCP3* in plants. The 30 directional genes from GO terms associated with chloroplast, mitochondria and abiotic stress supports the proposed idea that both *UCP1* and *UCP3* genes remotely influence the mitochondrial metabolism and also other pathways throughout the cell as a consequence of decreased uncoupling activity. Moreover, the comparative analysis via similarity matrix of these 30 directional genes from the two RNA-Seq data suggests a higher expression correlation among the abiotic stress-responsive genes than those associated with mitochondria and chloroplast for both intra- or intergroups. This reinforces published data demonstrating that genes responsive to abiotic stresses are markedly co-regulated in plants with altered expression of *UCP1* (Barreto et al., 2014; Barreto et al., 2015).

The generated metabolic profiles provide evidences that the double knockdown of *UCP* genes during the vegetative phase promotes an intense metabolic

reprogramming with consequences in redox homeostasis, energy balance and carbon flux. In this regard, significant alterations in several organic acids and sugars were observed. In comparison with previous studies that reported the metabolic profiles of *ucp1* and *ucp2* single mutant plants under normal conditions (Sweetlove et al. 2006; Arcuri et al. 2021), our data demonstrate a higher variation in the abundance of several metabolites. Our results also suggest that the three double mutant plants show disturbances in DNA metabolism as indicated by the common significant decrease in guanine levels. This finding is in line with the downregulation of many genes involved in DNA metabolism observed in the *ucp1 ucp3* transcriptome.

The significant increase in glutamate and aspartate levels in the *ucp1 ucp2* and *ucp2 ucp3* mutants could be indicative of an enhanced nitrogen uptake in these plants. These amino acids are important for nitrate assimilation and considered essential for plant stress tolerance (Pratelli et al., 2014; Hildebrandt et al., 2015). In addition, the accumulation of tyrosine, an aromatic amino acid that plays an important role in environmental responses (Maeda & Dudareva, 2012), also indicates that the mutant plants are experiencing an atypical situation. In parallel, the significant decreases in glycine and glycerate levels observed in these double mutants suggest possible changes in photorespiration through the well-known role of mitochondria in glycine oxidation and action of glyceric acid as carbon source for glycine synthesis (Voll et al., 2006; Igamberdiev & Kleczkowski, 2018). These findings are consistent with a previous study showing a strong reduction in glycine levels in the *ucp1* single mutants (Sweetlove et al. 2006).

The significant decrease in the levels of galactose and psicofuranose in *ucp1 ucp3* plants is suggestive of impairments in many cellular processes and mechanisms, including galactose transport, osmotic adjustment, regulation of energy and cellular redox balance, protection of cellular structures, as well as signaling regulation (Gibson, 2005; Rolland et al., 2006; Smeeckens et al., 2010). These data are consistent with previous reports showing that mitochondrial gene mutations resulted in decreased levels of several sugars (Fonseca-Pereira et al., 2018; Arcuri et al., 2021). Otherwise, the increased accumulation of arabinose, glycerol monostearate and myo-inositol-phosphate provide evidences for the occurrence of cellular toxicity or other type of stress in *ucp1 ucp3* plants (Williamson et al., 2002; Patrick et al., 2013; Zhao et al., 2019). Additionally, *ucp1 ucp3* plants showed increased levels of specific secondary

metabolites (dioctyl-isophthalate, erythrono-1,4-lactone, phenylpropanolamine and sinapinic acid) of several classes (e.g., flavonoids, terpenoids, alkaloids), of organic acids involved in GABA, methylglyoxal, TCA cycle and ascorbic acid pathways (4-hydroxybutyric acid, lactic, fumaric and threonic acids, respectively), and of two lipids (monopalmitin and sitosterol). Alterations in the levels of these organic acids may indicate anoxic and stressful conditions and could impair processes related to energy balance, such as photosynthesis, photorespiration and respiration (Schaeffer et al., 2001; Bouché & Fromm, 2004; Valpuesta & Botella, 2004; Maurino & Enggvist, 2015; Misra et al., 2016; Aboobucker & Suza, 2019). Overall, these results support the idea that both primary and secondary metabolisms are subjected to a UCP-mediated redox regulation.

In summary, the transcriptome analysis of *ucp1 ucp3* plants revealed broad alterations in genes associated with various cell compartments and processes (e.g., chloroplast, mitochondria, endoplasmic reticulum, DNA metabolism), which indicates that the double knockdown of these genes has severe consequences for the entire plant. Notably, the *ucp1 ucp3* plants displayed an upregulation of several abiotic stress-responsive genes suggesting that are permanently suffering from stress. Likewise, the double knockdown of *UCP* genes resulted in metabolic changes that significantly affected primary (amino acids, organic acids, sugars and nucleic acid compounds) and secondary metabolisms. Overall, the generated data highlights the importance of UCP activity for plant growth and development.

MATERIAL AND METHODS

Plant material and growth conditions

The *Arabidopsis thaliana ucp1 ucp3* double mutant (Col-0 ecotype) used in this study was previously characterized by Lima et al. (submitted). Wild-type (WT) Col-0 was used as control in all assays. WT and *ucp1 ucp3* seeds were kept at 4°C for at least 72 h in darkness for dormancy breaking and then germinated in Petri plates containing one-half-strength Murashige and Skoog medium (½ MS) (Murashige and Skoog, 1962) under normal conditions. The Petri plates were maintained in a growth chamber (Fitotron, Conviron® Model CPM6050) with 16 h day/8 h night photoperiod cycle, photosynthetic photon flux density (PPFD) of 150 $\mu\text{mol photons m}^{-2} \text{s}^{-1}$,

temperature of 19°C and relative humidity around 65%. Entire plants (21-day-old) were collected, immediately frozen in liquid nitrogen and stored at -80°C. Three biological replicates were sampled per genotype for the RNA-Seq analysis.

RNA extraction, cDNA library construction and Illumina sequencing

Total RNA from 21-day-old plants was extracted using the RNeasy Plant Mini Kit (Qiagen, Germany). The RNA was treated with DNase I (RQ1 RNase-Free DNase; Promega) to remove possible residual genomic DNA. RNA concentration and absorbance ratios were determined using a NanoDrop™ 1000 spectrophotometer (Thermo Fisher Scientific, Waltham, MA, USA). RNA quality of all samples was assessed in Bioanalyzer 2100 (Agilent technologies, Santa Clara, CA, United States) and an RNA integrity number (RIN) above seven was considered suitable for RNA-Seq. RNA samples were also quantified using the Quant-iT RiboGreen RNA Reagent (Invitrogen) to check if they have the minimum mass/concentration necessary for the preparation of cDNA libraries. Equal quantities of total RNA from the three biological replicates were pooled before cDNA library construction and sequencing. cDNA libraries were prepared using Illumina TruSeq Stranded mRNA Library Prep Kit (Illumina, San Diego, CA, United States). Each cDNA sample came from a single plant (n= 3 per genotype) and pooled to run in a single lane, each on a separate flow cell. Sequencing was performed with HiSeq SBS v4 High Output Kit (Illumina, San Diego, CA, United States) in an Illumina HiSeq 2500 system (Illumina, San Diego, CA, United States) at the Central Laboratory for High Performance Technologies (LaCTAD – UNICAMP, Campinas, São Paulo state, Brazil). Reads were 100 bp in length and generated from each end of the DNA fragments in paired-end sequencing.

Read mapping and differential expression analysis

The reads from all libraries were quality trimmed and then compared with the gene set (35386 transcripts; means size: 1534 bp) of the TAIR10 *Arabidopsis* reference genome (Berardini et al., 2015) using Kallisto (Bray et al., 2016) with default parameters. The Table S1 contains the statistics about read number and mapping from each sample. The *est_counts* from each library (obtained from Kallisto results in the file *abundance.tsv*) were submitted in DESeq2 package (Love et al., 2014) to identify differentially expressed transcripts between the conditions. The normalization method

of transcripts per kilobase million (TPM) was used in this study to calculate the expression level of each gene in the samples. For tune the thresh-old p-value, the adjusted p-value (P_{adj}) method was used.

Functional annotation and other analysis of the differentially expressed genes (DEGs)

Each DEG was functionally classified based on The Arabidopsis Information Resource (TAIR 10). Functional annotation was only performed for DEGs with TPM values that were significantly different between WT and *ucp1 ucp3* from adjusted p-value (P_{adj}) < 0.1. The complete lists of the up- [$\text{Log}_2(\text{Fold Change}) > 0$] and downregulated [$\text{Log}_2(\text{Fold Change}) < 0$] DEGs are available in Tables S2A and B. Gene Ontology (GO) framework and Kyoto Encyclopedia of Genes and Genomes (KEGG) pathway analysis were performed for term enrichment using the web tool DAVID bioinformatics resources 6.8 (<http://david.abcc.ncifcrf.gov/home.jsp>) (Jiao et al., 2012). GO functional description was divided into three categories: biological process (BP), molecular function (MF) and cellular component (CC). The hypergeometric test was used in each GO term and KEGG pathway with Benjamini-Hochberg test correction, and a corrected p-value ≤ 0.05 was considered as significantly enriched. Thereafter, corrected p-values were ranked from highest to lowest by the negative Log_{10} transformation and the top 30 ($-\text{Log}_{10}p \geq 4$ filter) were established. In this analysis, DEGs number of each GO term and pathway was taken into account and common GO terms and pathways found for both up- and downregulated DEGs were excluded. The up- and downregulated DEGs found in common between at least two terms and pathways were also analyzed. The protein-protein interactions (PPI) networks of the most enriched up- and downregulated DEGs were constructed using the STRING (search tool for recurring instances of neighboring genes) database (Version 11.5, released 12 August 2021) (<http://string-db.org/>), and adjusted by the Cytoscape software (an open source platform for complex network analysis and visualization, Version 3.8.2) (<https://cytoscape.org/>) with the parameter betweenness centrality. In order to get a high-quality PPI, it was established the filter of interactions with high confidence (0.700) from STRING.

The resulting up- and downregulated list of DEGs was used onto the biological pathways with MapMan software (Thimm et al., 2004). To reveal the impacts on

chloroplast and mitochondria, two organelles closely related to the activity of *UCP* genes, all DEGs from the CC category associated with the GO terms “chloroplast (GO:0009507)” and “mitochondria (GO: 0005739)” were selected. Subsequently, a classification based on the type and metabolic process was performed taking each DEG framed in these two terms. For chloroplast-related DEGs, the $\text{Log}_2(\text{Fold Change})$ and $-\text{Log}_{10}\text{P}_{\text{adj}}$ values were taken into account, while the TPM values of each biological replicate were considered for mitochondrial-related DEGs. At most, the top ten DEGs of each metabolic type and process were ranked, and some GO terms (BP and MF) and KEGG pathways were associated with each DEG. In parallel, GO terms within the BP category linked to different abiotic stress types were selected and associated with the identified DEGs. In addition, we also took into account the type of hormonal signaling for the upregulated DEGs or the type of biotic stress for the downregulated DEGs. All DEGs that appeared in common to more than one GO term was taken into account and classified as having more than one abiotic stress type. The GO terms that were linked to 'response to light' were sub-classified into 'stimulus' or 'absence'. In this analysis, the $\text{Log}_2(\text{Fold Change})$ and $-\text{Log}_{10}\text{P}_{\text{adj}}$ values were taken into account. At most, the top six upregulated and the top ten downregulated abiotic stress-responsive DEGs were ranked for each abiotic stress type.

The list of DEGs was also used against the *A. thaliana* Plant Transcription Factor Database (PlantTFDB 5.0) (Perez-Rodriguez et al., 2009) to identify differentially expressed transcription factors (TFs). The top ten up- or downregulated TFs differentially expressed between WT and *ucp1 ucp3* plants were selected. Selected publicly available experimental datasets of RNA-Seq libraries ('perturbations analysis' as 'condition search tools') from Genevestigator (Hruz et al., 2008) were used to check the expression of these top ten TFs in response to different types of abiotic stress. Datasets containing experiments that significantly affected each TF expression by more than $1-\text{Log}_2(\text{Fold Change})$ ($p\text{-value} \leq 0.01$) (Barreto et al. 2015) were selected using the filters 'stress', 'biotic' and 'light intensity'. TF expressions were ranked and the expression averages were determined for each stress condition. Only the relationship of TFs modulated by different types of perturbation in the same direction as our RNA-Seq were categorized, set at expression average $\geq 1-\text{Log}_2(\text{Fold Change})$.

Comparative analysis of *ucp1 ucp3* transcriptome with the selected dataset from WT *A. thaliana*

In order to validate the results from our RNA-Seq and to minimize transcriptome variability within the WT group, we generated, through bioinformatics analysis, a new transcriptional profile for the *ucp1 ucp3* double mutants relative to *A. thaliana* WT Col-0, using datasets from published studies and publicly available in online repositories databases. The FASTQs of WT transcriptome data were obtained from the Gene Expression Omnibus (GEO; National Center for Biotechnology Information - NCBI), respecting the same plant material growth procedures and conditions used in our RNA-Seq (21-day-old entire plants, ecotype Col-0, Illumina HiSeq, growth chamber with similar temperature and photoperiod). Two datasets were selected – GSE95473 (Krzyszton et al., 2018; SRR1_WT) and GSE75456 (Sun et al., 2016; SRR2_WT) – and a PCA was performed between the WT group and mutant of our RNA-Seq together with the SRR1_WT and SRR2_WT datasets, in order to verify which dataset is grouped closest to our WT group. As the SRR1_WT group was totally different from all the other three (Figure S4A), we chosen the SRR2_WT dataset to proceed with read mapping and differential expression analysis. The volcano-plot and the up- and downregulated DEGs number of *ucp1 ucp3*/SRR2_WT RNA-Seq is available in Figures S4B and S4C, respectively. A Venn diagram for comparison of the two RNA-Seq data and identification of the overlapping DEGs was created, as well as the direction type of these overlapping DEGs was also exhibited in relation to DEGs number. Thirty directional DEGs related to chloroplast, mitochondria and abiotic stress (ten of each) were selected for confirmation using TPM values for WT x SRR2_WT x *ucp1 ucp3*, and a similarity matrix from Log₂(Fold Change) values was also constructed with these DEGs, using Pearson correlation as metric. In addition, expression profiles of overlapping DEGs for the three groups from TPM values were exhibited through a hierarchical clustering performed with directional DEGs, using Euclidian distance as metric.

Metabolite profile of the *ucp* double mutants and analysis

Metabolite profiles were established for the *ucp1 ucp2*, *ucp1 ucp3* and *ucp2 ucp3* double mutants. Frozen samples (30 mg) collected from entire plants (21-day-old) grown in ½ MS medium under normal conditions were grounded with liquid

nitrogen using mortar and pestle. Metabolite extraction was initially performed using a solution containing methanol, chloroform and water (3:1:1) following the protocol described by Gullberg et al. (2004). The final supernatant was filtered (Millipore filter PVDF 0.22 μ m) and stored at -80°C. One hundred microliters of the organic phase of each sample were transferred to vials and completely dried. Thereafter, the samples were derivatized as described by Gullberg et al. (2004) using N-methyl-N-(trimethylsilyl) trifluoroacetamide (MSTFA) containing 1% trimethylchlorosilane (TMCS). A series of n-alkanes (C12-C40) to calculate retention indices (Schauer et al., 2005), as well as blank control samples, were used. The instrumental analysis was performed from one μ L of the derivatized samples injected in a split-less mode into a gas chromatograph 7890A (Agilent Technologies, Santa Clara, USA) coupled with a Comb-xt Autosampler mass spectrometer (Leap Technologies, Carrboro, USA), following the same GC-MS conditions described by Budzinski et al. (2019). Data processing including chromatograms were exported from ChromaTOF software v.4.51 (LECO Corp., St. Joseph, USA) to R software using TargetSearch package (Cuadros-Inostroza et al., 2009) to identify the metabolites via peak detection, retention time alignment and library matching. Five biological replicates were sampled per genotype for the GC-MS analysis.

Metabolite intensities were normalized by dry weight and total ion count (TIC). Metabolite screening and annotation were carried out using the Golm Metabolome Database (<http://csbdb.mpimp-golm.mpg.de>) (Kopka et al., 2005). The metabolite data were normalized by the Log₂ transformation to detect the relative abundance of each metabolite in the *ucp* double mutants relative to WT control. Significance was tested using the means with standard errors (\pm SE) by Student's *t* test (*p*-value \leq 0.05). A hierarchical clustering was performed from Log₂Fold Change values for WT and *ucp* double mutants using Euclidian distance as metric.

Data representation and analysis

Principal Component Analysis (PCA) plots were created using DESeq2 package, while volcano plots were constructed using VolcanoNoseR (<https://huygens.science.uva.nl/VolcanoNoseR/>). Bar plots, pie charts and scatter plots were made with Prism 8.0 (GraphPad Software Inc., US). Heatmaps, heat-scatter

plots, the matrix correlation and hierarchical clustering analysis were created using Morpheus (<https://software.broadinstitute.org/morpheus>).

Data availability

FASTQ files, raw gene counts and TPM values from *ucp1 ucp3* (21-day-old) transcriptome are available under the GEO accession number GSE205194 at the NCBI Gene Expression Omnibus.

Author Contributions

Conceptualization, R.P.M.L., J.S.O., P.B. and I.G.M.; methodology, R.P.M.L. and I.G.M.; validation, R.P.M.L. and L.C.N.; formal analysis, R.P.M.L., J.S.O., L.C.N., M.T.V.L., P.B. and I.G.M.; investigation, R.P.M.L.; resources, R.P.M.L., C.A.L. and I.G.M.; data curation, R.P.M.L., J.S.O., L.C.N. and M.T.V.L.; writing - original draft preparation, R.P.M.L. and I.G.M; writing - review and editing, R.P.M.L. and I.G.M; visualization, R.P.M.L., P.B. and I.G.M; supervision, I.G.M; project administration, I.G.M; funding acquisition, R.P.M.L., C.A.L. and I.G.M. All authors have read and agreed to the published version of the manuscript.

Funding

This research was funded by the Fundação de Amparo à Pesquisa do Estado de São Paulo (FAPESP), grant numbers #2017/25139-2 and #2018/19021-1. This study was also financed by the Coordenação de Aperfeiçoamento de Pessoal de Nível Superior (CAPES) - Finance Code 001. Funding was granted to R.P.M.L. and I.G.M.

Informed Consent Statement

Informed consent was obtained from all subjects involved in the study.

Acknowledgments

We thank Nicholas Vinicius da Silva for his valuable insights and discussions about transcriptome analysis, and Alice Nagai, Thaís Cataldi and Fabricio Moraes for their valuable insights and discussions about metabolome analysis.

Conflicts of Interest

The authors declare no conflict of interest. The funders had no role in the design of the study; in the collection, analyses, or interpretation of data; in the writing of the manuscript, or in the decision to publish the results.

REFERENCES

- Aboobucker, S.I.; Suza, W.P. Why do plants convert sitosterol to stigmasterol? *Front. Plant Sci.* **2019**, *10*, 354.
- Al-Whaibi, M.H. Plant heat-shock proteins: A mini review. *J. King Saud Univ. Sci.* **2010**, *23*, 139-150.
- Anelli, T.; Sitia, R. Protein quality control and in the early secretory pathway. *The EMBO J.* **2008**, *27*, 315-327.
- Arcuri, M.L.C.; Nunes-Laitz, A.V.; Lima, R.P.M.; Barreto, P.; Marinho, A.N.; Arruda, P.; Maia, I.G. The Knockdown of Mitochondrial Uncoupling Proteins 1 and 2 (AtUCP1 and 2) in *Arabidopsis thaliana* Impacts Vegetative Development and Fertility. *Plant Cell and Physiol.* **2021**, *00*, 1-15.
- Barreto, P.; Couñago, R.M.; Arruda, P. Mitochondrial uncoupling protein-dependent signaling in plant bioenergetics and stress response. *Mitochondrion* **2020**, *53*, 109-120.
- Barreto, P.; Dambire, C.; Sharma, G.; Vicente, J.; Osborne, R.; Yassitepe, J.; Gibbs, D.J.; Maia, I.G.; Holdsworth, M.J.; Arruda, P. Mitochondrial retrograde signaling through UCP1-mediated inhibition of the plant oxygen-sensing pathway. *Curr. Biol.* **2022**, *32*, 1-9.
- Barreto, P.; Okura, V.; Pena, I.A.; Maia, R.; Maia, I.G.; Arruda, P. Overexpression of mitochondrial uncoupling protein 1 (UCP1) induces a hypoxic response in *Nicotiana tabacum* leaves. *J. Exp. Bot.* **2015**, *67*, 301-313.
- Barreto, P.; Okura, V.K.; Neshich, L.A.; Maia, I.G.; Arruda, P. Overexpression of UCP1 in tobacco induces mitochondrial biogenesis and amplifies a broad stress response. *BMC Plant Biol.* **2014**, *14*, 144-159.
- Begcy, K.; Mariano, E.D.; Mattiello, L.; Nunes, A.V.; Mazzafera, P.; Maia, I.G.; MENOSSE M. An *Arabidopsis* mitochondrial uncoupling protein confers tolerance to drought and salt stress in transgenic tobacco plants. *PLOS ONE* **2011**, *6*, 1-10.

- Berardini, T.Z.; Reiser, L.; Li, D.; Mezheritsky, Y.; Muller, R.; Strait, E.; Huala, E. The Arabidopsis Information Resource: Making and mining the “gold standard” annotated reference plant genome. *Genesis* **2015**, 53, 474-485.
- Birke, H.; De Kok, L.J.; Wirtz, M.; Hell, R. The role of compartment-specific cysteine synthesis for sulfur homeostasis during H₂S exposure in *Arabidopsis*. *Plant Cell Physiol.* **2015**, 56, 358-367.
- Borecký, J.; Maia, I.G.; Arruda, P. Mitochondrial Uncoupling Proteins in Mammals and plants. *Biosci. Rep.* **2001**, 21, 201-212.
- Borecký, J.; Nogueira, F.T.S.; De Oliveira, K.A.P.; Maia, I.G.; Vercesi, A.E.; Arruda, P. The plant energy-dissipating mitochondrial systems: depicting the genomic structure and expression profiles of the gene families of uncoupling protein and alternative oxidase in monocots and dicots. *J. Exp. Bot.* **2006**, 57, 849-864.
- Bouché, N.; Fromm, H. GABA in plants: just a metabolite? *Trends Plant Sci.* **2004**, 9, 110-115.
- Brandalise, M.; Maia, I.G.; Borecky, J.; Vercesi, A.E.; Arruda, P. Overexpression of plant uncoupling mitochondrial protein in transgenic tobacco increases tolerance to oxidative stress. *J. Bioenerg. Biomembr.* **2003**, 35, 203-209.
- Bray, N.L.; Pimentel, H.; Melsted, P.; Pachter, L. Near-optimal probabilistic RNA-seq quantification. *Nature Biotech.* **2016**, 34, 525-527.
- Busi, M.V.; Gomez-Lobato, M.E.; Rius, S.P.; Turowski, V.R.; Casati, P.; Zabaleta, E.J.; Gomez-Casati, D.F.; Araya, A. Effect of mitochondrial dysfunction on carbon metabolism and gene expression in flower tissues of *Arabidopsis thaliana*. *Mol. Plant* **2011**, 4, 127-143.
- Chaumont, F.; Moshelion, M.; Daniels, M.J. Regulation of plant aquaporin activity. *Franois Bilogy Cells* **2000**, 97, 749-764.
- Chen, S.; Liu, A.; Ji, D.; Lin, X.; Liu, Z.; Xia, X.; Liu, D.; Ahammed, G.J. Silencing of tomato mitochondrial uncoupling protein disrupts redox poise and antioxidant enzymes activities balance under oxidative stress. *J. Plant Biol.* **2014**, 57, 9-19.
- Chen, S.; Liu, A.; Zhang, S.; Li, C.; Chang, R.; Liu, D.; Ahammed, G.J.; Lin, X. Overexpression of mitochondrial uncoupling protein conferred resistance to

- heat stress and *Botrytis cinerea* infection in tomato. *Plant Physiol. Biochem.* **2013**, 73, 245-253.
- Eprintsev, A.T.; Fedorin, D.N.; Cherkasskikh, M.; Igamberdiev, A.U. Effect of salt stress on the expression and promoter methylation of the genes encoding the mitochondrial and cytosolic forms of aconitase and fumarase in maize. *Int. J. Mol. Sci.* **2021**, 22, 6012.
- Figueira TRS, Arruda P. Differential expression of uncoupling mitochondrial protein and alternative oxidase in the plant response to stress. *J. Bioenerg. Biomembr.* **2011**, 43, 67-70.
- Fonseca-Pereira, P.; Daloso, D.M.; Gago, J.; Oliveira Silva, F.M.; Condori-Apfata, J.A.; Florez-Sarasa, I.; Tohge, T.; Reichheld, J.P.; Nunes-Nesi, A.; Fernie, A.R.; Araújo, W.L. The mitochondrial Thioredoxin system contributes to the metabolic responses under drought episodes in *Arabidopsis*. *Plant Cell Physiol.* **2018**, 60, 213-229.
- Fuchs, P.; Bohle, F.; Lichtenauer, S.; Ugalde, J. M.; Araujo, E.F.; Mansuroglu, B.; Ruberti, C.; Wagner, S.; Müller-Schüssele, S.J.; Meyer, A.J.; Schwarzländer, M. Reductive stress triggers ANAC017-mediated retrograde signaling to safeguard the endoplasmic reticulum by boosting mitochondrial respiratory capacity. *Plant Cell* 2022, 00, 1-21.
- Gandin, A.; Denysyuk, M.; Cousins, A.B. Disruption of the mitochondrial alternative oxidase (AOX) and uncoupling protein (UCP) alters rates of foliar nitrate and carbon assimilation in *Arabidopsis thaliana*. *J. Exp. Bot.* **2014**, 65: 3133-3142.
- Gawwad, M.R.A.; Šutković, J.; Mataković, L.; Musrati, M.; Zhang, L. Functional interactome of Aquaporin 1 sub-family reveals new physiological functions in *Arabidopsis Thaliana*. *Network Biol.* **2013**, 3, 1-10.
- Gibson, S.I. Control of plant development and gene expression by sugar signaling. *Curr. Opin. Plant Biol.* **2005**, 8, 93-102.
- Giraud, E.; Ho, L.H.M.; Clifton, R.; Carroll, A.; Estavillo, G.; Tan, Y.F.; Howell, K.A.; Ivanova, A.; Pogson, B.J.; Millar, A.H.; Whelan, J. The absence of ALTERNATIVE OXIDASE1a in *Arabidopsis* results in acute sensitivity to combined light and drought stress. *Plant Physiol.* **2008**, 147, 595-610.

- Han, Y.; Watanabe, S.; Shimada, H.; Sakamoto, A. Dynamics of the leaf endoplasmic reticulum modulate β -glucosidase-mediated stress-activated ABA production from its glucosyl ester. *J. Exp. Bot.* **2020**, 71, 2058-2071.
- Hildebrandt, T.M.; Nunes-Nesi, A.; Araújo, W.L.; Braun, H.P. Amino acid catabolism in plants. *Mol. Plant.* **2015**, 8, 1563-1579.
- Hruz, T.; Laule, O.; Szabo, G.; Wessendorp, F.; Bleuler, S.; Oertle, L.; Widmayer, P.; Gruissem, W.; Zimmermann, P. Genevestigator V3: a reference expression database for the meta-analysis of transcriptomes. *Adv. Bioinform.* **2008**, 420747.
- Igamberdiev, A.U.; Kleczkowski, L.A. The glycerate and phosphorylated pathways of serine synthesis in plants: the branches of plant glycolysis linking carbon and nitrogen metabolism. *Front. Plant Sci.* **2018**, 9, 318.
- Jarvis, P.; López-Juez, E. Biogenesis and homeostasis of chloroplasts and other plastids. *Nat. Rev. Mol. Cell Biol.* **2013**, 14, 787-802.
- Jiang, M.; Zhang, J. Effect of abscisic acid on active oxygen species, antioxidative defence system and oxidative damage in leaves of maize seedlings. *Plant Cell Physiol.* **2001**, 42, 1265-1273.
- Jiao, X.; Sherman, B.T.; Stephens, R.; Baseler, M.W.; Lane, H.C.; Lempicki, R.A. DAVID-WS: a stateful web service to facilitate gene/protein list analysis. *Bioinform.* **2012**, 28, 1805-1806.
- Kampinga, H.H.; Craig, E.A. The HSP70 chaperone machinery: J proteins as drivers of functional specificity. *Nat. Rev. Mol. Cell Biol.* **2010**, 11, 579-592.
- Kampinga, H.H.; Craig, E.A. The HSP70 chaperone machinery: J proteins as drivers of functional specificity. *Nat. Rev. Mol. Cell Biol.* **2010**, 11, 579-592.
- Kreps, J.A.; Wu, Y.; Chang, H.S.; Zhu, T.; Wang, X.; Harper, J.F. Transcriptome changes for *Arabidopsis* in response to salt, osmotic, and cold stress. *Plant Physiol.* **2002**, 130, 2129-2141.
- Krzyszton, M.; Zakrzewska-Placzek, M.; Kwasnik, A.; Dojer, N.; Karlowski, W.; Kufel, J. Defective XRN3-mediated transcription termination in *Arabidopsis* impacts expression of protein-coding genes. *Plant J.* **2019**, 47, 9.
- Laitz, A.V.N.; Acencio, M.L.; Lemke, N.; Ribolla, P.E.M.; Maia, I.G. Transcriptome response signatures associated with the overexpression of a

- mitochondrial uncoupling protein (AtUCP1) in tobacco. *PLOS ONE* **2015**, 10, 1-13.
- Lam, H.M.; Wong, P.; Chan, H.K.; Yam, K.M.; Chen, L.; Chow, C.M.; Coruzzi, G.M. Overexpression of the *ASN1* gene enhances nitrogen status in seeds of *Arabidopsis*. *Plant Physiol.* **2003**, 132, 926-935.
- Latijnhouwers, M.; Xu, X.M.; Moller, S.G. Arabidopsis stromal 70-kDa heat shock proteins are essential for chloroplast development. *Planta* **2010**, 232, 567-578.
- Leister, D.; Schneider, A. From genes to photosynthesis in *Arabidopsis thaliana*. *Int. Rev. Cytol.* 2003, 228, 31-83.
- Lensch, M.; Herrmann, R.G.; Sokolenko, A. Identification and characterization of SppA, a novel light-inducible chloroplast protease complex associated with thylakoid membranes. *J. Biol. Chem.* **2001**, 276, 33645-33661.
- Li, J.Y.; Fu, Y.L.; Pike, S.M.; Bao, J.; Tian, W.; Zhang, Y.; Chen, C.Z.; Zhang, Y.; Li, H.M.; Huang, J.; Li, L.G.; Schroeder, J.I.; Gassmann, W.; Gong, J.M. The *Arabidopsis* Nitrate Transporter NRT1.8 functions in nitrate removal from the xylem sap and mediates cadmium tolerance. *The Plant Cell* **2010**, 22, 1633-1646.
- Lima, R.P.M.; Nunes-Laitz, A.V.; Arcuri, M.L.C.; Campos, F.G.; Joca, T.A.C.; Monteiro, G.C.; Kushima, H.; Lima, G.P.P.; Almeida, L.F.R.; Barreto, P.; Maia, I.G. The Double Knockdown of the Mitochondrial Uncoupling Protein Isoforms Reveals Partial Redundant Roles During *Arabidopsis thaliana* Vegetative and Reproductive Development. *Submitted*.
- Liu, C.; Zhang, Y.; Cao, D.; He, Y.; Kuang, T.; Yang, C. Structural and functional analysis of the antiparallel strands in the lumenal loop of the major light-harvesting chlorophyll a/b complex of photosystem II (LHCIIb) by site-directed mutagenesis. *J. Biol. Chem.* **2008**, 283, 487-495.
- Love, M.; Huber, W.; Anders, S. Moderated estimation of fold change and dispersion for RNA-seq data with DESeq2. *Genome Biol.* 2014, 15, 1-21.
- Maeda, H.; Dudareva, N. The shikimate pathway and aromatic amino acid biosynthesis in plants. *Annu. Rev. Plant Biol.* **2012**, 63, 73-105.
- Maurino, V.G.; Engqvist, M.K.M. 2-Hydroxy Acids in Plant Metabolism. *The Arabidopsis Book* **2015**, e0182.

- Maxwell, D.P.; Wang, Y.; McIntosh, L. The alternative oxidase lowers mitochondrial reactive oxygen species production in plant cells. *Proc. Natl. Acad. Sci. USA* **1999**, 96, 8271-8276.
- McBride, H.M.; Neuspiel, M.; Wasjak, S. Mitochondria: more than just a powerhouse. *Cell Curr. Biol.* **2006**, 16, 551-560.
- Meier, K.; Ehbrecht, M.D.; Wittstock, U. Glucosinolate content in dormant and germinating *Arabidopsis thaliana* seeds is affected by non-functional alleles of classical myrosinase and nitrile-specifier protein genes. *Front. Plant Sci.* **2019**, 10, 1549.
- Millar, A.H.; Small, I.D.; Day, D.A.; Whelan, J. Mitochondrial biogenesis and function in *Arabidopsis*. *The Arabidopsis Book* **2008**, 6.
- Misra, B.B.; Yin, Z.; Geng, S.; Armas, E.; Chen, S. Metabolomic responses of *Arabidopsis* suspension cells to bicarbonate under light and dark conditions. *Sci. Rep.* **2016**, 6, 35778.
- Monné, M.; Daddabbo, L.; Gagneul, D.; Obata, T.; Hielscher, B.; Palmieri, L.; Miniero, D.V.; Fernie, A.R.; Weber, A.P.M.; Palmieri, F. Uncoupling proteins 1 and 2 (UCP1 and UCP2) from *Arabidopsis thaliana* are mitochondrial transporters of aspartate, glutamate, and dicarboxylates. *J. Biol. Chem.* **2018**, 293, 11, 4213-4227.
- Murashige T.; Skoog F.A. A revised medium for a rapid growth and bioassays with tobacco tissues cultures. *Plant Physiol.* **1962**, 15, 473-479.
- Nakano, R.T.; Piślewska-Bednarek, M.; Yamada, K.; Edger, P.P.; Miyahara, M.; Kondo, M.; Böttcher, C.; Mori, M.; Nishimura, M.; Schulze-Lefert, P.; Hara-Nishimura, I.; Bednarek, P. PYK10 myrosinase reveals a functional coordination between endoplasmic reticulum bodies and glucosinolates in *Arabidopsis thaliana*. *Plant J.* **2017**, 89, 204-220.
- Nicholls, D.G. A history of UCP1. *Biochem. Soc. Trans.* **2001**, 29, 751-755.
- Palmieri, F.; Pierri, C.L.; De Grassi, A.; Nunes-Nesi, A.; Fernie, A.R. Evolution, structure and function of mitochondrial carriers: a review with new insights. *The Plant J.* **2011**, 66, 161-181.
- Palmieri, L.; Picault, N.; Arrigoni, R.; Besin, E.; Palmieri, F.; Hodges, M. Molecular identification of three *Arabidopsis thaliana* mitochondrial dicarboxylate carrier isoforms: organ distribution, bacterial expression,

- reconstitution into liposomes and functional characterization. *Biochem. J.* **2008**, 410, 621-629.
- Pandey, S.P.; Somssich, I.E. The role of WRKY transcription factors in plant immunity. *Plant Physiol.* **2009**, 150, 1648-1655.
- Patrick, J.W.; Botha, F.C.; Birch, R.G. Metabolic engineering of sugars and simple sugar derivatives in plants. *Plant Biotech. J.* **2013**, 11, 142-156.
- Perez-Rodriguez, P.; Riano-Pachon, D.M.; Correa, L.G.G.; Rensing, S.A.; Kersten, B.; Mueller-Robber, B. PlnTFDB: updated content and new features of the plant transcription factor database. *Nucleic Acids Res.* **2009**, 38, 822-827.
- Pratelli, R.; Pilot, G. Regulation of amino acid metabolic enzymes and transporters in plants. *J. Exp. Bot.* **2014**, 65, 5535-5556.
- Pu, X.; Lv, X.; Tan, T.; Fu, F.; Qin, G.; Lin, H. Roles of mitochondrial energy dissipation systems in plant development and acclimation to stress. *Ann. Bot.* **2015**, 116, 583-600.
- Pu, Xiao-Jun; Li, Ya-Nan; Wei, Li-Jie; Xi, De-Hui; Lin, Hong-Hui. Mitochondrial energy-dissipation pathway and cellular redox disruption compromises Arabidopsis resistance to turnip crinkle virus infection. *Biochem. Biophys. Res. Commun.* **2016**, 473, 421-427.
- Rhoads, D.M.; Subbaiah, C.C. Mitochondrial retrograde regulation in plants. *Mitochondrion* **2007**, 7, 177-194.
- Rhoads, D.M.; White, S.J.; Zhou, Y.; Muralidharan, M.; Elthon, T.E. Altered gene expression in plants with constitutive expression of a mitochondrial small heat shock protein suggests the involvement of retrograde regulation in the heat stress response. *Physiol. Plant.* **2005**, 123, 435-444.
- Rolland, F.; Baena-Gonzalez, E.; Sheen, J. Sugar sensing and signaling in plants: conserved and novel mechanisms. *Annu. Rev. Plant Biol.* **2006**, 57, 675-709.
- Schaeffer, A.; Bronner, R.; Benveniste, P.; Schaller, H. The ratio of campesterol to sitosterol that modulates growth in Arabidopsis is controlled by STEROL METHYLTRANSFERASE 2;1. *Plant J.* **2001**, 25, 605-615.

- Schenk, P.M.; Kazan, K.; Rusu, A.G.; Manners, J.M.; Maclean, D.J. The *SEN1* gene of *Arabidopsis* is regulated by signals that link plant defence responses and senescence. *Plant Physiol. Biochem.* **2005**, 43, 997-1005.
- Silva-Filho, M.C. One ticket for multiple destinations: dual targeting of proteins to distinct subcellular locations. *Curr. Opin. Plant Biol.* **2003**, 6, 1-7.
- Smeekens, S.; Ma, J.K.; Hanson, J.; Rolland, F. Sugar signals and molecular networks controlling plant growth. *Curr. Opin. Plant Biol.* **2010**, 13, 274-279.
- Smith, A.M.; Ratcliffe, R.G.; Sweetlove, L.J. Activation and function of mitochondrial uncoupling protein in plants. *J. Biol. Chem.* **2004**, 279, 51944-51952.
- Sun, X.; Zhao, T.; Gan, S.; Ren, X.; Fang, L.; Karungo, S.K.; Wang, Y.; Chen, L.; Li, S.; Xin, H. Ethylene positively regulates cold tolerance in grapevine by modulating the expression of ETHYLENE RESPONSE FACTOR. *Sci. Rep.* **2016**, 6, 1-14.
- Sweetlove, L.J.; Lytovchenko, A.; Morgan, M.; Nunes-Nesi, A.; Taylor, N.L.; Baxter, C.J.; Eickmeier, I.; Fernie, A.R. Mitochondrial uncoupling protein is required for efficient photosynthesis. *Proc. Natl. Acad. Sci. USA* **2006**, 103, 19587-19592.
- Swindell, W.R.; Huebner, M. Weber, A.P. Transcriptional profiling of *Arabidopsis* heat shock proteins and transcription factors reveals extensive overlap between heat and non-heat stress response pathways. *BMC Genom.* **2007**, 8, 125.
- Thimm, O.; Blaesing, O.; Gibon, Y.; Nagel, A.; Meyer, S.; Krüger, P.; Selbig, J.; Müller, L.A.; Rhee, S.Y.; Stitt, M. MAPMAN: a user-driven tool to display genomics data sets onto diagrams of metabolic pathways and other biological processes. *The Plant J.* **2004**, 37, 914-939.
- Valpuesta, V.; Botella, M.A. Biosynthesis of L-ascorbic acid in plants: new pathways for an old antioxidant. *Trends Plant Sci.* **2004**, 9, 573-577.
- Vercesi, A.E.; Borecký, J.; Maia, I.G.; Arruda, P.; Cuccovia, I.M.; Chaimovich, H. Plant uncoupling mitochondrial proteins. *Ann. Rev. Plant Biol.* **2006**, 57, 383-404.
- Vishwakarma, K.; Upadhyay, N.; Kumar, N.; Yadav, G.; Singh, J.; Mishra, R.K.; Kumar, V.; Verma, R.; Upadhyay, R.G.; Pandey, M.; Sharma, S. Absciscic

- acid signaling and abiotic stress tolerance in plants: a review on current knowledge and future prospects. *Front. Plant Sci.* **2017**, 8, 161.
- Voll, L. M.; Jamai, A.; Renné, P.; Voll, H.; McClung, C. R.; Weber, A. P. The photorespiratory *Arabidopsis* shm1 mutant is deficient in SHM1. *Plant Physiol.* **2006**, 140, 59-66.
- Wang, H.; Wang, H.; Shao, H.; Tang, X. Recent advances in utilizing transcription factors to improve plant abiotic stress tolerance by transgenic technology. *Front. Plant Sci.* **2016**, 7, 67.
- Wang, P.; Song, C.-P. Guard-cell signalling for hydrogen peroxide and abscisic acid. *New Phytol.* **2008**, 178, 703-718.
- Wani, S.H.; Kumar, V.; Shriram, V.; and Sah, S.K. Phytohormones and their metabolic engineering for abiotic stress tolerance in crop plants. *Crop J.* **2016**, 4, 162–176.
- Wei, X.; Su, X.; Cao, P.; Liu, X.; Chang, W.; Li, M.; Zhang, X.; Liu, Z. Structure of spinach photosystem II-LHCII supercomplex at 3.2Å resolution. *Nat.* **2016**, 534, 69-74.
- Welchen, E.; García, L.; Mansilla, N.; Gonzalez, D.H. Coordination of plant mitochondrial biogenesis: keeping pace with cellular requirements. *Front. Plant Sci.* **2014**, 4, 551.
- Williamson, J.D.; Jennings, D.B.; Guo, W.W.; Pharr, D.M. Sugars alcohols, salt stress, and fungal resistance: polyols – multifunctional plant protection? *J. Amer. Soc. Hort. Sci.* **2002**, 127, 467-473.
- Woldesemayat, A.A.; Ntwasa, M. Pathways and network based analysis of candidate genes to reveal cross-talk and specificity in the Sorghum (*Sorghum bicolor* (L.) Moench) responses to drought and it's co-occurring stresses. *Front. Genet.* **2018**, 9, 557.
- Yonekura-Sakakibara, K.; Higashi, Y.; Nakabayashi, R. The Origin and Evolution of Plant Flavonoid Metabolism. *Front. Plant Sci.* **2019**, 10, 943.
- Yoon, Y.; Hyun Seo, D.; Shin, H.; Jin Kim, H.; Min Kim, C. The role of stress-responsive transcription factors in modulating abiotic stress tolerance in plants. *Agronomy* **2020**, 10, 788.

Zhang, X.; Zhang, L.; Dong, F.; Gao, J.; Galbraith, D.W.; Song, C.P. Hydrogen peroxide is involved in abscisic acid-induced stomatal closure in *Vicia faba*. *Plant Physiol.* **2001**, 126, 1438-1448.

Zhao, C.; Zayed, O.; Zeng, F.; Liu, C.; Zhang, L.; Zhu, P.; Hsu, C.C.; Tuncil, Y.E.; Tao, W.A.; Carpita, N.C.; Zhu, J.K. Arabinose biosynthesis is critical for salt stress tolerance in *Arabidopsis*. *New Phytol.* **2019**, 224, 274-290.

Supplementary Data

Table S1. Summary of the RNA-Seq reads and mapping statistics from *ucp1 ucp3* double mutant plants (21-day-old) compared with wild-type (WT) control.

Sample	Reads	Reads mapped (%)	Unique mapping (%)	Transcripts TPM > 0	Transcripts TPM ≥ 1	Transcripts TPM ≥ 2	Transcripts TPM ≥ 3	Transcripts TPM ≥ 5
WT_R1	10473764	91.9	61.4	25384	22185	19863	18120	15699
WT_R2	7340222	95.3	63.8	24875	22243	20080	18478	16030
WT_R3	9385814	90.3	60.9	25321	22192	19875	18175	15680
<i>ucp1_ucp3</i> _R1	9904360	90.6	61	25155	21822	19486	17779	15158
<i>ucp1_ucp3</i> _R2	23709422	95.3	63.7	27156	22504	20002	18251	15690
<i>ucp1_ucp3</i> _R3	2477978	95.5	63.9	21983	20393	18859	17486	15208
Mean	10548593	93	62	24979	21890	19694	18048	15578
Total of transcripts	35386							

Table S2. List of differentially expressed genes (DEGs) between *ucp1 ucp3* double mutant and wild-type (WT). (A) List of upregulated DEGs.

TAIR_ID	Gene Name	WT_R1	WT_R2	WT_R3	<i>ucp1</i> <i>ucp3</i> _R1	<i>ucp1</i> <i>ucp3</i> _R2	<i>ucp1</i> <i>ucp3</i> _R3	Log ₂ Fold Change	p value	p adjusted
AT1G01120	3-ketoacyl-CoA synthase 1(KCS1)	23.1255	25.725	25.4335	34.628	28.1206	48.7743	0.631398424	0.002451506	0.052638776
AT1G01620	plasma membrane intrinsic protein 1C(PIP1C)	306.529	339.929	224.47	513.05943	413.201155	528.356	0.841637651	1.83E-07	3.10E-05
AT1G02500	S-adenosylmethionine synthetase 1(SAM1)	284.9986	261.07129	223.7341	346.5245	314.3345	303.34036	0.425245933	0.001387851	0.037340805
AT1G02640	beta-xylosidase 2(BXL2)	25.0608	25.3801	15.6337	40.6655	39.4787	43.6787	0.996535514	6.74E-08	1.38E-05
AT1G02660	alpha/beta-Hydrolases superfamily protein(AT1G02660)	18.6035	21.4768	19.1379	29.055	23.9482	46.2153	0.794822568	0.000241897	0.011118431
AT1G03080	kinase interacting (KIP1-like) family protein(NET1D)	10.7285	13.2936	11.4539	15.9529	14.3707	14.4208	0.436894927	0.006823164	0.095820889
AT1G03090	methyl crotonyl-CoA carboxylase alpha chain(MCCA)	43.56723	41.88151	24.10433	78.4629	65.22689	69.398	1.062961667	3.21E-08	7.66E-06
AT1G03130	photosystem I subunit D-2(PSAD-2)	551.292	565.391	637.537	699.031	718.454	1040.17	0.574217765	0.000279016	0.012189675
AT1G03220	Eukaryotic aspartyl protease family protein(AT1G03220)	141.714	172.993	119.68	234.408	171.614	197.571	0.580202287	0.000484296	0.01737364
AT1G04240	AUX/IAA transcriptional regulator family protein(SHY2)	30.5341	28.3972	27.4019	37.0472	39.7136	55.438	0.646602131	0.001763722	0.043599003
AT1G05805	basic helix-loop-helix (bHLH) DNA- binding superfamily protein(AT1G05805)	45.0588	47.9922	43.3903	59.338	54.6317	72.0229	0.510137187	0.002696002	0.056113724
AT1G06570	4-hydroxyphenylpyruvate dioxygenase(PDS1)	27.5755	27.52191	19.22613	36.3463	34.00617	45.7665	0.703450313	0.000577621	0.019834667
AT1G06760	winged-helix DNA-binding transcription factor family protein(AT1G06760)	166.431	175.108	122.03	240.754	185.802	170.231	0.477183619	0.005972126	0.090292731
AT1G07000	exocyst subunit exo70 family protein B2(EXO70B2)	13.3032	13.5628	9.64686	22.595	18.2007	14.6812	0.738425016	0.001497912	0.039109691
AT1G07040	plant/protein(AT1G07040)	35.0815	35.262	32.5096	50.4479	45.0778	57.129	0.63831256	0.000181897	0.008630343
AT1G07600	metallothionein 1A(MT1A)	1278.25	1256.15	1127.84	2266.55	1406.14	1633.14	0.640160583	0.003602447	0.066929679
AT1G08110	lactoylglutathione lyase family protein / glyoxalase I family protein(AT1G08110)	90.12305	86.5295	81.5443	109.3158	108.07025	125.92296	0.483192045	0.001790751	0.044143519
AT1G08510	fatty acyl-ACP thioesterases B(FATB)	52.7507	53.5747	57.1198	66.75	68.4326	71.3207	0.422700152	0.002200633	0.049796374
AT1G08980	amidase 1(AMI1)	90.4254	89.7239	82.0649	105.553	104.749	134.809	0.468494119	0.001573707	0.040489695
AT1G09070	soybean gene regulated by cold- 2(SRC2)	106.941	107.487	122.793	140.956	126.192	184.424	0.493511793	0.002845871	0.058400671
AT1G09570	phytochrome A(PHYA)	28.60030007	31.49222	30.9259	42.5937	37.9542258	41.3233	0.51322227	0.000304698	0.012927696
AT1G09770	cell division cycle 5(CDC5)	42.6654	43.9812	36.2836	53.2778	49.9324	49.0379	0.408515098	0.004016614	0.0717357
AT1G10020	formin-like protein (DUF1005)(AT1G10020)	20.0524	18.0004	17.0565	31.1698	22.0741	28.1274	0.642898939	0.002125362	0.048524368

AT1G10070	branched-chain amino acid transaminase 2(BCAT-2)	11.3503	13.27543	5.73094	36.45184	23.938918	18.2544	1.521999024	2.86E-07	4.43E-05
AT1G11260	sugar transporter 1(STP1)	235.708	214.632	157.8	734.946	455.713	709.244	1.750358548	1.59E-20	1.41E-16
AT1G12240	Glycosyl hydrolases family 32 protein(ATBETAFRUCT4)	55.384	48.9771	38.1157	82.7649	89.0793	117.747	1.101026406	1.25E-10	7.86E-08
AT1G12440	A20/AN1-like zinc finger family protein(AT1G12440)	86.30501	83.119796	65.75156	104.37647	99.96428	107.885	0.495468555	0.002555466	0.054473409
AT1G12710	phloem protein 2-A12(PP2-A12)	24.4856	24.7952	30.4186	36.9141	35.832	38.4195	0.558007307	0.005280422	0.083977988
AT1G12780	UDP-D-glucose/UDP-D-galactose 4-epimerase 1(UGE1)	94.934	103.206	93.3327	114.972	127.852	130.869	0.445033761	0.000639762	0.021467307
AT1G14280	phytochrome kinase substrate 2(PKS2)	16.8894	15.6641	15.434	32.0254	25.4541	42.1234	1.09129653	2.03E-06	0.00022967
AT1G15380	Lactoylglutathione lyase / glyoxalase I family protein(GLY14)	44.8329	56.9777	46.3227	88.3052	59.0337	61.93368	0.615610303	0.004083055	0.072065923
AT1G16720	high chlorophyll fluorescence phenotype 173(HCF173)	98.3366	102.623	78.1194	110.664	112.494	149.069	0.497741246	0.00133438	0.036685066
AT1G18020	FMN-linked oxidoreductases superfamily protein(AT1G18020)	25.7194	25.2645	19.1025	52.738	42.2254	60.9219	1.216936492	2.32E-08	6.20E-06
AT1G19400	Erythronate-4-phosphate dehydrogenase family protein(AT1G19400)	40.16173	38.98761	36.20045	61.95807	48.7551	53.18006	0.601584578	0.001023219	0.02999969
AT1G19530	DNA polymerase epsilon catalytic subunit A(AT1G19530)	47.3028	51.4823	77.2651	104.424	85.801	97.365	0.793920357	0.000331009	0.013650266
AT1G19660	Wound-responsive family protein(AT1G19660)	91.66844	94.45709	93.9549	126.88691	119.97713	161.4609	0.616941036	4.47E-05	0.002819456
AT1G20440	cold-regulated 47(COR47)	280.826	419.152	278.449	495.281	351.795	418.674	0.479767536	0.006190069	0.091965246
AT1G20450	Dehydrin family protein(ERD10)	68.5028	88.6754	87.123585	107.73834	95.704761	123.17583	0.501481975	0.001845328	0.044832931
AT1G20510	OPC-8:0 CoA ligase1(OPCL1)	27.1217	26.51493	28.61799	33.748	41.92457	62.8756	0.792207825	9.34E-05	0.005046165
AT1G20620	catalase 3(CAT3)	1243.61102	1292.86623	1740.86024	2091.06182	1895.106297	2001.12	0.581011131	6.79E-05	0.004022917
AT1G21130	O-methyltransferase family protein(IGMT4)	456.67217	579.36312	399.96722	556.03843	575.5206	660.8898	0.416684422	0.003145053	0.061953339
AT1G21500	hypothetical protein(AT1G21500)	302.244	278.963	294.205	340.97	346.909	382.213	0.370485736	0.00595648	0.090292731
AT1G21680	DPP6 N-terminal domain-like protein(AT1G21680)	103.721	106.871	94.8596	132.175	130.523	148.941	0.518353919	4.00E-05	0.002670245
AT1G22690	Gibberellin-regulated family protein(AT1G22690)	188.5683	204.6978	178.3441	237.9914	223.9649	281.307	0.450077375	0.005003197	0.081313461
AT1G22740	RAB GTPase homolog G3B(RABG3B)	37.4293	32.6482	26.3661	46.8748	45.1545	48.0872	0.61924486	0.003234586	0.062923511
AT1G23030	ARM repeat superfamily protein(AT1G23030)	24.9678	27.0891	24.4276	32.0664	28.6211	44.8705	0.512751955	0.007237015	0.098103697
AT1G23310	glutamate:glyoxylate aminotransferase(GGT1)	705.428	790.681	569.90698	813.068	801.12994	1025.95	0.452701943	0.001681142	0.042028542
AT1G25275	thionin-like protein(AT1G25275)	491.01932	601.51938	601.5711	766.80589	647.8322	687.0486	0.410867016	0.004758307	0.07866464
AT1G26670	Vesicle transport v-SNARE family protein(VTI1B)	67.7284	74.8276	65.6226	94.1244	83.9037	99.024	0.493007409	0.002256642	0.050417371

AT1G27770	autoinhibited Ca ²⁺ -ATPase 1(ACA1)	18.4722	23.0882	23.2154	26.4686	29.3834	29.9462	0.492121089	0.001655986	0.042028542
AT1G28290	arabinogalactan protein 31(AGP31)	85.6772032	99.35857	78.3646	141.2250003	127.488	121.387	0.673069181	3.63E-06	0.000381588
AT1G28330	dormancy-associated protein-like 1(DYL1)	675.04959	718.5473	519.9129	1491.65787	904.945826	1131.9718	0.992335576	5.05E-08	1.12E-05
AT1G29395	COLD REGULATED 314 INNER MEMBRANE 1(COR413IM1)	25.1331	28.0263	49.6348	93.6969	72.1701	122.702	1.573778429	8.88E-05	0.004839504
AT1G29910	chlorophyll A/B binding protein 3(CAB3)	3360.02	3156.56	4008.69	4475.6	4094.83	5629.98	0.528621191	0.000439909	0.016127779
AT1G29920	chlorophyll A/B-binding protein 2(CAB2)	2609.47	2347.13	2129.25	2843.76	3156.51	4416.95	0.651770646	2.97E-05	0.002129878
AT1G29930	chlorophyll A/B binding protein 1(CAB1)	14318.2	13102.6	13812.6	21683	18450.2	23060.1	0.715782363	2.68E-08	6.56E-06
AT1G30380	photosystem I subunit K(PSAK)	2216.07	2072.53	2151.48	2316.59	2393.91	2970.25	0.347294421	0.00657564	0.094357756
AT1G30510	root FNR 2(RFNR2)	46.58058	60.4968776	46.91097	64.60599	67.19337	62.11097	0.438010331	0.005859309	0.08937017
AT1G30690	Sec14p-like phosphatidylinositol transfer family protein(AT1G30690)	31.63308	40.61812	25.93657	43.22227	40.700739	51.008	0.538893772	0.003331032	0.063766511
AT1G30880	hypothetical protein(AT1G30880)	119.492	117.139	91.3763	164.217	139.152	123.05	0.495458892	0.007281351	0.098103697
AT1G31330	photosystem I subunit F(PSAF)	3573.77	3409.11	3722.38	4241.41	4070.04	5001.42	0.410707217	0.000998573	0.029472939
AT1G32450	nitrate transporter 1.5(NRT1.5)	87.2646	113.078	70.4002	144.914	131.918	122.399	0.668179332	3.16E-05	0.002213611
AT1G32460	hypothetical protein(AT1G32460)	145.536	162.536	123.648	200.163	171.278	176.087	0.445191277	0.007021593	0.096931704
AT1G32640	Basic helix-loop-helix (bHLH) DNA-binding family protein(MYC2)	12.6127	17.0897	10.2611	19.9681	28.3482	45.6413	1.282208421	4.42E-07	6.20E-05
AT1G35580	cytosolic invertase 1(CINV1)	91.22456	101.27198	80.48631317	132.09957	105.254775	102.4676	0.424293307	0.005286024	0.083977988
AT1G42470	Patched family protein(AT1G42470)	9.97186	9.02575	7.71928	11.3432	12.0597	14.1683	0.551309318	0.004398237	0.075076285
AT1G44800	nodulin MtN21 /EamA-like transporter family protein(SIAR1)	13.4873	14.3227	19.8502	37.1464	33.9241	26.8645	1.159457165	1.55E-07	2.81E-05
AT1G45145	thioredoxin H-type 5(TRX5)	45.3252	57.8887	43.6576	91.016	72.1914	53.5455	0.707891587	0.001379886	0.037340805
AT1G47128	Granulin repeat cysteine protease family protein(RD21A)	290.586	330.743	272.342	351.894	328.884	372.912	0.333689787	0.007262794	0.098103697
AT1G50740	Transmembrane proteins 14C(AT1G50740)	25.3174	30.0366	20.1812	35.8298	32.3414	59.2554	0.765427874	0.005372462	0.084513325
AT1G51400	Photosystem II 5 kD protein(AT1G51400)	542.565	591.109	631.842	838.051	816.602	1256.04	0.806769353	1.24E-06	0.000152209
AT1G51760	peptidase M20/M25/M40 family protein(IAR3)	21.8474	24.532	20.5187	32.6642	31.1586	36.4909	0.657297331	0.000428286	0.015947767
AT1G52400	beta glucosidase 18(BGLU18)	11.519014	18.7976	15.225	36.017603	56.118592	78.35541	1.972860753	1.12E-16	2.48E-13
AT1G52410	TSK-associating protein 1(TSA1)	5.63653	7.12716	8.14906	7.1253	15.1316	15.1052	0.8935011	0.001372667	0.037340805
AT1G53580	glyoxalase II 3(GLY3)	56.7305	55.4121	56.94573	74.111696	70.6734	74.4636	0.460249545	0.003416394	0.064316541
AT1G53840	pectin methylesterase 1(PME1)	24.2461	27.447	27.1027	32.4522	34.8002	38.4504	0.497234783	0.002806447	0.057731686

AT1G56220	Dormancy/auxin associated family protein(AT1G56220)	789.5811	872.3043	820.7403	1266.8741	927.4012	1074.1591	0.499696791	0.000566442	0.019758294
AT1G57990	purine permease 18(PUP18)	64.425	87.5566	68.2512	81.5415	109.368	144.349	0.676616652	0.000274483	0.01211156
AT1G58200	MSCS-like 3(MSL3)	23.41587	21.5384	22.16575	27.44097251	26.48612	43.36890018	0.575958837	0.003383997	0.064316541
AT1G58290	Glutamyl-tRNA reductase family protein(HEMA1)	94.0956	89.274	83.7491	85.4961	117.284	148.486	0.467617108	0.005156207	0.082733691
AT1G59124	Disease resistance protein (CC-NBS-LRR class) family(AT1G59124)	5.91318	8.00719	4.61716	6.97495	8.98568	15.7054	0.803898799	0.003447141	0.064451315
AT1G61520	PSI type III chlorophyll a/b-binding protein(LHCA3)	2953.969567	3121.53096	3215.824094	3693.58305	3614.56006	5014.64464	0.504744685	0.000365387	0.014159645
AT1G61890	MATE efflux family protein(AT1G61890)	14.3051	14.5967	13.3533	22.9434	19.5763	34.0262	0.886530414	0.000102962	0.005473738
AT1G63800	ubiquitin-conjugating enzyme 5(UBC5)	70.4072	92.5718	71.0035	104.38	91.191	114.35	0.486155106	0.006099702	0.091119959
AT1G64720	Polyketide cyclase/dehydrase and lipid transport superfamily protein(CP5)	437.663	484.301	423.47	880.403	705.796	1034.31	1.061935576	1.39E-12	1.02E-09
AT1G65390	phloem protein 2 A5(PP2-A5)	23.4634	24.2052	35.4958	49.6634	42.684171	49.80558	0.852514946	4.41E-05	0.002798101
AT1G66100	Plant thionin(AT1G66100)	17.0047	18.471	25.7722	55.4775	50.8036	104.008	1.792710812	1.68E-09	7.07E-07
AT1G67865	hypothetical protein(AT1G67865)	86.9601	85.4044	101.62	126.881	115.961	186.547	0.674485238	0.002890585	0.058507818
AT1G67870	glycine-rich protein(AT1G67870)	201.855	170.382	150.876	255.877	207.268	211.883	0.469134267	0.002666883	0.055638876
AT1G68010	hydroxypyruvate reductase(HPR)	348.1527	331.637	229.55068	359.305	360.687	486.5009033	0.502017318	0.002576431	0.054787967
AT1G68020	UDP-Glycosyltransferase / trehalose-phosphatase family protein(ATTPS6)	13.254842	15.5946	12.9131	18.239	20.20731	22.08945	0.610704663	0.000616551	0.020767407
AT1G68520	B-box type zinc finger protein with CCT domain-containing protein(BBX14)	156.249	139.317	165.94	218.185	186.274	206.293	0.497419859	0.000414386	0.015695102
AT1G69840	SPFH/Band 7/PHB domain-containing membrane-associated protein family(AT1G69840)	33.09186	38.31906	38.455993	58.325759	50.910472	71.58714	0.77890542	4.06E-05	0.002671315
AT1G69890	actin cross-linking protein (DUF569)(AT1G69890)	39.8096	51.2725	41.9267	68.7744	55.1063	74.7564	0.65522445	0.000488597	0.017386569
AT1G70700	TIFY domain/Divergent CCT motif family protein(TIFY7)	39.76802	41.2284	24.4851	77.988772	104.725737	187.84601	1.903555485	1.72E-05	0.001342725
AT1G72150	PATELLIN 1(PATL1)	386.985	418.157	325.599	513.23	457.074	586.504	0.559882199	5.34E-05	0.003332858
AT1G72610	germin-like protein 1(GER1)	2191.72	1875.52	2274.23	2352.19	2625.43	2749.08	0.376370798	0.002236568	0.050223195
AT1G74920	aldehyde dehydrogenase 10A8(ALDH10A8)	79.1223	89.8568	79.9	105.714	99.34774	103.494	0.405136273	0.002418523	0.052440943
AT1G74950	TIFY domain/Divergent CCT motif family protein(TIFY10B)	25.5519	32.9725	25.9957	41.5593	58.3274	83.7468	1.167529789	1.53E-07	2.81E-05
AT1G75800	Pathogenesis-related thaumatin superfamily protein(AT1G75800)	103.372	108.441	95.5746	144.895	118.791	119.071	0.420852858	0.004159017	0.072917721
AT1G76100	plastocyanin 1(PETE1)	232.223	215.379	186.684	248.503	245.364	326.836	0.445672566	0.004274279	0.073857245
AT1G76490	hydroxy methylglutaryl CoA reductase 1(HMG1)	114.418	105.624	97.0491	147.662	141.946	156.498	0.583659893	4.00E-06	0.000401418

AT1G77120	alcohol dehydrogenase 1(ADH1)	26.215	36.7934	66.3153	82.5259	108.915	100.538	1.260027224	0.001985954	0.046833273
AT1G77180	chromatin protein family(SKIP)	51.21438	52.02472	49.28712	71.06	62.34995	71.9416	0.515628268	0.000365824	0.014159645
AT1G79040	photosystem II subunit R(PSBR)	5927.26	6474.97	5773.77	7784.86	6799.87	8722.96	0.459412541	0.000356505	0.014159645
AT1G79700	Integrase-type DNA-binding superfamily protein(WRI4)	30.90844	32.12406	17.7035	78.8201	49.0114	66.9089	1.369593983	2.50E-08	6.31E-06
AT1G80180	hypothetical protein(AT1G80180)	114.417	126.67	106.33	202.004	142.933	198.422	0.732535043	5.36E-05	0.003332858
AT1G80240	choice-of-anchor C domain protein. putative (Protein of unknown function. DUF642)(DGR1)	16.2452	22.8067	11.503	34.2114	20.832	23.6358	0.760340924	0.006292034	0.092703332
AT1G80420	BRCT domain-containing DNA repair protein(ATXRCC1)	17.896887	18.86644	12.28298	31.595737	24.606388	29.9301	0.8972701	0.000130888	0.006715599
AT1G80920	Chaperone DnaJ-domain superfamily protein(J8)	479.421	604.842	635.662	738.439	694.113	763.879	0.448214334	0.001095744	0.031294319
AT2G01450	MAP kinase 17(MPK17)	82.06253	85.24263171	81.11796701	104.02505	99.21932	114.914	0.439615566	0.00119621	0.033406822
AT2G05510	Glycine-rich protein family(AT2G05510)	62.26	53.7097	77.32244	136.0494	124.56102	76.2409	0.93354276	1.79E-05	0.001388345
AT2G05540	Glycine-rich protein family(AT2G05540)	170.99	161.141	167.769	353.194	303.553	336.414	1.082232582	4.70E-14	4.60E-11
AT2G06050	oxophytodienoate-reductase 3(OPR3)	24.798	26.6272	21.53217	53.475	59.20666	98.4298	1.581164996	4.32E-13	3.81E-10
AT2G06520	photosystem II subunit X(PSBX)	2906.96	2660.72	2719.65	3286.05	3125.69	4006.41	0.425288398	0.00112303	0.03186734
AT2G13790	somatic embryogenesis receptor-like kinase 4(SERK4)	19.4799	20.4104	19.2128	33.447	26.2449	31.2897	0.706178886	0.000139583	0.006920348
AT2G14890	arabinogalactan protein 9(AGP9)	143.87559	118.238483	113.376459	182.29087	153.13784	156.38269	0.487057027	0.00236123	0.051451502
AT2G15880	Leucine-rich repeat (LRR) family protein(AT2G15880)	67.6531	62.1001	55.8638	157.113	83.1021	161.379	1.219930368	0.000364959	0.014159645
AT2G15890	maternal effect embryo arrest 14(MEE14)	466.34322	510.8866	477.66333	639.4604	654.8515	735.4911	0.573852847	5.54E-07	7.64E-05
AT2G15960	stress-induced protein(AT2G15960)	708.59	738.951	687.288	1129.51	1038.62	1343.1	0.802072809	1.42E-08	3.91E-06
AT2G16660	Major facilitator superfamily protein(AT2G16660)	75.0725	56.8054	62.5423	130.385	149.409	192.06	1.355264935	1.58E-16	2.79E-13
AT2G17880	Chaperone DnaJ-domain superfamily protein(AT2G17880)	23.4802	27.3742	34.2493	53.1716	40.9889	42.6522	0.786825292	0.000662096	0.022049038
AT2G18280	tubby like protein 2(TLP2)	75.36952	86.95955	60.5094	105.94074	93.3604	106.9818	0.554342927	0.000369052	0.014222207
AT2G18700	trehalose phosphatase/synthase 11(TPS11)	41.5338	44.3659	24.6367	79.6712	66.7875	104.082	1.272865994	4.48E-10	2.64E-07
AT2G19810	CCCH-type zinc finger family protein(OZF1)	9.51373	13.8383	9.75553	23.9894	18.3289	23.0149	1.069293253	2.25E-05	0.00170052
AT2G20260	photosystem I subunit E-2(PSAE-2)	1107.69	1045.03	1046.05	1305.23	1194.36	1467.55	0.40250078	0.0016584	0.042028542
AT2G20670	sugar phosphate exchanger. putative (DUF506)(AT2G20670)	180.924	190.555	193.032	235.247	214.687	313.259	0.516439903	0.000848535	0.026367342
AT2G21045	Rhodanese/Cell cycle control phosphatase superfamily protein(AT2G21045)	45.1168	51.9089	39.5975	63.7782	60.3496	66.7097	0.564566135	0.006537792	0.094120741

AT2G22330	cytochrome P450. family 79. subfamily B. polypeptide 3(CYP79B3)	23.2108	23.6384	29.7326	39.4156	45.5981	43.4035	0.832418654	1.60E-06	0.0001831
AT2G22980	serine carboxypeptidase-like 13(SCPL13)	31.15968	19.24871	20.74299	33.74552	44.82092	51.16641	0.921114494	1.88E-05	0.001440466
AT2G24600	Ankyrin repeat family protein(AT2G24600)	22.50182	30.75641	22.19903967	34.321526	35.25927	43.89776	0.662158709	0.000266549	0.011940567
AT2G24945	transmembrane protein(AT2G24945)	17.0322	26.9433	26.5906	36.683	29.8399	34.9772	0.620930911	0.001382131	0.037340805
AT2G25900	Zinc finger C-x8-C-x5-C-x3-H type family protein(ATCTH)	77.7766	85.3465	66.955	117.833	113.151	144.231	0.787702985	1.77E-07	3.06E-05
AT2G27385	Pollen Ole e 1 allergen and extensin family protein(AT2G27385)	124.2930396	143.6870527	90.9994	181.4277809	183.914	317.051	0.997513175	2.79E-06	0.000307277
AT2G28910	CAX interacting protein 4(CXIP4)	210.537	238.621	196	283.812	242.178	268.261	0.398592193	0.003250386	0.063043198
AT2G29670	Tetratricopeptide repeat (TPR)-like superfamily protein(AT2G29670)	65.0265	63.203	59.2383	84.0341	118.439	150.91	0.987883282	1.16E-08	3.54E-06
AT2G29970	Double Clp-N motif-containing P-loop nucleoside triphosphate hydrolases superfamily protein(AT2G29970)	10.6854	10.1137	10.0576	13.5285	14.278	17.3101	0.601412585	0.00145613	0.038183737
AT2G29980	fatty acid desaturase 3(FAD3)	99.759	95.9224	101.405765	119.305	121.003682	135.561	0.419212891	0.001920439	0.045761892
AT2G30570	photosystem II reaction center W(PSBW)	2368.23	2386.28	2382.07	2766.28	2825.71	3603.28	0.46057476	0.000360413	0.014159645
AT2G31810	ACT domain-containing small subunit of acetolactate synthase protein(AT2G31810)	120.52543	122.35571	95.475124	184.30135	153.76988	158.57096	0.656231522	7.43E-06	0.000669306
AT2G31880	Leucine-rich repeat protein kinase family protein(SOBIR1)	36.8581	40.5681	41.2626	53.9457	44.7595	57.186	0.473571715	0.004082614	0.072065923
AT2G32090	Lactoylglutathione lyase / glyoxalase I family protein(AT2G32090)	35.26239	34.98131	25.61086	48.3232	48.87422	51.6606	0.715623002	0.002545435	0.054390962
AT2G32150	Haloacid dehalogenase-like hydrolase (HAD) superfamily protein(AT2G32150)	48.7639	62.6357	49.0424	96.0711	80.7189	128.77	0.997767284	2.79E-07	4.43E-05
AT2G32800	protein kinase family protein(AP4.3A)	4.95695	7.30377	7.27908	11.2965	10.9208	15.6405	0.999713041	5.54E-05	0.003393986
AT2G33830	Dormancy/auxin associated family protein(AT2G33830)	1399.0321	1540.568	983.07	3987.8112	2213.5248	3016.0927	1.345369932	3.12E-05	0.002204971
AT2G33850	E6-like protein(AT2G33850)	42.1536	33.5514	20.3998	53.9307	46.0535	80.166	0.954596926	0.000235359	0.010874567
AT2G34420	photosystem II light harvesting complex protein B1B2(LHB1B2)	5361.71	5317.67	6218.75	10618.2	7735.59	12295.9	0.961541494	5.54E-09	1.88E-06
AT2G34430	light-harvesting chlorophyll-protein complex II subunit B1(LHB1B1)	1914.31	2099.24	2429.79	6235.18	4375.67	6896.84	1.545278979	6.56E-20	2.89E-16
AT2G34510	choice-of-anchor C domain protein. putative (Protein of unknown function. DUF642)(AT2G34510)	72.6844	67.5901	38.2501	92.8681	94.5068	169.721	1.09546135	0.006822594	0.095820889
AT2G34660	multidrug resistance-associated protein 2(ABCC2)	12.5972	13.5131	11.4416	14.4656	16.11258	16.7182	0.414747297	0.00716122	0.097800392
AT2G34770	fatty acid hydroxylase 1(FAH1)	69.2335	64.6171	45.8318	74.035	77.2552	86.1908	0.481342028	0.007273273	0.098103697
AT2G36320	A20/AN1-like zinc finger family protein(AT2G36320)	72.4366	95.5441	72.772	112.347	100.867	100.893	0.488392598	0.001409344	0.037689263

AT2G36400	growth-regulating factor 3(GRF3)	19.8132	17.6358	12.2126	25.3442	21.8887	28.8184	0.675989882	0.00353874	0.066024063
AT2G38040	acetyl Co-enzyme a carboxylase carboxyltransferase alpha subunit(CAC3)	95.7895	87.3134	88.6772	108.0303	112.0986	117.8119	0.402693653	0.000854943	0.026473228
AT2G38400	alanine:glyoxylate aminotransferase 3(AGT3)	28.657306	44.8645	29.7781	79.352	57.36707	97.172	1.267353528	1.99E-09	7.31E-07
AT2G39700	expansin A4(EXPA4)	23.3425	30.0076	26.617	34.5351	36.1364	40.9799	0.554272554	0.004390617	0.075076285
AT2G39800	delta1-pyrroline-5-carboxylate synthase 1(P5CS1)	9.90337	10.4896	10.61282	17.79811	18.364923	30.97435	1.143901847	3.92E-07	5.67E-05
AT2G40205	Ribosomal protein L41 family(AT2G40205)	1580.2	1457.73	1451.2	2356.28	1911.03	2123.94	0.597133699	0.003267491	0.063079196
AT2G41100	Calcium-binding EF hand family protein(TCH3)	258.20459	390.6112269	335.2550392	568.1851197	446.72452	637.16816	0.847598785	5.94E-07	8.07E-05
AT2G41430	dehydration-induced protein (ERD15)(ERD15)	1216.985	1282.0603	1216.01966	1629.348	1427.3261	1835.1347	0.494221417	0.000138209	0.006920348
AT2G42840	protodermal factor 1(PDF1)	59.7217	62.274	25.528	86.0216	99.0244	138.848	1.23104901	0.003885114	0.070258465
AT2G43010	phytochrome interacting factor 4(PIF4)	30.87137	30.83	36.26765	52.72835	43.92699	83.01782	0.928417999	1.43E-05	0.001155303
AT2G43610	Chitinase family protein(AT2G43610)	22.0346	30.6668	14.3912	48.7803	35.6641	26.0253	0.872311463	0.001419275	0.037840199
AT2G45960	plasma membrane intrinsic protein 1B(PIP1B)	453.78528	476.23558	433.20932	601.26208	525.80409	620.28123	0.454518464	0.000280434	0.012191269
AT2G46800	zinc transporter(ZAT)	35.3116	39.8863	35.6154	47.8902	45.8697	53.4075	0.482970967	0.00479928	0.079017989
AT2G47060	Protein kinase superfamily protein(PT11-4)	26.129242	34.73477	28.40261	39.15021	41.73837	51.141	0.629610563	0.000907678	0.027585899
AT2G47440	Tetratricopeptide repeat (TPR)-like superfamily protein(AT2G47440)	26.5897	19.6067	17.9183	50.6999	28.2239	59.9847	1.209878759	0.002021405	0.047131747
AT3G01420	Peroxidase superfamily protein(DOX1)	86.5099	83.3908	70.7868	147.766	103.853	102.836	0.667820712	7.66E-05	0.004306455
AT3G03150	hypothetical protein(AT3G03150)	247.246	253.695	210.019	312.018	281.987	293.041	0.416084085	0.003407579	0.064316541
AT3G03870	transmembrane protein(AT3G03870)	16.85368	20.3384	21.93014	30.867807	24.7115	30.2573	0.614224476	0.006770216	0.095595449
AT3G04210	Disease resistance protein (TIR-NBS class)(AT3G04210)	25.7299	35.0036	38.4577	41.719	48.5026	58.4144	0.652740237	0.000434547	0.016112923
AT3G04730	indoleacetic acid-induced protein 16(IAA16)	134.467	150.314	115.068	159.923	165.141	186.36	0.441557376	0.001669905	0.042028542
AT3G05220	Heavy metal transport/detoxification superfamily protein(AT3G05220)	89.2432	87.0345	76.20585	110.9745	93.3538	118.6906	0.442116554	0.00285882	0.058400671
AT3G05900	neurofilament protein-like protein(AT3G05900)	39.5836	44.319	26.9354	50.4698	49.6437	63.608	0.644583801	0.000420895	0.015863987
AT3G06070	hypothetical protein(AT3G06070)	65.9929	43.0459	52.6678	64.8514	76.8764	97.9152	0.606892042	0.004616461	0.077013732
AT3G06080	trichome birefringence-like protein (DUF828)(TBL10)	39.6447	37.58633	30.19611	49.59377	47.3151	63.8672	0.649242639	0.000157888	0.007614003
AT3G06500	Plant neutral invertase family protein(A/N-InvC)	29.0477	36.1409	27.0113	35.5778	38.8652	51.2093	0.511873797	0.003264547	0.063079196
AT3G07310	phosphoserine aminotransferase. putative (DUF760)(AT3G07310)	44.3614	41.5939	36.9114	51.44	50.4374	73.7313	0.564357218	0.002284374	0.050693892

AT3G07360	plant U-box 9(PUB9)	22.1103	28.8442	25.509	34.5001063	30.7571	49.5524	0.633952228	0.002063928	0.047467086
AT3G07780	potyvirus VPg interacting protein (DUF1423)(OBE1)	50.5292	62.6315	47.2065	76.7433	58.4224	73.5627	0.474269358	0.005528482	0.08604736
AT3G08030	DNA-directed RNA polymerase subunit beta (Protein of unknown function. DUF642)(AT3G08030)	90.3527	86.4438	103.26406	117.737	113.008771	134.639	0.461569128	0.00186837	0.044927427
AT3G08940	light harvesting complex photosystem II(LHCB4.2)	815.192679	841.77284	1121.1627	1189.53608	1110.30655	1736.65858	0.632897651	0.000357801	0.014159645
AT3G09270	glutathione S-transferase TAU 8(GSTU8)	49.5311	68.0091	49.421	77.9858	75.8009	73.0808	0.549934597	0.0034286	0.064316541
AT3G10020	plant/protein(AT3G10020)	328.04985	381.445	333.427	532.37236	393.366	506.48	0.555279011	0.000346508	0.014027208
AT3G11410	protein phosphatase 2CA(PP2CA)	21.1532	19.227	13.7045	35.3367	23.1354	44.3774	0.981368013	9.38E-05	0.005046165
AT3G12120	fatty acid desaturase 2(FAD2)	460.1849	489.8023	412.4452	671.393	569.0169	655.4917	0.576519505	7.04E-06	0.000640591
AT3G13450	Transketolase family protein(DIN4)	49.7396	52.1816	36.5726	69.5054	63.4408	76.6677	0.678746584	0.000135341	0.00688358
AT3G13750	beta galactosidase 1(BGAL1)	326.114	378.361	176.493	549.974	547.353	678.564	1.115494478	0.000297843	0.012697899
AT3G14067	Subtilase family protein(AT3G14067)	55.7648	62.6107	46.5345	78.1495	70.6224	86.1214	0.599345358	7.17E-05	0.004121159
AT3G14180	sequence-specific DNA binding transcription factor(ASIL2)	15.3124	14.3063	11.584	22.257	18.643	19.0916	0.639381387	0.004609119	0.077013732
AT3G14595	Ribosomal protein L18ae family(AT3G14595)	53.8695	60.5303	42.182	89.075	70.7848	89.4472	0.75193859	0.000344822	0.014023294
AT3G14990	Class I glutamine amidotransferase-like superfamily protein(DJ1A)	280.5608	361.6220111	199.411	469.13339	337.58236	350.7238525	0.570422095	0.002356914	0.051451502
AT3G15353	metallothionein 3(MT3)	1919.1235	2018.14062	2156.5083	2285.76	2633.8799	2636.84068	0.401045249	0.000466394	0.016937957
AT3G15450	aluminum induced protein with YGL and LRDR motifs(AT3G15450)	1531.5442	1690.9312	1192.1104	2309.7123	2079.1003	2441.4742	0.731061418	1.71E-07	3.02E-05
AT3G15630	plant/protein(AT3G15630)	211.895	218.809	193.035	291.251	256.271	283.026	0.505667905	0.000340278	0.013902565
AT3G15880	WUS-interacting protein 2(WSIP2)	14.98817	14.80279096	13.40534	17.4837428	18.952276	19.08056	0.446637125	0.005394665	0.084644671
AT3G16240	delta tonoplast integral protein(DELTATIP)	749.708	612.274	566.661	1194.04	982.288	1194.7	0.904307299	5.15E-10	2.84E-07
AT3G16857	response regulator 1(RR1)	31.61802	28.92547	27.09905	40.41478	35.27648	38.70968	0.471767883	0.003689468	0.068259031
AT3G17510	CBL-interacting protein kinase 1(CIPK1)	29.329226	43.4183	30.19922	40.80387	48.6687	45.59602	0.49452041	0.005138034	0.082592258
AT3G17860	jasmonate-zim-domain protein 3(JAZ3)	9.38997	10.23771	10.27178	18.29255	19.49333	38.3632	1.349023283	1.54E-06	0.000178257
AT3G23080	Polyketide cyclase/dehydrase and lipid transport superfamily protein(AT3G23080)	26.1232	29.57443	25.4356	35.83988	41.30816	57.5551	0.775554997	7.02E-05	0.004102789
AT3G25190	Vacuolar iron transporter (VIT) family protein(AT3G25190)	37.5169	69.7219	38.1008	101.208	86.7316	67.8111	0.953047755	4.02E-05	0.002670245
AT3G26520	tonoplast intrinsic protein 2(TIP2)	1138.9	1089.75	1002.51	1641.78	1242.54	1546.11	0.557263999	7.07E-05	0.004102789
AT3G26740	CCR-like protein(CCL)	1182.33	1169.49	1586.85	1748.08	1547.56	1941.47	0.505061836	0.00101856	0.029962625

AT3G28345	ABC transporter family protein(ABCB15)	7.6595	9.6208	6.06867	12.2185	10.943	10.037	0.626610293	0.003141843	0.061953339
AT3G28550	Proline-rich extensin-like family protein(AT3G28550)	48.6524	60.6192	31.7065	119.009	74.3431	81.0858	1.074432224	0.002065423	0.047467086
AT3G28860	ATP binding cassette subfamily B19(ABCB19)	27.2753	28.5715	28.7994	32.7311	37.8626	45.8078	0.529424523	0.000338176	0.013880941
AT3G45300	isovaleryl-CoA-dehydrogenase(IVD)	21.8268	22.0831	14.88	31.175	24.5025	26.0742	0.579976488	0.002638649	0.055479184
AT3G47340	glutamine-dependent asparagine synthase 1(ASN1)	50.8164	50.58817	25.2594	354.08095	219.66222	350.09244	2.978258043	4.41E-14	4.60E-11
AT3G47470	light-harvesting chlorophyll-protein complex I subunit A4(LHCA4)	3377.02	3430.62	3554.86	3743.91	4177.7	5425.7	0.460070015	0.000929139	0.027927997
AT3G47620	TEOSINTE BRANCHED. cycloidea and PCF (TCP) 14(TCP14)	28.1967	32.7952	27.9829	36.0375	37.8218	51.3322	0.546447313	0.002227973	0.050157816
AT3G48360	BTB and TAZ domain protein 2(BT2)	351.1	352.797	293.905	345.078	422.851	496.525	0.428923256	0.002318263	0.050850918
AT3G50950	HOPZ-ACTIVATED RESISTANCE 1(ZAR1)	51.7704	52.9258	58.4445	71.099	55.9534	82.494	0.442131834	0.007512308	0.099843555
AT3G51730	saposin B domain-containing protein(AT3G51730)	152.759	156.649	129.277	178.897	169.597	189.725	0.383117624	0.006047145	0.090842158
AT3G51740	inflorescence meristem receptor-like kinase 2(IMK2)	9.7936	8.46565	5.7793	11.5021	11.9157	14.5596	0.717369356	0.002127924	0.048524368
AT3G53420	plasma membrane intrinsic protein 2A(PIP2A)	393.96448	484.1064	340.57666	527.48898	437.51777	574.23942	0.436930961	0.004362974	0.074909036
AT3G53990	Adenine nucleotide alpha hydrolases-like superfamily protein(AT3G53990)	205.808	294.646	248.03087	341.96096	275.089154	324.488	0.430923993	0.006727233	0.095448057
AT3G54580	Proline-rich extensin-like family protein(AT3G54580)	39.092	46.3777	29.4145	96.0507	67.0326	62.8401	1.091095471	1.04E-08	3.28E-06
AT3G54590	hydroxyproline-rich glycoprotein(HRGP1)	20.4469	24.356	17.9928	48.0507	34.9006	28.2407	0.959864836	3.55E-06	0.000381588
AT3G54890	chlorophyll a-b binding protein 6(LHCA1)	3348.32454	3327.16222	3428.3598	4301.292369	3951.27109	5518.4977	0.545099265	9.55E-05	0.005106778
AT3G55430	O-Glycosyl hydrolases family 17 protein(AT3G55430)	49.7463	51.0805	45.5615	62.773	54.4615	81.0887	0.502069777	0.003723269	0.068453843
AT3G57930	rho GTPase-activating gacO-like protein(AT3G57930)	25.27192	22.07294	23.3176	34.44804	28.91917	49.9157	0.690978713	0.006175785	0.091907761
AT3G58120	Basic-leucine zipper (bZIP) transcription factor family protein(BZIP61)	27.8961	23.2995	22.0921	39.9161	29.1034	47.0741	0.715965006	0.001038171	0.030237148
AT3G58490	Phosphatidic acid phosphatase (PAP2) family protein(SPP1)	15.7797	18.9573	13.71	24.4507	23.23558	28.273	0.717288262	0.001028431	0.030052666
AT3G59350	Protein kinase superfamily protein(AT3G59350)	89.59440001	99.42290352	57.4055	139.4444	112.9259	194.3799	0.95924601	0.003185878	0.062478611
AT3G60300	RWD domain-containing protein(AT3G60300)	72.39579	81.58316	64.4788	123.6512	92.44567	93.7105	0.614624167	0.000376262	0.014437025
AT3G61060	phloem protein 2-A13(PP2-A13)	69.91972	77.1286	53.73449	76.21722	88.6862	114.7	0.547747158	0.002012968	0.047131747
AT3G61260	Remorin family protein(AT3G61260)	223.514	231.699	151.397	389.905	288.009	401.469	0.929736391	2.84E-07	4.43E-05
AT3G61470	photosystem I light harvesting complex protein(LHCA2)	3636.92	3633.95	3799.81	4565.43	4363.45	5545.14	0.483928771	0.000138485	0.006920348

AT3G62040	Haloacid dehalogenase-like hydrolase (HAD) superfamily protein(AT3G62040)	43.7226	61.1935	35.7623	78.1367	75.1805	59.103	0.728206447	0.000571976	0.019834395
AT3G62290	ADP-ribosylation factor A1E(ARFA1E)	564.04639	672.334	475.639	751.896	671.572	664.266	0.389776539	0.005438068	0.084939731
AT3G62550	Adenine nucleotide alpha hydrolases-like superfamily protein(AT3G62550)	309.559	356.102	300.251	525.575	499.368	672.97	0.901985816	6.26E-10	3.25E-07
AT3G62650	hypothetical protein(AT3G62650)	74.83247	91.30431	66.8423	121.42	88.35982	108.683	0.544893587	0.006406495	0.09288466
AT3G62720	xylosyltransferase 1(XT1)	25.47494	26.37153	19.07457	29.6066	28.18223	50.4434	0.645782486	0.004656812	0.077394283
AT3G62980	F-box/RNI-like superfamily protein(TIR1)	35.8275	37.3895	32.6992	45.4746	44.8154	51.0217	0.494469662	0.000971583	0.028869417
AT4G05150	Octicosapeptide/Phox/Bem1p family protein(AT4G05150)	121.215	122.953	123.767	150.043	140.854	153.553	0.362297448	0.004593185	0.077013732
AT4G10340	light harvesting complex of photosystem II 5(LHCB5)	3397.04	3619.08	4050.74	4650.82	4519.61	6085.12	0.560073192	8.02E-05	0.004478854
AT4G12720	MutT/nudix family protein(NUDT7)	30.12991271	32.40097	44.70378694	54.50105	45.81782025	58.6543	0.643266165	0.001235055	0.034314475
AT4G13180	NAD(P)-binding Rossmann-fold superfamily protein(AT4G13180)	38.2623	43.728	28.7354	60.0053	54.9746	48.6004	0.682487783	0.000847978	0.026367342
AT4G13340	Leucine-rich repeat (LRR) family protein(LRX3)	102.205	78.0121	91.4543	135.468	93.6754	176.702	0.667617856	0.000752579	0.024239088
AT4G14500	Polyketide cyclase/dehydrase and lipid transport superfamily protein(AT4G14500)	42.56817	37.610995	38.846708	54.4689	54.436221	60.1077	0.581739989	0.000188528	0.008849791
AT4G14680	Pseudouridine synthase/archaeosine transglycosylase-like family protein(APS3)	14.8677	17.4176	15.7995	18.4312	25.0958	43.9388	0.876433738	0.00069094	0.022752031
AT4G15530	pyruvate orthophosphate dikinase(PPDK)	26.638596	29.96131314	26.56035	44.575635	32.80080977	39.0791	0.581601222	0.00077482	0.02477458
AT4G15760	monooxygenase 1(MO1)	55.3782	70.4798	46.2651	98.986	93.01524	105.462	0.883326176	9.18E-08	1.80E-05
AT4G16190	Papain family cysteine protease(AT4G16190)	331.775	350.249	278.511	424.674	356.028	398.335	0.395740221	0.003709621	0.068345316
AT4G16520	Ubiquitin-like superfamily protein(ATG8F)	162.653628	215.765	173.793	259.264	207.902	234.46	0.445788029	0.006355269	0.092703332
AT4G16830	Hyaluronan / mRNA binding family(AT4G16830)	62.9809	66.6027	65.4668	86.0568	75.9626	86.68341	0.436486608	0.003282195	0.063105392
AT4G17090	chloroplast beta-amylase(CT-BMY)	88.0481	100.46	65.3974	101.808	131.357	174.657	0.766338785	3.20E-05	0.002223346
AT4G17230	SCARECROW-like 13(SCL13)	24.3032	26.6005	24.0911	34.4631	30.0649	34.2196	0.480260742	0.005975179	0.090292731
AT4G17340	tonoplast intrinsic protein 2;2(TIP2;2)	133.755	122.906	77.0651	192.427	125.009	163.392	0.628816328	0.002768172	0.057211049
AT4G20260	plasma-membrane associated cation-binding protein 1(PCAP1)	481.38931	515.15995	385.72714	623.1105	501.59181	644.6652109	0.455505702	0.002311498	0.050850918
AT4G22485	Bifunctional inhibitor/lipid-transfer protein/seed storage 2S albumin superfamily protein(AT4G22485)	22.0816	23.4999	16.5523	30.3804	43.7993	20.1463	0.747833216	0.000909631	0.027585899
AT4G22505	Bifunctional inhibitor/lipid-transfer protein/seed storage 2S albumin superfamily protein(AT4G22505)	12.3295	12.872	9.96375	32.1944	29.5775	10.6225	1.212934501	1.37E-05	0.001128028

AT4G23180	cysteine-rich RLK (RECEPTOR-like protein kinase) 10(CRK10)	22.8341	29.6654	27.6099	40.8249	42.2091	56.7703	0.868115793	1.04E-06	0.000131142
AT4G23400	plasma membrane intrinsic protein 1;5(PIP1;5)	233.112	238.884	209.958	316.631	280.094	385.054	0.612680943	3.04E-05	0.002160085
AT4G24230	acyl-CoA-binding domain 3(ACBP3)	66.12287	71.96574	40.47757	113.09579	92.43019	97.2449	0.867328913	6.41E-06	0.000589536
AT4G25170	Uncharacterized conserved protein (UCP012943)(AT4G25170)	84.14864	81.74038	63.88712	110.68833	89.03509	112.487	0.529540525	0.001600692	0.0409815
AT4G26400	RING/U-box superfamily protein(AT4G26400)	20.4261	23.8126	23.2678	32.7303	30.3561	27.6581	0.538731059	0.007101055	0.09761185
AT4G26690	PLC-like phosphodiesterase family protein(SHV3)	38.5263	31.681	31.4197	39.0161	44.1352	59.6185	0.550936756	0.001387201	0.037340805
AT4G27450	aluminum induced protein with YGL and LRDR motifs(AT4G27450)	78.2872	81.1926	86.4772	136.344	141.81	142.52	0.863537857	7.15E-10	3.47E-07
AT4G28300	formin-like protein (DUF1421)(AT4G28300)	34.10441	31.96153	37.18706	57.34605	40.856	44.14429	0.564475791	0.002246614	0.050320742
AT4G28750	Photosystem I reaction centre subunit IV / PsaE protein(PSAE-1)	2296.51	2268.65	2354.7	2578.02	2659.51	3243.42	0.386793738	0.00185428	0.044832931
AT4G29900	autoinhibited Ca(2+)-ATPase 10(ACA10)	25.9094	33.9903	25.0783	35.7623	33.4529	40.5696	0.455496512	0.004170024	0.072917721
AT4G30140	GDSL-like Lipase/Acylhydrolase superfamily protein(CDEF1)	14.1641	15.6068	20.57	25.8934	27.4936	26.6416	0.75793047	0.000777837	0.024781269
AT4G30210	P450 reductase 2(ATR2)	70.2916	85.65784	66.689	87.194	92.9735	114.466	0.48805578	0.000811419	0.025574182
AT4G31290	ChaC-like family protein(AT4G31290)	95.0469	105.77	68.436	148.133	127.553	153.541	0.766891008	6.41E-06	0.000589536
AT4G31840	early nodulin-like protein 15(ENODL15)	31.8869	22.5232	19.9246	39.8858	38.1883	37.698	0.724777411	0.003093372	0.061484249
AT4G31910	HXXXD-type acyl-transferase family protein(BAT1)	12.059	12.036	8.37611	18.0805	15.7976	21.17	0.814948084	0.001244264	0.034314475
AT4G32060	calcium-binding EF hand family protein(AT4G32060)	164.789	162.212	156.287	184.75	179.87275	217.983	0.354866993	0.00597049	0.090292731
AT4G32340	Tetratricopeptide repeat (TPR)-like superfamily protein(AT4G32340)	187.958	198.365	180.677	235.054	220.673	223.865	0.357662423	0.006140517	0.09153727
AT4G34030	3-methylcrotonyl-CoA carboxylase(MCCB)	39.4791	39.9971	33.7339	50.2931	47.1043	48.2159	0.457242999	0.003143233	0.061953339
AT4G34150	Calcium-dependent lipid-binding (CaLB domain) family protein(AT4G34150)	57.0682	67.6498	74.0819	92.4737	78.7878	138.65	0.70104514	0.000547464	0.019248476
AT4G34950	Major facilitator superfamily protein(AT4G34950)	147.39	125.971	92.7638	157.544	190.207	203.254	0.678294315	2.55E-05	0.001908181
AT4G35100	plasma membrane intrinsic protein 3(PIP3)	320.359	320.775	228.658	427.90674	388.164	466.926	0.657099161	1.20E-05	0.001016231
AT4G35770	Rhodanese/Cell cycle control phosphatase superfamily protein(SEN1)	167.1232	199.28746	146.0563	575.64581	375.48386	495.624	1.603803101	1.12E-19	3.28E-16
AT4G36430	Peroxidase superfamily protein(AT4G36430)	14.8365	13.2503	21.1901	31.045	24.7164	27.6142	0.840015946	0.000925337	0.027927997
AT4G36730	G-box binding factor 1(GBF1)	44.92516	49.3364	38.11347	74.5588	51.44636	70.2063	0.658987882	0.000573118	0.019834395
AT4G36850	PQ-loop repeat family protein / transmembrane family protein(AT4G36850)	61.7883	62.142	37.8615	66.7691	89.7202	100.714	0.745175784	0.000143316	0.007026472

AT4G37300	maternal effect embryo arrest 59(MEE59)	180.668	215.605	188.929	263.458	246.341	290.593	0.540837588	7.27E-05	0.00413967
AT4G38470	ACT-like protein tyrosine kinase family protein(STY46)	125.792	155.936	81.249	167.574	157.117	162.199	0.52742547	0.003429705	0.064316541
AT4G38680	glycine rich protein 2(GRP2)	97.7511	84.4388	79.5343	121.22	104.468	110.341	0.454593578	0.003196266	0.062543339
AT4G38690	PLC-like phosphodiesterases superfamily protein(AT4G38690)	36.9659	36.7618	29.29	50.5475	48.7895	55.5589	0.664385833	0.000259336	0.011676757
AT5G01020	Protein kinase superfamily protein(AT5G01020)	46.2139	46.148	41.7943	53.8567	55.6857	57.8614	0.40396411	0.006470689	0.093459619
AT5G01530	light harvesting complex photosystem II(LHCB4.1)	3183.51	2751.9	3157.53	3457.65	3417.64	4125.24	0.36987361	0.003917827	0.070560859
AT5G02160	transmembrane protein(AT5G02160)	774.727	748.175	674.247	1172.15	1032.78	1327.45	0.780401186	6.79E-09	2.22E-06
AT5G04020	calmodulin binding protein(AT5G04020)	7.34457	7.82857	7.26538	8.98648	9.2672	14.04	0.555599727	0.00678195	0.095608161
AT5G04040	Patatin-like phospholipase family protein(SDP1)	22.1497	24.6463	23.8208	28.969	30.1697	35.7632	0.496503398	0.001243269	0.034314475
AT5G05100	Single-stranded nucleic acid binding R3H protein(AT5G05100)	31.7035	30.4536	29.2424	40.7449	39.154	48.8079	0.552742928	0.001759764	0.043599003
AT5G05600	2-oxoglutarate (2OG) and Fe(II)- dependent oxygenase superfamily protein(AT5G05600)	13.7116	15.5045	13.5564	28.2815	27.0863	37.4995	1.16459319	2.56E-07	4.19E-05
AT5G05690	Cytochrome P450 superfamily protein(CPD)	77.694486	79.36188	78.50222	106.01191	95.81131	106.26	0.475972543	0.000575746	0.019834667
AT5G06640	Proline-rich extensin-like family protein(EXT10)	10.8772	10.0054	11.3738	29.522	15.3805	13.8509	0.999351851	0.000292738	0.012602029
AT5G06700	trichome birefringence-like protein (DUF828)(AT5G06700)	46.1589	49.5082	50.4768	55.1039	61.8457	61.956	0.377522439	0.006306348	0.092703332
AT5G06870	polygalacturonase inhibiting protein 2(PGIP2)	33.5667	28.7421	19.988	57.0153	73.7128	138.431	1.792165702	4.20E-05	0.002745091
AT5G08330	TCP family transcription factor(TCP11)	62.9263	56.1408	50.3438	94.982	69.5158	106.971	0.748704225	0.000141312	0.006966912
AT5G09220	amino acid permease 2(AAP2)	58.6623	54.9822	60.4368	81.447	95.2978	82.5925	0.671780007	1.18E-06	0.000146993
AT5G10180	sulfate transporter 2;1(SULTR2;1)	15.7345	15.0003	25.4174	26.501	36.0624	27.4953	0.77774174	0.000278946	0.012189675
AT5G10450	G-box regulating factor 6(GRF6)	438.066307	436.68802	369.66097	576.60591	499.42888	550.819	0.485635093	0.000152639	0.007401294
AT5G11420	transmembrane protein. putative (Protein of unknown function. DUF642)(AT5G11420)	88.7065	84.1675	92.74	118.848	111.608	136.731	0.544645423	0.00017236	0.008222041
AT5G14120	Major facilitator superfamily protein(AT5G14120)	251.657	246.189	222.837	316.777	353.758	368.419	0.619366552	4.89E-08	1.11E-05
AT5G15230	GAST1 protein homolog 4(GASA4)	208.96102	232.263	259.765	381.613	387.230296	322.347	0.745063774	2.97E-07	4.52E-05
AT5G15350	early nodulin-like protein 17(ENODL17)	134.197	138.846	93.0779	156.489	138.726	194.095	0.494635017	0.007257349	0.098103697
AT5G15970	stress-responsive protein (KIN2) / stress-induced protein (KIN2) / cold- responsive protein (COR6.6) / cold- regulated protein (COR6.6)(KIN2)	68.7438	106.041	84.9519	102.348	126.211	182.908	0.705736769	0.002440581	0.052638776

AT5G16030	mental retardation GTPase activating protein(AT5G16030)	49.08774	59.97973	59.29328	86.44592	80.08774	131.82056	0.886307196	4.76E-06	0.000451318
AT5G16110	hypothetical protein(AT5G16110)	87.7718	85.7582	72.833	100.675	97.5374	109.568	0.404736583	0.005112761	0.082335975
AT5G18140	Chaperone DnaJ-domain superfamily protein(AT5G18140)	20.2892	26.1804	19.7915	34.9961	29.2012	36.7221	0.682550938	0.001879995	0.045084124
AT5G18170	glutamate dehydrogenase 1(GDH1)	97.4703	115.876	98.5509	174.912	132.094	138.028	0.61986883	7.39E-05	0.004182209
AT5G18630	alpha/beta-Hydrolases superfamily protein(AT5G18630)	23.84231	29.81594	26.74024	34.76664	35.56026	36.83111664	0.507773157	0.005072083	0.081980094
AT5G19010	mitogen-activated protein kinase 16(MPK16)	30.7828	30.8029	26.6364	35.8833	37.3918	37.0894	0.413871479	0.006026099	0.090751399
AT5G19140	aluminum induced protein with YGL and LRDR motifs(AILP1)	385.48362	379.62724	422.136	550.93803	473.589783	680.65453	0.613998026	4.40E-05	0.002798101
AT5G19450	calcium-dependent protein kinase 19(CDPK19)	25.12140102	29.31789525	22.1759	31.4178	34.4099	32.5972	0.460013043	0.006881736	0.095942055
AT5G19530	S-adenosyl-L-methionine-dependent methyltransferases superfamily protein(ACL5)	20.8994	25.8763	16.3285	34.66142	31.4173	35.7364	0.778066292	0.000313035	0.013092567
AT5G20230	blue-copper-binding protein(BCB)	151.025	138.91	99.0698	270.96	177.202	207.211	0.858913095	9.92E-06	0.000867043
AT5G20250	Raffinose synthase family protein(DIN10)	574.96918	582.9322	395.4438	629.1609	632.17562	712.20565	0.444453086	0.002263303	0.050438497
AT5G20830	sucrose synthase 1(SUS1)	19.134345	27.49008233	29.13692	31.869	35.0863	30.78811365	0.471677854	0.007351672	0.098263209
AT5G21170	5'-AMP-activated protein kinase beta-2 subunit protein(AKINBETA1)	61.48174	58.69103	52.0245	112.82027	79.947	95.4768	0.839835162	3.04E-06	0.000331671
AT5G24490	30S ribosomal protein(AT5G24490)	663.635	739.909	582.153	1007.35	901.879	1049.95	0.675111317	1.56E-07	2.81E-05
AT5G24800	basic leucine zipper 9(BZIP9)	43.3919	44.9156	31.8949	69.1707	59.7082	81.3357	0.873186217	1.43E-05	0.001155303
AT5G25280	serine-rich protein-like protein(AT5G25280)	81.21942	87.38743	76.3699	104.34917	97.46611	106.7033	0.422770002	0.001949536	0.046249079
AT5G25980	glucoside glucohydrolase 2(TGG2)	116.444	113.818	111.585	244.609	223.385	356.204	1.357743298	3.52E-16	5.18E-13
AT5G26000	thioglucoside glucohydrolase 1(TGG1)	538.575	506.61171	535.109	763.33958	788.216	1109.99	0.845348191	1.25E-08	3.57E-06
AT5G26340	Major facilitator superfamily protein(MSS1)	33.3946	34.1496	35.157	52.9929	63.7983	63.6966	0.894992243	1.97E-09	7.31E-07
AT5G27280	Zim17-type zinc finger protein(AT5G27280)	91.8928	99.0648	103.94	128.92	118.153	129.3	0.437370679	0.00629846	0.092703332
AT5G42900	cold regulated protein 27(COR27)	108.9419328	124.7859796	71.2033293	131.95733	133.5308224	152.6095	0.545987612	0.002646656	0.055479184
AT5G43780	Pseudouridine synthase/archaeosine transglycosylase-like family protein(APS4)	108.829	129.225	120.364	184.608	138.852	126.527	0.439982208	0.006451826	0.093339943
AT5G44680	DNA glycosylase superfamily protein(AT5G44680)	41.4415	40.5295	35.8108	65.1374	49.379	90.665	0.857710232	4.32E-05	0.002783514
AT5G46510	Disease resistance protein (TIR-NBS-LRR class) family(AT5G46510)	6.64885	8.1077	8.56148	11.1951	9.28749	13.2244	0.590998675	0.004057953	0.072065923
AT5G47220	ethylene responsive element binding factor 2(ERF2)	24.552	24.9271	25.476	46.6695	43.6459	63.4791	1.074410691	1.36E-06	0.000164311
AT5G47500	Pectin lyase-like superfamily protein(PME5)	24.9926	18.7788	11.8404	29.9088	29.4102	40.1746	0.893452201	0.000359769	0.014159645

AT5G48380	BAK1-interacting receptor-like kinase 1(BIR1)	35.6145	38.9646	36.0007	45.5729	41.6791	53.8007	0.424463223	0.005662835	0.087521053
AT5G49360	beta-xylosidase 1(BXL1)	227.971	259.825	127.264	340.126	336.334	443.156	0.967716083	0.00160211	0.0409815
AT5G49730	ferric reduction oxidase 6(FRO6)	36.9285	40.8049	38.6955	55.173	65.2052	82.5178	0.869617449	3.33E-08	7.73E-06
AT5G50950	FUMARASE 2(FUM2)	11.4005	9.7759144	13.632	18.98131173	23.5202933	54.9319	1.553725701	0.001990082	0.046833273
AT5G51070	Clp ATPase(ERD1)	70.6141	71.4834	60.0052	85.858	76.9547	87.3478	0.400453207	0.003105521	0.061587017
AT5G51400	PLAC8 family protein(AT5G51400)	71.0052	69.1441	72.4509	93.188	83.4952	96.922	0.440770199	0.007320795	0.098263209
AT5G51550	EXORDIUM like 3(EXL3)	78.471	72.8422	62.1666	121.591	104.114	170.175	0.96454671	1.55E-07	2.81E-05
AT5G53050	alpha/beta-Hydrolases superfamily protein(AT5G53050)	26.14835	30.75106	25.05742	27.95494	40.68586	49.12403	0.574006194	0.004260158	0.073857245
AT5G54080	homogentisate 1.2-dioxygenase(HGO)	26.11301	25.14814	21.35073	39.95451	32.42756	43.99198	0.744389246	0.000135722	0.00688358
AT5G54270	light-harvesting chlorophyll B-binding protein 3(LHCB3)	2135.92	2399.03	2825.26	3155.28	3265.29	4852.24	0.710791746	2.15E-05	0.001633928
AT5G55700	beta-amylase 4(BAM4)	14.151736	14.894	15.2177	23.8598	19.458493	26.24048	0.711159751	0.00072164	0.023586933
AT5G56980	cotton fiber protein(AT5G56980)	13.6784	14.804	12.1519	16.8605	18.6665	43.0645	0.954620637	0.000988322	0.029268264
AT5G57655	xylose isomerase family protein(AT5G57655)	135.1461	160.9736	121.48437	231.6607	196.9606	235.6017	0.767845724	8.35E-08	1.68E-05
AT5G58090	O-Glycosyl hydrolases family 17 protein(AT5G58090)	39.9891	37.8445	25.0273	53.1261	41.9487	57.3125	0.646996222	0.001384146	0.037340805
AT5G58110	chaperone binding / ATPase activator(AT5G58110)	51.0735	54.7185	42.0177	86.2962	58.2666	63.9727	0.605197615	0.004900388	0.080167419
AT5G58970	uncoupling protein 2(UCP2)	12.190573	10.332699	13.275009	27.09289	32.35972	20.39918	0.654359506	0.001560116	0.065703215
AT5G59030	copper transporter 1(COPT1)	51.6783	60.4698	53.2214	75.3598	69.8136	100.357	0.617944788	0.001973972	0.046703215
AT5G59950	RNA-binding (RRM/RBD/RNP motifs) family protein(AT5G59950)	66.92572	52.36867	48.7214	90.2782	65.493823	69.58321	0.525147871	0.006401055	0.09288466
AT5G63190	MA3 domain-containing protein(AT5G63190)	35.64885	41.03374	32.02742	51.9224	46.75	60.4931	0.629669233	8.14E-05	0.004517612
AT5G63600	flavonol synthase 5(FLS5)	56.63271	67.326475	52.690697	109.584965	80.25061	69.82465	0.678083368	0.00024572	0.011203566
AT5G64240	metacaspase 3(MC3)	38.70394	47.80599	29.30476	52.48497	51.27933	51.81669	0.526482321	0.004493804	0.075682858
AT5G64840	general control non-repressible 5(ABCF5)	48.6271	56.9684	41.4407	50.925	65.8967	81.2461	0.502956566	0.003221936	0.062906155
AT5G65207	hypothetical protein(AT5G65207)	152.064	184.023	141.44	272.316	192.991	268.009	0.701349754	0.000685862	0.022669403
AT5G65470	O-fucosyltransferase family protein(AT5G65470)	19.9004	15.5515	15.1157	19.1524	23.5727	35.2573	0.646803127	0.004445346	0.075409772
AT5G65660	hydroxyproline-rich glycoprotein family protein(AT5G65660)	167.228	201.05	130.915	213.205	205.892	211.124	0.43556659	0.007345525	0.098263209
AT5G65730	xyloglucan endotransglucosylase/hydrolase 6(XTH6)	64.4039	59.31	54.7849	70.9147	92.8486	113.39	0.690388145	0.000108244	0.005686049
AT5G66210	calcium-dependent protein kinase 28(CPK28)	19.587029	28.80634	25.89711	35.31535	33.35012	43.53015	0.666909315	0.000402309	0.015303358

AT5G66880	sucrose nonfermenting 1(SNF1)- related protein kinase 2.3(SNRK2.3)	33.5186	36.7162	34.6967	41.1768	44.6058	57.1678	0.497609111	0.005328915	0.083977988
-----------	---	---------	---------	---------	---------	---------	---------	-------------	-------------	-------------

Table S2. List of differentially expressed genes (DEGs) between *ucp1 ucp3* double mutant and wild-type (WT). (B) List of downregulated DEGs.

TAIR_ID	Gene Name	WT_R1	WT_R2	WT_R3	<i>ucp1</i> <i>ucp3</i> _R1	<i>ucp1</i> <i>ucp3</i> _R2	<i>ucp1</i> <i>ucp3</i> _R3	Log ₂ Fold Change	p value	p adjusted
AT1G01080	RNA-binding (RRM/RBD/RNP motifs) family protein(AT1G01080)	93.1594	93.1109	89.83139	58.8872	73.948865	59.723	-0.411390767	0.005399994	0.084644671
AT1G02475	Polyketide cyclase/dehydrase and lipid transport superfamily protein(AT1G02475)	104.181	89.0463	100.448	53.3465	76.4873	70.9139	-0.471578424	0.007130155	0.097744155
AT1G04980	PDI-like 2-2(PDIL2-2)	22.4572	18.3416	28.1227	10.8925	14.6183	5.72465	-0.934133151	0.000601504	0.020495264
AT1G05300	zinc transporter 5 precursor(ZIP5)	26.928179	25.5087	28.774953	14.6978	17.788851	14.995	-0.665701008	0.002286865	0.050693892
AT1G06950	translocon at the inner envelope membrane of chloroplasts 110(TIC110)	102.653	97.1645	101.441	63.549	86.4157	62.2471	-0.40359784	0.002909658	0.05875911
AT1G09310	plant/protein (Protein of unknown function. DUF538)(AT1G09310)	765.118	814.315	1156.28	491.845	688.496	595.797	-0.53688668	0.001111793	0.031650228
AT1G09530	phytochrome interacting factor 3(PIF3)	24.7492	19.4785	33.8762	11.91244	14.46593	8.12115	-1.02055426	3.53E-05	0.002414348
AT1G10490	GNAT acetyltransferase (DUF699)(AT1G10490)	12.3974	12.4867	12.2317	6.05923	10.2326	5.62188	-0.602823581	0.006409831	0.09288466
AT1G10522	Serine/Threonine-kinase(PRIN2)	67.9419	54.4463	53.1967	24.754449	44.52863	22.1763	-0.78128943	0.001062735	0.030674734
AT1G11210	cotton fiber protein. putative (DUF761)(AT1G11210)	45.6559	53.1034	50.334	30.0311	36.4698	30.2602	-0.509636441	0.005281117	0.083977988
AT1G13820	alpha/beta-Hydrolases superfamily protein(AT1G13820)	56.3905	57.8717	50.5964	28.0945	46.3119	29.1154	-0.537736769	0.006862916	0.095831063
AT1G14140	Mitochondrial substrate carrier family protein(UCP3)	13.5128	18.1642	14.1774	1.64085	4.0777	3.9988	-0.696796632	0.004231981	0.076815679
AT1G14210	Ribonuclease T2 family protein(AT1G14210)	70.7283	76.2336	89.5247	45.9256	60.7428	33.5593	-0.595528981	0.003657766	0.067814671
AT1G17100	SOUL heme-binding family protein(HBP1)	102.216	101.648	81.7154	59.7164	68.7231	62.9224	-0.480510698	0.004376858	0.075001493
AT1G19450	Major facilitator superfamily protein(AT1G19450)	46.9745	53.1529	50.7165	28.5377	38.9539	36.6265	-0.451551972	0.004888375	0.080167419
AT1G23020	ferric reduction oxidase 3(FRO3)	44.75988	36.5279	65.3292	29.09415	32.08237	28.0959	-0.622128846	0.002039585	0.04736668
AT1G24530	Transducin/WD40 repeat-like superfamily protein(AT1G24530)	50.6669	48.5816	64.3869	24.5166	32.0537	26.9431	-0.87118868	3.68E-06	0.000381588
AT1G26230	TCP-1/cpn60 chaperonin family protein(Cpn60beta4)	23.2735	22.98165	21.08493	10.6887	17.879344	12.3734	-0.590557892	0.006724458	0.095448057
AT1G27020	plant/protein(AT1G27020)	489.633	523.643	780.452	291.75	337.882	256.217	-0.923259782	6.36E-08	1.34E-05
AT1G27330	Ribosome associated membrane protein RAMP4(AT1G27330)	255.53	228.721	279.323	149.221	196.828	124.581	-0.564425878	0.001835946	0.044757525
AT1G27970	nuclear transport factor 2B(NTF2B)	174.633	152.154	194.04	117.773	127.421	92.2553	-0.503516549	0.002606558	0.055162773

AT1G28660	GDSL-like Lipase/Acylhydrolase superfamily protein(AT1G28660)	33.5474	27.95	42.2338	16.9124	21.6414	15.4903	-0.81319276	0.000390857	0.014932086
AT1G30410	multidrug resistance-associated protein 13(ABCC12)	16.2153	14.1854	15.0233	7.48633	12.3603	8.80908	-0.553727373	0.00370892	0.068345316
AT1G30680	toprim domain-containing protein(AT1G30680)	21.6553	19.8428	20.3364	11.4102	16.9942	5.31754	-0.676185137	0.006365377	0.092703332
AT1G31660	bystin-like protein(AT1G31660)	32.1371	33.6962	34.3095	17.707	25.6771	10.3662	-0.705130682	0.002018899	0.047131747
AT1G31970	DEA(D/H)-box RNA helicase family protein(STRS1)	60.4782	54.7186	53.3257	34.65	43.7457	37.7287	-0.439691614	0.004475531	0.075519236
AT1G36060	Integrase-type DNA-binding superfamily protein(AT1G36060)	30.3948	28.36	45.3381	19.9884	16.7381	12.5146	-0.944222619	4.27E-05	0.002769685
AT1G36370	serine hydroxymethyltransferase 7(SHM7)	37.0753	28.5838	35.9176	19.6861	25.0641	19.2252	-0.555152006	0.002854286	0.058400671
AT1G45332	Translation elongation factor EFG/EF2 protein(AT1G45332)	16.1166	16.3855	17.9594	7.66491	13.8021	6.88154	-0.66837822	0.005589747	0.086543015
AT1G48570	zinc finger (Ran-binding) family protein(AT1G48570)	38.2529	40.2827	41.1083	19.5967	32.975	22.1088	-0.555196135	0.005780441	0.088717207
AT1G48630	receptor for activated C kinase 1B(RACK1B_AT)	136.755	126.892	136.899	78.5695	107.938	63.8369	-0.55146512	0.000842828	0.026367342
AT1G48920	nucleolin like 1(NUC-L1)	335.234	290.642	332.107	213.876	278.164	205.555	-0.362296126	0.006206147	0.091988775
AT1G51790	Leucine-rich repeat protein kinase family protein(AT1G51790)	28.3122	26.0104	37.4575	12.9532	17.6963	11.4122	-0.99532199	6.07E-07	8.11E-05
AT1G51800	Leucine-rich repeat protein kinase family protein(LOS1)	68.3007	50.4531	80.3333	22.9418	34.975	22.8484	-1.195256843	7.86E-10	3.47E-07
AT1G51820	Leucine-rich repeat protein kinase family protein(AT1G51820)	20.3198	14.5621	23.2509	3.64275	10.82	7.67355	-1.318587944	0.004441878	0.075409772
AT1G51850	Leucine-rich repeat protein kinase family protein(AT1G51850)	51.458	37.1535	73.3583	20.1218	29.6561	18.5781	-1.152308332	0.000872994	0.026750607
AT1G51890	Leucine-rich repeat protein kinase family protein(AT1G51890)	18.3609511	17.1648	20.7756	10.54665	11.58287	6.28359	-0.809179361	0.000147838	0.007208135
AT1G52200	PLAC8 family protein(AT1G52200)	393.038	349.046	396.4	257.389	277.687	209.308	-0.503911352	0.000227197	0.010552712
AT1G52930	Ribosomal RNA processing Brix domain protein(AT1G52930)	41.7307	40.4522	48.5151	21.2966	33.0033	21.9385	-0.643284371	0.003405599	0.064316541
AT1G53240	Lactate/malate dehydrogenase family protein(mMDH1)	263.011	255.438	271.759	176.981	211.251	161.097	-0.420750472	0.000801901	0.025456039
AT1G55490	chaperonin 60 beta(CPN60B)	505.49279	472.1	425.09825	287.969083	384.41033	309.599	-0.42125326	0.000680749	0.022585012
AT1G56050	GTP-binding protein-like protein(AT1G56050)	53.7078	49.1956	48.9742	23.2903	36.2198	26.5224	-0.704915775	0.000171347	0.008218134
AT1G56110	NOP56-like pre RNA processing ribonucleoprotein(NOP56)	113.786	100.698	109.444	68.5123	82.0383	73.0826	-0.441173573	0.001094119	0.031294319
AT1G57770	FAD/NAD(P)-binding oxidoreductase family protein(AT1G57770)	43.8486	39.431	34.4813	22.6653	31.9472	21.6668	-0.498642937	0.007042202	0.096953875
AT1G58380	Ribosomal protein S5 family protein(XW6)	63.1623	68.0069	64.9919	41.3482	47.0775	31.6653	-0.558515629	0.001820861	0.044678844
AT1G59359	Ribosomal protein S5 family protein(AT1G59359)	501.582	459.233	468.615	338.385	390.032	328.123	-0.338345438	0.003793877	0.069318761
AT1G59990	DEA(D/H)-box RNA helicase family protein(EMB3108)	41.9159	38.6139	36.6923	19.1499	31.0038	16.8753	-0.66111028	0.000940414	0.028132715

AT1G60000	RNA-binding (RRM/RBD/RNP motifs) family protein(AT1G60000)	109.946	118.451	113.671	69.9816	94.7428	61.5822	-0.463007636	0.005559712	0.086229278
AT1G60600	UbiA prenyltransferase family protein(ABC4)	39.4068	34.1643	37.951	18.32739	28.64363	27.0882	-0.52109069	0.006947201	0.096453025
AT1G61380	S-domain-1 29(SD1-29)	23.6032	17.9741	25.5692	10.0904	14.5988	6.71469	-0.926459481	6.12E-05	0.003699001
AT1G62180	5'adenylylphosphosulfate reductase 2(APR2)	69.2865	58.259	63.368	33.81219	40.43759	28.43905	-0.763480956	4.09E-06	0.000401655
AT1G62380	ACC oxidase 2(ACO2)	695.017	756.389	959.361	460.573	484.693	423.139	-0.721628368	2.48E-07	4.13E-05
AT1G62780	dimethylallyl. adenosine tRNA methyl thiotransferase(AT1G62780)	206.075	211.673	196.563	109.762	170.325	153.984	-0.418381949	0.006850956	0.095820889
AT1G62790	Bifunctional inhibitor/lipid-transfer protein/seed storage 2S albumin superfamily protein(AT1G62790)	103.6119	112.1277	120.6733	80.1402	77.9207	68.6141	-0.457668443	0.0072133	0.098085315
AT1G63810	nucleolar protein(AT1G63810)	14.1291	10.6474	13.4808	5.93267	8.67508	7.50124	-0.704347097	0.001192607	0.033406822
AT1G64170	cation/H+ exchanger 16(CHX16)	51.3232	47.3265	75.8308	26.6785	33.2633	18.8458	-1.018458546	8.22E-07	0.000106651
AT1G65040	RING/U-box superfamily protein(Hrd1B)	43.70078	38.74956	50.3722	19.81209	30.63233	26.31665	-0.708008788	0.00046037	0.01678827
AT1G65370	TRAF-like family protein(AT1G65370)	32.5658	24.4397	35.3726	12.2791	18.0442	15.9083	-0.91613841	0.000218317	0.010193888
AT1G65845	transmembrane protein(AT1G65845)	317.984	228.569	410.334	170.101	189.183	109.534	-0.899652347	3.80E-05	0.002581205
AT1G66920	Protein kinase superfamily protein(AT1G66920)	26.53	25.30065	22.28403	10.49741	14.09946	9.90432	-0.961493092	3.93E-06	0.000398995
AT1G67120	midasin-like protein(AT1G67120)	4.13588	4.17299	3.96981	2.00611	3.2002	2.20278	-0.605044326	0.001393187	0.037370451
AT1G67480	Galactose oxidase/kelch repeat superfamily protein(AT1G67480)	59.33455	57.1152	58.38134	40.91664	43.04313	28.8718	-0.491349155	0.002795291	0.057636556
AT1G68590	Ribosomal protein PSRP-3/Ycf65(PSRP3/1)	633.48712	599.62513	584.669	351.94817	506.78	448.33205	-0.388585098	0.00388274	0.070258465
AT1G69200	fructokinase-like protein(FLN2)	42.8534	36.4757	36.9387	15.7144	31.0394	21.8768	-0.659353006	0.001559019	0.040271763
AT1G69450	Early-responsive to dehydration stress protein (ERD4)(AT1G69450)	25.752547	26.7523	32.809178	13.924	22.2728	12.92456	-0.657053699	0.001560673	0.040271763
AT1G69850	nitrate transporter 1:2(NRT1:2)	72.6129	78.9638	70.3035	43.0184	55.3765	43.4417	-0.534768338	0.000186622	0.008807144
AT1G69870	nitrate transporter 1.7(NRT1.7)	54.4256	47.5872	48.878	21.2156	34.4197	33.6396	-0.691128709	0.000116605	0.006017791
AT1G73110	P-loop containing nucleoside triphosphate hydrolases superfamily protein(AT1G73110)	53.4709	55.8377	51.8324	30.4614	43.3209	35.2552	-0.459643574	0.006574611	0.094357756
AT1G73600	S-adenosyl-L-methionine-dependent methyltransferases superfamily protein(AT1G73600)	149.733893	159.21912	175.41243	60.2942	97.98409	76.199554	-0.953087046	1.95E-09	7.31E-07
AT1G73680	alpha dioxxygenase(ALPHA DOX2)	44.0382	40.5738	55.49064	25.2287	27.7086000	22.9198	-0.777288656	7.95E-06	0.000708596
AT1G73990	signal peptide peptidase(SPPA)	32.1001	27.3835	26.5005	8.50053	9.49938	9.91228	-1.558469671	8.40E-15	1.06E-11
AT1G75750	GAST1 protein homolog 1(GASA1)	1308.27764	964.31017	1439.33959	508.22184	611.15158	339.521	-1.245826647	1.47E-11	9.99E-09
AT1G77030	putative DEAD-box ATP-dependent RNA helicase 29(AT1G77030)	19.0189	17.4165	18.5356	9.17048	14.3487	10.5532	-0.573813439	0.00488612	0.080167419

AT1G77510	PDI-like 1-2(PDIL1-2)	69.0223	58.6159	81.5032	37.1699	53.9839	32.2885	-0.639188651	0.00069481	0.022794405
AT2G01670	nudix hydrolase homolog 17(NUDT17)	42.1261	32.5149	52.3431	24.0703	28.4194	24.254	-0.629107061	0.004276606	0.073857245
AT2G03420	hypothetical protein(AT2G03420)	167.462	149.575	125.921	63.8014	110.398	94.7023	-0.63808172	0.001443712	0.038145972
AT2G04360	transmembrane protein(AT2G04360)	58.3292	53.7152	49.0133	26.7497	42.9795	34.5335	-0.528842055	0.006662814	0.095135248
AT2G04530	Metallo-hydrolase/oxidoreductase superfamily protein(CPZ)	27.0102	21.8883	23.4578	11.7567	17.3906	12.8493	-0.66232564	0.006996824	0.096782083
AT2G16430	purple acid phosphatase 10(PAP10)	47.4315	35.1625	47.1948	18.0625	34.9156	22.2932	-0.673704565	0.003013369	0.060374973
AT2G16600	rotamase CYP 3(ROC3)	1095.49	1184.23	1340.5	841.31	1008.01	746.212	-0.382811516	0.003743972	0.068548866
AT2G18900	Transducin/WD40 repeat-like superfamily protein(AT2G18900)	16.8645	16.0381	18.1421	8.99841	12.7606	10.3045	-0.56471679	0.005173954	0.082867779
AT2G18940	Tetratricopeptide repeat (TPR)-like superfamily protein(AT2G18940)	21.0318	22.5801	18.5012	10.4901	16.0684	10.9273	-0.594771847	0.003173959	0.06238349
AT2G18950	homogentisate phytyltransferase 1(HPT1)	22.1052	14.5952	29.1515	9.55433	15.3485	9.76709	-0.801626873	0.003573203	0.066526409
AT2G19190	FLG22-induced receptor-like kinase 1(FRK1)	41.1483	25.6654	48.6725	10.6177	17.3453	14.0157	-1.375177225	2.77E-09	9.76E-07
AT2G19540	Transducin family protein / WD-40 repeat family protein(AT2G19540)	69.1184	68.7312	76.72	48.6346	51.2882	46.6855	-0.450053496	0.002429707	0.052554334
AT2G20020	RNA-binding CRS1 / YhbY (CRM) domain-containing protein(CAF1)	33.3208	35.2131	27.4763	18.1221	25.0158	20.6113	-0.485300378	0.006498148	0.093702867
AT2G21860	violaxanthin de-epoxidase-like protein(AT2G21860)	52.7294	36.7722	41.1436	19.5102	31.6156	34.1248	-0.568228817	0.007307317	0.098263209
AT2G23670	homolog of Synechocystis YCF37(YCF37)	197.524	192.086	192.23	110.51	140.594	132.114	-0.517861409	0.000521909	0.018423376
AT2G24120	DNA/RNA polymerases superfamily protein(SCA3)	34.313345	30.09086	26.195246	16.06602	25.480127	15.9412	-0.535361012	0.003848496	0.069882673
AT2G25450	2-oxoglutarate (2OG) and Fe(II)- dependent oxygenase superfamily protein(AT2G25450)	550.485	652.979	787.254	415.05	485.82	469.539	-0.447869857	0.001442915	0.038145972
AT2G25830	YebC-like protein(AT2G25830)	48.118	51.7607	54.3639	26.6932	41.2711	30.7337	-0.531182163	0.004610376	0.077013732
AT2G26440	Plant invertase/pectin methylesterase inhibitor superfamily(AT2G26440)	46.399	47.0784	56.3191	24.2783	30.9782	18.3046	-0.874415002	3.66E-06	0.000381588
AT2G27660	Cysteine/Histidine-rich C1 domain family protein(AT2G27660)	27.3758	22.8707	28.1464	13.672	14.9568	8.04906	-0.920341634	1.14E-05	0.000980619
AT2G27840	histone deacetylase-related / HD-like protein(HDT4)	48.4966	47.8490237	53.41773	22.5285	35.8439	16.4034	-0.810090424	0.001052678	0.030558825
AT2G27920	serine carboxypeptidase-like 51(SCPL51)	19.07138	21.5134	27.008	13.78426	14.33114	9.90397	-0.682414418	0.003374832	0.064316541
AT2G28000	chaperonin-60alpha(CPN60A)	369.269	331.583	338.181	187.995	279.886	190.375	-0.564698279	7.19E-05	0.004121159
AT2G29320	NAD(P)-binding Rossmann-fold superfamily protein(AT2G29320)	29.7883	35.1479	46.1707	12.3037	24.8796	22.0418	-0.83687571	0.001426083	0.037907171
AT2G31060	elongation factor family protein(EMB2785)	27.80627	25.1023	32.115067	15.896443	23.47726	11.2710215	-0.58924018	0.006102198	0.091119959
AT2G31170	Cysteinyl-tRNA synthetase. class Ia family protein(SYCO ARATH)	29.1825	27.7836	26.25145	14.5839	21.98829	10.7006	-0.642324205	0.003321638	0.063724904

AT2G31400	s uncoupled 1(GUN1)	119.521	128.605	127.063	77.6945	104.566	85.4248	-0.391440967	0.001923814	0.045761892
AT2G31890	RAP(RAP)	28.5439	28.1723	26.2434	15.4224	23.0913	11.7895	-0.568571594	0.004421187	0.075322338
AT2G32230	proteinaceous RNase P 1(PRORP1)	62.8108	60.7541	57.9017	35.3199	48.714	37.3638	-0.470460723	0.002518382	0.053943491
AT2G34357	ARM repeat superfamily protein(AT2G34357)	18.5586	17.597	21.2872	10.6241	15.0521	13.4399	-0.469735796	0.007143907	0.097744155
AT2G36690	2-oxoglutarate (2OG) and Fe(II)-dependent oxygenase superfamily protein(AT2G36690)	115.396	81.3274	158.351	47.8239	67.934	53.3515	-0.979358026	5.52E-06	0.000518211
AT2G37270	ribosomal protein 5B(RPS5B)	227.64053	201.23419	226.12578	149.002	181.23061	134.563	-0.384582077	0.007369936	0.098263209
AT2G37600	Ribosomal protein L36e family protein(AT2G37600)	172.06565	162.267	153.089	111.691	109.14	93.2294	-0.51813985	0.002291996	0.050693892
AT2G37690	phosphoribosyl aminoimidazole carboxylase, putative / AIR carboxylase(AT2G37690)	19.3917	16.5818	17.1025	8.1707	13.3735	7.31374	-0.717223418	0.002080931	0.047699266
AT2G38470	WRKY DNA-binding protein 33(WRKY33)	35.7827	54.017	61.9673	21.313	36.9943	37.1723	-0.601194055	0.006851329	0.095820889
AT2G39200	Seven transmembrane MLO family protein(MLO12)	68.4521	48.4593	62.5572	19.5095	38.2112	21.5339	-1.059606959	1.43E-06	0.000170796
AT2G39210	Major facilitator superfamily protein(AT2G39210)	45.7857	36.4293	42.9587	20.4026	21.0883	13.5317	-1.033255534	5.39E-08	1.16E-05
AT2G39518	Uncharacterized protein family (UPF0497)(AT2G39518)	64.8335	36.0554	72.1888	16.7546	33.2329	31.4389	-1.039824343	0.000426189	0.015936944
AT2G40100	light harvesting complex photosystem II(LHCB4.3)	32.773282	39.139	28.236	20.19421	20.6031	17.9732	-0.649352362	0.004016834	0.0717357
AT2G40400	DUF399 family protein, putative (DUF399 and DUF3411)(AT2G40400)	34.28352	34.90943	37.35664	13.41686	25.28932	23.7721	-0.704675847	0.00044043	0.016127779
AT2G41410	Calcium-binding EF-hand family protein(AT2G41410)	73.5729	75.7909	113.714	51.6384	57.6391	45.6453	-0.654390831	0.000840875	0.026367342
AT2G41700	ATP-binding cassette A1(ABCA1)	17.309607	21.057879	23.2487	9.856467	14.291271	12.0529	-0.673431624	8.42E-05	0.004645219
AT2G42280	basic helix-loop-helix (bHLH) DNA-binding superfamily protein(FBH4)	20.78974	19.20298	19.6578	9.840298	13.36622	14.4042	-0.617787349	0.006614726	0.094764542
AT2G43620	Chitinase family protein(AT2G43620)	169.566	115.308	297.011	25.7554	68.9701	21.8047	-2.241909864	0.000355559	0.014159645
AT2G44210	carboxyl-terminal peptidase (DUF239)(AT2G44210)	56.472	55.8751	68.12347	29.7564	46.5083	36.259	-0.583348803	0.001166766	0.032896844
AT2G44370	Cysteine/Histidine-rich C1 domain family protein(AT2G44370)	51.5227	41.4631	63.9109	20.524	22.0427	19.7425	-1.235065199	2.49E-08	6.31E-06
AT2G44380	Cysteine/Histidine-rich C1 domain family protein(AT2G44380)	31.2923	33.2414	46.197	23.4418	20.6627	13.5022	-0.778543027	0.002642544	0.055479184
AT2G44670	senescence-associated family protein (DUF581)(AT2G44670)	105.718	80.7431	99.7132	49.9458	79.929	29.8485	-0.671433874	0.005322715	0.083977988
AT3G01060	lysine-tRNA ligase(AT3G01060)	30.4319	31.8942	37.5239	14.6257	22.4905	19.4344	-0.730796841	0.000436836	0.016127779
AT3G02550	LOB domain-containing protein 41(LBD41)	71.5258	67.4587	63.8113	21.4585	35.2217	16.4004	-1.296693611	7.79E-10	3.47E-07
AT3G03780	methionine synthase 2(MS2)	92.4116931	84.65	113.025004	53.8586910	82.4003883	50.6053001	-0.532041523	0.002184796	0.049692858

AT3G04070	NAC domain containing protein 47(NAC047)	30.8611	24.9723	61.0456	14.0429	17.854	7.49084	-1.443766169	0.005318608	0.083977988
AT3G04110	glutamate receptor 1.1(GLR1.1)	12.935	11.9588	16.4578	6.88381	8.94137	7.76351	-0.71472821	0.001866946	0.044927427
AT3G04840	Ribosomal protein S3Ae(AT3G04840)	528.122	493.81	527.363	358.276	433.841	325.488	-0.370554194	0.003017038	0.060374973
AT3G05730	defensin-like protein(AT3G05730)	571.985	528.845	512.287	283.519	399.85	317.388	-0.590959628	2.95E-05	0.002129878
AT3G06530	ARM repeat superfamily protein(AT3G06530)	13.57852	11.0873505	11.85733	4.62176000	8.85358	7.1578495	-0.739827427	0.000290081	0.012548865
AT3G06980	DEA(D/H)-box RNA helicase family protein(AT3G06980)	71.2165	65.3082	64.8782	39.3117	58.1173	44.4867	-0.405340594	0.007382267	0.098263209
AT3G09440	Heat shock protein 70 (Hsp 70) family protein(AT3G09440)	99.4368	93.9463	145.7448	53.1427	67.166	43.9814	-0.938312873	3.89E-07	5.67E-05
AT3G10040	sequence-specific DNA binding transcription factor(AT3G10040)	22.8391	17.3414	22.8978	5.89449	14.4993	6.69862	-1.050129357	0.00042244	0.015863987
AT3G11964	RIBOSOMAL RNA PROCESSING 5(AT3G11964)	15.9816	14.3436	13.7939	7.95924	11.4565	6.93859	-0.60490763	0.000960205	0.028627725
AT3G13470	TCP-1/cpn60 chaperonin family protein(Cpn60beta2)	128.625	122.609	105.4	56.9378	90.792	55.218	-0.702876638	2.77E-05	0.002040281
AT3G14210	GDSL-like lipase/acylhydrolase superfamily protein(ESM1)	559.365	500.237	876.13	238.275	426.758	250.712	-1.001803123	0.006748549	0.095480799
AT3G14230	related to AP2 2(RAP2.2)	149.61473	141.3487	190.18143	114.65552	121.95498	100.601	-0.411599783	0.006322453	0.092703332
AT3G14390	Pyridoxal-dependent decarboxylase family protein(AT3G14390)	41.7856	32.2522	37.5208	18.5365	28.7608	21.7447	-0.589947585	0.002322144	0.050850918
AT3G16560	Protein phosphatase 2C family protein(AT3G16560)	22.6052	20.2731	23.8913	11.5163	17.62	11.8252	-0.57409621	0.006663293	0.095135248
AT3G16670	Pollen Ole e 1 allergen and extensin family protein(AT3G16670)	292.705	261.75	275.451	146.987	252.64	116.79	-0.566173891	0.004062369	0.072065923
AT3G18080	B-S glucosidase 44(BGLU44)	316.08	333.232	403.039	169.265	290.755	231.158	-0.521974102	0.001371003	0.037340805
AT3G18130	receptor for activated C kinase 1C(RACK1C_AT)	94.7389	81.9005	103.388	52.5342	75.0347	46.0287	-0.564270523	0.00182977	0.04473052
AT3G18290	zinc finger protein-like protein(BTS)	33.5341	31.5694	55.3645	22.0767	24.5162	18.253	-0.789837576	8.81E-05	0.004828236
AT3G18600	P-loop containing nucleoside triphosphate hydrolases superfamily protein(AT3G18600)	25.777	20.5445	26.5189	12.1433	18.481	13.8358	-0.602327341	0.004914513	0.080167419
AT3G18680	Amino acid kinase family protein(AT3G18680)	160.265	160.411	145.951	87.688	124.754	94.8408	-0.498420239	0.000599593	0.020495264
AT3G19810	BTB/POZ domain protein. putative (DUF177)(AT3G19810)	56.4702	44.2629	50.3812	26.4569	42.3128	24.2644	-0.56283611	0.006751277	0.095480799
AT3G19930	sugar transporter 4(STP4)	92.7422	90.7556	109.579	66.9233	76.1425	67.7509	-0.37982819	0.0062125	0.091988775
AT3G20440	Alpha amylase family protein(EMB2729)	17.905	16.4872577	15.567113	4.35702	10.871172	6.65604014	-1.067226958	2.83E-05	0.002065968
AT3G21300	RNA methyltransferase family protein(AT3G21300)	16.0676	16.0236	16.8289	7.10699	11.7922	7.8086	-0.730293154	0.003273685	0.063079196
AT3G22120	cell wall-plasma membrane linker protein(CWLP)	1602.49	1021.18	1752.65	735.633	944.49	620.989	-0.84096857	4.60E-06	0.000446307

AT3G22200	Pyridoxal phosphate (PLP)-dependent transferases superfamily protein(POP2)	262.707	290.613	273.64053	196.385	223.145152	181.338	-0.358573217	0.002057139	0.047467086
AT3G22370	alternative oxidase 1A(AOX1A)	33.3242	33.7968	23.5789	13.3765	14.6201	12.2506	-0.746371685	0.002029818	0.006067341
AT3G23620	Ribosomal RNA processing Brix domain protein(AT3G23620)	46.7375	48.1568	45.4862	26.1893	35.7415	17.5904	-0.643721346	0.001849338	0.044832931
AT3G23810	S-adenosyl-L-homocysteine (SAH) hydrolase 2(SAHH2)	140.088	151.294	146.205	84.8351	127.486	86.9297	-0.443419765	0.002879381	0.058479546
AT3G23990	heat shock protein 60(HSP60)	66.0281	73.2408	71.2552	43.3627	55.8271	46.7975	-0.426695363	0.002635252	0.055479184
AT3G25230	rotamase FKBP 1(ROF1)	51.5723	53.0498	50.5171	34.3191	39.6136	35.4245	-0.405081887	0.005863493	0.08937017
AT3G25410	Sodium Bile acid symporter family(AT3G25410)	39.2266	34.5353	34.8689	17.4056	25.7363	16.1834	-0.729407727	0.000296379	0.01269684
AT3G25520	ribosomal protein L5(ATL5)	576.81207	584.8608	560.958	409.725	497.731	389.632	-0.310480823	0.0072081	0.098085315
AT3G25540	TRAM. LAG1 and CLN8 (TLC) lipid-sensing domain containing protein(LAG1)	23.7848	20.5044	25.1482	10.7041	16.565	10.1829	-0.740994421	0.001674183	0.042028542
AT3G26290	cytochrome P450. family 71. subfamily B. polypeptide 26(CYP71B26)	69.243	59.6289	91.5797	24.2949	43.7621	28.6809	-1.081547272	4.25E-07	6.04E-05
AT3G26710	cofactor assembly of complex C(CCB1)	144.32	144.469	130.296	70.507	107.288	86.5801	-0.567844978	0.00031972	0.013246634
AT3G29035	NAC domain containing protein 3(NAC3)	20.5439	22.3833	29.3337	15.0969	14.7449	10.7358	-0.687745551	0.004650819	0.077394283
AT3G30720	qua-quine starch(QQS)	95.3023	85.3316	104.642	8.93843	28.5464	8.49133	-2.459296904	3.74E-06	0.000383633
AT3G43600	aldehyde oxidase 2(AAO2)	18.9121	22.2455	22.6449	11.4301	15.6801	16.4549	-0.4844914	0.004451954	0.075409772
AT3G44310	nitrilase 1(NIT1)	479.6595	494.797	730.7746	358.581	443.52208	353.33	-0.470768018	0.003955876	0.070956515
AT3G44750	histone deacetylase 3(HDA3)	87.8372	84.1588	85.4214	49.5236	70.7447	37.9797	-0.549217658	0.004227667	0.073588086
AT3G44990	xyloglucan endo-transglycosylase-related 8(XTH31)	36.1588	55.2126	76.0029	24.7667	38.4199	27.8177	-0.771392798	0.001762386	0.043599003
AT3G45140	lipoxygenase 2(LOX2)	88.7591	73.2586	139.344	37.9315	53.4768	49.1065	-1.018965753	0.001548489	0.040192396
AT3G46280	kinase-like protein(AT3G46280)	232.664	137.093	300.525	78.461	96.085	46.8581	-1.508785704	0.000487049	0.017386569
AT3G47520	malate dehydrogenase(MDH)	103.186	98.9737	108.787	65.8988	86.3083	53.4975	-0.470893557	0.003056269	0.060883907
AT3G48730	glutamate-1-semialdehyde 2.1-aminomutase 2(GSA2)	204.17	204.176	178.865	122.366	165.839	139.122	-0.363751382	0.005677524	0.087594664
AT3G49680	branched-chain aminotransferase 3(BCAT3)	98.6093	88.15245	113.274	61.7799	85.919699	48.107	-0.493605735	0.006052713	0.090842158
AT3G51600	lipid transfer protein 5(LTP5)	1103.65	1016.15	1291.41	772.271	837.62	726.375	-0.451344118	0.000512819	0.018175212
AT3G51870	Mitochondrial substrate carrier family protein(AT3G51870)	35.2199	28.8925	33.1106	18.0718	22.3003	16.3336	-0.648983871	0.001513389	0.039397221
AT3G52140	tetratricopeptide repeat (TPR)-containing protein(NOXY38)	46.38577	43.6356	47.5416	27.1042	38.5352	26.9349	-0.465179411	0.001668209	0.042028542
AT3G52340	sucrose-6F-phosphate phosphohydrolase 2(SPP2)	34.5794	27.63245	35.12316	19.03726	19.96473	18.7725	-0.662436481	0.000904564	0.027585899

AT3G53560	Tetratricopeptide repeat (TPR)-like superfamily protein(AT3G53560)	53.8635	52.0096	56.5788	27.0563	43.7077	30.0019	-0.569448535	0.00287749	0.058479546
AT3G54090	fructokinase-like 1 (FLN1)	66.8253	52.1883	53.4642	26.6134	50.6464	24.8934	-0.624073779	0.004768905	0.07866464
AT3G54110	plant uncoupling mitochondrial protein 1(UCP1)	63.7648	63.5799	68.5789	26.0758	32.4032	24.3507	-0.747347981	0.003140492	0.051349875
AT3G54400	Eukaryotic aspartyl protease family protein(AT3G54400)	112.386	85.2098	116.927	56.4666	69.1546	49.0355	-0.736158563	1.45E-05	0.001163986
AT3G54470	uridine 5'-monophosphate synthase / UMP synthase (PYRE-F) (UMPS)(AT3G54470)	48.3992	48.2104	48.4202	28.6004	36.7522	33.6097	-0.462533179	0.00461098	0.077013732
AT3G55010	phosphoribosyl formyl glycinamide cyclo-ligase. chloroplast / phosphoribosyl-aminoimidazole synthetase / AIR synthase (PUR5)(PUR5)	32.81304	30.76853	32.57591	17.85973	22.63422	14.2707	-0.655719857	0.001458121	0.038183737
AT3G55250	calcium homeostasis regulator(PDE329)	111.929	104.174	113.714	67.4922	85.6026	79.4228	-0.418843555	0.005021123	0.081454796
AT3G55400	methionyl-tRNA synthetase / methionine-tRNA ligase / MetRS (cpMetRS)(OVA1)	50.22913	41.55053	52.5637	26.71983	41.07938	24.0198	-0.526917725	0.005693502	0.087687878
AT3G56070	rotamase cyclophilin 2(ROC2)	95.5129	83.877	88.6825	52.4771	67.3159	44.94495	-0.562728381	0.002416638	0.052440943
AT3G59930	defensin-like protein(AT3G59930)	42.0907	130.123	58.7692	24.4907	15.4441	18.2256	-1.873764095	0.000650789	0.021754581
AT3G61440	cysteine synthase C1(CYSC1)	466.87738	496.4123	608.45451	383.88146	425.522851	304.181	-0.398271399	0.006365804	0.092703332
AT3G61770	Acid phosphatase/vanadium-dependent haloperoxidase-related protein(AT3G61770)	35.228	29.2846	38.826	16.2259	23.0574	23.085	-0.66989214	0.003928736	0.070613224
AT3G62530	ARM repeat superfamily protein(AT3G62530)	462.519	422.403	399.814	238.365	329.927	272.415	-0.518370645	0.00011355	0.005929474
AT3G62600	DNAJ heat shock family protein(ATERDJ3B)	64.8255	55.7989	74.0287	34.4506	51.5412	33.8251	-0.580826421	0.002194011	0.049774156
AT3G62870	Ribosomal protein L7Ae/L30e/S12e/Gadd45 family protein(AT3G62870)	529.013	492.073	513.272	356.499	426.697	363.649	-0.324402321	0.005317796	0.083977988
AT4G01037	Ubiquitin carboxyl-terminal hydrolase family protein(WTF1)	50.1826	46.543	51.3029	25.8113	36.4995	26.384	-0.621505333	0.000272623	0.012089961
AT4G01250	WRKY family transcription factor(WRKY22)	34.8393	21.4123	40.3206	15.9974	20.7728	19.7731	-0.703048958	0.005987655	0.090326588
AT4G01720	WRKY family transcription factor(WRKY47)	24.4397	25.8285	25.1006	16.7769	17.7878	11.4468	-0.549449506	0.006948619	0.096453025
AT4G02330	Plant invertase/pectin methylesterase inhibitor superfamily(ATPMEPCRB)	49.3912	40.1422	77.9715	9.90508	20.7328	9.97608	-1.94349569	1.36E-05	0.001128028
AT4G02380	senescence-associated gene 21(SAG21)	968.3953	818.3891	985.4512	664.60547	774.195	549.958	-0.379241896	0.006723832	0.095448057
AT4G02930	GTP binding Elongation factor Tu family protein(AT4G02930)	72.056	67.4861	69.5217	46.9068	54.8369	37.1116	-0.459818375	0.003237085	0.062923511
AT4G02990	Mitochondrial transcription termination factor family protein(BSM)	48.6571	47.136	46.8672	24.0072	36.6869	28.079	-0.57765309	0.00086761	0.026678238
AT4G04020	fibrillin(FIB)	102.411	111.449	102.725	47.8826	78.225	64.3204	-0.641288091	0.000114955	0.005967532

AT4G04940	transducin family protein / WD-40 repeat family protein(AT4G04940)	10.5563	10.1773	11.0875	5.31931	7.02865	4.41077	-0.762481123	0.001185862	0.033328777
AT4G05390	root FNR 1(RFNR1)	46.59522	51.3357	62.05612	32.858	37.60919	31.4917	-0.541186182	0.002666164	0.055638876
AT4G09420	Disease resistance protein (TIR-NBS class)(AT4G09420)	23.2162	19.9181	22.7161	9.26527	11.6496	14.6669	-0.877903064	0.000246288	0.011203566
AT4G09730	RH39(RH39)	49.4781	45.8066	50.778	28.7796	39.9319	28.4105	-0.47184577	0.004207309	0.073378468
AT4G11460	cysteine-rich RLK (RECEPTOR-like protein kinase) 30(CRK30)	19.43	17.13	24.029	6.76018	13.851	7.04289	-0.973853435	0.000254387	0.01151265
AT4G12060	Double Clp-N motif protein(AT4G12060)	119.688	96.2954	115.102	62.1655	89.2946	66.8318	-0.495963291	0.004076643	0.072065923
AT4G12290	Copper amine oxidase family protein(AT4G12290)	54.6517	49.8432	50.215	23.9597	36.6014	23.4208	-0.757289853	1.12E-05	0.000972336
AT4G12320	cytochrome P450. family 706. subfamily A. polypeptide 6(CYP706A6)	49.1884	56.4409	57.983	16.3621	33.8563	32.2321	-0.927121106	1.47E-05	0.001163986
AT4G12470	azelaic acid induced 1(AZI1)	1788.21	987.907	2674.94	472.636	594.232	323.888	-1.88938555	3.49E-05	0.002405832
AT4G12480	Bifunctional inhibitor/lipid-transfer protein/seed storage 2S albumin superfamily protein(EARLI1)	2781.7	1737.1	4177.28	567.737	896.488	348.119	-2.187748137	1.48E-05	0.001163986
AT4G12490	Bifunctional inhibitor/lipid-transfer protein/seed storage 2S albumin superfamily protein(AT4G12490)	1458.33	652.398	1469.43	105.673	270.061	75.1927	-2.920738028	4.67E-06	0.000448243
AT4G12500	Bifunctional inhibitor/lipid-transfer protein/seed storage 2S albumin superfamily protein(AT4G12500)	192.541	48.3859	314.921	24.3907	56.9382	11.949	-2.502983247	0.005832294	0.089202769
AT4G12600	Ribosomal protein L7Ae/L30e/S12e/Gadd45 family protein(AT4G12600)	151.400284	151.365329	161.511	95.4076	125.518252	80.9478	-0.487723616	0.0037407	0.068548866
AT4G13170	Ribosomal protein L13 family protein(AT4G13170)	108.417	98.6632	107.346	67.748	70.6913	76.3423	-0.48037859	0.003415152	0.064316541
AT4G13850	glycine-rich RNA-binding protein 2(GR-RBP2)	341.3546	264.049	285.28406	182.7963	240.6179	169.966	-0.475849504	0.002935967	0.059155052
AT4G15233	ABC-2 and Plant PDR ABC-type transporter family protein(ABCG42)	18.42845	15.11628	19.72838	6.95878	11.25039	5.87721	-0.993661337	4.10E-06	0.000401655
AT4G15490	UDP-Glycosyltransferase superfamily protein(UGT84A3)	28.4578	30.533	25.616	15.6897	21.7282	16.7479	-0.52314157	0.007251201	0.098103697
AT4G15640	adenylyl cyclase(AT4G15640)	20.0175	20.6153	24.471	8.5375	16.7695	10.1181	-0.733188301	0.005711416	0.087810529
AT4G16390	pentatricopeptide (PPR) repeat-containing protein(SVR7)	46.0165	44.6156	42.2748	25.3805	34.8315	31.2621	-0.450765232	0.004151396	0.072917721
AT4G16660	heat shock protein 70 (Hsp 70) family protein(AT4G16660)	49.6057	44.8589	60.9038	27.792	41.0332	36.6735	-0.477113252	0.004954494	0.080670491
AT4G21105	cytochrome-c oxidase/ electron carrier(AT4G21105)	344.65	295.516	427.622	224.837	284.331	206.149	-0.471889875	0.00607642	0.091043134
AT4G21410	cysteine-rich RLK (RECEPTOR-like protein kinase) 29(CRK29)	38.6022	40.6702	42.039	26.1691	30.6356	24.3606	-0.462860873	0.003432645	0.064316541
AT4G21680	NITRATE TRANSPORTER 1.8(NRT1.8)	20.8085	20.9446	31.2982	11.746	13.7418	6.43138	-1.010564785	3.91E-05	0.002637156
AT4G21990	APS reductase 3(APR3)	88.8253	81.5102	77.5451	62.258	60.9484	29.1792	-0.557460182	0.004768653	0.07866464

AT4G22470	protease inhibitor/seed storage/lipid transfer protein (LTP) family protein(AT4G22470)	324.429	152	285.805	74.8098	120.95	73.2079	-1.419563166	0.00031054	0.013050082
AT4G23010	UDP-galactose transporter 2(UTR2)	51.48323	43.394987	72.08918	34.0504	33.706856	24.60189	-0.731576664	0.000482182	0.017368402
AT4G23210	cysteine-rich RLK (RECEPTOR-like protein kinase) 13(CRK13)	13.66154	9.81149	18.59604	4.28074	9.17076	8.03770019	-0.904058718	0.00244579	0.052638776
AT4G23260	cysteine-rich RLK (RECEPTOR-like protein kinase) 18(CRK18)	46.0756	45.2565	40.3073	21.3465	31.6629	30.1874	-0.585950818	0.000614391	0.020767407
AT4G23290	cysteine-rich RLK (RECEPTOR-like protein kinase) 21(CRK21)	35.83595	31.31591	45.09752	19.4224	27.12295	27.62632	-0.533613593	0.005412335	0.084687695
AT4G23300	cysteine-rich RLK (RECEPTOR-like protein kinase) 22(CRK22)	32.7136	26.4763	45.9641	13.2983	23.0532	20.2551	-0.822378258	0.00035023	0.014113158
AT4G24240	WRKY DNA-binding protein 7(WRKY7)	56.9974	59.3645	55.1218	32.9565	37.1422	31.1669	-0.646303351	6.09E-05	0.003699001
AT4G24350	Phosphorylase superfamily protein(AT4G24350)	60.09889	61.1653	60.40729	32.6471	45.29327	43.82553	-0.502298941	0.003821988	0.069688107
AT4G25630	fibrillarin 2(FIB2)	66.8945	66.2715	73.9802	40.6861	48.787	31.3476	-0.63406261	0.000308038	0.01300686
AT4G26200	1-amino-cyclopropane-1-carboxylate synthase 7(ACS7)	23.6646	18.4328	30.3686	3.17269	9.17302	7.67021	-1.788603865	1.24E-08	3.57E-06
AT4G27730	oligopeptide transporter 1(OPT6)	16.8115	11.2555	20.3417	6.86071	10.3197	4.22191	-0.99349411	0.000364961	0.014159645
AT4G27820	beta glucosidase 9(BGLU9)	28.5254	25.8087	27.2246	12.0158	20.2972	17.8023	-0.623543315	0.004313921	0.074211221
AT4G28450	WD repeat and SOF domain-containing protein 1(AT4G28450)	28.5279	27.5808	26.4223	17.5071	18.598	9.17526	-0.67329822	0.002024128	0.047131747
AT4G29520	nucleophosmin(AT4G29520)	36.6727	33.4756	44.7648	20.4447	26.5216	18.313	-0.679560136	0.002321698	0.050850918
AT4G30825	Tetratricopeptide repeat (TPR)-like superfamily protein(AT4G30825)	15.3836	15.2841	14.5351	4.5238	10.9023	10.0036	-0.771553674	0.002739508	0.056751546
AT4G30990	ARM repeat superfamily protein(AT4G30990)	8.35763	6.56457	8.47938	4.20679	6.01106	2.78439618	-0.684698334	0.001822593	0.044678844
AT4G31210	DNA topoisomerase. type IA. core(AT4G31210)	20.4218	17.9911	21.8884	8.8521	16.7649	12.7152	-0.562367943	0.005322496	0.083977988
AT4G31550	WRKY DNA-binding protein 11(WRKY11)	90.6954	101.2796	130.5754	64.6865	77.1307	71.1774	-0.508799656	0.003038187	0.060660637
AT4G31700	ribosomal protein S6(RPS6)	474.094	443.545	490.584	349.605	383.707	292.293	-0.353095026	0.005933286	0.090278023
AT4G33220	pectin methylesterase 44(PME44)	69.4366	67.4711	85.3915	44.7466	60.4551	48.3914	-0.434640149	0.007029608	0.096931704
AT4G34230	cinnamyl alcohol dehydrogenase 5(CAD5)	57.79783	48.126	59.16	33.0744	40.298617	28.7343	-0.56591124	0.002222824	0.050157816
AT4G36220	ferulic acid 5-hydroxylase 1(FAH1)	61.9522	63.6337	76.5452	32.3352	45.8163	41.2254	-0.675445351	5.48E-05	0.003381887
AT4G36810	geranylgeranyl pyrophosphate synthase 1(GGPS1)	79.704	75.2884	75.2235	46.859	61.2749	51.3098	-0.429826303	0.004666699	0.077412825
AT4G37520	Peroxidase superfamily protein(AT4G37520)	190.64249	164.528000	261.878	114.821	102.462418	72.1723079	-0.977347106	3.92E-07	5.67E-05
AT4G37800	xyloglucan endotransglucosylase/hydrolase 7(XTH7)	204.856	203.034	267.946	92.9936	168.287	126.814	-0.713316404	0.000105906	0.005596544

AT4G37910	mitochondrial heat shock protein 70-1(mthSc70-1)	72.7028	73.3322	77.875	49.8681	63.2385	44.458	-0.391498699	0.006672943	0.095135248
AT4G39730	Lipase/lipoxygenase. PLAT/LH2 family protein(PLAT1)	198.024	202.824	211.358	140.293	157.312	139.866	-0.384488407	0.006962105	0.096453025
AT5G01410	Aldolase-type TIM barrel family protein(RSR4)	158.683	153.899	145.006	103.347	117.827	114.539	-0.359070915	0.00553932	0.086064252
AT5G02050	Mitochondrial glycoprotein family protein(AT5G02050)	38.3066	42.117	38.1704	22.6932	28.7899	21.4683	-0.567293619	0.005798036	0.08883275
AT5G02490	Heat shock protein 70 (Hsp 70) family protein(Hsp70-2)	16.9755	14.4983	23.8452	7.18143	8.87924	6.38112	-1.170477734	2.43E-06	0.000271654
AT5G02760	Protein phosphatase 2C family protein(AT5G02760)	33.128	34.6718	35.1244	20.7703	14.599	10.5438	-1.002069776	9.78E-06	0.000863147
AT5G02830	Tetratricopeptide repeat (TPR)-like superfamily protein(AT5G02830)	18.1346	18.9873	14.9163	6.91262	12.4616	11.8329	-0.670317931	0.002592132	0.054989338
AT5G04950	nicotianamine synthase 1(NAS1)	66.2955	63.1844	72.5991	35.3643	48.8057	41.921	-0.586894109	0.000741779	0.024018386
AT5G05190	hypothetical protein (DUF3133)(AT5G05190)	15.7577	11.0585	11.3664	5.95714	8.63649	4.79907	-0.809516292	0.002059972	0.047467086
AT5G07830	glucuronidase 2(GUS2)	39.7254	38.338	41.6365	26.6288	30.2688	24.4041	-0.44256015	0.007134188	0.097744155
AT5G08610	P-loop containing nucleoside triphosphate hydrolases superfamily protein(PDE340)	58.9261	56.3347	50.2954	25.59	44.6525	26.7348	-0.656227272	0.000316794	0.013187301
AT5G09590	mitochondrial HSO70 2(MTHSC70-2)	32.4221	30.7515	34.1114	19.2973	24.1357	18.1733	-0.537155357	0.00145436	0.038183737
AT5G09650	pyrophosphorylase 6(PPa6)	252.972	253.897	256.22	146.429	219.185	166.719	-0.422818352	0.003014175	0.060374973
AT5G11450	PsbP domain protein (Mog1/PsbP/DUF1795-like photosystem II reaction center PsbP family protein)(PPD5)	170.243	167.91	144.964	83.6312	138.666	111.44	-0.442272868	0.007365987	0.098263209
AT5G12130	integral membrane TerC family protein(PDE149)	44.0359	40.4967	43.2036	23.3722	31.6448	29.1343	-0.519194708	0.004136047	0.072855515
AT5G12860	dicarboxylate transporter 1(DiT1)	305.97741	243.33	262.837	171.008	226.097	194.062	-0.36835282	0.006333243	0.092703332
AT5G13490	ADP/ATP carrier 2(AAC2)	30.17792	22.8203	33.65466	12.19511	20.624	8.81456215	-0.87673104	0.000864304	0.026669529
AT5G13740	zinc induced facilitator 1(ZIF1)	28.3095	31.3429	49.7735	21.8378	22.6648	23.4258	-0.607723591	0.005480417	0.085449961
AT5G20700	senescence-associated family protein. putative (DUF581)(AT5G20700)	280.654	302.343	399.817	196.831	248.099	177.668	-0.558946043	0.000477601	0.01727389
AT5G20720	chaperonin 20(CPN20)	755.035116	779.736516	694.360435	439.968086	631.341992	490.855	-0.419076308	0.001236887	0.034314475
AT5G21105	Plant L-ascorbate oxidase(AT5G21105)	59.916442	50.369	76.8226	33.50088	44.795	45.6437685	-0.522793968	0.003913517	0.070560859
AT5G26860	lon protease 1(LON1)	17.5555	14.5436	16.431	9.09237	11.068	6.05503	-0.719668798	0.000554562	0.019420688
AT5G27120	NOP56-like pre RNA processing ribonucleoprotein(AT5G27120)	54.5389	53.3144	55.9988	30.2976	37.8867	29.0366	-0.635067862	6.23E-05	0.003742199
AT5G28540	heat shock protein 70 (Hsp 70) family protein(BIP1)	175.766	158.427	227.86	112.491	145.188	113.216	-0.507674109	0.001138353	0.032198594

AT5G28750	Bacterial sec-independent translocation protein mttA/Hcf106(AT5G28750)	285.721	307.991	255.638	171.973	236.453	178.157	-0.423642571	0.005109181	0.082335975
AT5G35220	Peptidase M50 family protein(EGY1)	57.1175	53.3184	53.795	28.8936	41.7145	38.8064	-0.509860073	0.00188532	0.045089287
AT5G37600	hypothetical protein(GSR 1)	381.837	322.506	440.705	228.521	234.81	163.263	-0.766298009	1.48E-06	0.000174007
AT5G38430	Ribulose biphosphate carboxylase (small chain) family protein(RBCS1B)	4229.33	4042.81	3801.82	2876.66	3167.44	2850.28	-0.345994379	0.000810354	0.025574182
AT5G39050	HXXXD-type acyl-transferase family protein(PMAT1)	28.2774	22.9823	26.5701	15.5897	17.5228	10.3549	-0.671413877	0.003388268	0.064316541
AT5G39580	Peroxidase superfamily protein(AT5G39580)	236.3889	172.34318	228.0703	87.3546	138.05011	106.97	-0.848716912	8.69E-07	0.000111082
AT5G39610	NAC domain containing protein 6(NAC6)	44.4191	34.4989	64.5932	29.0277	26.6839	14.1818	-0.875583394	0.000743005	0.024018386
AT5G40480	embryo defective 3012(EMB3012)	12.9094	12.2987	11.2579	6.23121	10.1917	6.58641	-0.537910651	0.005062912	0.081980094
AT5G41670	6-phosphogluconate dehydrogenase family protein(AT5G41670)	108.4015	103.7375	119.215	79.3766	87.2071	63.6388	-0.409884055	0.004461919	0.075433778
AT5G42020	Heat shock protein 70 (Hsp 70) family protein(BIP2)	136.241	131.395	177.079	80.3056	119.187871	82.1618	-0.563243529	0.000603897	0.020497669
AT5G43745	ion channel POLLUX-like protein. putative (DUF1012)(AT5G43745)	13.92	18.1452	17.9729	8.02275	13.561	7.3759	-0.627257115	0.007170182	0.097800392
AT5G44572	transmembrane protein(AT5G44572)	161.925	176.904	219.735	91.3263	98.8031	74.2455	-0.948792511	6.91E-07	9.10E-05
AT5G44575	hypothetical protein(AT5G44575)	162.605	68.44	142.04	56.3825	68.5164	57.6938	-0.941751341	0.000759541	0.024374375
AT5G44580	transmembrane protein(AT5G44580)	173.442	225.035	226.249	135.461	134.47	110.83	-0.591954596	0.00073944	0.024018386
AT5G44785	organellar single-stranded DNA binding protein 3(OSB3)	38.84323	37.21852	35.04162	16.2215	30.26069	24.054	-0.562548951	0.007376735	0.098263209
AT5G44910	Toll-Interleukin-Resistance (TIR) domain family protein(AT5G44910)	52.2456	46.2528	67.7907	23.0338	34.3836	17.6246	-0.96846299	0.000269563	0.012014618
AT5G45140	nuclear RNA polymerase C2(NRPC2)	10.6317	11.233	13.2879	6.1177	9.07408	6.03358	-0.591237942	0.006244387	0.092306061
AT5G45800	Leucine-rich repeat protein kinase family protein(MEE62)	17.1189	19.266	20.9296	10.8908	12.8488	12.8296	-0.570727801	0.004254509	0.073857245
AT5G46580	pentatricopeptide (PPR) repeat-containing protein(AT5G46580)	67.089	59.9181	57.4742	28.1876	51.2564	35.7627	-0.578736997	0.001613336	0.041149385
AT5G48470	hypothetical protein(AT5G48470)	33.6515	31.9942	26.0808	13.7213	23.5743	19.1128	-0.603905614	0.006952702	0.096453025
AT5G49910	chloroplast heat shock protein 70-2(cpHsc70-2)	195.673	171.114	174.957	79.2485	144.194	96.7076	-0.668134954	7.06E-05	0.004102789
AT5G50200	nitrate transmembrane transporter(WR3)	87.1526	63.8843	88.5601	54.7624	54.9936	43.2275	-0.529586005	0.006335733	0.092703332
AT5G52780	transmembrane protein. putative (DUF3464)(AT5G52780)	106.041	105.159	98.4163	59.8295	73.2915	65.498	-0.543133198	0.004172629	0.072917721
AT5G53450	OBP3-responsive protein 1(ORG1)	69.10521	63.8091	144.3299	39.6643	44.46715	38.5686	-1.088927812	0.006834078	0.095820889
AT5G53550	YELLOW STRIPE like 3(YSL3)	44.4584	54.0045	45.5306	30.84485	35.2071	28.5209	-0.489993777	0.001069332	0.030738942
AT5G54160	O-methyltransferase 1(OMT1)	294.296	289.675	310.602	176.975	232.339	221.882	-0.418181288	0.001063623	0.030674734

AT5G55280	homolog of bacterial cytokinesis Z-ring protein FTSZ 1-1(FTSZ1-1)	106.13	87.2061	90.2158	51.02	78.036	57.2939	-0.503173846	0.002703049	0.056128015
AT5G55920	S-adenosyl-L-methionine-dependent methyltransferases superfamily protein(OLI2)	36.4518	30.8942	35.0723	16.3871	26.6871	17.3271	-0.639782593	0.000930406	0.027927997
AT5G56010	heat shock protein 81-3(HSP81-3)	117.167	107.701	143.672	74.2723	83.8404	60.3639	-0.646772645	2.72E-05	0.002019854
AT5G56030	heat shock protein 81-2(HSP81-2)	138.03	131.101	159.672	83.5534	106.691	82.3163	-0.555572849	6.42E-05	0.003826998
AT5G57180	chloroplast import apparatus 2(CIA2)	20.26621	25.3528	18.27494	9.20384	14.080048	15.9068	-0.66016539	0.00383994	0.069871078
AT5G58250	YCF54(EMB3143)	382.876	327.72	357.86	223.628	299.006	242.309	-0.387061542	0.004905455	0.080167419
AT5G59850	Ribosomal protein S8 family protein(AT5G59850)	228.79	204.72	227.733	127.056	180.361	128.473	-0.492013056	0.001677507	0.042028542
AT5G61520	Major facilitator superfamily protein(AT5G61520)	25.4793	32.113	37.5727	17.3399	19.20273	13.97701	-0.777236132	0.000139537	0.006920348
AT5G61790	calnexin 1(CNX1)	156.64	138.516	175.242	83.8578	112.616	86.645	-0.635630947	1.36E-05	0.001128028
AT5G62680	Major facilitator superfamily protein(GTR2)	49.9791	46.5229	81.9131	34.5429	43.0797	33.8109	-0.582280177	0.004285368	0.073864016
AT5G64120	Peroxidase superfamily protein(AT5G64120)	972.792	691.559	951.819	386.419	436.829	335.043	-1.080933839	9.65E-13	7.74E-10
AT5G64580	AAA-type ATPase family protein(EMB3144)	36.9819	35.6689	35.6517	15.4905	30.4191	22.9681	-0.561149763	0.004023702	0.0717357
AT5G65010	asparagine synthetase 2(ASN2)	202.679	214.423	220.926	113.405	183.867376	144.794	-0.440236222	0.002882561	0.058479546
AT5G66470	GTP-binding protein Era-like protein(AT5G66470)	54.3495	56.0688	60.8611	30.2784	47.0705	35.9179	-0.492231307	0.005261316	0.083977988
AT5G67370	DUF1230 family protein (DUF1230)(CGLD27)	49.7925	51.1463	60.9105	26.6989	35.5015	40.3557	-0.613620387	0.001746144	0.043530273

Table S3. List of chloroplastic differentially expressed genes (DEGs) between *ucp1 ucp3* double mutant and wild-type (WT) assessing their metabolic type and process.

Upregulated						
GO:0009507~chloroplast	Gene Symbol	Metabolic type and Process	Functions	Log ₂ Fold Change	p value	p adjusted
AT1G52400	BGLU44	Carbon and AA metabolism	carbohydrate metabolic process/response to wounding	1.972860753	1.123E-16	2.47743E-13
AT4G35770	SEN1	Plant Growth, Development and response to stress	senescence process/response to oxidative stress	1.603803101	1.116E-19	3.28148E-16
AT1G29395	COR413IM1	Plant Growth. Development and response to stress	response to cold	1.573778429	8.884E-05	0.004839504
AT5G50950	FUM2	Carbon and AA metabolism	pyruvate metabolic process	1.553725701	0.0019901	0.046833273

AT2G34430	LHB1B1	Photosynthesis	Photosynthesis - antenna proteins	1.545278979	6.556E-20	2.89277E-16
AT1G10070	BCAT-2	Carbon and AA metabolism	aspartate and isoleucine metabolic process	1.521999024	2.861E-07	4.42892E-05
AT5G25980	TGG99	Carbon and AA metabolism	tryptophan and carbohydrate metabolic process	1.357743298	3.523E-16	5.1814E-13
AT2G16660	AT2G16660	Plant Growth, Development and response to stress	response to karrikin/growth regulators	1.355264935	1.579E-16	2.78708E-13
AT2G39800	P5CS1	Carbon and AA metabolism	proline metabolic process	1.143901847	3.92E-07	5.67107E-05
AT2G27385	AT2G27385	Plant Growth, Development and response to stress	growth regulators	0.997513175	2.786E-06	0.000307277
AT2G29670	AT2G29670	DNA metabolism	RNA processing	0.987883282	1.163E-08	3.54052E-06
AT2G34420	LHB1B2	Photosynthesis	Photosynthesis - antenna proteins	0.961541494	5.541E-09	1.88069E-06
AT5G56980	AT5G56980	Unknown	protein of unknown function DUF761 and DUF4408	0.954620637	0.0009883	0.029268264
AT3G16240	DELTA-TIP	Transport activity	water transport	0.904307299	5.149E-10	2.84006E-07
AT1G52410	TSA1	Carbon and AA metabolism	tryptophan metabolic process	0.8935011	0.0013727	0.037340805
AT1G61890	AT1G61890	Transport activity	drug transmembrane transport	0.886530414	0.000103	0.005473738
AT4G14680	APS3	DNA metabolism	sulfate assimilation/purine metabolism	0.876433738	0.0006909	0.022752031
AT1G65390	PP2-A5	Signaling pathway	defense response/signal transduction	0.852514946	4.407E-05	0.002798101
AT5G26000	TGG00	Carbon and AA metabolism	tryptophan and carbohydrate metabolic process	0.845348191	1.252E-08	3.56554E-06
AT1G01620	PIP1C	Transport activity	water transport	0.841637651	1.827E-07	3.10093E-05
AT2G22330	CYP79B3	Carbon and AA metabolism/Transport activity	tryptophan metabolic process	0.832418654	1.598E-06	0.0001831
AT1G51400	AT1G51400	Photosynthesis	photosystem II	0.806769353	1.242E-06	0.000152209
AT1G20510	OPCL1	Lipid metabolism/Signaling pathway	JA signaling	0.792207825	9.342E-05	0.005046165

AT2G17880	AT2G17880	Carbon and AA metabolism	protein folding	0.786825292	0.0006621	0.022049038
AT5G02160	AT5G02160	Plant Growth, Development and response to stress	heat shock protein binding	0.780401186	6.792E-09	2.21991E-06
AT1G69840	AT1G69840	Carbon and AA metabolism	histidine metabolism	0.77890542	4.056E-05	0.002671315
AT4G17090	CT-BMY	Carbon and AA metabolism	starch and sucrose metabolism	0.766338785	3.2E-05	0.002223346
AT3G15450	AT3G15450	Carbon and AA metabolism	glutamine metabolic process	0.731061418	1.711E-07	3.02052E-05
AT1G29930	CAB1	Photosynthesis	Photosynthesis - antenna proteins	0.715782363	2.675E-08	6.55823E-06
AT5G55700	BAM77	Carbon and AA metabolism	starch and sucrose metabolism	0.711159751	0.0007216	0.023586933
AT5G54270	LHCB3	Photosynthesis	Photosynthesis - antenna proteins	0.710791746	2.148E-05	0.001633928
AT5G15970	KIN2	Plant Growth, Development and response to stress	response to osmotic and cold stresses	0.705736769	0.0024406	0.052638776
AT1G06570	PDS55	Carbon and AA metabolism	phenylalanine and tyrosine metabolic process	0.703450313	0.0005776	0.019834667
AT5G18140	AT5G18140	Carbon and AA metabolism	protein folding	0.682550938	0.00188	0.045084124
AT4G34950	AT4G34950	Plant Growth, Development and response to stress	response to karrikin/growth regulators	0.678294315	2.551E-05	0.001908181
AT1G57990	PUP99	Transport activity	purine nucleobase transport	0.676616652	0.0002745	0.01211156
AT5G24490	AT5G24490	DNA metabolism	translation/structural constituent of ribosome	0.675111317	1.558E-07	2.80569E-05
AT5G66210	CPK28	Carbon and AA metabolism	serine and threonine metabolism/plant-pathogen interaction	0.666909315	0.0004023	0.015303358
AT1G51760	IAR3	Signaling pathway	proteolysis	0.657297331	0.0004283	0.015947767
AT2G31810	AT2G31810	Carbon and AA metabolism	isoleucine and valine metabolic process	0.656231522	7.433E-06	0.000669306
AT1G29920	CAB2	Photosynthesis	Photosynthesis - antenna proteins	0.651770646	2.969E-05	0.002129878
AT1G07040	AT1G07040	Unknown	protein of unknown function DUF1338	0.63831256	0.0001819	0.008630343

AT3G08940	LHCB4.2	Photosynthesis	Photosynthesis - antenna proteins	0.632897651	0.0003578	0.014159645
AT4G17340	TIP2;2	Transport activity	water transport	0.628816328	0.0027682	0.057211049
AT4G15530	PPDK	Carbon and AA metabolism	pyruvate metabolic process	0.581601222	0.0007748	0.02477458
AT1G20620	CAT3	Transport activity	response to oxidative stress/inorganic ion transport	0.581011131	6.792E-05	0.004022917
AT1G03130	PSAD-2	Photosynthesis	photosystem I	0.574217765	0.000279	0.012189675
AT2G15890	MEE14	Plant Growth, Development and response to stress	defense response to fungus	0.573852847	5.538E-07	7.63665E-05
AT3G14990	DJ1A	DNA metabolism	regulation of transcription from RNA polymerase II promoter	0.570422095	0.0023569	0.051451502
AT3G07310	AT3G07310	Unknown	protein of unknown function DUF760	0.564357218	0.0022844	0.050693892
AT4G10340	LHCB5	Photosynthesis	Photosynthesis - antenna proteins	0.560073192	8.019E-05	0.004478854
AT1G72150	PATL1	Transport activity	cell cycle	0.559882199	5.337E-05	0.003332858
AT3G26520	TIP2	Transport activity	water transport	0.557263999	7.067E-05	0.004102789
AT3G54890	LHCA1	Photosynthesis	Photosynthesis - antenna proteins	0.545099265	9.548E-05	0.005106778
AT1G29910	CAB3	Photosynthesis	Photosynthesis - antenna proteins	0.528621191	0.0004399	0.016127779
AT2G20670	AT2G66	Unknown	protein of unknown function DUF506	0.516439903	0.0008485	0.026367342
AT3G26740	CCL	Plant Growth, Development and response to stress	circadian rhythm	0.505061836	0.0010186	0.029962625
AT1G61520	LHCA3	Photosynthesis	Photosynthesis - antenna proteins	0.504744685	0.0003654	0.014159645
AT1G68010	HPR00	Carbon and AA metabolism	coenzyme metabolism	0.502017318	0.0025764	0.054787967
AT1G16720	HCF173	DNA metabolism/Photosynthesis	photosystem II	0.497741246	0.0013344	0.036685066
AT4G30210	ATR22	Transport activity	inorganic ion transport/oxidation-reduction process	0.48805578	0.0008114	0.025574182
AT5G10450	GRF6	DNA metabolism	regulation of transcription	0.485635093	0.0001526	0.007401294

AT3G61470	LHCA2	Photosynthesis	Photosynthesis - antenna proteins	0.483928771	0.0001385	0.006920348
AT1G08110	AT1G08110	Carbon and AA metabolism	carbohydrate and lactate metabolic process	0.483192045	0.0017908	0.044143519
AT1G58290	HEMA1	DNA metabolism	glutamyl-tRNA reductase activity	0.467617108	0.0051562	0.082733691
AT3G08030	AT3G08030	Unknown	protein of unknown function DUF642	0.461569128	0.0018684	0.044927427
AT2G30570	PSBW	Photosynthesis	photosystem II	0.46057476	0.0003604	0.014159645
AT3G47470	LHCA4	Photosynthesis	Photosynthesis - antenna proteins	0.460070015	0.0009291	0.027927997
AT1G79040	PSBR	Photosynthesis	photosystem II	0.459412541	0.0003565	0.014159645
AT4G20260	PCAP1	Plant Growth, Development and response to stress	N-terminal protein myristylation	0.455505702	0.0023115	0.050850918
AT2G45960	PIP1B	Transport activity	water transport	0.454518464	0.0002804	0.012191269
AT1G23310	GGT1	Carbon and AA metabolism	glycine and alanine metabolic process/photorespiration response to light stimulus	0.452701943	0.0016811	0.042028542
AT1G80920	J8	Photosynthesis	response to light stimulus	0.448214334	0.0010957	0.031294319
AT1G76100	PETE1	Photosynthesis	oxidation-reduction process	0.445672566	0.0042743	0.073857245
AT5G20250	DIN10	Carbon and AA metabolism	galactose metabolism	0.444453086	0.0022633	0.050438497
AT5G43780	APS4	DNA metabolism	sulfate assimilation/purine metabolism	0.439982208	0.0064518	0.093339943
AT1G30510	RFNR55	Carbon and AA metabolism/Photosynthesis	oxidation-reduction process	0.438010331	0.0058593	0.08937017
AT5G27280	AT5G27280	Carbon and AA metabolism	protein folding	0.437370679	0.0062985	0.092703332
AT3G53420	PIP2A	Transport activity	water transport	0.436930961	0.004363	0.074909036
AT2G06520	PSBX	Photosynthesis	photosystem II	0.425288398	0.001123	0.03186734
AT1G08510	FATB	Lipid metabolism	fatty acid biosynthetic process	0.422700152	0.0022006	0.049796374
AT2G29980	FAD3	Lipid metabolism	fatty acid biosynthetic process	0.419212891	0.0019204	0.045761892
AT1G31330	PSAF	Photosynthesis	photosystem I	0.410707217	0.0009986	0.029472939
AT1G09770	CDC5	DNA metabolism	DNA repair and RNA regulation	0.408515098	0.0040166	0.0717357

AT1G74920	ALDH10A8	Carbon and AA metabolism	glycine metabolism	0.405136273	0.0024185	0.052440943
AT2G38040	CAC3	Lipid metabolism	acetyl-CoA carboxylase activity	0.402693653	0.0008549	0.026473228
AT2G20260	PSAE-2	Photosynthesis	photosystem I	0.40250078	0.0016584	0.042028542
AT5G51070	ERD00	DNA metabolism	ATP binding/ATPase activity	0.400453207	0.0031055	0.061587017
AT4G28750	PSAE-1	Photosynthesis	photosystem I	0.386793738	0.0018543	0.044832931
AT1G21500	AT1G21500	Unknown	autophagy process	0.370485736	0.0059565	0.090292731
AT5G01530	LHCB4.1	Photosynthesis	Photosynthesis - antenna proteins	0.36987361	0.0039178	0.070560859
AT1G30380	PSAK	Photosynthesis	photosystem I	0.347294421	0.0065756	0.094357756
AT1G47128	RD21A	Signaling pathway	defense response to fungus/proteolysis	0.333689787	0.0072628	0.098103697
Downregulated						
GO:0009507~chloroplast	Gene Symbol	Metabolism type	Functions	Log2Fold Change	p value	p adjusted
AT1G73990	SPPA	Signaling pathway	proteolysis	-1.558469671	8.402E-15	1.05931E-11
AT5G53450	ORG1	DNA metabolism	protein phosphorylation/ATP binding	-1.088927812	0.0068341	0.095820889
AT3G20440	EMB2729	Carbon and AA metabolism	starch and sucrose metabolism	-1.067226958	2.833E-05	0.002065968
AT2G39518	AT2G39518	Unknown	unknown	-1.039824343	0.0004262	0.015936944
AT2G39210	AT2G39210	Plant Growth, Development and response to stress	response to karrikin/growth regulators	-1.033255534	5.385E-08	1.15913E-05
AT3G45140	LOX2	Lipid metabolism	fatty acid metabolic process	-1.018965753	0.0015485	0.040192396
AT3G14210	ESM1	Lipid metabolism	lipid metabolic process	-1.001803123	0.0067485	0.095480799
AT3G09440	AT3G09440	DNA metabolism	Spliceosome/ATP binding	-0.938312873	3.888E-07	5.67107E-05
AT1G04980	PDIL2-2	Carbon and AA metabolism	protein processing in endoplasmic reticulum/cell redox homeostasis	-0.934133151	0.0006015	0.020495264
AT4G12320	CYP706A6	Secondary metabolism	oxidation-reduction process/secondary metabolites process	-0.927121106	1.47E-05	0.001163986

AT5G13490	AAC2	Transport activity	ATP:ADP antiporter activity/mitochondrial carrier protein	-0.87673104	0.0008643	0.026669529
AT2G18950	HPT1	Secondary metabolism	terpenoid metabolic process	-0.801626873	0.0035732	0.066526409
AT4G30825	AT4G30825	DNA metabolism	protein processing in endoplasmic reticulum	-0.771553674	0.0027395	0.056751546
AT1G62180	APR2	Carbon and AA metabolism	sulfate assimilation/cysteine metabolic process	-0.763480956	4.091E-06	0.000401655
AT3G54110	UCP1	Transport activity	mitochondrial transport/photorespiration	-0.747347981	0.0031405	0.051349875
AT3G06530	AT3G06530	DNA metabolism	ribosome biogenesis	-0.739827427	0.0002901	0.012548865
AT3G54400	AT3G54400	Signaling pathway	proteolysis	-0.736158563	1.453E-05	0.001163986
AT3G01060	AT3G01060	Plant Growth, Development and response to stress	circadian rhythm	-0.730796841	0.0004368	0.016127779
AT3G25410	AT3G25410	Transport activity	inorganic ion transport	-0.729407727	0.0002964	0.01269684
AT5G26860	LON1	Carbon and AA metabolism	protein catabolic process	-0.719668798	0.0005546	0.019420688
AT2G37690	AT2G37690	DNA metabolism	purine metabolism/ATP binding	-0.717223418	0.0020809	0.047699266
AT1G56050	AT1G56050	DNA metabolism	ATP and GTP binding	-0.704915775	0.0001713	0.008218134
AT2G40400	AT2G40400	Unknown	unknown	-0.704675847	0.0004404	0.016127779
AT3G13470	Cpn60beta2	DNA metabolism	RNA degradation/ATP binding	-0.702876638	2.774E-05	0.002040281
AT1G30680	AT1G30680	DNA metabolism	DNA replication, recombination and repair	-0.676185137	0.0063654	0.092703332
AT5G02830	AT5G02830	DNA metabolism	protein processing in endoplasmic reticulum	-0.670317931	0.0025921	0.054989338
AT5G49910	cpHsc70-2	DNA metabolism	spliceosome/protein processing in endoplasmic reticulum	-0.668134954	7.062E-05	0.004102789
AT2G04530	CPZ	DNA metabolism	tRNA processing/RNA transport	-0.66232564	0.0069968	0.096782083
AT1G59990	EMB3108	DNA metabolism	RNA binding/ATP binding	-0.66111028	0.0009404	0.028132715
AT5G57180	CIA2	DNA metabolism	regulation of transcription	-0.66016539	0.0038399	0.069871078
AT5G08610	PDE340	DNA metabolism	RNA binding/ATP binding	-0.656227272	0.0003168	0.013187301
AT3G55010	PUR5	DNA metabolism	purine metabolism	-0.655719857	0.0014581	0.038183737

AT2G40100	LHCB4.3	Photosynthesis	Photosynthesis - antenna proteins	-0.649352362	0.0040168	0.0717357
AT3G51870	AT3G51870	Transport activity	transmembrane transport	-0.648983871	0.0015134	0.039397221
AT2G31170	SYCO ARATH	DNA metabolism	tRNA processing/ATP binding	-0.642324205	0.0033216	0.063724904
AT4G04020	FIB	Plant Growth, Development and response to stress	Protein binding	-0.641288091	0.000115	0.005967532
AT1G77510	PDIL1-2	Carbon and AA metabolism	protein processing in endoplasmic reticulum	-0.639188651	0.0006948	0.022794405
AT2G03420	AT2G03420	Unknown	Hypothetical protein	-0.63808172	0.0014437	0.038145972
AT5G61790	CNX1	DNA metabolism	protein folding/protein processing in endoplasmic reticulum	-0.635630947	1.361E-05	0.001128028
AT5G43745	AT5G43745	Transport activity	transmembrane transport	-0.627257115	0.0071702	0.097800392
AT3G54090	FLN1	DNA metabolism	chloroplast organization	-0.624073779	0.0047689	0.07866464
AT5G67370	CGLD27	Unknown	unknown	-0.613620387	0.0017461	0.043530273
AT5G48470	AT5G48470	Unknown	unknown	-0.603905614	0.0069527	0.096453025
AT2G18940	AT2G18940	DNA metabolism	RNA binding	-0.594771847	0.003174	0.06238349
AT5G45140	NRPC2	DNA metabolism	transcription/RNA polymerase/purine and pyrimidine metabolism	-0.591237942	0.0062444	0.092306061
AT1G26230	Cpn60beta4	DNA metabolism	RNA degradation/ATP binding	-0.590557892	0.0067245	0.095448057
AT3G14390	AT3G14390	Carbon and AA metabolism	lysine metabolic process	-0.589947585	0.0023221	0.050850918
AT2G31060	EMB2785	DNA metabolism	translation	-0.58924018	0.0061022	0.091119959
AT5G46580	AT5G46580	Unknown	unknown	-0.578736997	0.0016133	0.041149385
AT4G02990	BSM	DNA metabolism	chloroplast organization	-0.57765309	0.0008676	0.026678238
AT3G53560	AT3G53560	DNA metabolism	Protein binding	-0.569448535	0.0028775	0.058479546
AT2G31890	RAP	DNA metabolism	rRNA processing/RNA binding	-0.568571594	0.0044212	0.075322338
AT2G21860	AT2G21860	Secondary metabolism	xanthophyll cycle	-0.568228817	0.0073073	0.098263209
AT3G26710	CCB1	Carbon and AA metabolism	cytochrome complex/electron transport	-0.567844978	0.0003197	0.013246634
AT2G28000	CPN60A	DNA metabolism	ATP binding	-0.564698279	7.192E-05	0.004121159

AT5G42020	BIP2	DNA metabolism	ATP binding/protein processing in endoplasmic reticulum	-0.563243529	0.0006039	0.020497669
AT3G19810	AT3G19810	DNA metabolism	rRNA processing	-0.56283611	0.0067513	0.095480799
AT5G44785	OSB3	DNA metabolism	DNA replication	-0.562548951	0.0073767	0.098263209
AT4G31210	AT4G31210	DNA metabolism	DNA binding/DNA replication	-0.562367943	0.0053225	0.083977988
AT5G64580	EMB3144	Signaling pathway	proteolysis/ATP binding	-0.561149763	0.0040237	0.0717357
AT1G58380	XW6	DNA metabolism	translation/structural constituent of ribosome	-0.558515629	0.0018209	0.044678844
AT4G21990	APR3	Carbon and AA metabolism	cysteine metabolic process/sulfur metabolism	-0.557460182	0.0047687	0.07866464
AT1G48570	AT1G48570	DNA metabolism	metal binding	-0.555196135	0.0057804	0.088717207
AT5G52780	AT5G52780	Unknown	unknown	-0.543133198	0.0041726	0.072917721
AT4G05390	RFNR1	Photosynthesis	oxidation-reduction process	-0.541186182	0.0026662	0.055638876
AT5G09590	MTHSC70-2	DNA metabolism	spliceosome/ATP binding/protein processing in endoplasmic reticulum	-0.537155357	0.0014544	0.038183737
AT2G24120	SCA3	DNA metabolism	transcription	-0.535361012	0.0038485	0.069882673
AT3G03780	MS2	Carbon and AA metabolism	cysteine and methionine metabolic process	-0.532041523	0.0021848	0.049692858
AT2G25830	AT2G25830	DNA metabolism	transcriptional regulatory protein	-0.531182163	0.0046104	0.077013732
AT2G04360	AT2G04360	Lipid metabolism	Cardiolipin synthase activity	-0.528842055	0.0066628	0.095135248
AT3G55400	OVA1	DNA metabolism	tRNA processing	-0.526917725	0.0056935	0.087687878
AT3G18080	BGLU44	Carbon and AA metabolism	carbohydrate metabolic process	-0.521974102	0.001371	0.037340805
AT1G60600	ABC4	Secondary metabolism	terpenoid metabolic process	-0.52109069	0.0069472	0.096453025
AT3G62530	AT3G62530	Transport activity	energy production and conversion	-0.518370645	0.0001136	0.005929474
AT2G23670	YCF37	Unknown	unknown	-0.517861409	0.0005219	0.018423376
AT5G35220	EGY1	DNA metabolism	chloroplast organization	-0.509860073	0.0018853	0.045089287

AT5G28540	BIP1	DNA metabolism	ATP binding/protein processing in endoplasmic reticulum	-0.507674109	0.0011384	0.032198594
AT5G55280	FTSZ1-1	DNA metabolism	Cell division and chromosome partitioning	-0.503173846	0.002703	0.056128015
AT1G57770	AT1G57770	Secondary metabolism	carotenoid metabolic process	-0.498642937	0.0070422	0.096953875
AT3G18680	AT3G18680	DNA metabolism	pyrimidine metabolic process	-0.498420239	0.0005996	0.020495264
AT4G12060	AT4G12060	DNA metabolism	ATP binding/protein metabolic process	-0.495963291	0.0040766	0.072065923
AT3G49680	BCAT3	Carbon and AA metabolism	aspartate and isoleucine metabolic process	-0.493605735	0.0060527	0.090842158
AT5G66470	AT5G66470	DNA metabolism	GTP binding/rRNA processing	-0.492231307	0.0052613	0.083977988
AT5G59850	AT5G59850	DNA metabolism	translation/ribosome	-0.492013056	0.0016775	0.042028542
AT2G20020	CAF1	DNA metabolism	RNA binding/mRNA process	-0.485300378	0.0064981	0.093702867
AT3G43600	AAO2	Carbon and AA metabolism	tryptophan metabolic process	-0.4844914	0.004452	0.075409772
AT1G17100	HBP1	Carbon and AA metabolism	heme binding	-0.480510698	0.0043769	0.075001493
AT4G16660	AT4G16660	DNA metabolism	ATP binding/protein processing in endoplasmic reticulum	-0.477113252	0.0049545	0.080670491
AT4G09730	RH39	DNA metabolism	rRNA processing/ATP binding	-0.47184577	0.0042073	0.073378468
AT3G47520	MDH	Carbon and AA metabolism	carbohydrate metabolic process	-0.470893557	0.0030563	0.060883907
AT3G44310	NIT1	Carbon and AA metabolism	tryptophan metabolic process	-0.470768018	0.0039559	0.070956515
AT2G32230	PRORP1	DNA metabolism	tRNA processing/RNA transport	-0.470460723	0.0025184	0.053943491
AT3G52140	NOXY38	DNA metabolism	RNA binding	-0.465179411	0.0016682	0.042028542
AT1G60000	AT1G60000	DNA metabolism	RNA binding	-0.463007636	0.0055597	0.086229278
AT1G73110	AT1G73110	DNA metabolism	ATP binding/ATPase activity	-0.459643574	0.0065746	0.094357756
AT4G16390	SVR7	DNA metabolism	chloroplast organization/RNA binding	-0.450765232	0.0041514	0.072917721
AT5G11450	PPD5	Photosynthesis	oxygen involving process	-0.442272868	0.007366	0.098263209

AT4G36810	GGPS1	Secondary metabolism	terpenoid metabolic process	-0.429826303	0.0046667	0.077412825
AT5G28750	AT5G28750	Transport activity	protein transport/protein secretion	-0.423642571	0.0051092	0.082335975
AT5G09650	PPa6	DNA metabolism	oxidative phosphorylation	-0.422818352	0.0030142	0.060374973
AT1G55490	CPN60B	DNA metabolism	RNA degradation/ATP binding	-0.42125326	0.0006807	0.022585012
AT1G53240	mMDH1	Carbon and AA metabolism	pyruvate metabolic process/carbohydrate and malate metabolic process	-0.420750472	0.0008019	0.025456039
AT5G20720	CPN20	DNA metabolism	protein folding	-0.419076308	0.0012369	0.034314475
AT3G55250	PDE329	Signaling pathway	calcium homeostasis	-0.418843555	0.0050211	0.081454796
AT1G62780	AT1G62780	DNA metabolism	RNA binding	-0.418381949	0.006851	0.095820889
AT1G01080	AT1G01080	DNA metabolism	chloroplast rRNA processing	-0.411390767	0.0054	0.084644671
AT5G41670	AT5G41670	Carbon and AA metabolism	carbon metabolism/response to sucrose, fructose and glucose	-0.409884055	0.0044619	0.075433778
AT3G06980	AT3G06980	DNA metabolism	RNA binding/ATP binding	-0.405340594	0.0073823	0.098263209
AT1G06950	TIC110	Transport activity	protein import into stroma	-0.40359784	0.0029097	0.05875911
AT3G61440	CYSC1	Carbon and AA metabolism	cysteine and methionine metabolic process	-0.398271399	0.0063658	0.092703332
AT2G31400	GUN1	Signaling pathway	signal transduction/DNA binding	-0.391440967	0.0019238	0.045761892
AT1G68590	PSRP3/1	DNA metabolism	translation/structural constituent of ribosome	-0.388585098	0.0038827	0.070258465
AT5G58250	EMB3143	Carbon and AA metabolism	chlorophyll metabolic process	-0.387061542	0.0049055	0.080167419
AT2G37270	RPS5B	DNA metabolism	Ribosome/rRNA binding	-0.384582077	0.0073699	0.098263209
AT4G39730	PLAT1	Plant Growth, Development and response to stress	regulation of plant growth	-0.384488407	0.0069621	0.096453025
AT2G16600	ROC3	Signaling pathway	signal transduction	-0.382811516	0.003744	0.068548866
AT4G02380	SAG21	Plant Growth, Development and response to stress	senescence process/response to oxidative stress	-0.379241896	0.0067238	0.095448057
AT3G04840	AT3G04840	DNA metabolism	translation/ribosome	-0.370554194	0.003017	0.060374973

AT5G12860	DIT1	Transport activity	inorganic ion transport	-0.36835282	0.0063332	0.092703332
AT3G48730	GSA2	Secondary metabolism	tetrapyrroles metabolic process	-0.363751382	0.0056775	0.087594664
AT4G31700	RPS6	DNA metabolism	rRNA processing	-0.353095026	0.0059333	0.090278023
AT5G38430	RBCS1B	Carbon and AA metabolism	carbon fixation	-0.345994379	0.0008104	0.025574182
AT3G25520	ATL5	DNA metabolism	Ribosome/rRNA binding	-0.310480823	0.0072081	0.098085315

Table S4. List of mitochondrial differentially expressed genes (DEGs) between *ucp1 ucp3* double mutant and wild-type (WT) assessing their metabolic type and process.

Downregulated						
GO:0005739~mitochondrion	Gene Symbol	Metabolic type and Process	Functions	Log ₂ Fold Change	p value	p adjusted
AT3G30720	QQS	Carbon and AA metabolism	starch metabolic process	-2.459296904	3.73852E-06	0.000383633
AT5G44575	AT5G44575	Unknown	unknown	-0.941751341	0.000759541	0.024374375
AT5G13490	AAC2	Transport activity	ATP:ADP antiporter activity/mitochondrial carrier protein	-0.87673104	0.000864304	0.026669529
AT4G30825	AT4G30825	DNA metabolism	protein processing in endoplasmic reticulum	-0.771553674	0.002739508	0.056751546
AT3G54110	UCP1	Transport activity	mitochondrial transport/photorespiration	-0.747347981	0.003140492	0.051349875
AT3G22370	AOX1A	Cellular respiration	mitochondria-nucleus signaling pathway/oxidation-reduction process	-0.746371685	0.002029818	0.006067341
AT4G15640	AT4G15640	DNA metabolism	mRNA binding	-0.733188301	0.005711416	0.087810529
AT5G26860	LON1	Carbon and AA metabolism	protein catabolic process/mitochondrion organization	-0.719668798	0.000554562	0.019420688
AT2G37690	AT2G37690	DNA metabolism	purine metabolism/ATP binding	-0.717223418	0.002080931	0.047699266
AT3G13470	Cpn60beta2	DNA metabolism	RNA degradation/ATP binding	-0.702876638	2.77432E-05	0.002040281

AT1G14140	UCP3	Transport activity	mitochondrial transport	-0.696796632	0.004231981	0.076815679
AT1G30680	AT1G30680	DNA metabolism	DNA replication.	-0.676185137	0.006365377	0.092703332
AT5G02830	AT5G02830	DNA metabolism	recombination and repair	-0.670317931	0.002592132	0.054989338
AT1G45332	AT1G45332	DNA metabolism	protein processing in endoplasmic reticulum	-0.66837822	0.005589747	0.086543015
AT3G55010	PUR5	DNA metabolism	mitochondrial translational elongation	-0.655719857	0.001458121	0.038183737
AT3G51870	AT3G51870	DNA metabolism	purine metabolism	-0.648983871	0.001513389	0.039397221
AT2G31170	SYCO	Transport activity	transmembrane transport	-0.642324205	0.003321638	0.063724904
AT5G61790	ARATH CNX1	DNA metabolism	tRNA processing/ATP binding	-0.635630947	1.36128E-05	0.001128028
AT2G01670	NUDT17	DNA metabolism	protein folding/protein processing in endoplasmic reticulum	-0.629107061	0.004276606	0.073857245
AT2G18940	AT2G18940	DNA metabolism	nucleoside catabolic process	-0.594771847	0.003173959	0.06238349
AT5G44580	AT5G44580	DNA metabolism	RNA binding	-0.591954596	0.00073944	0.024018386
AT2G31060	EMB2785	Transport activity	transport transmembrane	-0.58924018	0.006102198	0.091119959
AT4G02990	BSM	DNA metabolism	translation	-0.57765309	0.00086761	0.026678238
AT5G02050	AT5G02050	DNA metabolism	chloroplast organization/regulation of transcription/RNA splicing	-0.567293619	0.005798036	0.08883275
AT2G28000	CPN60A	Signaling pathway	mitochondrial glycoprotein	-0.564698279	7.1916E-05	0.004121159
AT1G27330	AT1G27330	DNA metabolism	ATP binding	-0.564425878	0.001835946	0.044757525
AT3G56070	ROC2	Carbon and AA metabolism	protein glycosylation/response to oxidative stress	-0.562728381	0.002416638	0.052440943
AT5G44785	OSB3	Carbon and AA metabolism	protein peptidyl-prolyl isomerization/protein folding	-0.562548951	0.007376735	0.098263209
AT5G64580	EMB3144	DNA metabolism	DNA replication	-0.561149763	0.004023702	0.0717357
		Signaling pathway	proteolysis/ATP binding			

AT5G56030	HSP81-2	Plant Growth, Development and response to stress	protein folding/response to heat/response to stress	-0.555572849	6.41808E-05	0.003826998
AT5G09590	MTHSC70-2	DNA metabolism	spliceosome/ATP binding/protein processing in endoplasmic reticulum transcription	-0.537155357	0.00145436	0.038183737
AT2G24120	SCA3	DNA metabolism		-0.535361012	0.003848496	0.069882673
AT4G23290	CRK21	Signaling pathway	protein phosphorylation/defense response to bacterium	-0.533613593	0.005412335	0.084687695
AT3G55400	OVA1	DNA metabolism	tRNA processing	-0.526917725	0.005693502	0.087687878
AT3G62530	AT3G62530	Transport activity	energy production and conversion	-0.518370645	0.00011355	0.005929474
AT1G57770	AT1G57770	Secondary metabolism	carotenoid metabolic process	-0.498642937	0.007042202	0.096953875
AT4G13850	GR-RBP2	Plant Growth, Development and response to stress	response to salt and osmotic stress/cold acclimation	-0.475849504	0.002935967	0.059155052
AT4G21105	AT4G21105	Cellular respiration	mitochondrial transport transmembrane	-0.471889875	0.00607642	0.091043134
AT3G47520	MDH	Carbon and AA metabolism	carbohydrate metabolic process	-0.470893557	0.003056269	0.060883907
AT2G32230	PRORP1	DNA metabolism	tRNA processing/RNA transport	-0.470460723	0.002518382	0.053943491
AT1G60000	AT1G60000	DNA metabolism	RNA binding	-0.463007636	0.005559712	0.086229278
AT4G02930	AT4G02930	DNA metabolism	translation	-0.459818375	0.003237085	0.062923511
AT1G31970	STRS1	DNA metabolism	rRNA processing/ATP binding	-0.439691614	0.004475531	0.075519236

AT3G23990	HSP60	DNA metabolism	mitochondrion organization/RNA degradation/response to heat	-0.426695363	0.002635252	0.055479184
AT1G53240	mMDH1	Carbon and AA metabolism	pyruvate metabolic process/carbohydrate and malate metabolic process	-0.420750472	0.000801901	0.025456039
AT5G20720	CPN20	DNA metabolism	protein folding	-0.419076308	0.001236887	0.034314475
AT3G55250	PDE329	Signaling pathway	calcium homeostasis	-0.418843555	0.005021123	0.081454796
AT5G41670	AT5G41670	Carbon and AA metabolism	carbon metabolism/response to sucrose, fructose and glucose	-0.409884055	0.004461919	0.075433778
AT3G61440	CYSC1	Carbon and AA metabolism	cysteine and methionine metabolic process	-0.398271399	0.006365804	0.092703332
AT4G37910	mtHsc70-1	DNA metabolism	protein folding/ATP binding/response to heat	-0.391498699	0.006672943	0.095135248
AT4G02380	SAG21	Plant Growth, Development and response to stress	senescence process/response to oxidative stress	-0.379241896	0.006723832	0.095448057
AT5G12860	DiT1	Transport activity	inorganic ion transport	-0.36835282	0.006333243	0.092703332
AT1G48920	NUC-L1	DNA metabolism	rRNA processing/nucleotide binding	-0.362296126	0.006206147	0.091988775
AT3G22200	POP2	Carbon and AA metabolism	sucrose and glutamate metabolic process	-0.358573217	0.002057139	0.047467086
AT4G31700	RPS6	DNA metabolism	rRNA processing	-0.353095026	0.005933286	0.090278023

Table S5. List of abiotic stress-responsive differentially expressed genes (DEGs) between *ucp1 ucp3* double mutant and wild-type (WT) assessing their metabolic type and process.

Upregulated					
TAIR_ID	Gene Symbol	Response type	Log ₂ Fold Change	p value	p adjusted
AT3G47340	ASN1	Response to light *absence	2.978258043	4.40901E-14	4.60483E-11
AT1G52400	BGLU18	Response to water deprivation/salt stress	1.972860753	1.12291E-16	2.47743E-13
AT4G35770	SEN1	Response to oxidative stress/wounding	1.603803101	1.11552E-19	3.28148E-16
AT1G29395	COR413IM1	Response to cold/water deprivation	1.573778429	8.88385E-05	0.004839504
AT5G50950	FUM2	Response to salt stress	1.553725701	0.001990082	0.046833273
AT2G34430	LHB1B1	Response to light *stimulus	1.545278979	6.55586E-20	2.89277E-16
AT5G25980	TGG2	Response to salt stress	1.357743298	3.52277E-16	5.1814E-13
AT1G32640	MYC2	Response to wounding/to oxidative stress	1.282208421	4.424E-07	6.19711E-05
AT1G77120	ADH1	Response to cold/water deprivation/salt stress	1.260027224	0.001985954	0.046833273
AT2G39800	P5CS1	Response to water deprivation/salt stress/oxidative stress	1.143901847	3.91995E-07	5.67107E-05
AT2G19810	OZF1	Response to oxidative stress	1.069293253	2.25451E-05	0.00170052
AT3G11410	PP2CA	Response to cold/water deprivation	0.981368013	9.37758E-05	0.005046165
AT2G34420	LHB1B2	Response to light *stimulus	0.961541494	5.54084E-09	1.88069E-06
AT5G26340	MSS1	Response to water deprivation/salt stress	0.894992243	1.96598E-09	7.31123E-07
AT5G49730	FRO6	Response to light *stimulus	0.869617449	3.33005E-08	7.73361E-06
AT4G24230	ACBP3	Response to light/hypoxia *absence	0.867328913	6.41308E-06	0.000589536

AT5G20230	BCB	Response to light/oxidative stress/wounding *absence	0.858913095	9.9231E-06	0.000867043
AT2G41100	TCH3	Response to light *absence	0.847598785	5.94108E-07	8.06616E-05
AT5G26000	TGG1	Response to salt stress	0.845348191	1.25248E-08	3.56554E-06
AT1G01620	PIP1C	Response to water deprivation	0.841637651	1.82718E-07	3.10093E-05
AT4G36430	AT4G36430	Response to oxidative stress	0.840015946	0.000925337	0.027927997
AT4G31910	BAT1	Response to abiotic stress	0.814948084	0.001244264	0.034314475
AT4G17090	CT-BMY	Response to cold	0.766338785	3.1996E-05	0.002223346
AT3G58490	SPP1	Response to abiotic stress	0.717288262	0.001028431	0.030052666
AT1G29930	CAB1	Response to light *stimulus	0.715782363	2.67531E-08	6.55823E-06
AT5G54270	LHCB3	Response to light *stimulus	0.710791746	2.14771E-05	0.001633928
AT1G45145	TRX5	Response to oxidative stress	0.707891587	0.001379886	0.037340805
AT5G15970	KIN2	Response to cold/water deprivation/osmotic stress	0.705736769	0.002440581	0.052638776
AT4G34150	AT4G34150	Response to cold	0.70104514	0.000547464	0.019248476
AT5G65730	XTH6	Response to water deprivation	0.690388145	0.000108244	0.005686049
AT3G13450	DIN4	Response to light *absence	0.678746584	0.000135341	0.00688358
AT5G63600	FLS5	Response to light *stimulus	0.678083368	0.00024572	0.011203566
AT2G36400	GRF3	Response to cold	0.675989882	0.00353874	0.066024063
AT3G01420	DOX1	Response to oxidative stress	0.667820712	7.66134E-05	0.004306455
AT4G35100	PIP3	Response to water deprivation	0.657099161	1.1976E-05	0.001016231
AT1G29920	CAB2	Response to light *stimulus	0.651770646	2.96856E-05	0.002129878
AT4G12720	NUDT7	Response to salt stress/oxidative stress	0.643266165	0.001235055	0.034314475

AT1G07600	MT1A	Response to light *stimulus	0.640160583	0.003602447	0.066929679
AT3G08940	LHCB4.2	Response to light *stimulus	0.632897651	0.000357801	0.014159645
AT1G01120	KCS1	Response to cold/light	0.631398424	0.002451506	0.052638776
AT2G47060	PTI1-4	Response to oxidative stress	0.629610563	0.000907678	0.027585899
AT5G18170	GDH1	Response to light/salt stress *absence	0.61986883	7.39291E-05	0.004182209
AT1G20620	CAT3	Response to cold/light/oxidative stress	0.581011131	6.79223E-05	0.004022917
AT1G03220	AT1G03220	Response to salt stress	0.580202287	0.000484296	0.01737364
AT4G10340	LHCB5	Response to light *stimulus	0.560073192	8.0188E-05	0.004478854
AT3G10020	AT3G10020	Response to oxidative stress	0.555279011	0.000346508	0.014027208
AT3G47620	TCP14	Response to abiotic stress *Regulation	0.546447313	0.002227973	0.050157816
AT5G42900	COR27	Response to cold	0.545987612	0.002646656	0.055479184
AT3G54890	LHCA1	Response to cold/light *stimulus	0.545099265	9.54808E-05	0.005106778
AT3G28860	ABCB19	Response to light *stimulus	0.529424523	0.000338176	0.013880941
AT1G29910	CAB3	Response to light *stimulus	0.528621191	0.000439909	0.016127779
AT1G77180	SKIP	Response to salt stress	0.515628268	0.000365824	0.014159645
AT1G09570	PHYA	Response to light *stimulus	0.51322227	0.000304698	0.012927696
AT1G61520	LHCA3	Response to cold/light *stimulus	0.504744685	0.000365387	0.014159645
AT1G20450	ERD10	Response to cold/water deprivation	0.501481975	0.001845328	0.044832931
AT5G66880	SNRK2.3	Response to water deprivation/salt stress/osmotic stress	0.497609111	0.005328915	0.083977988
AT3G17510	CIPK1	Response to salt stress/osmotic stress	0.49452041	0.005138034	0.082592258
AT2G41430	ERD15	Response to water deprivation/light *stimulus	0.494221417	0.000138209	0.006920348
AT3G61470	LHCA2	Response to cold/light *stimulus	0.483928771	0.000138485	0.006920348

AT1G20440	COR47	Response to cold/water deprivation/osmotic stress	0.479767536	0.006190069	0.091965246
AT3G16857	RR1	Response to water deprivation	0.471767883	0.003689468	0.068259031
AT5G20830	SUS1	Response to cold/water deprivation/osmotic stress/hypoxia	0.471677854	0.007351672	0.098263209
AT1G58290	HEMA1	Response to light	0.467617108	0.005156207	0.082733691
AT1G53580	GLY3	Response to salt stress	0.460249545	0.003416394	0.064316541
AT3G47470	LHCA4	Response to cold/light *stimulus	0.460070015	0.000929139	0.027927997
AT4G20260	PCAP1	Response to cold/water deprivation	0.455505702	0.002311498	0.050850918
AT4G38680	GRP2	Response to cold/water deprivation	0.454593578	0.003196266	0.062543339
AT2G45960	PIP1B	Response to water deprivation/salt stress	0.454518464	0.000280434	0.012191269
AT1G80920	J8	Response to light	0.448214334	0.001095744	0.031294319
AT5G20250	DIN10	Response to cold/oxidative stress	0.444453086	0.002263303	0.050438497
AT3G53420	PIP2A	Response to water deprivation	0.436930961	0.004362974	0.074909036
AT4G16830	AT4G16830	Response to salt stress/osmotic stress	0.436486608	0.003282195	0.063105392
AT3G53990	AT3G53990	Response to cold/oxidative stress/heat	0.430923993	0.00672733	0.095448057
AT3G48360	BT2	Response to cold/salt stress	0.428923256	0.002318263	0.050850918
AT1G02500	SAM1	Response to salt stress	0.425245933	0.001387851	0.037340805
AT1G74920	ALDH10A8	Response to water deprivation/salt stress	0.405136273	0.002418523	0.052440943
AT5G01530	LHCB4.1	Response to light *stimulus	0.36987361	0.003917827	0.070560859
AT1G47128	RD21A	Response to water deprivation	0.333689787	0.007262794	0.098103697

Downregulated

TAIR_ID	Gene Symbol	Response type	Log ₂ Fold Change	p value	p adjusted
---------	-------------	---------------	------------------------------	---------	------------

AT5G02490	Hsp70-2	Response to cadmium ion/heat	-1.170477734	2.4318E-06	0.000271654
AT4G21680	NRT1.8	Response to cadmium ion	-1.010564785	3.91465E-05	0.002637156
AT3G09440	AT3G09440	Response to cadmium ion/heat	-0.938312873	3.88764E-07	5.67107E-05
AT5G49910	cpHsc70-2	Response to cadmium ion/heat	-0.668134954	7.06223E-05	0.004102789
AT5G56010	HSP81-3	Response to heat	-0.646772645	2.72366E-05	0.002019854
AT1G77510	PDIL1-2	Response to cadmium ion	-0.639188651	0.00069481	0.022794405
AT2G38470	WRKY33	Response to heat	-0.601194055	0.006851329	0.095820889
AT5G42020	BIP2	Response to cadmium ion/heat	-0.563243529	0.000603897	0.020497669
AT3G56070	ROC2	Response to cadmium ion	-0.562728381	0.002416638	0.052440943
AT5G56030	HSP81-2	Response to heat	-0.555572849	6.41808E-05	0.003826998
AT1G36370	SHM7	Response to cadmium ion	-0.555152006	0.002854286	0.058400671
AT5G09590	MTHSC70-2	Response to cadmium ion/heat	-0.537155357	0.00145436	0.038183737
AT3G03780	MS2	Response to cadmium ion	-0.532041523	0.002184796	0.049692858
AT5G28540	BIP1	Response to heat	-0.507674109	0.001138353	0.032198594
AT3G54470	AT3G54470	Response to cadmium ion	-0.462533179	0.00461098	0.077013732
AT4G02930	AT4G02930	Response to cadmium ion	-0.459818375	0.003237085	0.062923511
AT3G23990	HSP60	Response to cadmium ion/heat	-0.426695363	0.002635252	0.055479184
AT5G09650	PPa6	Response to cadmium ion	-0.422818352	0.003014175	0.060374973
AT1G53240	mMDH1	Response to cadmium ion	-0.420750472	0.000801901	0.025456039
AT5G20720	CPN20	Response to cadmium ion	-0.419076308	0.001236887	0.034314475
AT5G41670	AT5G41670	Response to cadmium ion	-0.409884055	0.004461919	0.075433778
AT3G25230	ROF1	Response to cadmium ion/heat	-0.405081887	0.005863493	0.08937017

AT4G37910	mtHsc70-1	Response to cadmium ion/heat	-0.391498699	0.006672943	0.095135248
AT3G22200	POP2	Response to cadmium ion	-0.358573217	0.002057139	0.047467086

Table S6. List of differentially expressed transcription factors (TFs) between *ucp1 ucp3* double mutant and wild-type (WT) control.

TFs upregulated				
TAIR_ID	Family	Gene Symbol	Gene Description	Log ₂ FoldChange
AT1G79700	AP2	WRI4	AP2 family protein	1,369593983
AT1G32640	bHLH	MYC2	bHLH family protein	1,282208421
AT5G47220	ERF	ERF2	ethylene responsive element binding factor 2	1,074410691
AT2G19810	C3H	OZF1	C3H family protein	1,069293253
AT2G43010	bHLH	PIF4	phytochrome interacting factor 4	0,928417999
AT5G24800	bZIP	BZIP9	basic leucine zipper 9	0,873186217
AT2G25900	C3H	ATCTH	C3H family protein	0,787702985
AT5G08330	TCP	TCP21	TCP family protein	0,748704225
AT3G58120	bZIP	BZIP61	bZIP family protein	0,715965006
AT2G36400	GRF	GRF3	growth-regulating factor 3	0,675989882
AT4G36730	bZIP	GBF1	G-box binding factor 1	0,658987882
AT3G14180	Trihelix	ASIL2	sequence-specific DNA binding transcription factors	0,639381387
AT3G47620	TCP	TCP14	TEOSINTE BRANCHED, cycloidea and PCF (TCP) 14	0,546447313
AT1G05805	bHLH	BHLH128	bHLH family protein	0,510137187
AT1G68520	CO-like	BBX14	B-box type zinc finger protein with CCT domain	0,497419859
AT4G17230	GRAS	SCL13	SCARECROW-like 13	0,480260742
AT3G16857	ARR-B	RR1	Response Regulator 1	0,471767883
AT1G09770	MYB	CDC5	cell division cycle 5	0,408515098
TFs downregulated				
TAIR_ID	Family	Gene Symbol	Gene Description	Log ₂ FoldChange
AT3G14230	ERF	RAP2.2	Related to AP2 2	-0,411599783

AT4G31550	WRKY	WRKY11	WRKY DNA-binding protein 11	-0,508799656
AT3G44750	C2H2	HDA3	histone deacetylase 3	-0,549217658
AT4G01720	WRKY	WRKY47	WRKY family protein	-0,549449506
AT2G38470	WRKY	WRKY33	WRKY DNA-binding protein 33	-0,601194055
AT2G42280	bHLH	FBH4	bHLH family protein	-0,617787349
AT4G24240	WRKY	WRKY7	WRKY DNA-binding protein 7	-0,646303351
AT3G29035	NAC	NAC3	NAC domain containing protein 3	-0,687745551
AT4G01250	WRKY	WRKY22	WRKY family protein	-0,703048958
AT5G39610	NAC	NAC6	NAC domain containing protein 6	-0,875583394
AT1G36060	ERF	ERF055	ERF family protein	-0,944222619
AT1G09530	bHLH	PIF3	phytochrome interacting factor 3	-1,02055426
AT3G10040	Trihelix	HRA1	sequence-specific DNA binding transcription factors	-1,050129357
AT3G02550	LBD	LBD41	LOB domain-containing protein 41	-1,296693611
AT3G04070	NAC	NAC047	NAC domain containing protein 47	-1,443766169

Table S7. Levels of the metabolites identified in the wild-type (WT) and *ucp* double mutant plants (21-day-old).

Source metabolite	ucp1 ucp2 _R1	ucp1 ucp2 _R2	ucp1 ucp2 _R3	ucp1 ucp2 _R4	ucp1 ucp2 _R5	ucp1 ucp3 _R1	ucp1 ucp3 _R2	ucp1 ucp3 _R3	ucp1 ucp3 _R4	ucp1 ucp3 _R5	ucp2 ucp3 _R1	ucp2 ucp3 _R2	ucp2 ucp3 _R3	ucp2 ucp3 _R4	ucp2 ucp3 _R5	WT _R1	WT _R2	WT _R3	WT _R4	WT _R5
Formyl piperidine	0	0	0	0	0	0	0	1	0	0	0	0	0	0	0	0	0	0	0	0
Diethyl isophthalate	1	1	1	1	1	1	1	2	1	2	2	1	1	1	1	1	1	1	1	1
2-amino benzo xazole	0	0	0	0	0	0	0	0	0	0	0	0	0	1	0	0	0	0	0	0
1,3-butanediol	32	0	217	161	0	0	0	0	0	0	0	64	138	69	81	0	0	0	0	0
Putrescine	0	0	0	0	0	0	0	0	1	0	0	0	0	0	0	1	0	0	0	1
alpha-methyl-6-fluoro tryptamine	0	0	1	1	1	5	1	1	0	101	0	0	1	0	0	1	1	1	0	0
Fumaric acid	3	12	5	3	3	6	8	25	6	9	16	3	5	4	2	4	3	3	8	4

2-Furoic acid	0	0	0	0	0	0	0	0	0	0	0	0	0	0	0	0	0	0	0	0
Erythrono-1,4-lactone	0	0	0	0	0	0	0	1	0	1	0	0	0	0	0	0	0	0	0	0
Threonic acid	0	0	1	0	0	1	1	1	1	1	1	0	0	0	0	0	0	1	0	1
Dimethoxy mandelic acid	3	20	27	27	9	52	75	24	59	178	11	12	15	15	19	39	20	22	20	8
Methyl 4-oxo-1-(trifluoro acetyl)-2-pyrrolidine carboxylate	0	0	0	0	0	0	0	0	0	0	0	0	0	0	0	0	0	0	0	0
Phytol	0	0	0	0	0	0	0	0	0	0	0	0	0	0	0	0	0	0	0	0
Cytosine	0	0	0	0	0	0	0	0	0	0	16	13	19	10	2	0	0	0	0	0
1,2,3,4-Tetrahydro-6-methoxy-1-salicyl-7-iso quinolinol	0	0	0	0	0	0	0	0	0	0	0	0	0	0	0	0	0	6	0	0
Adenine	2	5	2	1	1	2	1	4	3	2	4	4	2	2	1	2	1	1	4	3
Alanine	1	3	2	3	4	163	4	1	6	5	3	3	2	58	3	3	3	3	4	6
Alanine, N-methyl-n-butoxycarbonyl-, octyl ester	0	0	0	0	0	0	0	0	0	0	0	0	0	0	0	0	0	0	0	0
Alanine, N-methyl-N-methoxycarbonyl-, undecyl ester	68	1	0	18	1	0	0	8	28	4	17	0	34	52	31	0	19	156	1	2
Manno pyranose	492	253	46	9	130	197	84	206	360	225	279	83	106	177	136	183	207	112	142	276
Xylose	1	1	0	0	0	8	0	1	1	0	65	1	1	7	0	1	0	0	0	0
Galactose	2	25	122	73	77	1	0	1	0	0	0	0	0	0	0	36	177	102	2	0

Linolenic acid	0	0	0	0	0	0	0	4	2	2	0	0	0	0	0	0	0	0	0	0
Sitosterol	0	0	0	0	0	2	1	4	2	2	0	0	0	0	0	1	0	0	0	0
Methyl (3,4-dimethoxyphenyl) (hydroxy) acetate	0	0	0	0	0	0	0	0	0	0	0	0	0	0	0	0	0	0	25	2
Glycolic acid	0	0	0	0	0	0	0	1	0	1	1	0	1	0	0	0	0	0	0	0
Diglycolic acid	0	0	0	0	0	0	0	0	0	0	0	0	0	0	0	0	0	0	0	0
Adenosine	0	0	0	0	0	0	0	0	0	0	0	0	0	0	0	0	0	0	0	0
Epinephrine	0	0	0	0	0	0	2	0	1	0	0	0	0	0	0	0	0	0	0	0
Alanyl glycine	0	0	0	0	0	0	0	0	0	0	0	0	0	0	0	0	15	0	0	16
Arabino furanose	0	39	0	0	0	0	0	0	0	0	38	21	0	50	0	0	0	0	0	0
Asparagine	0	27	8	7	11	9	6	5	12	1	10	14	18	10	7	7	13	7	8	26
Aucubin	1	2	1	1	4	2	2	3	1	2	12	5	39	2	4	2	8	1	7	24
2,3-Butanediol	0	0	8	0	0	1	0	0	1	0	0	0	0	0	0	0	0	0	0	0
Malic acid	14	29	19	9	14	11	14	40	12	22	31	9	17	14	6	11	7	7	17	14
Succinic acid	0	0	0	0	0	0	0	0	0	0	0	0	0	0	0	19	0	9	24	37
Methyl Succinic acid	4	1	0	0	0	0	0	0	0	0	0	0	0	0	0	0	0	0	0	0
3-Deoxy tetronic acid	0	0	0	0	0	0	0	0	0	0	0	0	0	0	0	0	0	0	0	0
4-Hydroxy butyric acid	2	1	1	1	0	2	2	2	1	3	0	0	1	0	0	1	0	0	0	1
Amino butyric acid	3	16	8	6	8	14	10	40	24	12	16	9	9	9	5	11	8	9	17	20
Sinapinic acid	1	2	1	1	1	1	2	4	2	2	4	1	1	1	0	1	1	1	1	1

Cyclopentane carboxylic acid, 3-oxo-, methyl ester	0	0	0	0	0	0	0	0	0	0	0	0	0	6	1	0	0	1	21	3
3-Methyl Cyclopentanone	0	0	0	0	0	0	0	0	0	0	0	0	1	0	0	0	0	0	0	0
Psicofuranose	111	227	275	332	342	174	125	39	39	24	207	151	168	151	203	398	163	271	97	154
Arabinose	0	0	1	0	0	1	0	1	1	0	0	3	0	0	1	0	0	0	0	0
2-Deoxy-D-erythro-pentopyranose	0	0	0	0	0	0	0	0	0	0	0	0	0	0	0	0	0	0	0	0
d-Erythrotetrofuranose, tris-O-(trimethylsilyl)-	0	0	0	0	0	0	0	0	0	4	0	0	0	0	0	0	0	0	0	0
Gluconic acid	0	1	0	0	1	1	1	3	2	1	3	1	1	0	0	1	0	1	1	1
Glucose	78	0	0	90	2	0	0	0	0	0	0	101	0	0	81	0	1	0	79	0
D-Mannopyranose 6-phosphate	0	1	0	0	1	1	0	0	0	2	2	1	1	0	0	0	1	1	1	1
Galactose methoxamine	1	4	2	1	4	1	0	9	2	5	5	1	7	2	0	2	1	2	8	5
Rhamnose	10	1	1	0	1	1	0	3	1	1	0	1	2	0	7	0	2	0	2	4
Psicose	17	0	0	15	50	0	0	0	0	0	0	0	0	0	0	0	18	17	27	0
Ribose-5-phosphate	0	0	0	0	0	0	0	0	0	0	0	0	0	0	0	0	0	0	0	0
Phthalic acid	0	0	0	0	0	0	0	0	0	0	0	0	0	0	0	0	0	0	0	0
Laudanosoline hydrobromide	0	0	0	0	0	0	0	0	0	0	0	0	0	0	0	0	0	0	0	0

Ethyl-D-glucopyranoside	11	11	9	6	9	35	26	122	45	25	6	5	18	5	35	24	29	50	7	1
Galactaric acid	1	0	1	1	2	0	0	0	0	0	1	0	2	1	1	2	1	1	1	0
Glutamic acid	0	2	2	1	1	1	1	0	1	0	1	1	1	1	0	1	0	0	0	1
Glycerol	4	18	0	5	82	0	60	1	0	21	0	0	0	0	0	0	0	0	0	0
Glycerylglycoside	0	1	1	0	0	1	0	1	1	1	2	1	0	0	0	0	0	0	1	0
Glycine	0	0	0	1	0	32	10	31	13	7	13	7	10	3	8	20	9	10	26	38
Methyl hexopyranoside	0	0	1	0	1	0	5	2	12	56	1	0	13	0	0	1	4	11	92	5
Guaicol-d-glucopyranoside	0	0	0	0	0	0	0	0	0	0	0	0	0	0	0	0	0	0	0	0
Mono palmitin	2	0	3	13	0	17	19	37	17	18	0	0	0	0	5	3	3	6	8	2
Palmitic acid	2	1	1	3	1	3	5	19	4	8	1	0	1	0	1	4	2	1	5	1
Ascorbic acid	1	0	0	0	0	0	0	0	0	0	0	0	0	0	0	0	0	0	0	0
Aspartic acid	0	17	8	5	7	7	6	4	9	16	17	7	12	10	4	6	4	4	2	7
Cysteine	0	0	0	0	0	0	0	0	0	0	0	0	0	0	0	0	0	0	0	0
Glutamine	0	123	83	105	106	0	0	0	0	0	84	174	193	100	98	78	90	85	145	135
Isoleucine	0	0	0	0	0	0	0	0	0	0	0	0	0	0	0	0	0	0	0	0
Proline	0	3	0	0	0	0	0	0	0	0	0	0	0	0	0	0	0	0	0	0
Pyro glutamic acid	22	22	13	8	11	11	10	84	16	28	16	13	19	20	8	8	8	8	20	19
Tryptophan	0	0	0	0	0	0	0	0	0	0	0	0	0	0	0	0	0	0	0	0
Tyrosine	0	0	0	0	0	0	0	0	0	0	0	0	0	0	0	0	0	0	0	0
Valine	0	1	0	0	1	0	0	0	0	0	1	1	1	0	0	0	0	0	0	1
Levo glucosan	53	0	1	0	0	0	0	0	0	0	0	0	0	0	0	0	0	0	0	0
Meso-Erythritol	0	0	0	0	0	0	0	4	0	1	0	0	0	0	0	0	0	0	0	0

Myo-Inositol	5	12	7	4	8	5	4	11	5	5	18	7	14	7	4	6	5	5	9	10
Myo-Inositol [phosphate]	0	0	0	0	0	0	0	1	1	0	0	0	0	0	0	0	0	0	0	0
N-Acetyl-D- gluco samine	0	0	0	0	0	0	0	0	0	0	0	0	0	0	0	1	0	0	0	3
2-Pyrro lidinone	0	1	0	0	0	0	0	2	0	1	0	0	0	0	0	0	0	0	1	0
Guanine	0	0	0	0	0	0	0	0	0	0	0	0	0	0	0	0	0	0	0	0
Phenyl alanine	0	0	0	0	0	0	0	0	0	0	0	0	0	0	0	0	0	0	0	0
Threonine	1	6	3	2	2	2	2	1	3	3	5	2	3	2	1	2	2	2	2	4
Glycerol mono stearate	1	0	2	6	0	7	9	16	7	8	0	0	0	0	0	3	2	3	3	2
Stearic acid	2	1	1	2	1	2	2	2	2	2	1	0	1	0	1	3	2	1	2	1
Ornithine	0	1	0	0	0	1	0	0	0	0	0	1	1	1	0	0	0	0	0	1
β -Hydroxy- β -methyl glutaric acid	2	1	1	0	0	2	1	2	0	2	0	0	0	0	0	0	0	0	0	0
Phenyl propanol amine	0	0	98	68	84	200	486	1	270	111	59	39	99	129	52	92	54	61	76	58
Glycero phosphoric acid	0	0	0	0	0	0	1	153	0	50	0	0	0	0	0	0	0	0	0	0
Phosphoric acid, mono methyl ester	4	2	1	0	1	0	0	1	1	1	2	1	2	1	0	1	0	0	1	1
1,2- Benzenedic arboxylic acid	0	0	0	0	0	0	0	42	0	0	0	0	0	0	0	0	0	0	0	0
Malonic acid	0	0	0	0	0	0	0	0	0	0	0	0	0	0	0	0	0	0	0	0
Lactic acid	0	0	0	0	0	0	1	1	0	0	0	162	0	0	0	0	0	0	0	0
Propanoic acid	0	0	0	0	0	0	0	1	0	0	0	0	0	0	0	0	0	0	0	0

Glyceric acid	2	3	2	1	2	3	3	10	4	6	3	1	2	1	2	3	2	2	5	5
2-Methyl alanine	0	0	0	0	0	0	0	3	0	0	0	0	0	0	0	0	0	0	0	0
Thymine	0	0	0	0	0	0	0	0	0	0	0	0	0	0	0	0	0	0	0	0
Ribitol	2	79	0	0	0	0	0	0	0	0	7	64	0	64	176	0	103	0	61	68
Ribonic acid	1	1	1	0	1	0	0	0	0	0	0	0	1	1	0	0	0	0	0	0
2-(Dimethylamino) ethyl (1Z)-2-(dimethylamino)-N-hydroxy-2-oxoethanimidothioate	0	0	0	0	0	0	0	0	0	0	0	0	0	0	0	0	0	0	0	0
Serine	7	42	19	15	26	25	18	28	32	26	30	21	28	15	12	23	15	16	21	44
Urea	33	1	2	0	1	0	0	1	1	6	1	1	1	1	0	0	0	0	0	1
Uridine	0	0	0	0	0	0	0	1	1	1	1	0	1	0	0	0	0	0	1	1

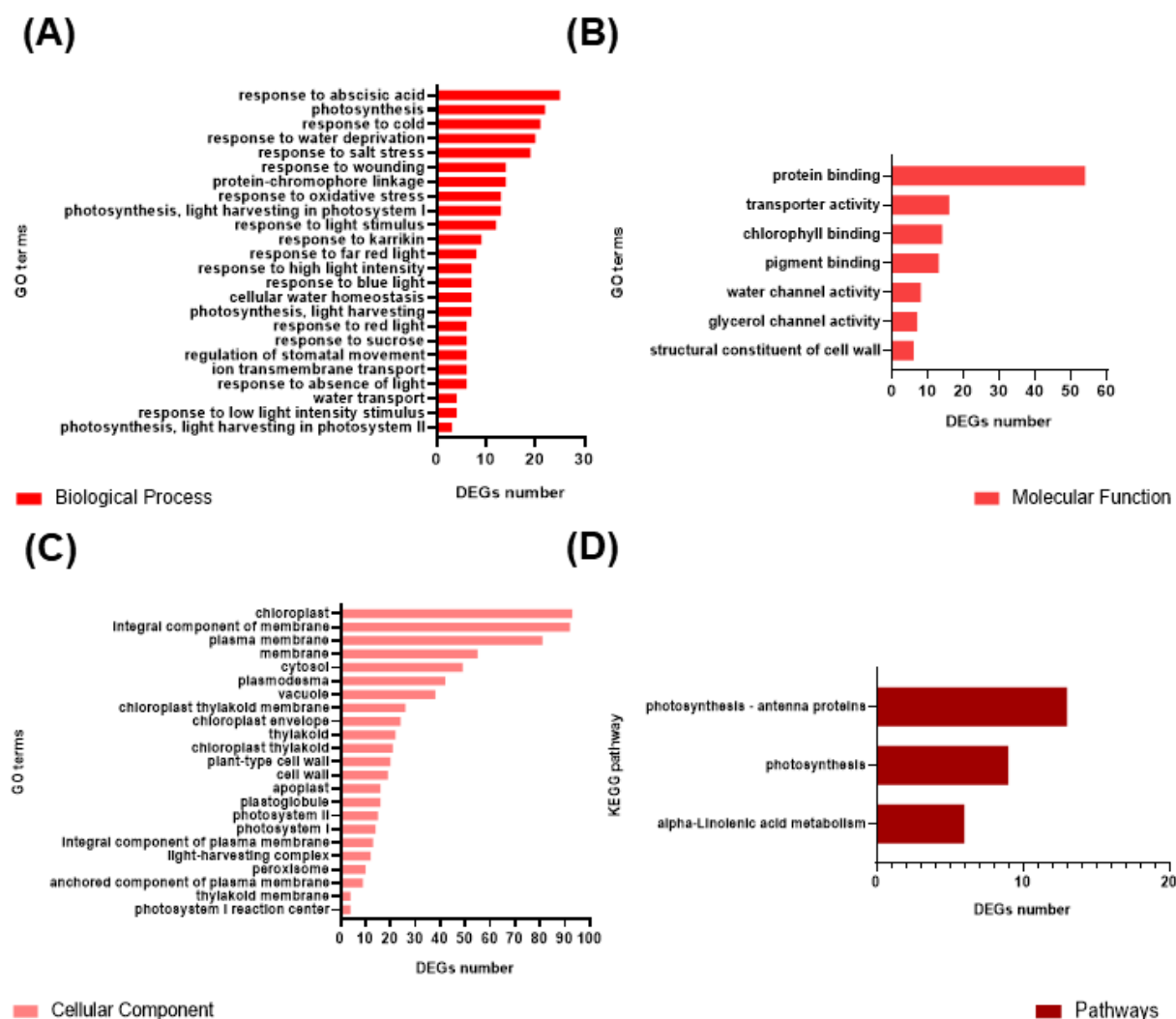


Figure S1. Overview of GO and KEGG enrichment analysis for the upregulated differentially expressed genes (DEGs) between the *ucp1 ucp3* mutant and the wild-type (WT). (A) Biological Process. (B) Molecular Function. (C) Cellular Component. (D) Pathways. The bars represent the number of DEGs relative to each GO term or KEGG pathway. GO terms and pathways with corrected p-value ≤ 0.05 were considered significantly enriched. GO: Gene Ontology; KEGG: Kyoto Encyclopedia of Genes and Genomes.

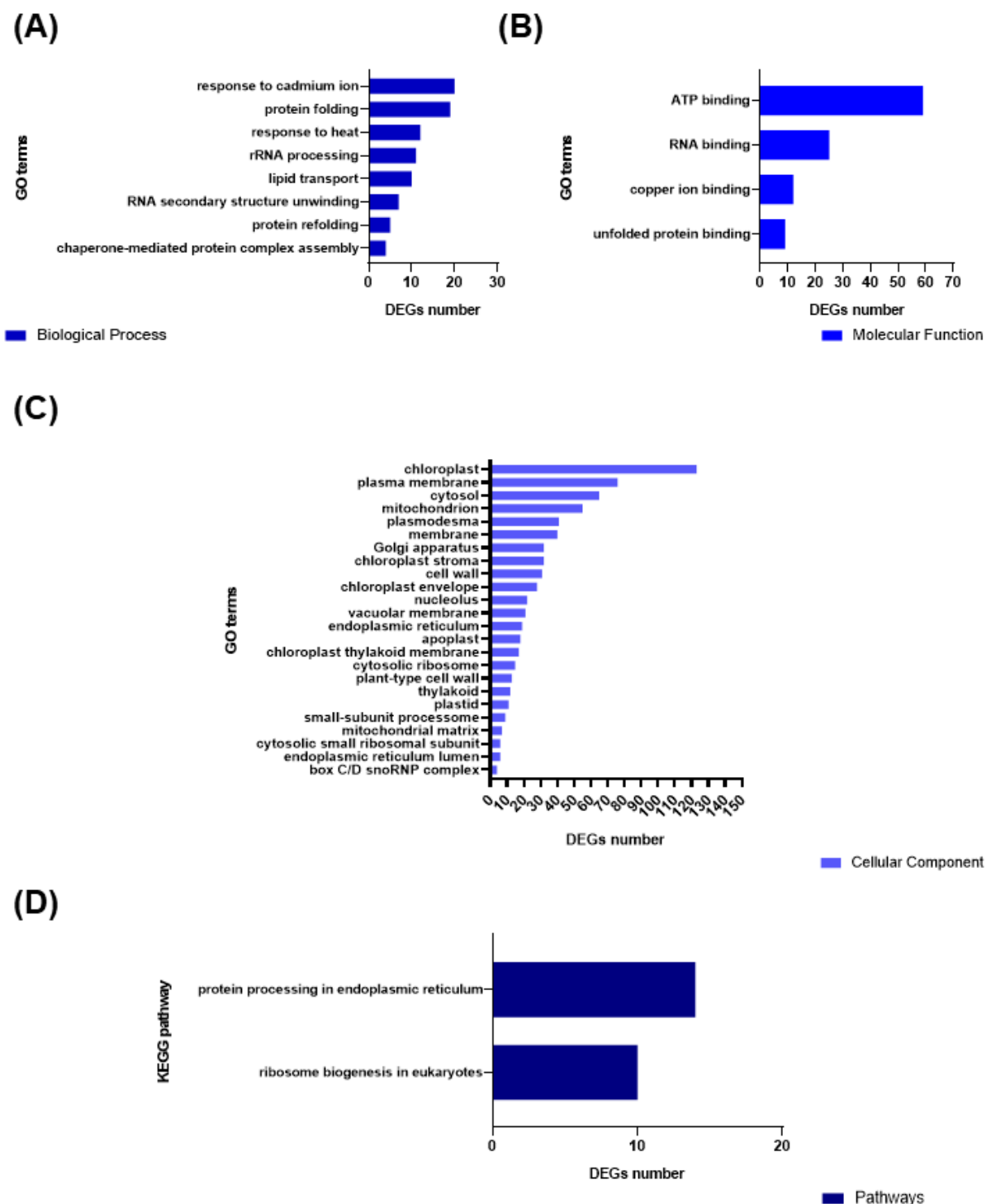


Figure S2. Overview of GO and KEGG enrichment analysis for the downregulated differentially expressed genes (DEGs) between the *ucp1 ucp3* mutant and the wild-type (WT). (A) Biological Process. (B) Molecular Function. (C) Cellular Component. (D) Pathways. The bars represent the number of DEGs relative to each GO term or pathway. GO terms and KEGG pathways with corrected p-value ≤ 0.05 were considered significantly enriched. GO: Gene Ontology; KEGG: Kyoto Encyclopedia of Genes and Genomes.

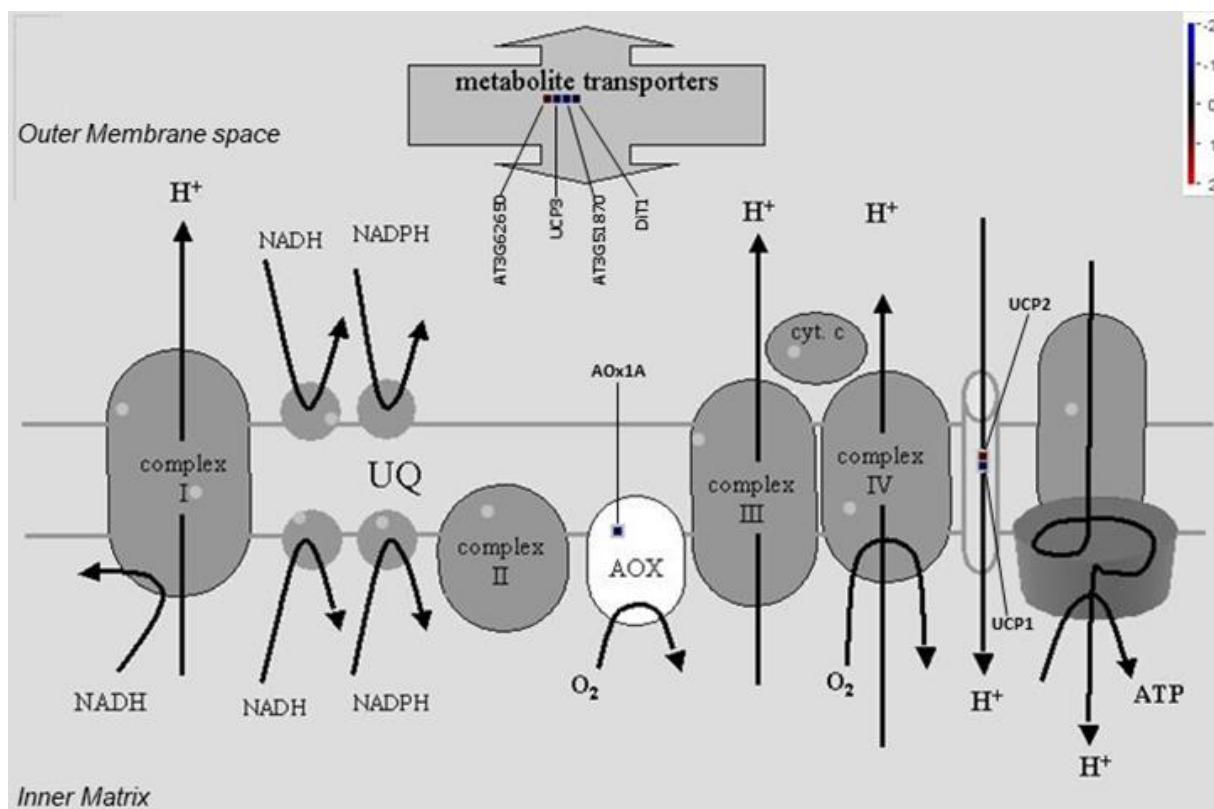
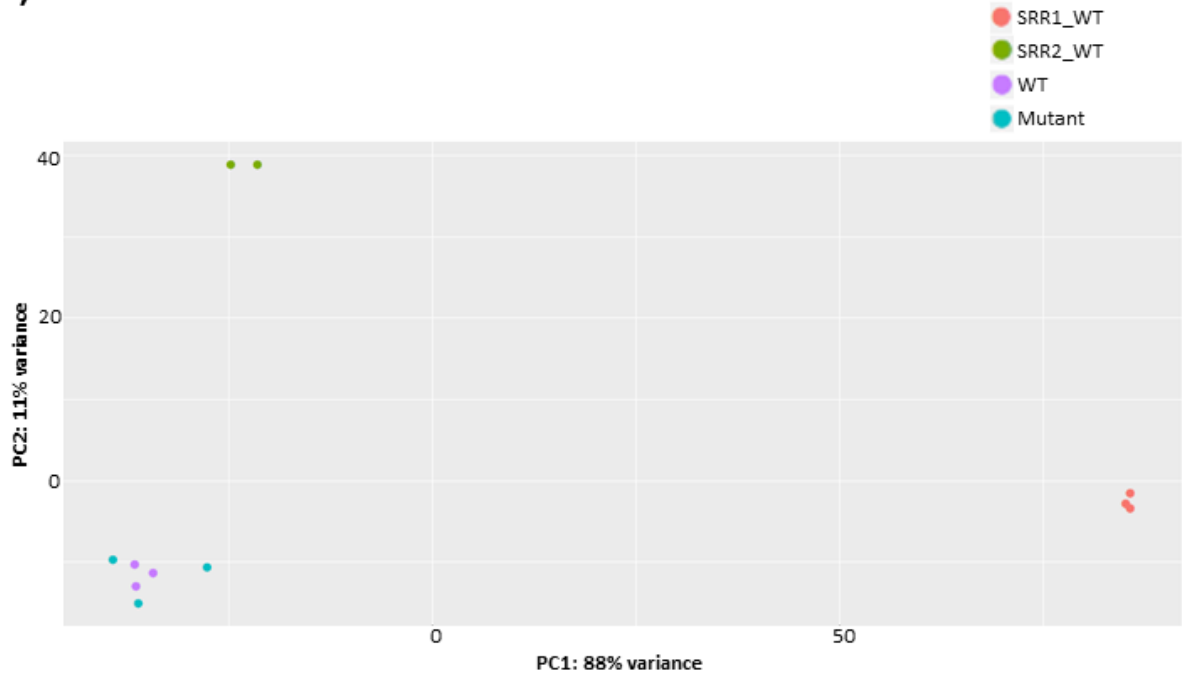
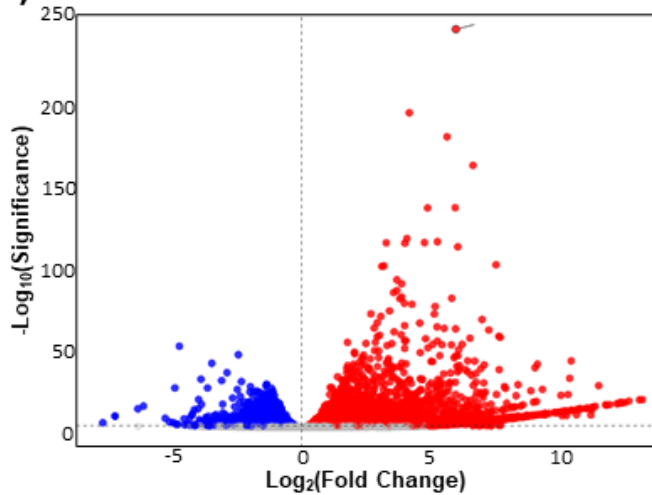


Figure S3. MapMan overview of the DEGs related to mitochondrial electron transport chain and metabolite transporters. The 668 DEGs ($P_{\text{adj}} < 0.1$) were used against the *Arabidopsis thaliana* mitochondrial metabolite transport. The $\text{Log}_2(\text{Fold Change})$ values for each up- and downregulated DEG detected from this MapMan analysis were plotted onto boxes. Red and blue boxes indicate up- and downregulated DEGs, respectively. DEG: differentially expressed gene; P_{adj} : adjusted p-value.

(A)



(B)



(C)

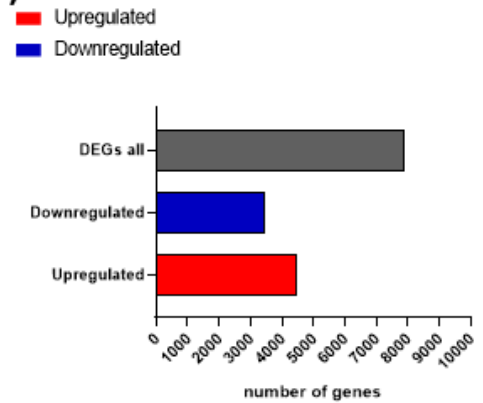
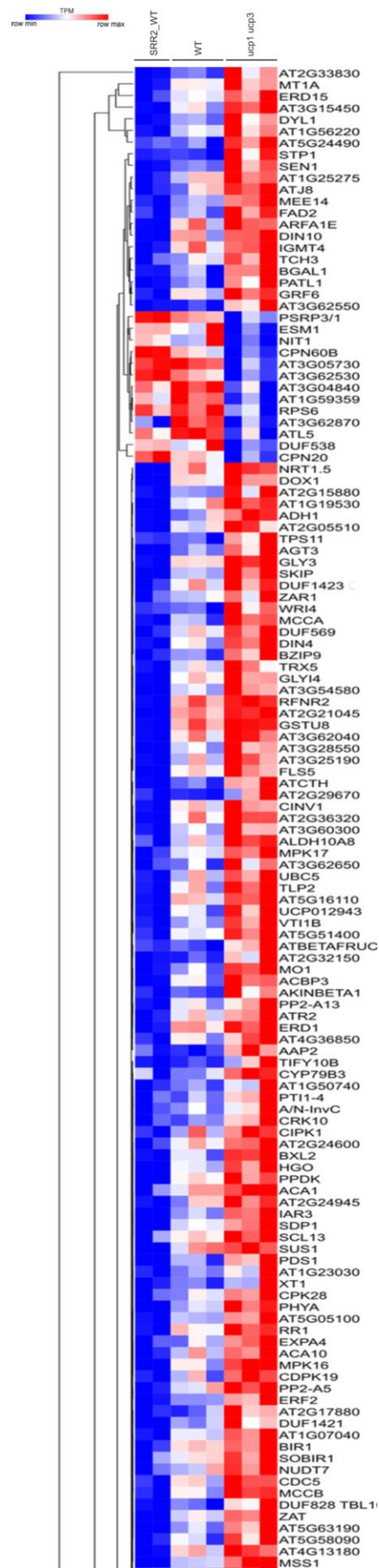
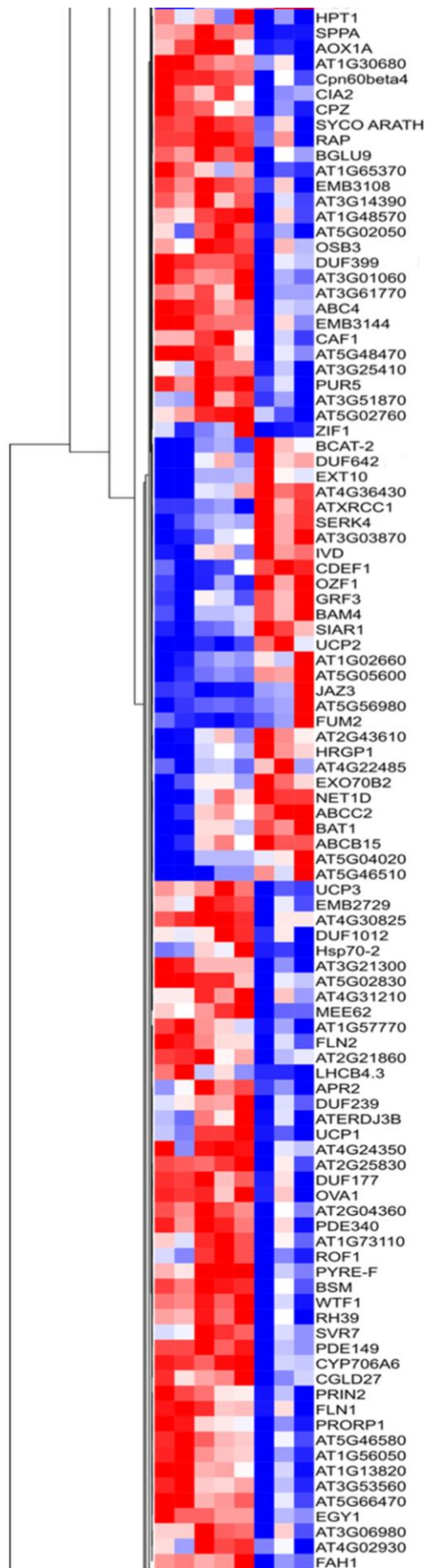


Figure S4. Overview of *ucp1 ucp3* mutant transcriptome using wild-type (WT) datasets. (A) PCA of normalized count data from WT and mutant groups of the transcriptome together with SRR1_WT and SRR2_WT selected datasets. (B) Volcano plot of negative log-transformed Padj ($-\log_{10}(\text{Padj})$) and $\log_2(\text{Fold Change})$ for each gene in *ucp1 ucp3* plants compared with proceeded SRR2_WT dataset. (C) Number of DEGs all, up- and downregulated DEGs in *ucp1 ucp3* plants compared with SRR2_WT proceeded dataset. DEGs were identified using DESeq2 package and defined by $\text{Padj} < 0.1$. Up- and downregulated DEGs are shown in red and blue, respectively. PCA: Principal Component Analysis; Padj: adjusted p-value; DEG: differentially expressed gene.





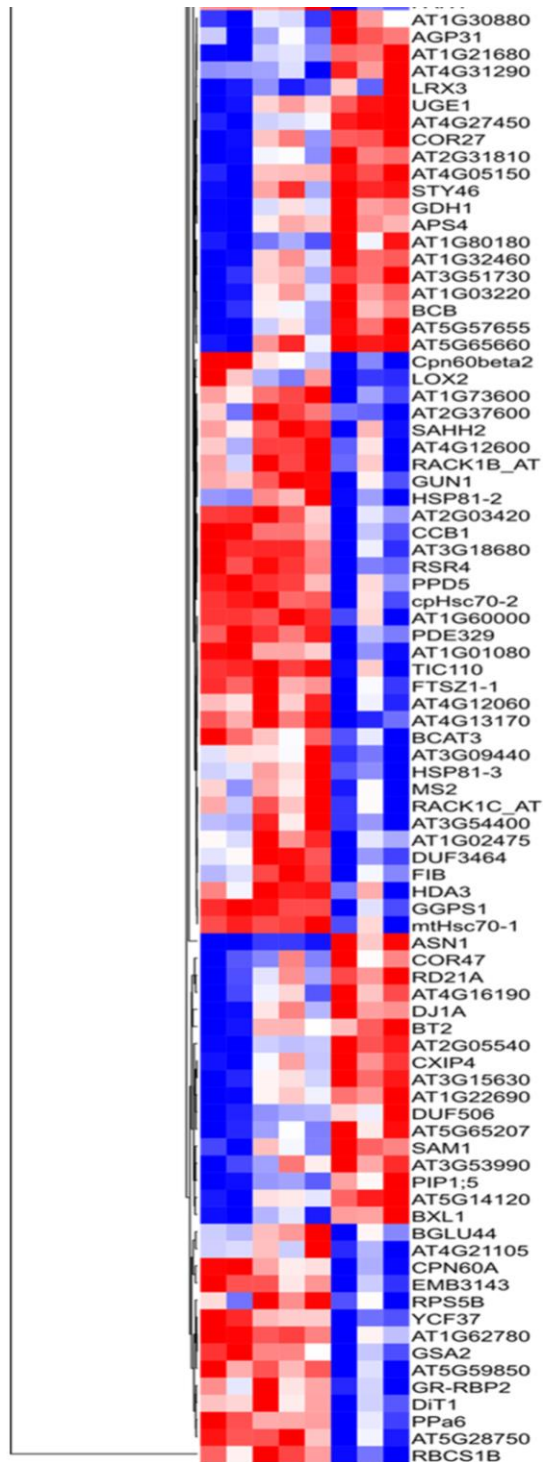


Figure S5. Hierarchical clustering analysis of differentially expressed genes (DEGs) in *ucp1 ucp3* plants compared with the two wild-type (WT) treatments in each RNA-Seq counterpart. DEGs were identified using DESeq2 package and defined by $P_{adj} < 0.1$. The heatmap was constructed using TPM data from WT and mutant groups together with SRR2_WT preceded dataset. Pearson correlation was used as metric. The expression scale according to TPM data of the three biological replicates per genotype varies from dark blue (downregulation) to dark red (upregulation). P_{adj} : adjusted p-value; TPM: Transcripts Per Kilobase Million.

Considerações Finais

Os resultados obtidos a partir da utilização dos duplo-mutantes de inserção gerados no presente trabalho revelaram que a expressão reduzida dos genes alvos provoca profundos impactos (fenótipos alterados, alterações no metabolismo mitocondrial, no balanço redox, nos cloroplastos e por toda a célula) em toda a planta. Estes impactos puderam ser observados durante os estágios de desenvolvimento vegetativo e reprodutivo. Os dados gerados no capítulo I forneceram novos *insights* para o melhor entendimento do papel desempenhado pelas três isoformas, indicando uma redundância funcional parcial entre elas. Os dados de RNA-Seq no capítulo II revelam que uma intensa reprogramação transcricional ocorre em decorrência da mutação concomitante dos genes *AtUCP1* e *AtUCP3*. Diversos dos genes desregulados estão associados a vários compartimentos, processos e mecanismos internos por toda a célula, a exemplo de transcritos de genes mitocondriais, de cloroplastos, responsivos a estresses abióticos, bem como aqueles relacionados ao metabolismo de DNA e energético. Em concordância com as análises do transcriptoma de plantas *ucp1 ucp3*, as análises do metaboloma de plantas *atucp* duplamente mutantes revelaram distúrbios tanto no metabolismo primário, com mudanças importantes nas concentrações de aminoácidos, ácidos orgânicos, açúcares e componentes de ácidos nucleicos, quanto no secundário, com alterações de metabólitos vinculados às classes dos flavonoides, terpenos e alcaloides. Portanto, um importante ajuste metabólico se faz necessário para compensar a expressão reduzida dos genes *AtUCP1-3*. Os dados apresentados, além de fornecer subsídios importantes para melhor compreender as respectivas funções em plantas das referidas proteínas, poderão ser empregados em aplicações futuras visando a aquisição de tolerância a estresses.